Production of magnetic bacteria and their use in biotechnology

Mary Aubry

PSL
UNIVERSITÉ PARIS

THÈSE DE DOCTORAT
DE L'UNIVERSITÉ PSL

Préparée à l'Ecole Normale Supérieure

Production of magnetic bacteria and their use in biotechnology

Production de bactéries magnétiques et leurs utilisations en biotechnologie

Soutenue par
Mary AUBRY
Le 11 Décembre 2020

Ecole doctorale n° 388
Chimie Physique et Chimie Analytique de Paris-Centre

Spécialité
Chimie Physique

ENS

Composition du jury :

Jérôme, BONNET	Chargé de Recherche, Université de Montpellier	*Rapporteur*
Laurence, LEMELLE	Chargée de Recherche, ENS Lyon	*Rapportrice*
Damien, FAIVRE	Directeur de Recherche, CEA	*Examinateur*
Claire, WILHELM	Directrice de Recherche, Université Paris Diderot	*Examinatrice*
Zoher, GUEROUI	Directeur de Recherche, ENS Ulm	*Directeur de thèse*
François, GUYOT	Professeur, MNHN, Sorbonne Université	*Invité*

Présidente du jury : Claire WILHELM

REMERCIEMENTS

Ces trois années de thèse ont été extrêmement riches. J'ai beaucoup appris au laboratoire et j'ai donc énormément de personnes à remercier que ce soit pour leur aide précieuse, pour leur implication dans mon projet de thèse ou pour leur présence chaleureuse au laboratoire.

Avant toute chose, je souhaiterais remercier les membres du jury : Jérôme Bonnet et Laurence Lemelle pour avoir accepté de rapporter mon travail ; Damien Faivre et Claire Wilhelm pour avoir accepté de l'examiner. Merci pour les nombreuses discussions pendant la soutenance !

Un grand merci à Zoher. Merci pour m'avoir fait confiance pendant ces presque 4 années au laboratoire. J'ai beaucoup appris à ton contact et j'ai énormément apprécié toute la liberté d'action que tu m'as donnée pour ce projet. Grâce à toi j'ai pu explorer plein d'expériences, j'ai eu la chance de discuter avec beaucoup de scientifiques et tu m'as aidée à rester motivée tout au long de cette thèse. Je m'estime très chanceuse d'avoir fait partie de ton équipe !

Je voulais aussi remercier tous les collaborateurs qui ont pris du temps pour me montrer de nouvelles expériences et pour discuter du projet. Un grand merci à François Guyot qui a été une aide constante pendant toute cette thèse. Merci pour ta disponibilité, et pour toutes les discussions autour des *MagEcoli.* Ça a été un réel plaisir de travailler avec toi. Merci aussi à Alice Lebreton. Tu m'as ouvert les portes de ton laboratoire pour les expériences d'invasion avec beaucoup de bienveillance. J'aimerais plus tard être aussi rigoureuse, créative et passionnée que toi ! Merci à Olivier Espeli. Merci pour ta disponibilité pendant les expériences de live microscopie et pour tous tes conseils sur les bactéries, leur croissance et leur génétique. Tu m'as fait comprendre plein de choses sur la microbiologie avec beaucoup de patience ! Je voulais aussi remercier Yohan Guyodo pour les expériences de magnétométrie. Merci pour avoir pris le temps de répondre à toutes mes questions sur le magnétisme. Merci à Jean-Michel Guigner et sa patience pendant toutes les séances de microscopie électronique pour aller chercher des bactéries magnétiques à regarder ! Merci à Guillaume Morin pour son avis éclairant sur la composition des *MagEcoli* et pour m'avoir laissé assister à une expérience au synchrotron, je ne l'oublierai pas de sitôt ! Pour les expériences d'IRM je voudrais remercier Philippe Pelupessy qui a su prendre le temps de m'expliquer la RMN et qui m'a beaucoup aidée pour les mesures ! Enfin j'ai eu la chance de travailler avec des *C. elegans*. Merci à Marie-Anne Félix et Aurélien Richaud pour m'avoir accueillie et accompagnée pendant ces expériences !

Je voulais maintenant adresser mes remerciements au pôle de physique et de chimie biologique de la matière vivante et plus largement au département chimie de l'ENS. Merci Ludovic Jullien pour ton accueil dans ce groupe et tes questions toujours pertinentes pendant mes présentations aux pôle meetings.

Merci à l'administration – Anne, Pauline, Nathalie et Elza – en particulier ces dernières semaines pour la préparation de ma soutenance.

A présent je voudrais remercier plus particulièrement quelques membres du laboratoire. D'abord ceux de l'équipe de Zoher. Je garderai un très bon souvenir des anciens. Alexandra, merci pour ton aide et tes conseils, et en particulier sur les calculs de diffusion lors de mon stage de M2. Merci à Shunnichi pour ta bonne humeur et tes conseils avisés lorsque j'étais bloquée sur des clonages. Merci aussi à Wei-An pour m'avoir encadrée avec beaucoup de patience pendant mon stage et continué à m'aider au début de ma thèse ensuite. C'était très agréable de travailler en binôme avec toi ! Merci aussi à Marina. Heureusement que tu as été là lors de la première moitié de ma thèse, que ce soit du point de vue scientifique et humain. Ça a été un véritable plaisir de tous vous connaitre et de débuter une thèse dans une si bonne atmosphère. Enfin je souhaite remercier ceux qui restent dans l'équipe. Audrey et Marie-Aude, merci pour à peu près tout ! Tout me manquera sauf le lab cleaning peut-être: les discussions le soir sur les manips bien sûr mais aussi les goûters, les fou-rires et surtout le body tonic (heureusement j'ai Sissy). Je pourrais adresser les mêmes remerciements, body tonic mis à part, à Lucas, qui ne fait pas partie de l'équipe mais que je vois avec plaisir aussi souvent qu'Audrey et Marie-Aude. Je suis sûre qu'on trouvera les temps de tous se revoir l'année prochaine ! Léonard, merci et bon courage pour ta très belle thèse qui s'annonce. Enfin je remercie les deux stagiaire que j'ai eu le plaisir d'encadrer. Eugénia, merci et bon courage pour ta thèse à Edimbourg. C'était très chouette d'apprendre à encadrer avec toi ! Elisa ensuite, ça a été un grand plaisir de travailler avec toi. Garde ta motivation et ton optimisme ! Quant à moi je garde tes jolis schémas colorés de métabolisme.

Merci à d'autres permanents du groupe : Emmanuelle, Isabelle et Thomas. Je suis très contente de vous avoir rencontrés et c'était toujours très chouette de discuter un peu au détour d'un couloir, d'une paillasse ou d'un déjeuner ! Merci aux autres membres non permanents. Je garde un très bon souvenir de nos échanges lors des déjeuners du midi ou d'une bière à la montagne: Raja, Jordi, Kaithlin, Bea, David, Alienor et les autres.

Merci aussi à Arnaud Gautier et son équipe. J'ai beaucoup appris en travaillant à côté d'Alison et merci pour tous tes conseils de qualité ! Merci aussi à Fanny, Louise et Hela qui me manqueront aussi beaucoup. Mais on se revoit bientôt autour d'un brunch, d'un goûter ou d'une balade en avion.

D'autres remerciements sont destinés à mes proches. Anyssa qui me connait depuis 15 ans déjà mais aussi mes amis de l'ESPCI et puis ma famille plus généralement. Ils m'ont tous écoutée avec beaucoup de patience raconter mes expériences de bactéries magnétiques, quand elles marchaient mais aussi quand elles ne fonctionnaient pas. Enfin mon dernier remerciement est pour Arthur. Un petit peu parce que tu m'as poussée à coder pour traiter des résultats de ma thèse, mais essentiellement parce que tu as été d'un profond soutien tous les jours. Je n'y serai pas arrivée avec autant de sérénité sans ta présence.

Table of contents

Preface

We are surrounded by microorganisms. They are everywhere: in soil, in water, on our skin, in our food, in our gut… The microbial world is rich and diverse. Nowadays, we know that microorganisms and especially bacteria can do more complex actions than just growing and dividing. They can communicate with each other, they can organize between themselves to colonize surfaces (by secreting biofilms for instance), they can transfer genes to foreign strains (via horizontal gene transfer), and they can even secrete antibiotics to kill others…

As our knowledge on microorganisms is improving, we can use them and try to control them to accomplish various applications. The most ancient example dates back over millennia with the fermentative processes leading to bread, beer or wine; and underwent under many improvements. Even without seeing and knowing the existence of microorganisms, fermentation was used to make alcohol and food. With the invention of the microscope, microbes were seen, and Pasteur later explained the process of alcoholic fermentation. Today, we genetically reprogram bacteria or yeast to make them produce at the large scale specific kinds of alcohol, like biofuels. Bacteria and other reprogrammed (or not) microorganisms are now used in various fields such as in medicine, in environmental applications, in mining, in food industry…

Thus, following the advances of biology to modify a microorganism, in order to use it for specific biotechnological applications, my PhD work aimed to give magnetic properties to reprogrammed *E. coli*. Indeed, magnetic interactions have the advantages of being contactless, remote-controlled, and to penetrate deeply into thick living matters. We wanted to obtain magnetic bacteria in order to precisely control their spatio-temporal localization with magnetic forces. Indeed, in the context of biosensing or therapy mediated by reprogrammed bacteria, magnetism could be a tool to precisely localize bacteria in space, as well as monitoring their position via magnetic resonance imaging for instance. If we control the position of the reprogrammed object with magnetism, we can get better results and avoid dissemination. During my work, I engineered my magnetic *E. coli,* later referred as *MagEcoli*, to become a versatile platform, so that they could later help in medical or environmental context (depollution, disease diagnostic or therapy for example). I modified them to accomplish some actions such as invading

cells, targeting other bacteria, communicating; all in presence of magnetic forces to localize and enhance their actions. Thus the modified *E. coli* would be a remote-controlled living object that could serve for various applications *in vitro* and *in vivo* (**Fig. 1**).

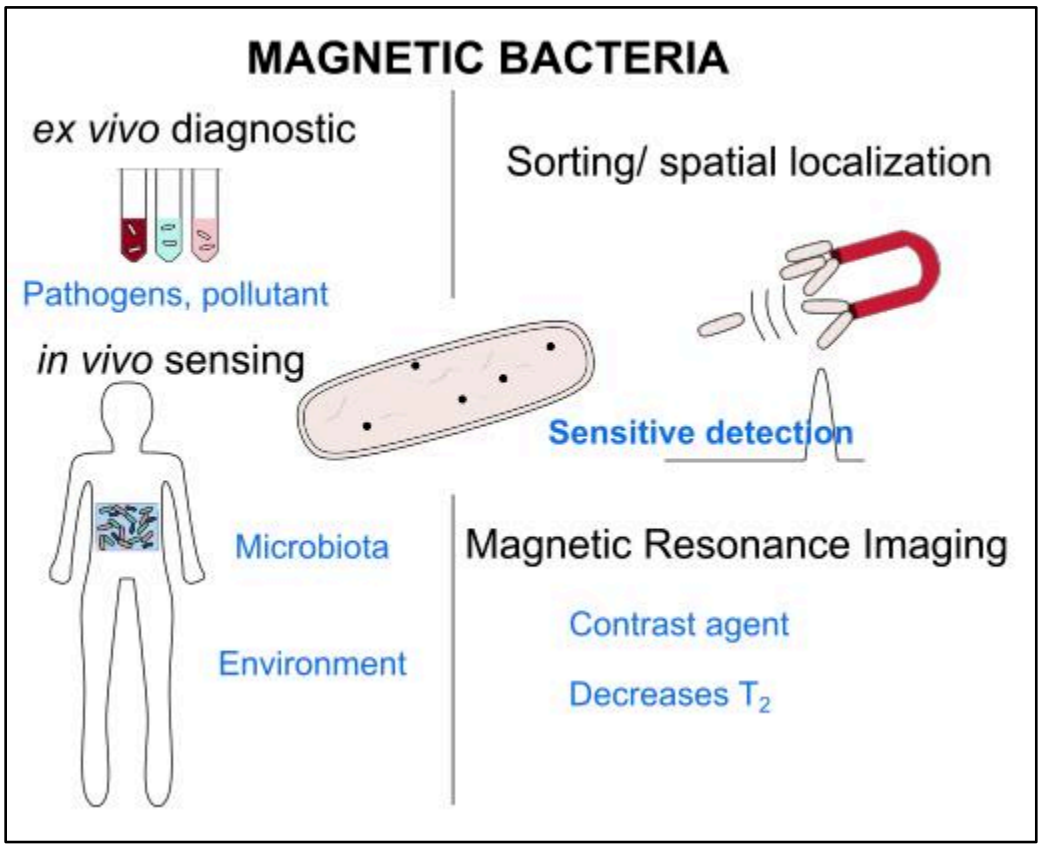

Figure 1: A reprogrammed magnetic bacteria, which can be a versatile platform for environmental and medical purposes.

Organization of the manuscript

The manuscript is based on 2 articles and 1 deposited patent. It is divided in 4 chapters.

In the first chapter, I describe a general state-of-the-art about microorganisms and their use in various applications.

In the second chapter, I present an article accepted in *ACS Synthetic Biology*. In this part, I genetically modified *E. coli* to make them overexpress a ferritin protein (from the archaeon:

Pyrococcus furiosus) fused with a fluorescent protein (GFP or mCherry). I developed a chemical protocol of biomineralization that conferred magnetic properties to the bacteria. I characterized the magnetic properties and the structure of the synthesized iron oxide crystals. As bacteria are living objects, I studied the impact of biomineralization on their growth and the reciprocal impact of bacterial division on magnetic properties. I performed two proof-of-concept assays in which *MagEcoli* locally invade mammalian cells or concentrate a targeted bacterial population towards a magnet.

In the third chapter, I present an article in preparation for submission. Here, I studied the effect of magnetic localization on a bacterial communication, called quorum sensing, used by some pathogens, and mediated for Gram-negative by a small molecule: AHL. As quorum sensing is a complex process, I simplified the problem: my reprogrammed *MagEcoli* can either send this AHL, or detect AHL and become fluorescent. I had the idea of using magnetic bacteria either as a spatially-controllable source of AHL or as a spatially-controllable biosensor. Yet, I figured out that localized sending of AHL was not sufficient to induce a local detection. However, with bacteria which were able to detect AHL, I investigated the idea of having a more sensitive biosensor in liquid medium. Indeed, a magnetic concentration of fluorescent bacteria raised locally the fluorescence signal and could be a way to improve the sensitivity of fluorescent biosensors.

Finally, in the fourth chapter of the manuscript, I investigated the idea of using magnetic bacteria for *in vivo* applications. With a simple multicellular organism, *C. elegans*, I studied the survival of *MagEcoli* inside their gut. I showed that the magnetic properties seemed to be unaltered in the gut of the worms. Besides, as magnetic bacteria showed a signal in nuclear magnetic resonance (NMR) measurements, I investigated the idea of using them *in vivo* with magnetic resonance imaging (MRI) to monitor their localization.

Chapter 1: Engineering microorganisms for specific functions

Content

1.1 – Nature has a rich microbial biodiversity

In nature, there is a large biodiversity of microorganisms. Bacteria, fungi, archaea and viruses have taken different evolutionary paths to develop. If we think about a bacterium, we have already various representations in mind. Generally we visualize an organism, whose shape can vary from a coccus to a bacillus, with a typical size of 1 µm and that lives in or around us, in soil or water. In reality, some bacteria can be much smaller, like *Mycoplasma pneumoniae* a parasite for our cells whose size ranges between 0.3 and 0.8 µm for the spherical shape[1]. Some can be significantly larger such as the giant bacterium *Thiomargarita namibiensis* (700 µm) that was found in sediment, can be seen without a microscope, and grows in a hostile environment: a sulfur-rich medium[2]. Other bacteria display original behaviors like, for example, living in an arsenic and sulfur-rich medium (*Acidithiobacillus thiooxidans,* isolated in 1921[3], releases sulfuric acid during growth) or infecting plant cells by plasmid injection (*Agrobacterium tumefaciens*[4]), or even living in symbiosis with an abyssal fish like the bioluminescent bacteria of the *Enterovibrio* family which produce the light needed to attract preys for *Melanocetus johnsonii*[5].

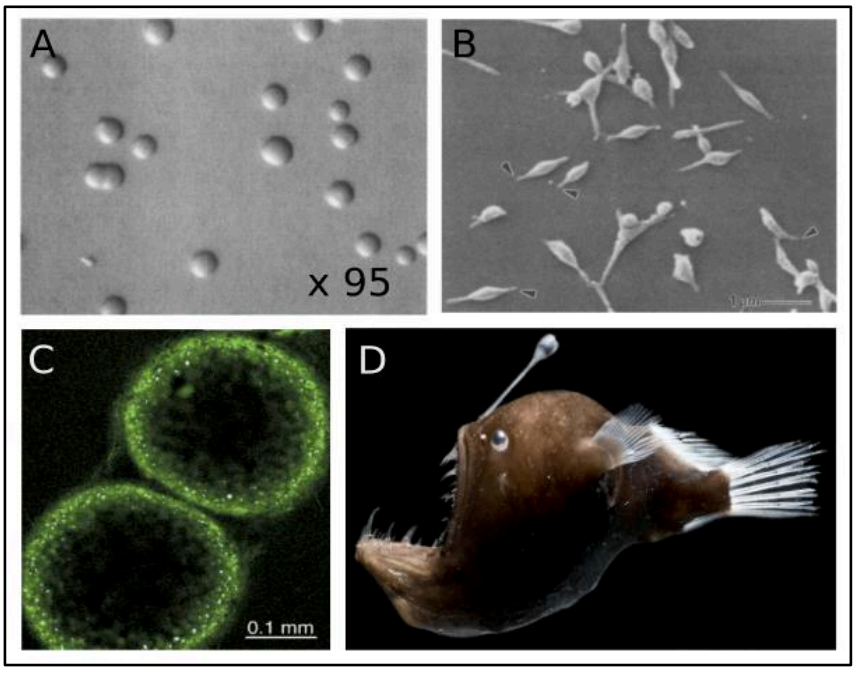

Figure 1.1: Images of various bacteria, from the smallest to the largest ones; from the nearest to the deepest ones. (A) *Mycoplasma pneumoniae* on agar, extracted from[1]. **(B)** *Mycoplasma pneumoniae,* scanning electron micrograph, extracted from[1]. **(C)** *Thiomargarita namibiensis*, confoncal laser scanning micrograph, with cytoplasm stained in green, extracted from[2]. **(D)** *Melanocetus johnsonii*, adult female, extracted from[5].

1.1.a - Selecting a microorganism to achieve specific purposes

Since microorganisms exist in a wide variety, some researchers have tried to exploit their original properties for technological applications by selecting the right strains and trying to understand how they act. For instance, in an environmental context, *A. thiooxidans* can be used to filter biogas. This bacteria can remove H_2S from gas thanks to its natural ability to reduce sulfur[6]. This same strain, along with other bacterial strains, is also employed in biomining: they can extract metals via bioleaching thanks to their ability to solubilize metals[7] (**Fig. 1.2**).

Commercial biomining microorganisms.

Microorganisms	Commercial biomining operations
Acidithiobacillus thiooxidans, *A. ferrooxidan*, *A. caldus*, *Acidiphilium*, *Acidimicrobium*, *Ferromicrobium*, *Ferroplasma acidiphilum*, *Sulfolobus*, *Acidianus*, *Metallosphaera*, *Sulfobacillus* and *Sulfurisphaera*	Sulfur and/or iron(II) bioleaching (Rohwerder et al., 2003; Pradhan et al., 2008)
Acidithiobacillus and *Leptospirillum*, *Acidianus brierleyi*, *A. ferrooxidans* and *A. thiooxidans*	Ni–Cu sulfide bioleaching (Zhiguo et al., 2010; Zhao and Fang, 2002)
Aspergillus, *Penicillium*, *Rhizopus*, *Leptospirillum ferriphilum* and *Acidithiobacillus caldus*	Cu bioleaching (Rohwerder et al., 2003; Zhou et al., 2009)
Acidithiobacillus ferrooxidans, *Acidithiobacillus thiooxidans* and *Leptospirillum ferrooxidans*	Zn sulfide bioleaching (Rawlings, 1995)

Figure 1.2: Non-exhaustive list of selected strains of bacteria used in biomining, extracted from[7].

As microorganisms are self-reproducing, provided that they are put in the right conditions to grow and live, they can fulfil their role while reducing costs and being greener. For the example of mining, traditional methods of metal extraction can be harmful to the environment and biomining was developed in the idea of reducing costs.

However, for some applications, we cannot always use natural strains directly as they are, as illustrated by the example of *A. tumefaciens* and its applications in food industry. After its discovery in 1897[4], scientists have studied how it induced crown gall disease: at the contact of the plant, the bacterium integrates its DNA plasmid into the plant genome, hence genetically modifying the plant's cells. Thus, thanks to its unique function, *A. tumefaciens* might have opened the way to genetically modified plants. This bacterium revealed an opportunity to introduce genes into plants. Yet, to inject desired genes (and not the ones from *A. tumefaciens*), bacteria were genetically modified[8]. *A. tumefaciens* and its use in food industry illustrate the fact that sometimes microorganisms have to be modified to improve their performances or to obtain novel features of interest.

1.1.b - Programming a microorganism for the desired functions

1.1.b.i) Genetic modifications

When a microorganism is needed for a specific application, instead of selecting a pre-existing strain, one strategy is to take a simple-to-handle organism (well-known and robust) and to change it in order to confer it the desired novel features.

The first, commonly used technique is to genetically modify it[9]. Indeed, with the discovery of the *lac* operon, by Monod and Jacob in 1961[10], gene regulations and molecular interactions began to be better understood and the idea of acting on genes to transform an organism's phenotype rose. With progress in molecular biology, especially cloning strategies[11] and DNA recombinant techniques in the 70s, foreign genes were successfully cloned in bacteria or yeast using plasmids (round portions of DNA) to give new functions.

Yet, at this time, designing complex genetic circuits remained impossible. The advances of sequencing (like the complete sequencing of the genomes of *Escherichia coli* and *Saccharomyces cerivisiae*, the 2 main models used in genetic engineering, achieved in the 90s) led to a better understanding of the complexity of gene regulation. Knowledge on cell's machinery began to rise. This led to the birth of 'systems biology'[12]: a field that brings together techniques from biology and mathematical models. Systems biology was made possible by the development of omics fields - e.g. genomics, proteomics - to acquire a large range of data.

Next, in the 2000s, more complex genetic circuits were engineered and this represented an important step leading to what we now call synthetic biology. Logic gates[13] and oscillators[14,15,16], for example, were integrated into microorganisms to engineer individual or group functions. Simultaneously, for 20 years, the field of metabolic engineering has evolved[17]. It consists in understanding biological and metabolic pathways. It is especially useful when it allows to hijacks the metabolic routes in order to transform them (and bio-produce desired compounds of interest).

On **Figure 1.3** is displayed a chronology of some of the main advances from molecular biology to synthetic biology.

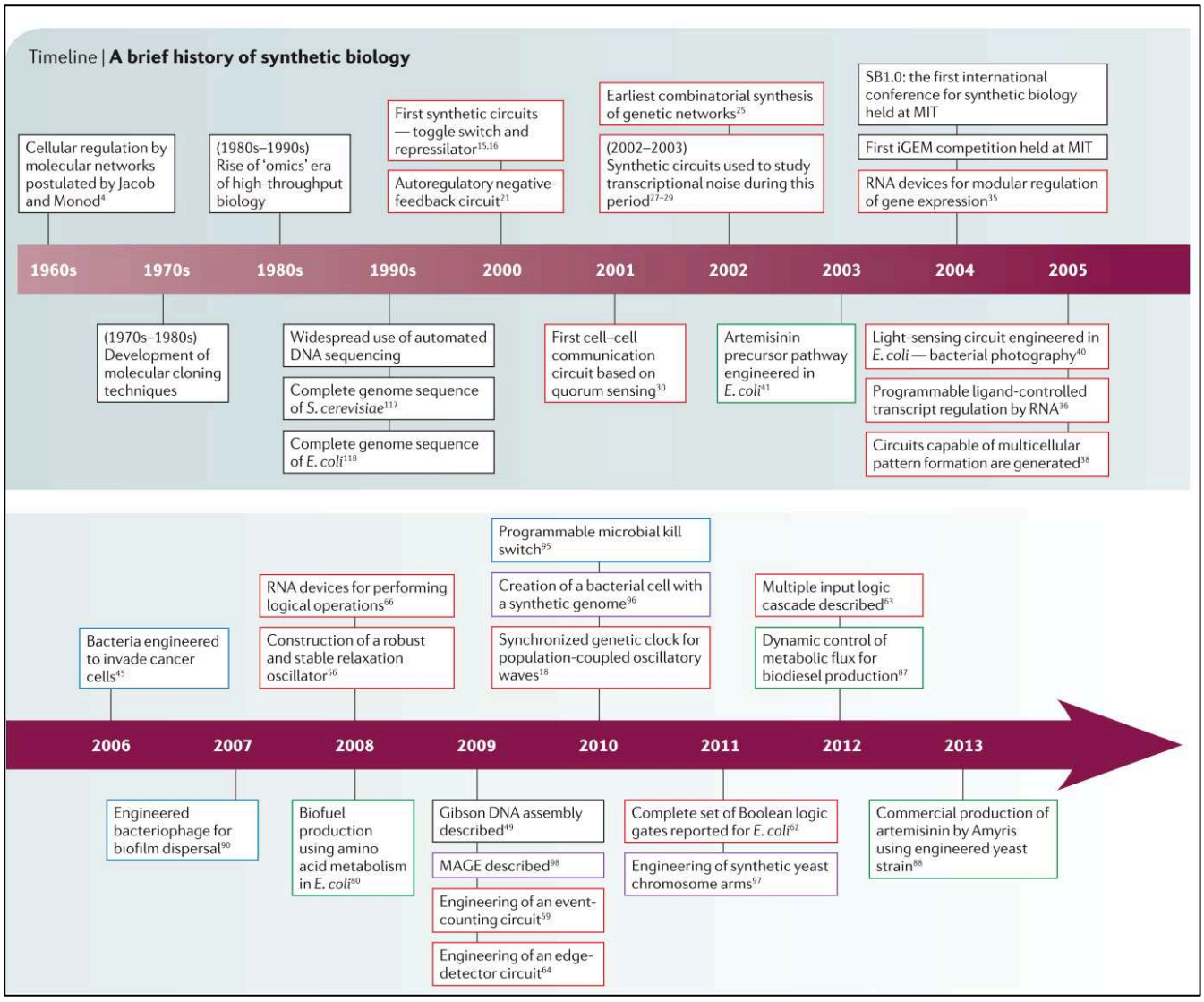

Figure 1.3: Timeline of the main advances from discovery of molecular networks to synthetic biology, extracted from[9].

Novel functions can also be acquired through directed evolution, which does not require the insertion of a foreign or synthetic gene[18]. Inspired by evolution which naturally selects organisms based on their ability to survive and reproduce in specific conditions, directed evolution reproduces this process artificially. It consists in genetically inducing various random mutations to create a large diversity amongst a microbial population, and selecting the most desired ones. The idea is that amongst this population few mutants might have the desired abilities. Several rounds of "selection → gene diversification" are applied to only form and keep the best mutants. Often, at the end, they are fully genetically characterized to understand what mutation created the desired properties.

1.1.b.ii) Chemical modifications

Instead of genetically changing a strain, chemical modifications can be used to confer the wanted features. One strategy is to use bioorthogonal chemistry, in other words to employ *in situ* a chemical reaction that does not affect the biological process of the living organism. It is mostly used to study the mechanisms of action of biomolecules. For instance, glycans or lipids can be tagged with this method to be visualized with microscopy[19,20]. Another chemical strategy is to create biohybrids[21]. Biohybrids consist of a living part, e.g. a microorganism (bacterium, yeast, mammalian cell…) and of a synthetic part (a magnetic particle, a loaded vesicle), chemically fused together. Contrarily to genetic modified organisms (GMOs), biohybrids are not mutated or genetically changed to bear a new function. However, the conjugation of the living part with the synthetic part can sometimes take several iterative steps, be more difficult to perform with a high yield and take more time, in comparison to genetically modified microorganisms.

1.1.b.iii) Genetic modifications and ethics

Nowadays, having a genetically modified microorganism is of great interest especially for bio-production, for ecological applications (the microbes can sense pollutants in soil or water, treat wastes or even help to produce energy), or for medical purposes (they can be used for drug-therapy or diagnostic). However, regulations have to be strict because the modified microorganisms can represent a risk[22]. Indeed, since the beginning of DNA recombinant techniques, scientists have raised some issues[23]: for instance modified bacteria might transfer their novel genes to their close environment (other bacteria or cells) leading to unpredictable consequences. Thus genetically-modified microorganisms must be handled with caution, especially when their application is to interact with nature. For instance, the Cartagena protocol of 2000 on biosafety regulates the handling of GMOs worldwide and is now ratified by 173 countries[i]. To prevent uncontrollable dissemination of GMOs, a kill switch can be introduced into the modified microorganisms. It can consist of a genetic circuit which triggers cell death after chemical induction. The first example of it dates back to 1988, with the production of a lethal polypeptide by a *hok* gene which was inducible by a *lac* promoter[24]. In this first version of kill switch the authors have shown that it was efficient *in vitro* and in soil, but needed improvement for real use in nature. Thus, the GMOs can carry out their action and die afterwards, preventing them from replicating or transferring their genes to other organisms in the environment. It can represent a solution to this problem.

In the next sections of this chapter, I will discuss several innovative applications performed to give novel features to microorganisms. I will talk about how genetic modifications, metabolic engineering, synthetic biology or even chemical transformations add new properties to microbes. First, I will focus on synthesis and sensing properties in a single microorganism, then on how new structural and group functions can be generated. Finally I will examine physical properties that can be engineered in microbes. In this introduction, I will focus on microorganisms and not discuss about synthetic biology in mammalian cells, even though this domain exists. I will consider mostly the cases of bacteria and more specifically *E. coli* because it is the main and historical strain of bacteria employed for genetic modifications[11].

1.2 – Modification at the single microbe scale for secretion and sensing

One purpose of modifying microorganisms is to use them to secrete a molecule of interest or sense the environment. Microorganisms can be modified to become living cell factories to produce proteins or other molecules of interest and even metal nanoparticles. They can probe the environment to search for pollutants and pathogens. A final goal is to have a versatile microorganism that does both and might be used for *in vivo* diagnostic and therapy.

1.2.a - Production of specific molecules and materials

1.2.a.i) Protein production

Bacteria, and especially *E. coli,* have been designated as efficient organisms to become living factories. To do so, *E. coli* strains have been genetically modified and improved to mass produce recombinant proteins, using recombinant DNA techniques. The most used *E. coli* strains are BL21 because they can read rare codon (proteins from another organism), can keep a foreign plasmid in their cytoplasm, and lack proteins that could degrade the foreign expressed proteins (OmpT and Lon protease). In a review, the authors discuss the different parameters that can be adjusted with BL21 genetic modifications: which plasmid to insert, which promoter to use, which fusion tag to add to purify the protein after lysis of bacteria[25]. Usually arabinose[26] or Isopropyl-β-D-

1-thiogalactopyranoside (IPTG)[27] inducible promoters allow bacteria to express proteins on demand. Tag like Histidine-tag can be fused to collect the proteins on Ni-NTA beads during purification[28].

In most cases, expressing recombinant proteins with *E. coli* leads to the formation of inclusion bodies[29]. The expressed proteins aggregate in insoluble phases at the extremity of the bacteria. This is a way for the bacterium to avoid metabolic disturbances due to an over-concentration of foreign proteins, but it should be avoided for bio-production. Indeed, the inclusion bodies are lost during the step of protein purification, resulting in a reduced yield of production.

If we focus on an example of a widely-bio-produced protein in the industry, we can look at recombinant insulin, a drug for diabetic patients. In 1982 human insulin produced by *E. coli* using recombinant DNA techniques was commercialized for the first time by Genentech and Eli Lilly[ii]. It was a huge success. Now, insulin is produced predominantly by yeasts and bacteria and has replaced insulin obtained from pig and cattle. Even now, *E. coli* strains are improved for optimal production of insulin. For example, in 2019, a study[30] found that expressing a heat shock protein (DcHsp70) raised the quantity and folding of insulin produced by bacteria and might help to solubilize the inclusion bodies. Beside, in this article, the plasmid for the production of insulin is a typical example of those used in recombinant protein expression (**Fig. 1.4**).

Even if *E. coli* is a preferred organism for bio-production, it can still be fastidious: *E. coli* have sometimes a low rate of production, the proteins can remain trapped in inclusion bodies, which are difficult to extract and collect after lysis, and some proteins can be toxic for the bacteria[25]. For insulin expression, alternatives can be found such as yeasts like *Saccharomyces cerevisiae* and even plants[31].

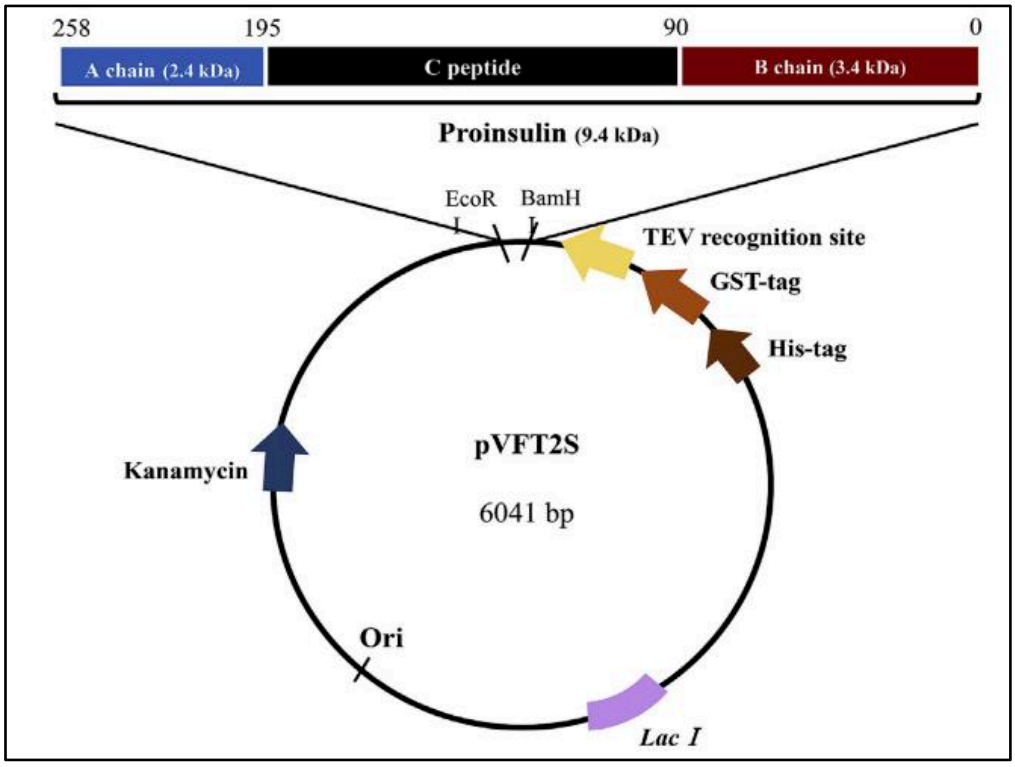

Figure 1.4: A plasmid used for the production of insulin by *E. coli*, extracted from[30]. The plasmid has the gene for proinsulin, an antibiotic resistance gene (Kanamycin, to avoid plasmid loss during bacterial division), an IPTG inducible promoter (Lac I, to express proinsulin on demand) and a Histidine-tag for purification.

1.2.a.ii) Small molecule bio-synthesis

Small molecules can also be bio-synthesized by microbes. A common way, for the production of biofuels for instance, is to add a plasmid that changes the preexisting metabolic pathways of the microorganism. It is called metabolic engineering. If we look at *E. coli* or *S. cerevisiae*, we know that they can use, in anaerobic conditions, a fermentative metabolic pathway that leads to the assimilation of some amino acids by degrading them into various alcohols (Ehrlich pathway)[32]. One strategy is to add a plasmid that can interfere with this metabolic process to obtain the desired alcohols composing biofuels.

Thus, with this method, scientists have increased the production of isobutanol and other derivative alcohols from glucose by *E. coli*[33]. They inserted foreign plasmids which code for different 2-keto-acid decarboxylases. These enzymes are intermediates in the pathway that leads to the production of various alcohols. The resulting modified *E. coli* were able to take different

pathways to synthesize isobutanol, 1-butanol, 2-methyl-1-butanol, 3-methyl-1-butanol, and 2-phenylethanol (**Fig. 1.5**).

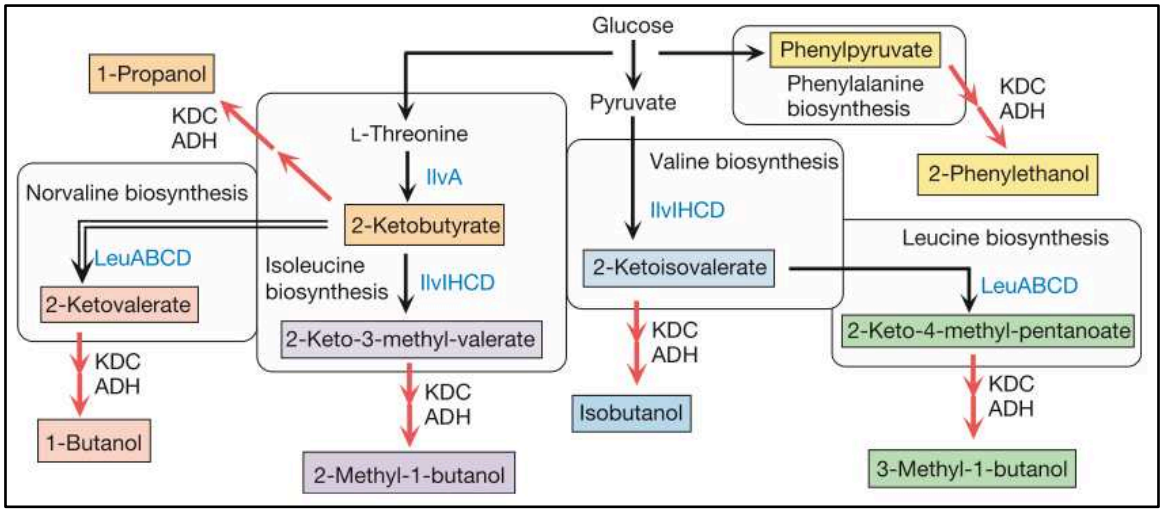

Figure 1.5: The synthetic pathway used to produce different alcohols by genetically modified *E. coli*, extracted from[33].

Moreover, with metabolic engineering, a team has discovered a way to synthesize a precursor of Taxol, an antitumor agent[34]. They worked on the level of expression of P450, a cytochrome that can oxidize *in situ* Taxa-4(5),11(12)-diene, a molecule produced by modified *E. coli*, to form Taxadien-5α-ol. The author improved the yield of the metabolic reaction by 5 times, regarding their previous assays. This broadens our perspective for biosynthesis of anticancer drugs.

Another successful example of molecule synthesis is artemisinin production by microorganisms. Artemisinin is the major treatment for malaria and is initially produced by the plant *Artemisia annua.* By expressing the genes of *A. annua* in *E. coli* or *S. cerevisiae*, after optimization (codon optimization, expression of other genes from *A. annua* like the ones for the cytochrome P450 enzyme), the teams of J. Keasling managed to obtain precursors of artemisinin on a large scale (several grams per Liter)[35,36].

1.2.a.iii) Material bio-synthesis

Bacteria can also be improved to produce more complex and larger molecular structures, as illustrated by the following example of cellulose. Some strains are naturally known to secrete

cellulose, and their growth medium was changed to make cellulose from by-product and to increase the yield[37]. However, in 2016, scientists[38] went further. They were interested in producing a cellulose-based material with additional properties. They inserted a synthetic plasmid which produces fluorescent protein upon induction (Red Fluorescent Protein, RFP) in a naturally cellulose-producing strain (*Komagataeibacter rhaeticus)*. With this method, the cellulose contained the bacteria and was patterned with fluorescent proteins as the bacteria were creating it (**Fig. 1.6**).

This opened the way to novel types of biomaterials: living and environmentally-responsive materials. By creating a hybrid material, mixing polymers and living bacteria, this study let us envision other types of bio-materials. We can imagine having cellulose patterned with environmentally-responsive bacteria (bacteria which produce fluorescence upon a change in the environment for example). These types of material might be of great use in the field of pathogen detectors. We can also think about creating a bio-material filled with bacteria which could secrete a drug or an antibiotic. With this, we could use this system to create "living" bandages, curing and avoiding pathogenic bacterial infections from wounds. However, all these applications require times and improvements to be developed.

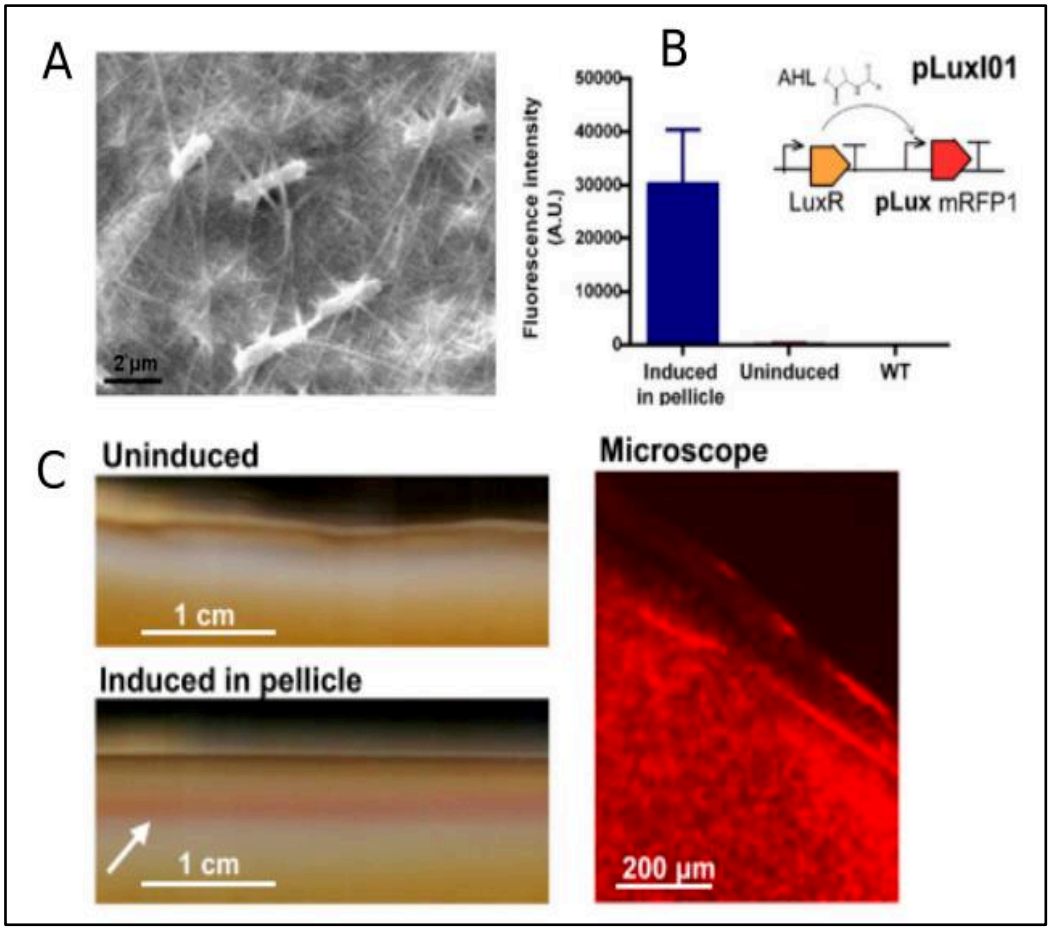

Figure 1.6: Cellulose-making bacteria modified with an RFP-producing inducible plasmid, extracted from[38]. (A) Bacterial cellulose with *K. rhaeticus*, scanning electron micrograph. **(B)** The AHL-inducible system to express RFP in an induced pellicle of cellulose. **(C) Left panel**: Images of induced and uninduced cellulose pellicle. The white arrow indicates the visible RFP section, observed in granular fluorescence on the **right panel**.

1.2.a.iv) Crystal bio-synthesis

Due to the presence of metals in the environment (in soils), evolution has led various bacteria to naturally interact with metals and produce minerals. For instance, tellurium is formed by *E. coli* K12. *Shewanella putrefaciens* and *Geobacter metallireducens* reduce Tc(VIII). *Enterobacter cloacea, Desulfovibrio desulfuricans* and *Rhodospirillum rubrum* turn selenite into selenium[39]. The strain *Pseudomonas stutzeri* AG259 precipitates silver ions in its periplasm[39] to survive its cytotoxic effect. Indeed, as some metals might be toxic (silver is a bactericide[40,41]), turning metallic ions into crystals help bacteria to detoxify their cytoplasm. A silver-tolerant yeast which forms silver nanoparticles, MKY3, has even been discovered through screening among other microbes in soil[42]. Inspired by these microorganisms, bacteria have been transformed to produce metal nanoparticles.

One of the advantages of biologically synthesized crystals is that they can be perfectly nanostructured, which enhanced their properties[43]. Instead of using naturally biomineralizing strains, such as sulfate-reducing bacteria which create pyrite, scientists can take the option of employing genetic modifications. For instance, a study in 2010[44] exploited recombinant *E. coli* to produce diverse nanoparticles. They incubated the bacteria with semiconductors (Cd, Se, Zn, Te), alkali-earth metals (Cs, Sr), rare elements (Pr, Gd), magnetic metals (Fe, Co, Ni, Mn) and noble ones (Au, Ag). The *E. coli* were engineered to express two proteins (phytochelatin synthase and metallothionein) that bind to different metals. As a result, bacteria have formed nanoparticles of different sizes (depending on the concentration of incubated ions) and characteristics. Semiconductors were synthesized (CdSe, CdTe), as well as gold, silver, rare metal alloys (PrGd), and new semi-conducting and alkali-earth metal (CdCs) nanoparticles (**Fig. 1.7**).

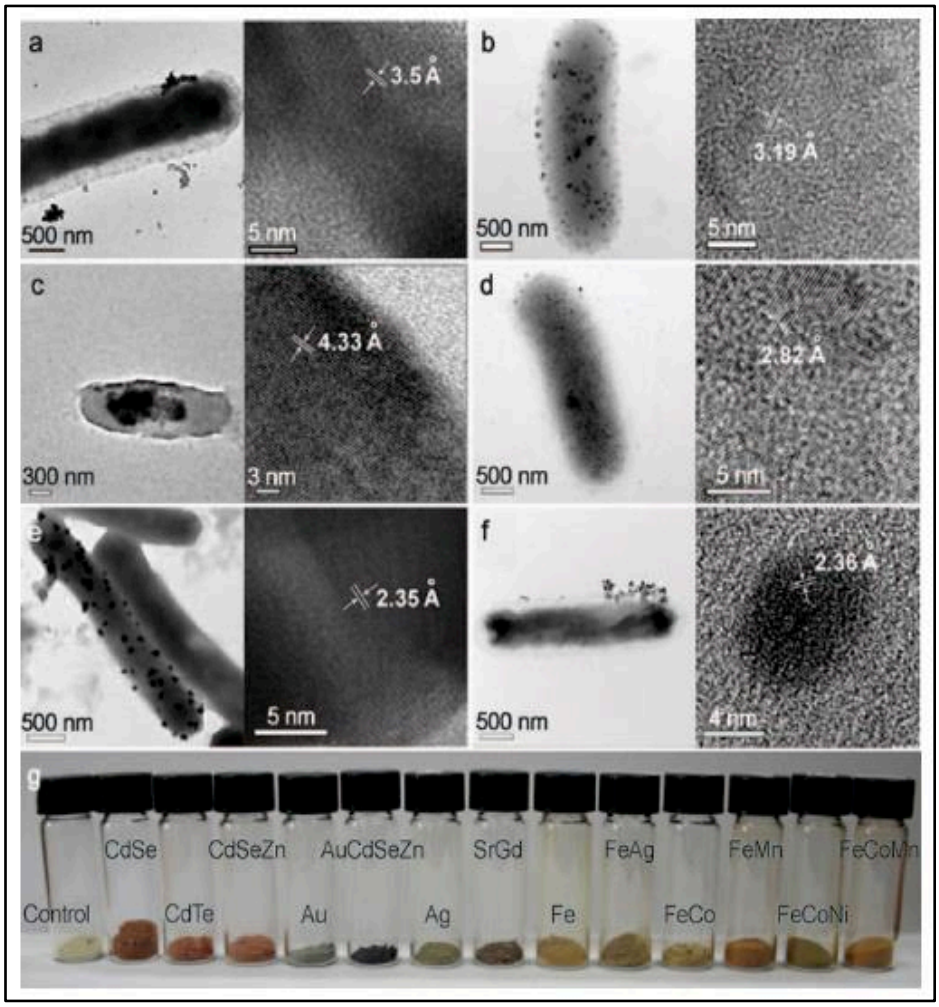

Figure 1.7: Diverse materials synthesized by recombinant *E. coli*, extracted from[44]. Upper panel: Transmission electron micrographs of diverse material producing bacteria. **(a)** CdSeZn, **(b)** PrGd, **(c)** CdCs, **(d)** FeCo, **(e)** Au, **(f)** Ag. **Lower panel:** picture of dried bacteria that contained the different nanoparticles.

To note, recent works[45] showed that even our human cells are able to synthesize iron oxides nanoparticles (in ferritins) from internalized then degraded iron oxides. This might reveal the mechanisms responsible for the magnetite nanoparticles found in brain.

1.2.b – Using microorganisms to sense the environment: whole-cell biosensors

1.2.b.i) Sensing based on a gene reporter

In addition to producing proteins or materials, microbes can be genetically modified to sense the environment: to detect the presence of pollutant, to probe pathogens, to recognize cancer cells… Bacteria can become whole-cell biosensors for health and environmental purposes[46,47].

To monitor a compound or organism that is toxic for the bacterium (and induces stress or/and death), one strategy is to insert a plasmid which has a reporter gene (production of fluorescent proteins, luminescence…). Different methods can be employed. The plasmid's promoter can be constitutive. In this configuration, the sensor bacteria continuously express the reporter gene, under normal conditions. In presence of toxicity, the bacteria die and the level of reporter gene expression is diminished, thus nonspecifically indicating the presence of pathogen or toxic metals or pollutants (**Fig. 1.8**). Another way is to use an inducible plasmid. In this case, the expression of the reporter gene can be triggered either by the metabolites involved in bacterial stress-response or by a specific toxic inducer. In the first method, the response (increase of expression of reporter gene) is not specific to a unique toxic compound, as the same stress-response can be induced by different factors. In the second case, the detector is highly specific to a compound, or a pathogen (**Fig. 1.8**)[48].

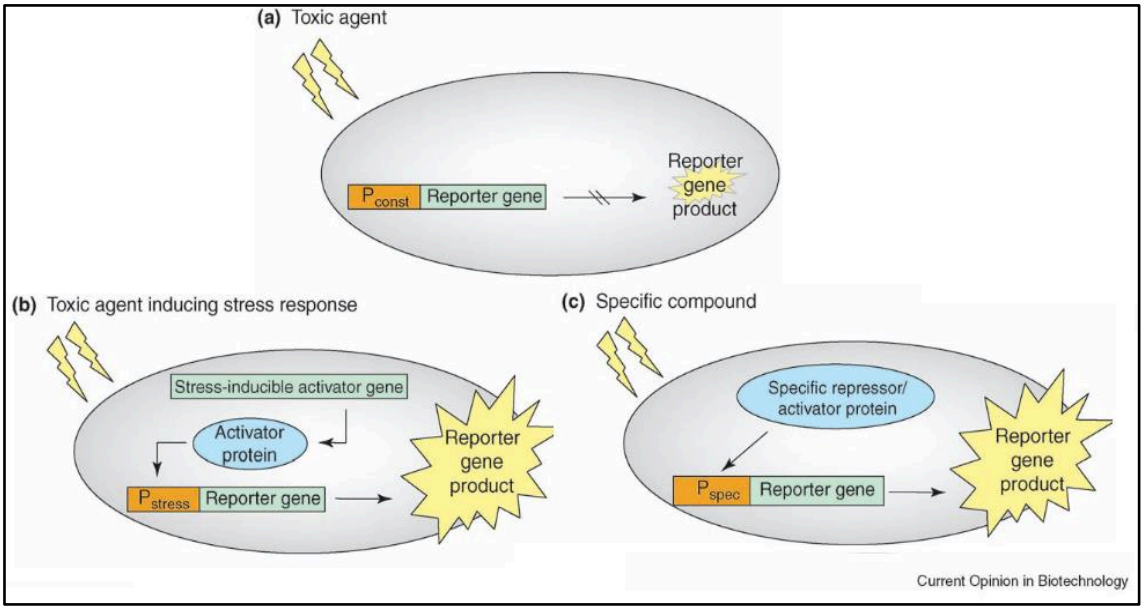

Figure 1.8: Schematic representation of the three common types of biosensors, extracted from[48]. (a) The constitutive promoter. **(b)** The inducible promoter responding to stress-response. **(c)** The inducible promoter responding to a specific chemical.

One example of biosensing with a constitutive plasmid is the commercially available Microtox assay[iii,49]. It uses luminescent bacteria, *Vibrio fischeri*. In the detector kit, when a toxic compound is applied on the sample, *V. fischeri* are killed and the level of bioluminescence decreases. This loss of bioluminescence is the reporter for the presence of toxicity in the medium.

For specific detection, a team gave to *Bacillus subtilis* a plasmid which expressed luciferase, making the bacteria luminescent, upon cadmium detection. This plasmid was made inducible by the cadmium resistance operon from *Staphylococcus aureus,* and this operon regulated the expression of luciferase (inducible promoter *cad*)[50]. This system led to the detection of cadmium, but also lead and antimony because of the lack of specificity from the promoter *cad*[51].

1.2.b.ii) Specific sensing based on quorum sensing response

Quorum sensing is a communication used by Gram-negative and Gram-positive bacteria involved in group behavior. It is a way for bacteria to sense how numerous they are and to trigger the expression of specific genes when their number is high enough. Bacteria secrete with a positive feedback a small chemical (AHL) or peptide (AIP), called autoinducer, that is specific for each bacterial strain. The autoinducer triggers the expression of genes. At low cell density, there are not enough autoinducers. But at high cell density the concentration of autoinducers has risen enough to trigger the expression of genes which code for the formation of a biofilm, bioluminescence or the secretion of toxins[52–54] , for example (**Fig. 1.9**).

This quorum sensing communication is well-characterized and used by pathogens like *Pseudomonas aeroginusa* and *Burkholderia cepacia* for example. Moreover, bacteria can be genetically transformed to detect these specific pathogens, by monitoring the presence of quorum sensing communication. Some are engineered to respond to the presence of the autoinducer and thus selectively detect the pathogens. Many bacterial sensors are based on this method.

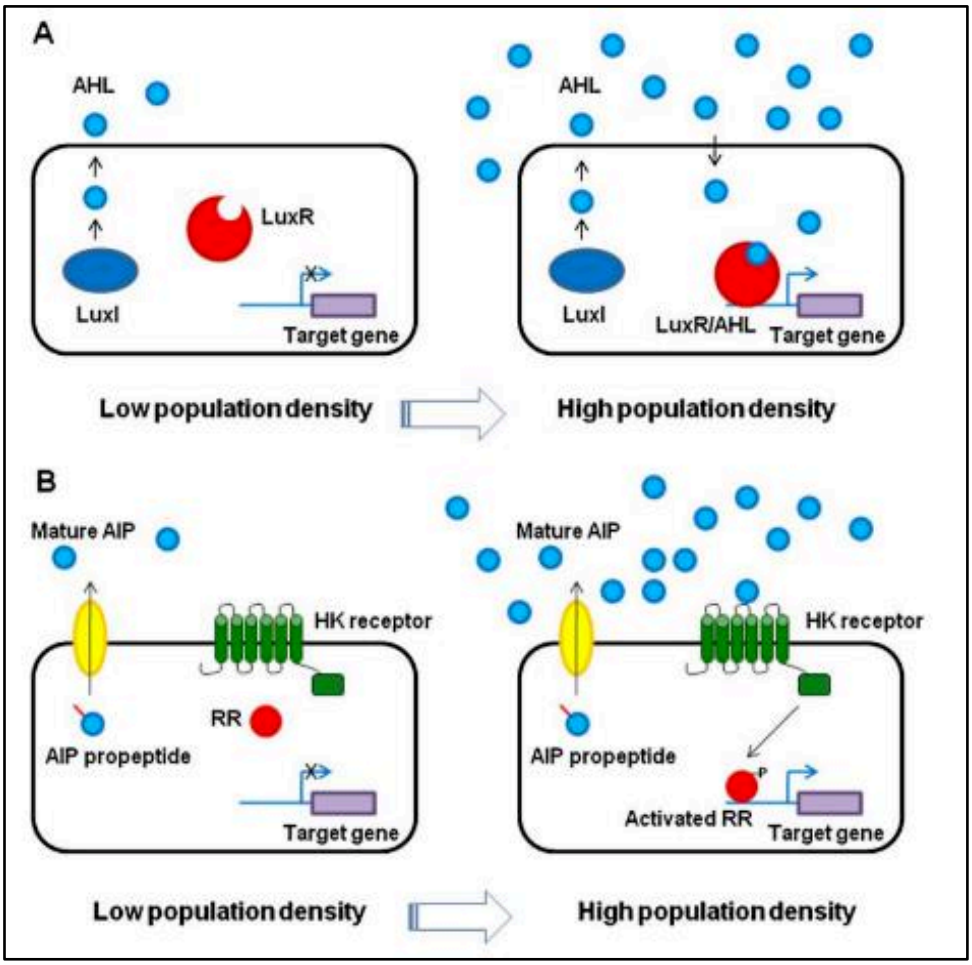

Figure 1.9: Representation of quorum sensing at low and high-cell density, extracted from[55]. **(A)** For Gram-negative bacteria AHL is the auto-inducer. **(B)** For Gram-positive bacteria AIP is the auto-inducer.

In 2018 the team of Karen Polizzi[56] has developed 6 plasmids that respond to 6 different autoinducers (AHL) sent by various bacterial species (*V. fisheri*, *P. aeruginosa*, *Rhizobium leguminosarum*, *A. tumefaciens*, *Rhodopseudomonas palustris*). The team has engineered *E. coli* bacteria with these plasmids. The 6 autoinducers triggered the expression of a gene that code for a fluorescence protein (**Fig. 1.10**), with more or less specificity. The modified *E. coli* in presence of a specific AHL will monitor its presence by fluorescence. They have tested the system with 3 plasmids and 3 different fluorescent colors to monitor the selectivity, and the strength of the inducible promoters. This system is very interesting, since it could be used for simultaneous detection of different pathogens in the same medium!

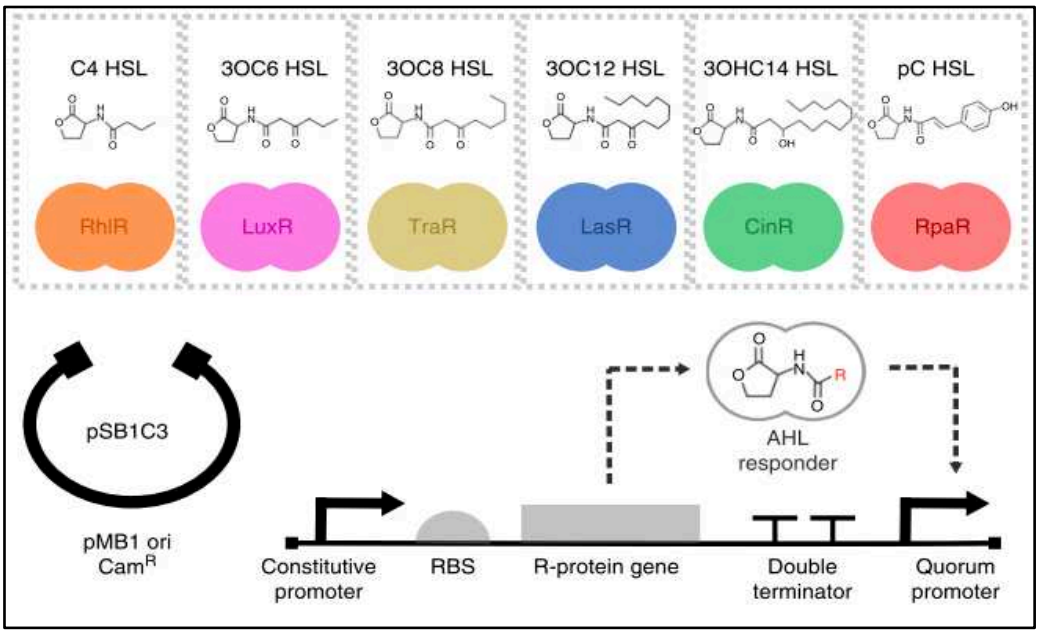

Figure 1.10: The plasmid construction which can detect the presence of an autoinducer, extracted from[56]. Depending on the promoter, one of the six AHL autoinducer triggers gene expression.

With the same idea of monitoring AHL presence, a bacterial biosensor[57] has been developed to detect *P. aeruginosa* in saliva. The inserted plasmid had an inducible promoter (inspired by the *lasR/lasI* quorum sensing system of *P. aeruginosa*) and triggered the expression of β-galactosidase in *E. coli.* Thus, bacteria turned blue in presence of XgaI and gave the sensing signal (**Fig. 1.11**).

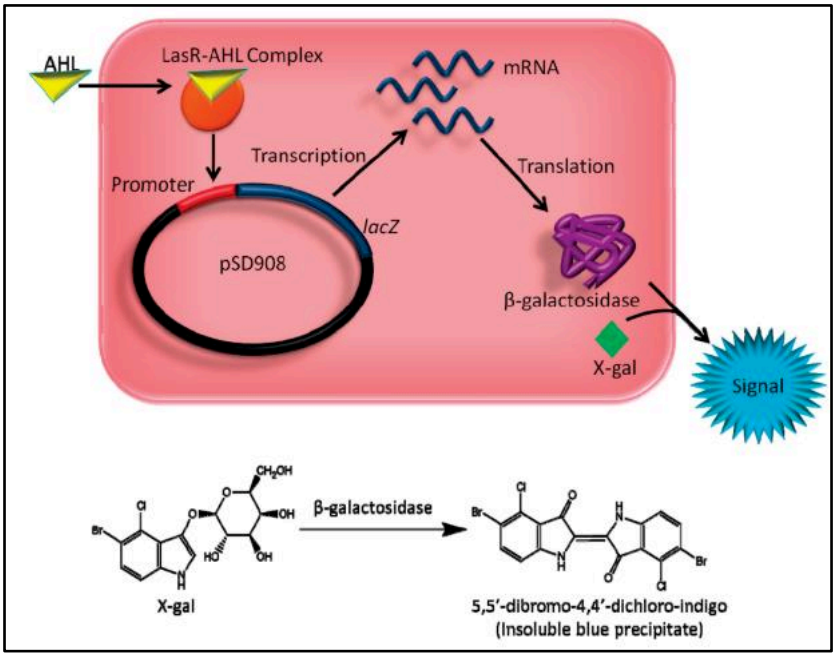

Figure 1.11: The plasmid inserted in bacteria to sense the AHL of *P. aeruginosa*, extracted from[57].

The quorum sensing genetic circuit was also engineered to detect other toxic compounds such as toxic metals in water. As it is based on a positive feedback, parts of the quorum sensing genes can be added to enhance the expression of the reporter gene, to amplify the signal of detection. In 2016, a team has turned *E. coli* to detect metal ions[58]. They put in the bacteria a metal-dependent promoter that controls the *luxI* gene extracted from *V. fisheri*. When metals are sensed, *luxI* is expressed and the quorum sensing positive loop led to the amplification of GFP production. This method improved the performance of the bio-detector for copper**.**

1.2.b.iii) Sensing based on aggregation

There are other ways to reprogram bacteria to detect specific compounds in the medium. For instance, bacteria can be modified with a plasmid which expresses a nanobody at the membrane. The nanobody is specific to an antigen; and in the presence of this antigen (which is at the membrane of a pathogen or freely diffusing in the medium) the modified bacteria agglutinate around it. Agglutination induces an optical change which can be monitored. That was done in a recent assay[59]. The authors have engineered *E. coli* to make them express antibodies that recognize fibrinogen markers in plasma samples.

1.2.c – Microorganisms designed to secrete or/and sense: towards *in vivo* applications

1.2.c.i) Bacteria programmed to sense *in vivo*

Modified microorganisms which might detect pathogens or cancer cells are being investigated in order to develop *in vivo* applications. Many teams have studied the opportunity to have an *in situ* diagnosis of diseases thanks to engineered bacteria. Researchers generally work with strains that are well-tolerated by the body and do not induce an immune response, or on strains that naturally colonize cancer regions such as *Salmonella Typhimurium* or *E. coli*[60].

In an assay[61], T. Danino et al. have engineered a probiotic strain, *E. coli Nissle* 1917*,* to monitor liver cancer. As the hepatic portal vein delivers blood from the gut to the liver, the authors hypothesized that orally administrating the sensor *Nissle* 1917 would result in selectively targeting the liver, colonizing it and then searching for cancer cells. For the sensing part, they genetically

modified the bacteria with a self-maintaining plasmid that has a PROP-Z platform. On one hand, PROP-Z allows bacteria to produce a luminescent signal, in order to monitor their position in the organism. On the other hand, there is an IPTG-inducible *lacZ* gene that converts an orally administrated substrate LuGaI into luciferase. The author showed that the enzymatic activity of *lacZ* on LuGaI was 3.6 times higher when there was a tumor in the liver. At the end luciferase went into the urine and was detected by a luciferase assay (**Fig. 1.12**). Thus they have developed a two-stage technique to monitor cancer metastasis in liver: **(i)** orally delivering sensor *Nissle* 1917 with LuGaI **(ii)** monitoring a luciferase increase in the urine that revealed tumor presence in liver.

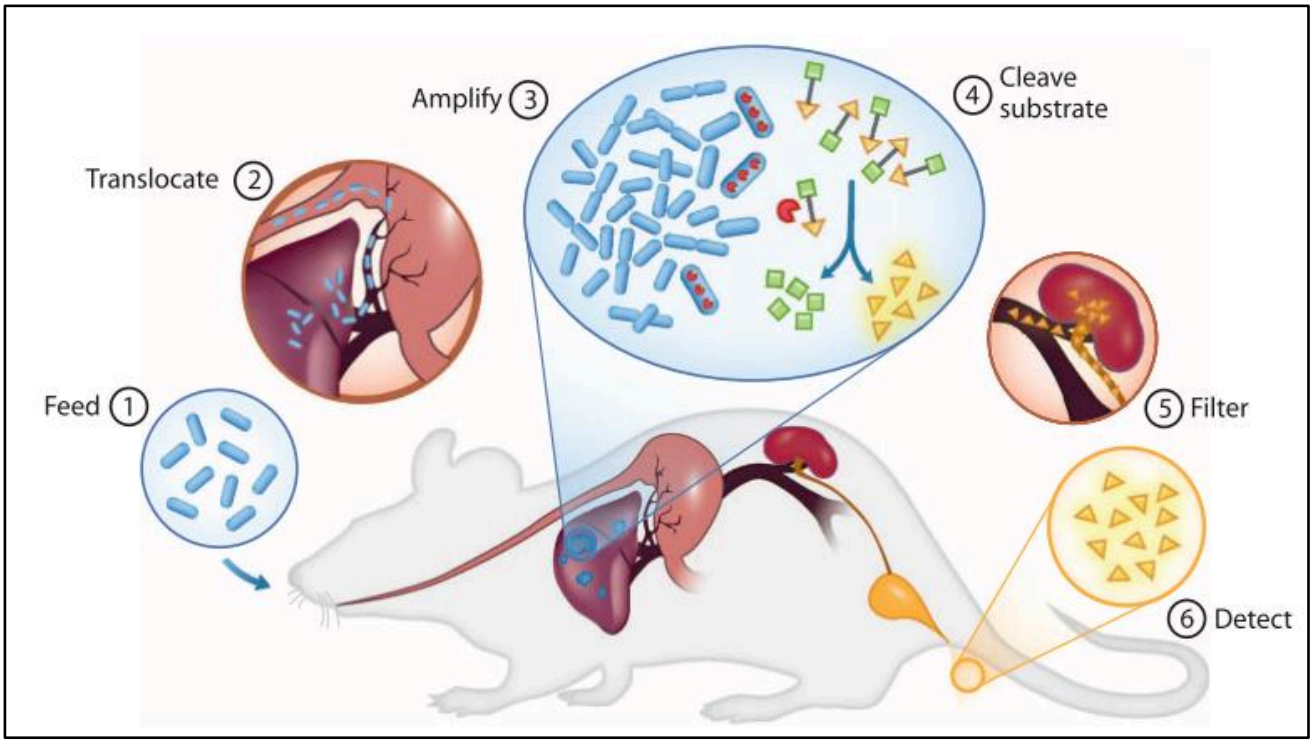

Figure 1.12: Schematic representing the assay of cancer detection in urine, based upon genetic programming of *E. coli*, extracted from[61]. 1 Bacteria (and LuGaI) are orally ingested by mice. **2** They go to the liver via blood flow. **3** They colonize the tumor. **4** They cleave substrates via *lacZ* enzymatic activity. **5** The cleaved substrates go to urine. **6** They are detected in urine.

In the same idea of having a probiotic to diagnose disease, a sensor that monitors gastro-intestinal health was developed[62]. In this article, they genetically modified *E. coli* to detect blood with a plasmid that triggers the expression of luminescence upon heme sensing. They built up an ingestible device: a capsule that contains the blood-sensitive bacteria and that electronically monitors the increase of luminescence. They tested their system in pig's gut and were able to detect the presence of ingested blood. This set up could be a way to monitor troubles in intestine like inflammations.

1.2.c.ii) Bacteria programmed to deliver molecules *in vivo*

Instead of sensing, bacteria can secrete *in vivo,* in order to cure diseases like pathogen infections or cancer. *In vivo* delivery which efficiently targets the sick cells has been studied for a few years. Bacteria, viruses or even cells are employed for drug-delivery[63].

For instance, based on quorum sensing, J. Hasty and coworkers have created a synthetic circuit in *S. typhimurium*, in order to use them for *in vivo* delivery[64]. With the *luxI/luxR* genes, they created a genetic system to make bacteria grow, then express sfGFP when they are numerous enough and lyse with their own secretion of Haemolysin E. This system led to an oscillation of bacterial density and was tested on tumor in mice. Indeed, *S. typhimurium* preferentially colonize tumor cells, and Haemolysin E is toxic. Thus this system leads to lysis and toxic secretion only in tumor regions and worked well to destroy cancer cells in mice when combined with chemotherapy.

In 2019, N. S. Joshi and his team transformed the *E. coli Nissle* 1917 to cure gut inflammation[65]. The inserted plasmid coded for the membrane expression of curli fibers, whose extremity contains human cytokines (**Fig. 1.13**). These cytokines could restitute the epithelium in gut, in addition to anti-inflammatory activity.

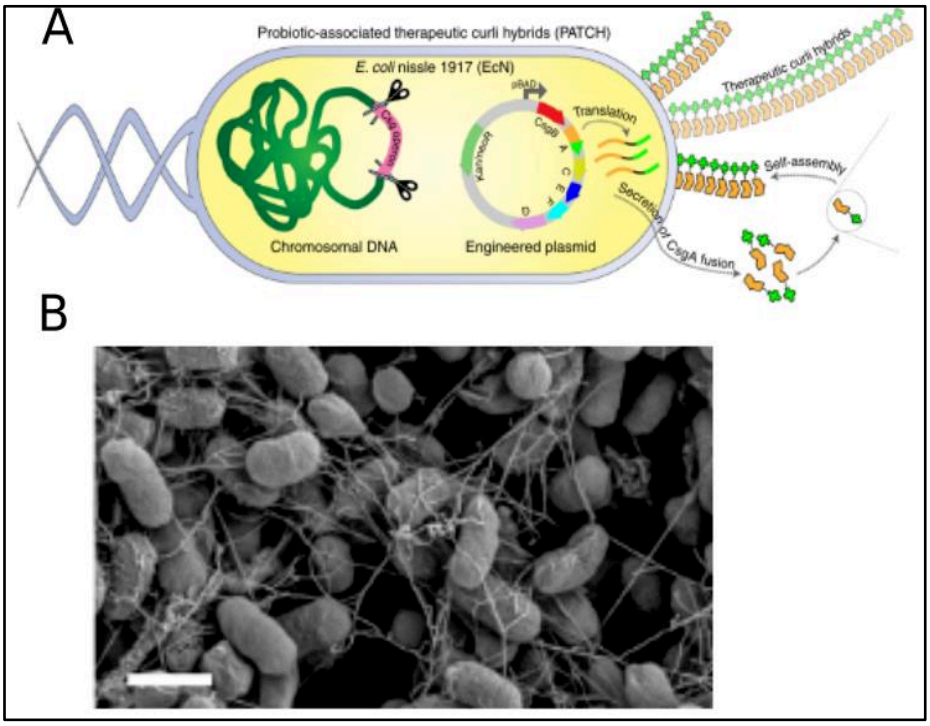

Figure 1.13: The reprogrammed bacteria used to cure bowel inflammation, extracted from[65]. **(A)** The plasmid codes for the production of curing curli fibers. **(B)** Scanning electron micrograph of the fiber-displaying bacteria, scale bar = 1µm.

To make bacteria deliver drugs in targeted cells, another strategy is to create biohybrids. For instance a highly-motile, chemotactic attenuated strain of *S. typhimurium* was linked by biotin-streptavidin interaction to a fluorescent bead for a proof-of-concept experiment[66]. The author showed that thanks to the bacterial properties of being attracted by (and proliferating into) tumor cells, the biohybrid was preferentially visualized in tumors during mouse model assays. With biohybrids, new modes of in vivo medical applications are envisioned[67]. For instance, flagellated bacteria can be linked with a liposome via antigen/antibody interaction[68] (**Fig. 1.14**). As lipid vesicles can store drugs, this type of biohybrid could swim to deliver medicine to targeted areas. Following this idea, *E. coli* were attached to a red blood cell (RBC) via biotin/avidin interactions[69]. The bacteria had flagella to swim and the RBC was loaded with an anti-tumoral drug (doxorubicin) and superparamagnetic nanoparticles (**Fig. 1.14**). Thus the scientists were able to control the swimming of the biohybrid with magnetic forces and the RBC delivered the drug.

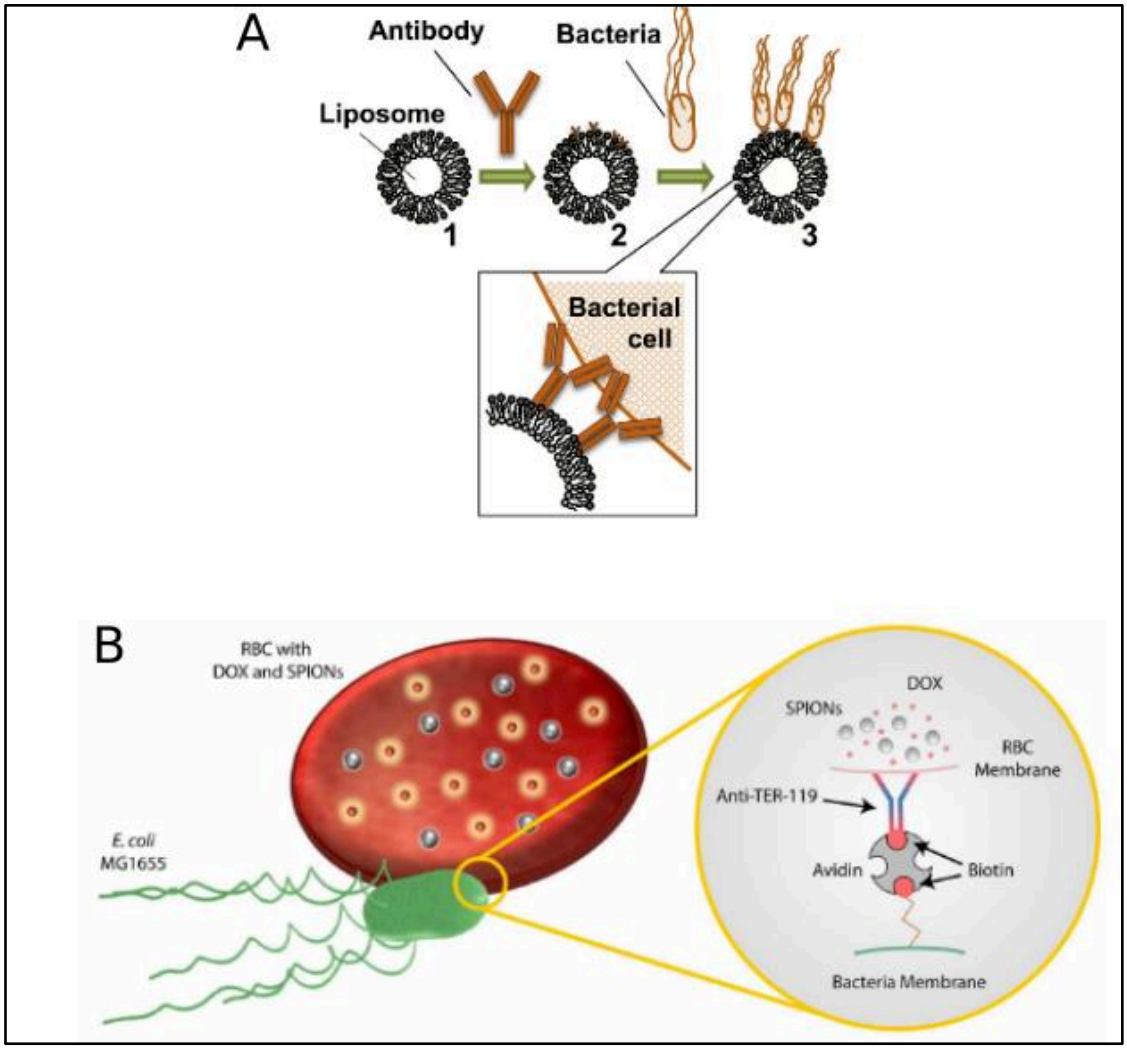

Figure 1.14: Two types of biohybrids that deliver drug *in vivo*. (A) The bacterium is linked to a liposome with antibody, extracted from[68]. **(B)** The bacterium is linked via avidin/biotin interaction to a loaded and magnetic red blood cell, extracted from[69].

More recently, following the same idea, the same team has conjugated with biotin/streptavidin interaction swimming *E. coli* MG1655 with nanoerythrosomes, which are nanometric red blood cells (fabricated via a process of extrusion)[70]. The nanoerythrosomes surrounded the bacterial membrane. They visualized these biohybdrids by conjugating the biotin with a fluorophore. With smaller objects linked on the bacterium, the swimming properties (directionality and speed) were enhanced as well as the penetration into targeted areas.

1.2.c.iii) Bacteria programmed to sense and secrete *in vivo*

To go further, we can combine both abilities to secrete and sense in the idea of having *in vivo* applications.

One example of such living object was done by R. Weiss and his team with genetically transformed *E. coli*[71]. They designed *E. coli* to make them sense and kill *P. aeruginosa* via one of their quorum sensing autoinducer, 3OC12HSL. To do so, they inserted in a plasmid a "detection module": a reporter gene which codes for GFP, and a *pLas* promoter extracted from *P. aeruginosa* (sensitive to 3OC12HSL). Upon detection of 3OC12HSL, the *E. coli* produced GFP as a fluorescent reporter. Then a "destruction module" was added: a gene which codes for bacteriocin, *CoPy*, under the *pLas* promoter. The toxin was exported outside the *E. coli* via a "secretion module": a secretion tag encoded just before the bacteriocin gene (**Fig. 1.15**). So these *E. coli* were able to sense *P. aeruginosa*, to become fluorescent on its contact and to kill them with a secreted toxin.

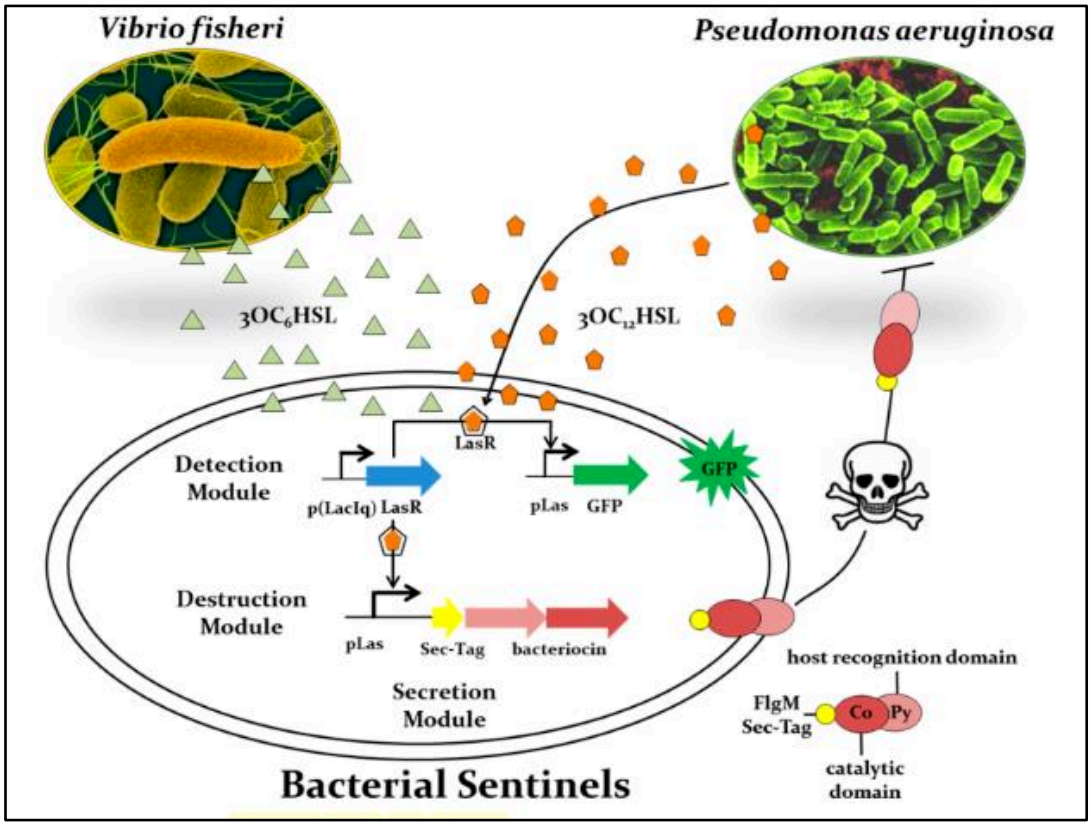

Figure 1.15: The sensing and killing system engineered in *E. coli,* extracted from[71]. The bacteria specifically sense *P. aeruginosa* and kill them.

By detecting the same quorum sensing molecule, 3OC12HSL, but with a different genetic circuit, another team has transformed *E. coli* to make them sense and kill *P. aeruginosa*[72]. For sensing, they used the *lasR* and *gfp* genes. With it, bacteria sensed the presence of the LasR-3OC12HSL complex and became fluorescent. For the destruction of pathogens, the authors have placed two genes after two *pLux* promoters: one which codes for S5 pycocin, a bacteriocin, and one which codes for the E7 lysis protein (**Fig. 1.16**). When *P. aeruginosa* were detected, the pyocin accumulated into the *E. coli* cytoplasm, and the E7 lysis proteins were formed. At one point, the lysis proteins broke the membrane of the *E. coli,* resulting in external release of pyocin and eradication of pathogens.

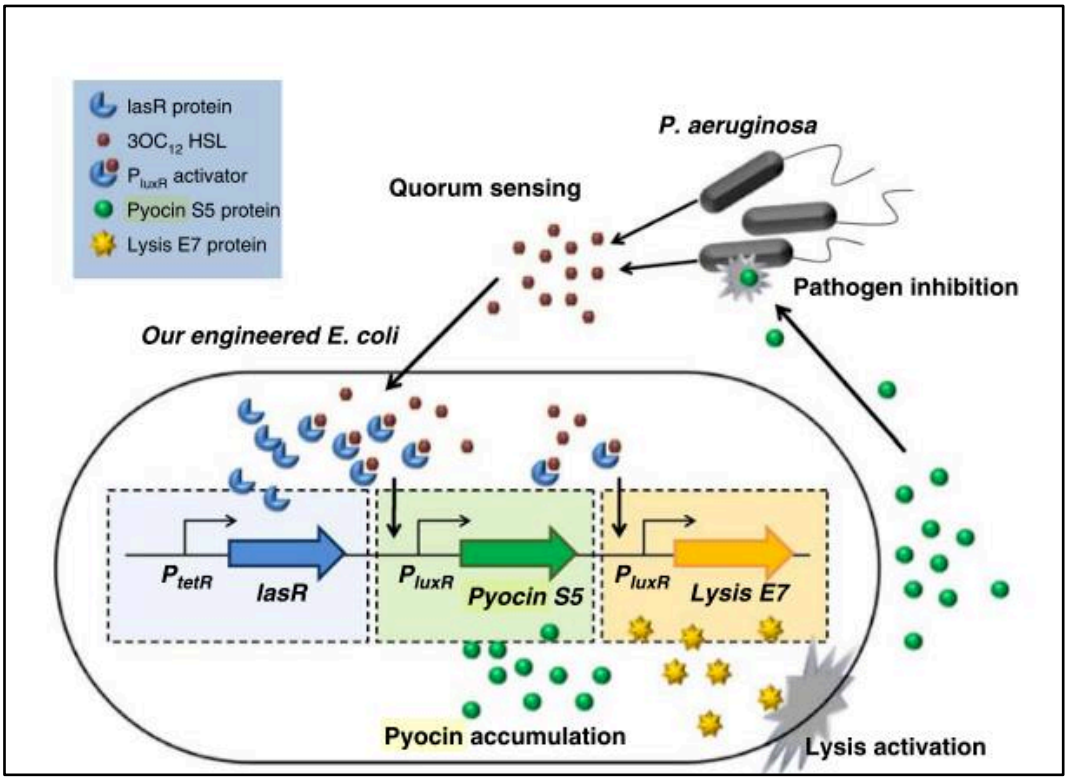

Figure 1.16: The genetic circuit inserted in *E. coli* to destroy *P. aeruginosa*, extracted from[72].

Those two genetic systems worked *in vitro*. However, for *in vivo* applications, some modifications must be made. These bacteria secrete toxins which can kill all types of surrounding microbes, and not only the targeted pathogens. They might destroy other bacteria, non-pathogenic ones, and induce damages in organs. This raises biosafety concerns.

Moreover, for *in vivo* applications, we have to take into account supplementary parameters. For instance, the injected bacteria must be non-pathogenic and specific to the targeted area (gut, tumors). They must not mutate and keep their plasmid during the therapy. Eventually, they should be eliminated from the body. In their review, D. Riglar and P. Silver[73] talk about these constraints and explore new advances in this domain. They mention that several strains of bacteria can be chosen depending on the desired application: *Lactococcus lactis* or *E. coli* for the guts, attenuated *Salmonella enterica* or *S. Typhimurium* to target hypoxic tumors, attenuated *Listeria monocytogenes* to trigger anticancer response. They discuss the different genetic circuits which are implemented in these strains to obtain sensitive and responsive bacteria ("logic gates" and "memory circuits"), and bacteria which represent no harm, with kill switches. The process to have an optimal strain for sensing and drug delivery is long and must be optimized at each step. Until now, no recombinant bacterium has been totally approved for use in human!

1.3 – Modifications conferring new structural functions and group behaviors

Reprogramming microbes, genetically or chemically, does not only consist in enhancing their secreting or sensing properties. Indeed other features can simply be added. The organisms can be modified to gain swimming abilities, to have new membrane properties, to acquire the ability to form biofilms, to invade cells, to change their collective behavior… In this second part, I will discuss several examples of what can be done with microbes.

1.3.a – Microorganisms with enhanced swimming properties

A first example of properties that can be artificially given to microbes is motility. Many teams have attempted and succeeded in making cells motile or controlling how they swim (especially their directionality).

One largely used technique is the formation of biohybrid. For instance, inspired by how spermatozoids swim, a team has given these properties to cardiomyocyte cells[74]. They used a PDMS filament whose extremity is coated with a cell-adherent matrix. Thus the filament binds to the cardiomyocyte (**Fig. 1.17**). This type of cell is highly contractile. Hence, the strength of contraction gives the impulsion needed to bend the PDMS filament and to initiate the swimming movement.

For bacterial biohybrids, the opposite strategy is usually chosen. Some bacterial strains can be highly motile, and even chemotactic. Therefore, for bacterial biohybrid systems, the biological part – the bacteria – provides the motile feature, whereas the non-living part – the liposome, the particle… - provides other properties: drug, magnetism, fluorescence...[66–68] Motile bacteria are even the source of inspiration for the motility of inorganic microrobots[75].

To illustrate this, we can take the example of biohybrid microtube swimmers. They were formed by a combination of motile *E. coli* and electropolymerized microtubes[76]. These microtubes were made of a polypyrrole Au-polycarbonate membrane. To attract the *E. coli* inside, they were coated with polydopamine (**Fig. 1.17**). The authors of the article showed that bacteria trapped in the tube had more directional and less random motion. Moreover, they added extra properties via

further chemical functionalization of the microtube. With a different layer of polydopamine they improved the conjugation step by selectively attracting only one bacterium per microtube. With nickel in the layer, they controlled the swimming trajectory with magnetic forces. With urease on the layer, they added a kill switch activated upon addition of urea. At the end, they managed to have a better swimming object than motile *E. coli* (better directionality) and they added various functionalities.

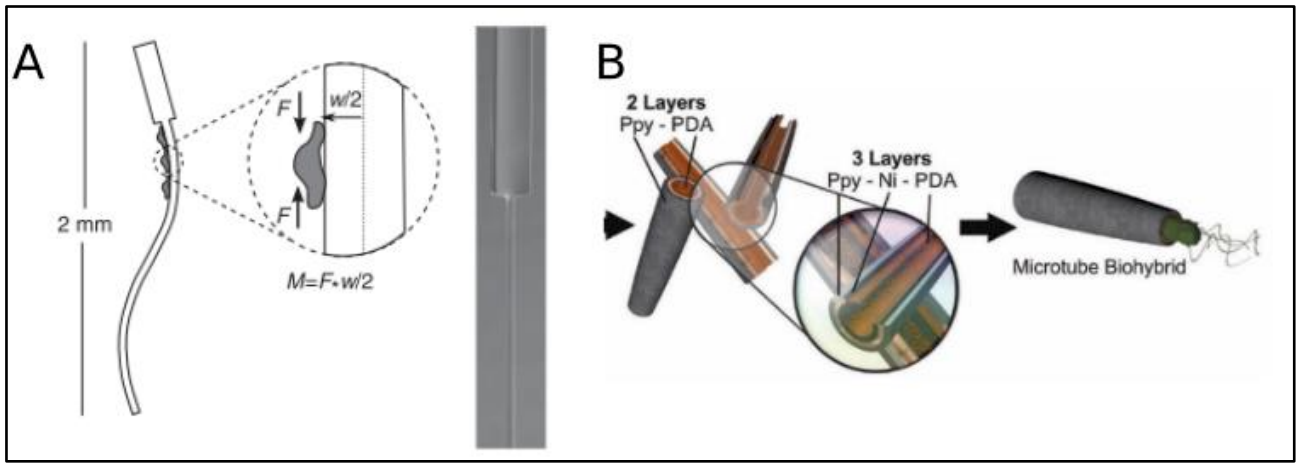

Figure 1.17: Two types of swimmers. (A) Self-propelled cardiomyocyte, extracted from[43]. **(B)** Microtube swimmers, extracted from[76].

1.3.b – Microorganisms with adhesive properties

Microbes can be engineered to adhere to each other and to other cells. In nature, bacteria naturally produce biofilms to adhere to surfaces[77]. A biofilm is made of extracellular organic matter, especially adhesion proteins. It surrounds the bacteria and makes them stick to their surroundings. It also protects bacteria from external aggressions and helps them to colonize surfaces and organs. However, a biofilm is not surface or cell-selective. Being able to tune the adhesive properties (to select to which substrate bacteria will adhere or how bacteria will stick to each other) is interesting for applications, as illustrated by the examples given below.

Bacteria adhering to gut cells and provoking inflammations, like enterohemorrhagic and enteropathogenic *E. coli* strains, have naturally strong adhesive proteins displayed on their outer membrane: the intimins. Inspired by the intimin design, and especially the export portion responsible for the display of intimin at the membrane (β-barrel), synthetic biology has achieved to give non-pathogenic *E coli* adhesive properties. The β-barrel was bonded with different proteins and

had been cloned in bacteria. For instance, in 2018 Glass et al.[78] fused it with an antigen or the corresponding nanobody. In this configuration, modified antigen-displaying *E. coli* bound to the ones with the complementary nanobody, with strong affinity. His team has engineered different couples of nanobody/antigen at the surface of *E. coli*, making bacteria adhere with each other with different aggregative structures. It was not a complete biofilm, because no other external adhesive proteins were secreted, but thanks to this system, different kinds of structures have been made, leading to various topologies (**Fig. 1.18**).

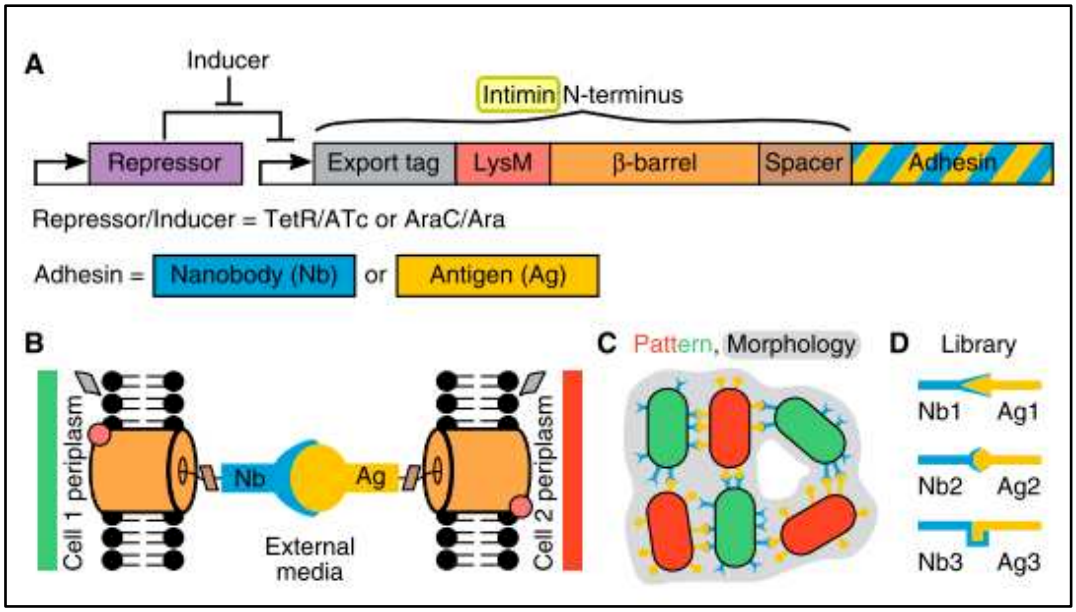

Figure 1.18: A synthetic adhesive protein engineered in *E. coli*, extracted from[78]. (A) The gene construction used to display nanobody or antigen. **(B)** Antigen and the corresponding nanobody bind with each other. **(C)** The different binding patterns. **(D)** The library of antigen/nanobody.

Following the same idea, synthetic adhesins have been engineered to make *E. coli* adhere to various substrates[79]. The β-barrel of intimin was fused with antibodies that recognize antigen coated on a surface, antigen on cells or even antigen on tumors in mice. This resulted in bacteria selectively adhering on target tissues (the tumor) instead of other organs (spleen and liver) probably due to the repression of unselective and natural adhesins of bacteria.

Another team made *E. coli* BL21 adhere to each other with a different scaffold that exports proteins to the membrane: eCPX. It is a transmembrane protein that usually presents peptides at the surface of *E. coli*[80]. They fused it with cohesin and dockerin domains from *Acetivibrio cellulolyticus*. Aggregation was induced via cohesin/cohesin and dockerin/dockerin interactions alone. This

aggregation, reversible when proteinase K was applied, allowed bacteria to better survive in a hostile environment such as *Caenorhabditis elegans* gut, or in the presence of a biocide agent.

1.3.c – Microorganisms with invasive properties

We can genetically modify bacteria not only to adhere but also to preferentially enter into cells. Indeed, some pathogenic bacteria naturally invade cells thanks to membrane proteins, like the invasin of *Yersinia pseudotuberculosis*[81,82]. With this protein, a team has genetically modified *E. coli* to preferentially invade cancer cells[83]. They transformed their bacteria with the *invasin* gene and fused it with different promoters. One was the *arabinose* operon which triggers gene expression upon external arabinose addition. They also used a promoter which belongs to the quorum sensing system of *V. fisheri*. With this one, bacteria produced invasin when they were numerous enough, 10^8 bacteria/mL. They finally used the promoter from the *fdhF* gene which codes for formate dehydrogenase. This promoter is of great interest because it leads to gene expression under hypoxic conditions. Knowing that tumor regions are hypoxic, they could have had invasin only after anaerobic growth, so in contact of cancer cells (**Fig. 1.19**). Their system is great. If all the promoters were combined in an "AND gate", the bacteria would invade cells when arabinose is externally added, when they are numerous enough to have an effect, and only in hypoxic so cancer regions. Unfortunately, the authors only tested the promoters separately. It was difficult because of the different translation rates of the promoters which could induce errors in a logic gate. Nevertheless, their technique let us envision the use of this bacterium for targeted anticancer therapy: the bacteria could invade cancer cells, and deliver a drug or a toxin directly inside the cytoplasm of sick cells.

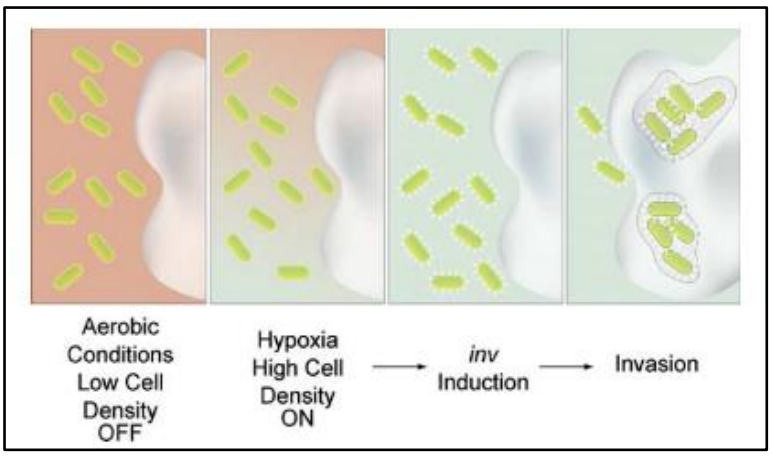

Figure 1.19: Schematic of the inducible invasion of cancer cells, extracted from[83].

1.3.d – Modifying the behavior of groups of microorganisms

Multicellular transformation can be achieved amongst microbes with synthetic biology. By mastering bacterial communication, it is possible to change the behavior of a whole population of bacteria instead of acting at the single cell level. Most studies are based on modifying quorum sensing to induce a change in a group of bacteria[84].

For example, if we go back to a previous example, the team of J. Hasty[64] has used quorum sensing to create self-limitating populations of bacteria. They cloned inside *S. typhimurium* the *luxI/luxR* system which codes for quorum sensing communication. With two other genes, one for GFP, and the lysis gene *ϕX174E*, under the *pLux* promoter, their system began to be auto-regulated. When bacteria grew, they accumulated AHL. Once a threshold was reached, they became fluorescent and died upon lysis. This led to a drastic decrease in bacterial number. Then the remaining surviving bacteria repeated the periodic cycle of "growth → GFP and lysis → death". J. Hasty and coworkers have managed to have a population in which the number of cells is oscillating over time (**Fig. 1.20**). In another article[85], they went further by co-culturing two different communities of bacteria that were competitive, with the use of orthogonal self-lysing.

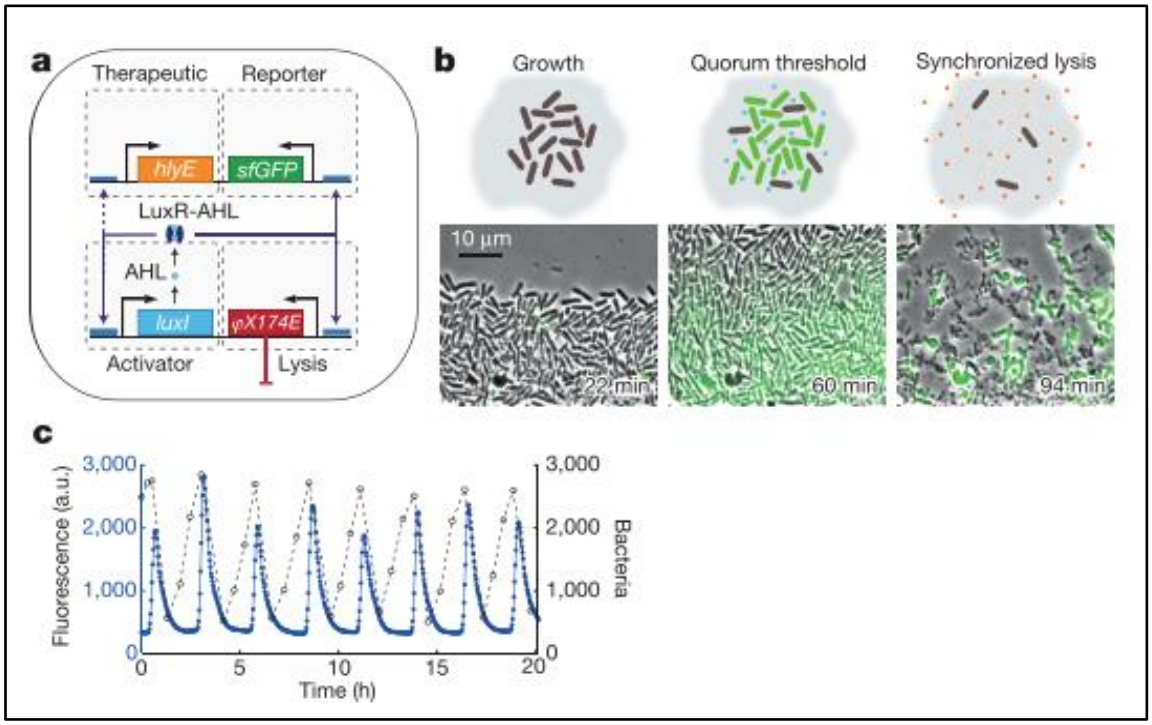

Figure 1.20: The autoregulated population of bacteria, extracted from[64]. (A) The synthetic circuit. **(B)** The main states in which the bacterial population can be: growth, fluorescence, death. **(C)** The periodic number of bacteria in this system over time.

Instead of focusing on controlling the growth of microbes in a community, other teams have tried to create color patterns in bacterial colony, on the long range scale (macroscopic one). For instance, in an article[86], with a logic gate based on quorum sensing, with three different reporters, the author have engineered bacteria to produce different fluorescent proteins upon addition of two AHL molecules. They applied AHL gradients on solid surface and with their logic gate, the bacteria macroscopically patterned in a gradient of fluorescence color (**Fig. 1.21**).

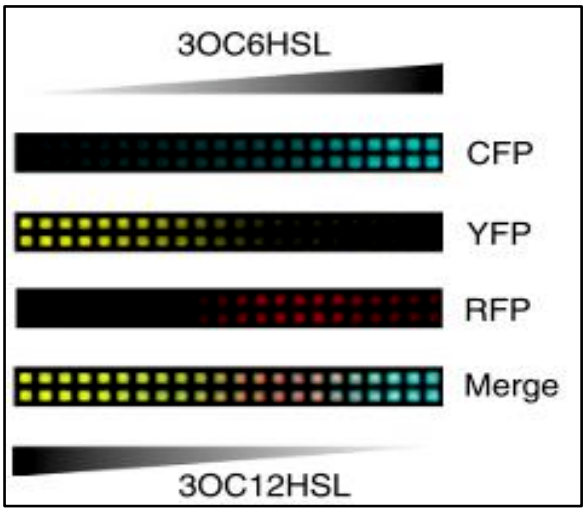

Figure 1.21: The fluorescent pattern observed in bacteria spread on a solid surface with gradient of AHL, extracted from[86].

Another team has done the same kind of color pattern in microbial population[87]. They trapped bacteria in a microfluidic channel and used synthetic circuits based on quorum sensing (on activator/repressor system). When the two kinds of bacteria grew in their device (the activator and the repressor), the oscillations of each population density synchronized. Over time, a stabilization of the spatial arrangement of cells followed a transient oscillation regime. With local interactions between cells they have built a macroscopic multicellular system with a stabilized group behavior at the end.

Finally another study was achieved to produce Turing-type pattern at the macroscopic level amongst bacterial population[88]. The author used two circuits based on quorum sensing: one that resulted in red fluorescence, the other one in green. They obtained a multicellular behavior which displayed Turing-like pattern. In a recent article on BiorXiv[89], the team of Elowitz has used quorum sensing communication to induce collective group behavior and population size control in mammalian cell lines.

1.4 – Modifying the physical properties of microorganisms

In addition to secreting, sensing, structural and group properties, microbes can be reprogrammed to get physical characteristics. Here are a few examples of novel properties which are very different to their natural "biological" ones. Their mechanisms are so dissimilar that we can visualize/control these new characteristics without affecting the biological environment. Hence, it is a good way to have an effect only affecting the modified microbes.

1.4.a – Microorganisms with optical properties

One first example is based on chemical techniques (formation of biohybrids) to transform bacteria in order to control them with light, e.g. induce an action upon light exposure. Indeed, a team has managed to do cancer therapy delivered by light using bacterial biohybrids[90]. They called it photo-controlled bacterial metabolite therapy, PMT. They harnessed a semi-conductor (carbon nitride C_3N_4) on an *E. coli.* According to the authors, the *E. coli* strain MG1655 is preferentially homing in tumor and has an endogenous nitrate/nitrite reductase activity. With the presence of carbon nitride, the reduction of NO_3 into cytotoxic NO is enhanced, when light is applied. Indeed, upon light irradiation, the semi-conductor produces photoelectrons that are transmitted to the bacterial enzyme that creates NO. With this system they achieved a 37-fold increase in the rate of NO emitted and managed to affect the surrounding cancer cells. With PMT, they have reduced tumor growth in mice *in vivo* by around 80% (**Fig. 1.22**).

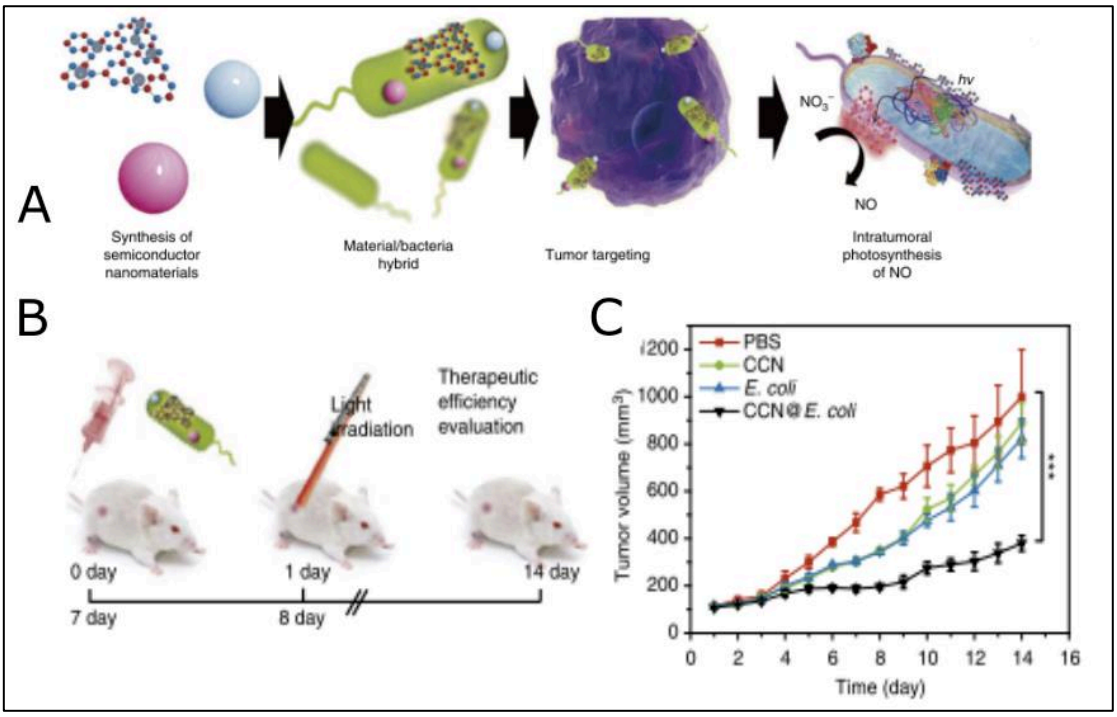

Figure 1.22: System of PMT engineered with light-activated biohybrids, extracted from[90]. (A) Schematic of the biohydbrid formation. **(B)** Protocol used to study anti-cancer activity in mice (PMT treatment). **(C)** Tumor growth as a function of time (days). In black the data corresponding to the PMT treatment, in red the control, in green the semi-conductor alone, in blue the bacteria alone.

1.4.b – Microorganisms with acoustic properties

It is also possible to confer acoustic properties with genetic modifications. Recently, Shapiro et. al have used gas nanostructures produced by bacteria for ultrasound imaging. Indeed, for imaging, ultrasounds have the advantages of penetrating deeply in the living matter, being cheap and having a high spatial resolution (nanoscale range). That is why scientists began by a preliminary assay to study the possibility of using gas vesicles, naturally formed by *Anabaena flos-aquae* and *Halobacterium NRC-1,* as contrast agents for ultrasound imaging[91]. They explored the characteristics of the vesicles produced by each strain: they can be distinguished in the same medium thanks to their different collapse pressure; the signal is better when vesicles aggregate. As they appeared to be good candidates for *in vivo* sensing, they injected the gas vesicles in mice and successfully detected a contrast signal in ultrasound imaging.

Next, in another study[92], M. Shapiro and coworkers genetically encoded the gas vesicles in *E. coli* and *S. typhimurium*. To do so, his team inserted a genetic circuit made by combining gas-vesicles producing genes from *A. flos-aquae* and *Bacillus megaterium*. The team tested several conditions until finding the best combination for ultrasound imaging (**Fig. 1.23A**). Then, the whole

modified bacterium was used for imaging (not only the vesicles contrary to the first article). By testing it in mice, his team gave a proof-of-concept of imaging a probiotic (here the gas-vesicles forming *E. coli Nissle*) in the gut. In general it is difficult to monitor gut microbiota, but here they were able to find more precisely the position on bacteria in the digestive system with ultrasound rather than with a bioluminescent control (**Fig. 1.23**). They also used their imaging technique to see modified *S. typhimurium* in tumor.

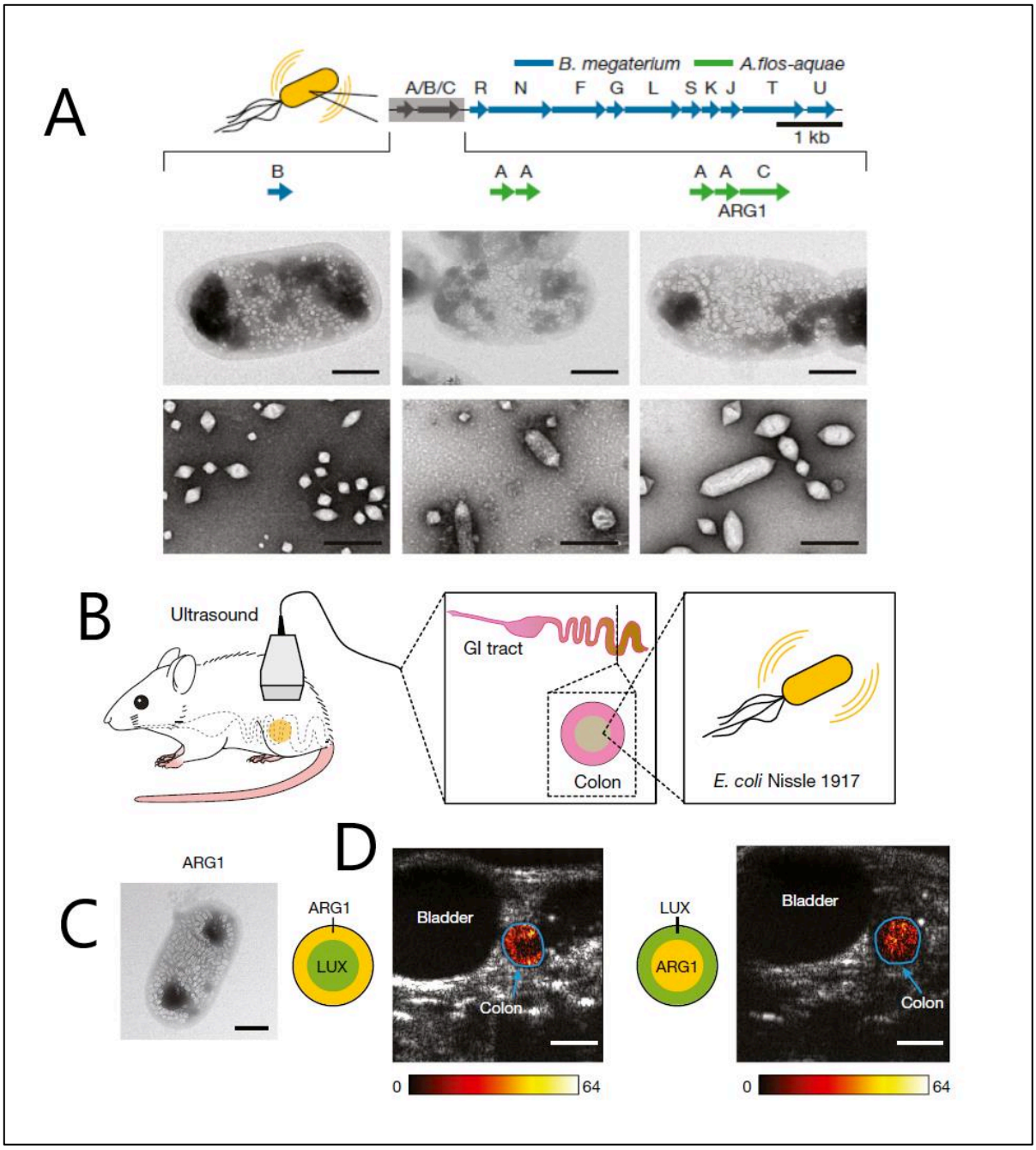

Figure 1.23: Modified *E. coli* that produce gas-vesicles for ultrasound imaging, extracted from[92]. (A) On the **top:** Schematic of the different combinations of genes inserted in *E. coli* to create internal gas vesicles good enough for reporter imaging. **Below:** Transmission electron micrographs of genetically modified bacteria (**middle**) or extracted vesicles (**bottom**). On the **left**: genes from *B. magetarium* end in small vesicles undetectable with ultrasounds. On the **middle**:

vesicles from both strains are larger. On the **right**: another combination of genes from both strains ended up in the desired reporter gene clusters, ARG1, with large and elongated gas vesicles, suitable for ultrasound imaging. **(B)** Schematic of the *in vivo* ultrasound imaging with ARG1-bearing *E. coli* introduced in gut as the reporter agent. **(C)** Transmission electron micrograph of a modified *Nissle* which presented gas-vesicles. **(D)** Transverse ultrasound image of a mouse whose colon is colonized by, **for the left panel:** luminescent *E. coli* in the lumen and ultrasonic *E. coli* at the colon wall, **for the right panel**: ultrasonic *E. coli* in the lumen and luminescent *E. coli* at the colon wall.

1.4.c – Microorganisms with magnetic properties

Another feature which can be given to bacteria is magnetism. Magnetism is a complex notion which covers different states of matter. Indeed, materials can possess a magnetic moment. This moment depends on spins' organization and arrangement of material's atoms. If the atoms have spins which are all counterbalanced (no single spin in the orbital layers), the matter is diamagnetic (no magnetic moment). It is the case of most living systems made of organic molecules. On the contrary when single spins exist, the magnetic moment of atoms is non-zero. Thus the repartition of magnetic moments can take various forms. It can be random, if the moments do not interact with each other, and the matter is called paramagnetic. In this case the sum of magnetic moments is null when no external field is applied. If there is an interaction of magnetic moments of atoms (occurring at a certain range of temperature), they can organize themselves and different states exist: ferromagnetic (they are all orientated along the same direction), antiferromagnetic (the sum of magnetic moments is zero, due to the orientation of magnetic moments which are in the opposite direction, like in hematite, wüstite), ferrimagnetic (like magnetite, maghemite)[93,94]… (**Fig. 1.24**).

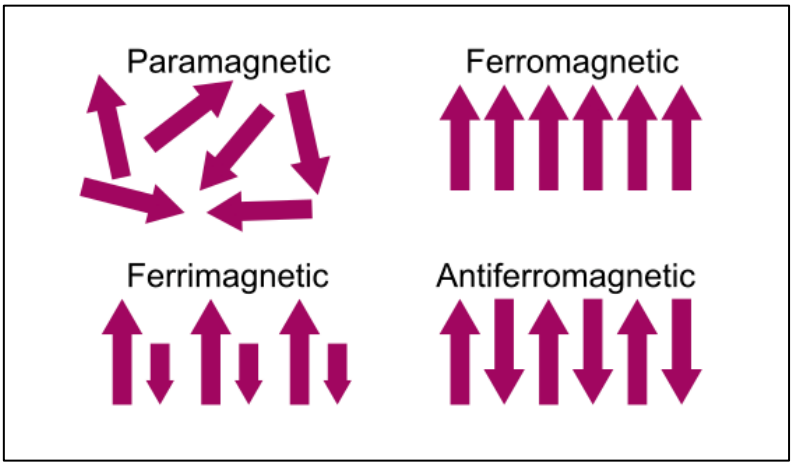

Figure 1.24: Orientation of magnetic moments inside a "magnetic" material. For paramagnetism, the magnetic moments are randomly distributed, resulting in zero spontaneous magnetization, in the absence of an external magnetic field. For ferromagnetism, the magnetic moments are oriented in the same direction. For ferrimagnetism and antiferromagnetism, they are

orientated in opposite directions, but the opposition is unequal in ferrimagnetism leading to a no-zero permanent magnetization.

Thus paramagnetic, ferromagnetic and other non-diamagnetic materials respond to a magnetic field. When an external magnetic field is applied a magnetization is induced in these objects: the magnetic moments align, following the direction of the external magnetic field. For paramagnetic matter it means that under a field, the matter becomes magnetized through the alignment of the initially randomly oriented magnetic moments with the external magnetic field. For ferromagnetic materials (most of our everyday life magnets), we could suppose, as magnetic moments of atoms are all in the same direction, that the magnetization is extremely high even without an external field. It is not exactly the case. In fact, macroscopically, a ferromagnetic material is often divided in several magnetic domains. In each domain the magnetic moments have naturally the same orientation, but the domains are randomly oriented inside the material. Thus with no external field, a ferromagnetic material likely has a low magnetization. However, when a magnetic field is applied, the domains align with each other all along the external magnetic field, inducing a strong magnetization. When the external field is removed, the orientation of domains remains, creating a remanent magnetization: the matter becomes a magnet (**Fig. 1.25**)!

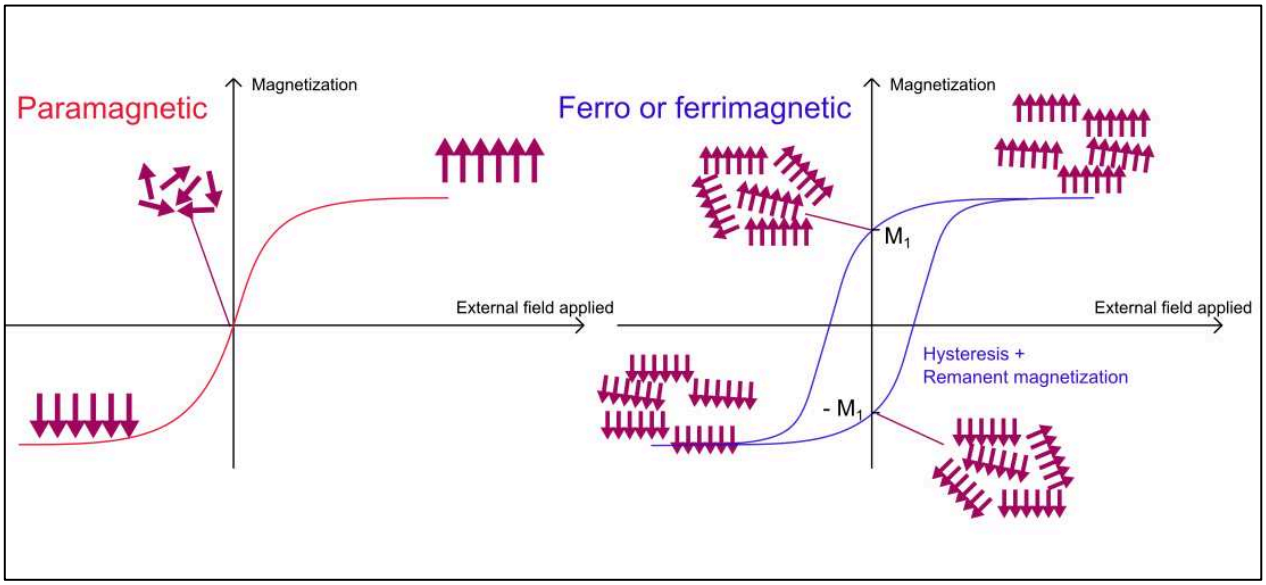

Figure 1.25: Magnetization curves of paramagnetic or ferro/ferrimagnetic materials.

To note, when ferromagnetic particles are small (below around 76 nm for magnetite[95]), with a size smaller than a monodomain of magnetic moment orientation, the material is called

superparamagnetic. As thermic agitation is sufficient enough to reverse the magnetization, no remanent magnetization exists and the curves look like the ones for paramagnetic objects.

Usually, when we want to provide "magnetic" properties to a microorganism, the ability to strongly follow magnetic field gradients is required. That is why paramagnetic, ferrimagnetic or even superparamagnetic materials are looked for. With these properties, the microorganism could be controlled with an external magnetic field (to concentrate it in space, to do hyperthermia with an alternative field[96]) and could even represent a contrast agent in medical magnetic resonance imaging (contrary to light which can be scattered, magnetic fields penetrate well in living matters).

1.4.c.i) Naturally magnetic microbes: magnetotactic bacteria

In nature, most organisms are diamagnetic, but some of them have developed "magnetic" properties. Some species of fish like the pacific salmon (*Oncorhynchus nerka)*[97] can imprint the Earth magnetic field of their lake to find their way back after migration. Birds are also well-known for their ability of magnetoreception. If we focus more on microorganisms, some naturally magnetic bacteria have been described in the mid-70s in the United States, by Blakemore: the magnetotactic bacteria[98]. These specific bacteria, discovered in lake sediments, can orient themselves by aligning with the Earth magnetic field[99]. It is called magnetotaxis. To do so, these bacteria synthesize magnetosomes in their cytoplasm: ferrimagnetic magnetite ($Fe^{(II)}Fe^{(III)}{}_2O_4$) or even greigite ($Fe^{(II)}Fe^{(III)}{}_2S_4$), with a well-defined structure and size, enclosed in a lipid membrane and organized into chains to enhance their magnetic properties. Several processes are involved in the biogenesis of magnetosomes such as the formation of the lipid vesicle, the process of iron uptake, the growth of magnetite crystal and the alignment in chains[100]. The biomineralization process, perfectly controlled in shape by the geometry and proteins of the vesicle, and in structure by the redox conditions in the magnetosome, leads to a strongly magnetic crystal (**Fig. 1.26**).

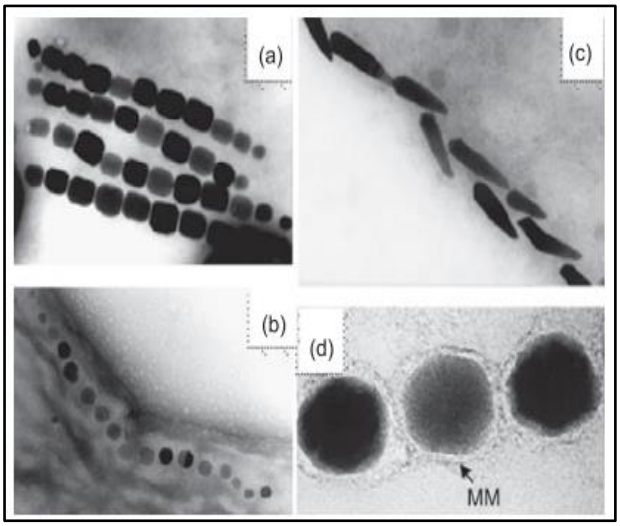

Figure 1.26: Transmission electron micrograph of magnetosomes with various shapes, extracted from[100]. (A) "Elongated prisms". **(B) "**Cubo-octahedral". **(C) "**Bullet-shaped". **(D)** Zoom of the "bullet-shaped" coated with the magnetosome membrane (MM).

If we look closer at the biosynthesis of magnetite crystals in the magnetosomes, we can note that they require a well-defined process. To create perfect magnetite crystals, whose size is between 35-120 nm, whose structure can be octahedral, dodecahedral or cubic, and aligned in one or several chains (**Fig. 1.27**), iron has to enter into cells and to be turned into iron oxides.

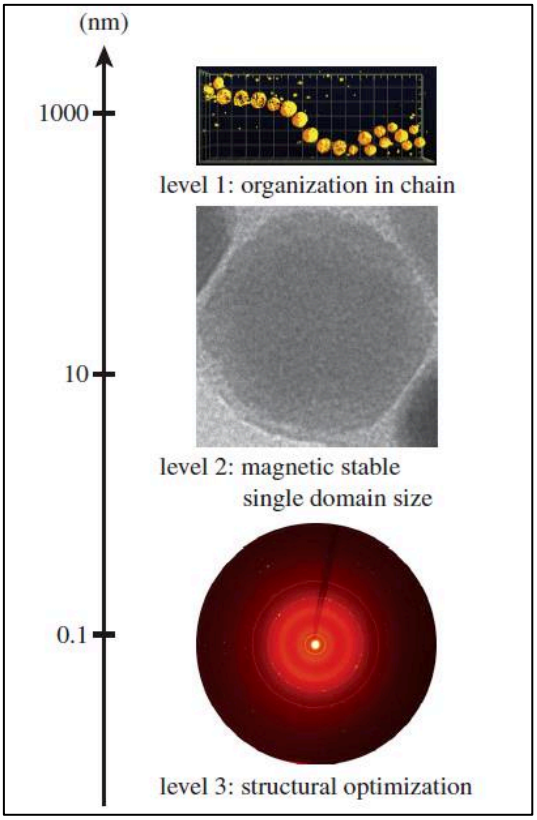

Figure 1.27: Organization of magnetite particles in magnetotactic bacteria, at different levels, extracted from[101]. The magnetite crystals assemble in chain, they are perfectly shaped monodomains of magnetite at nanometer and sub-nanometer scale. At **the top**: reconstruction of a chain from the strain MSR-1. In **the middle**: transmission electron micrograph of magnetosome. Image width, 50 nm. At **the bottom**: diffractrogram in 2 dimensions of AMB-1 bacteria.

In order to take iron from the environment, magnetotactic bacteria can adopt various strategies: they can use iron transporters to make it bioavailable[102]; they can employ periplasmic proteins like *Magnetospirillum* AMB-1[103]; or they can incorporate iron III through an energetic process like *M. gryphiswaldense*[103]. For biomineralization, in his review[103], D. Schüler discusses the mechanism proposed for *Magnetospirillum* species of magnetotactic bacteria. His mechanism was in agreement with the 3-step process historically found by Frankel et. al[104] in *Aquaspirillum magnetotacticum* strain MS-1: hydrous ferric oxide leads to ferrihydrite then magnetite. Indeed, according to D. Schüler, iron III is uptaken by the bacteria, after a reducing step, and then ferrihydrite structures nucleate, via an oxidizing and dehydratative process. Next, 1/3 of iron III is reduced and water is lost to form ferrimagnetic magnetite in the magnetosomes' membranes (**Fig. 1.28**). D. Schüler has additionally shown that in the case of *Magnetospirillum gryphiswaldense,* magnetite is formed under low concentration of O_2 (microaerobic conditions)[105].

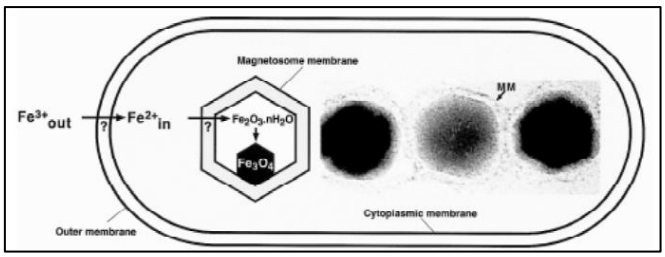

Figure 1.28: Hypothesis of biomineralization in *Magnetospirillum* bacteria, extracted from[103].

Still, the process of iron incorporation from cytoplasm into magnetosomes vesicles remained unclear at the time. Thus, a more recent study has specified the mechanism of magnetosomes biomineralization[106]. By working on the strain *M. magneticum* strain AMB-1, and using techniques of X-ray absorption spectroscopy and transmission electron microscopy, the authors have monitored the mineralization of magnetotactic bacteria. They have revealed that before making ferrihydrite-like structures in magnetosomes, iron is stored in cytoplasmic ferritin under the form of a ferric hydroxide phase, enriched in phosphate. Then iron and phosphate separated, leading to a precipitation of iron in a ferrihydrite form in magnetosome vesicles. According to the assays, ferrihydrite quickly turns into magnetite (**Fig. 1.29**).

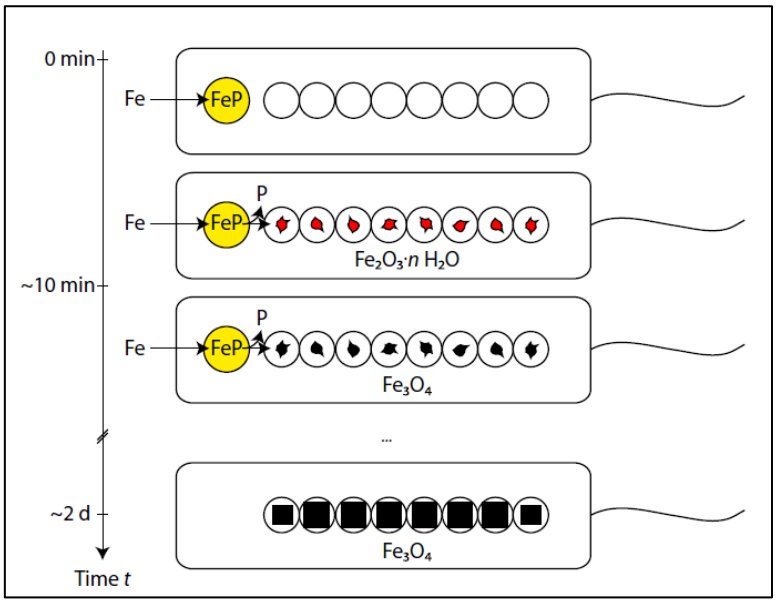

Figure 1.29: Mechanisms of biomineralization in magnetotactic bacteria extracted from[106].

In addition to the chemical process that allows to obtain pure crystals, a defined growth, phase, size and alignment of magnetite particles are also controlled by the magnetosome membrane and specifically associated proteins[107]. Indeed, this membrane made of phospholipids and proteins is encoded by a large genomic island of hundreds of genes. The proteins of the magnetosome membrane are numerous (Mam, Mms, Mtx families…) and are involved in general magnetosome structure or even nucleation and mineralization process, by acting on the crystal surface (**Fig. 1.30**). For example, a study in 2014[108] on various genes of *M. gryphiswaldense* has shown that *Mms6* operon was importantly linked with crystal size, whereas the *MamAB* operon was involved in mineralization. Another study has shown that the protein MamJ is essential to bind magnetosome vesicles on a cytoskeletal filament to form an elongated chain, also in *M. gryphiswaldense*[109].

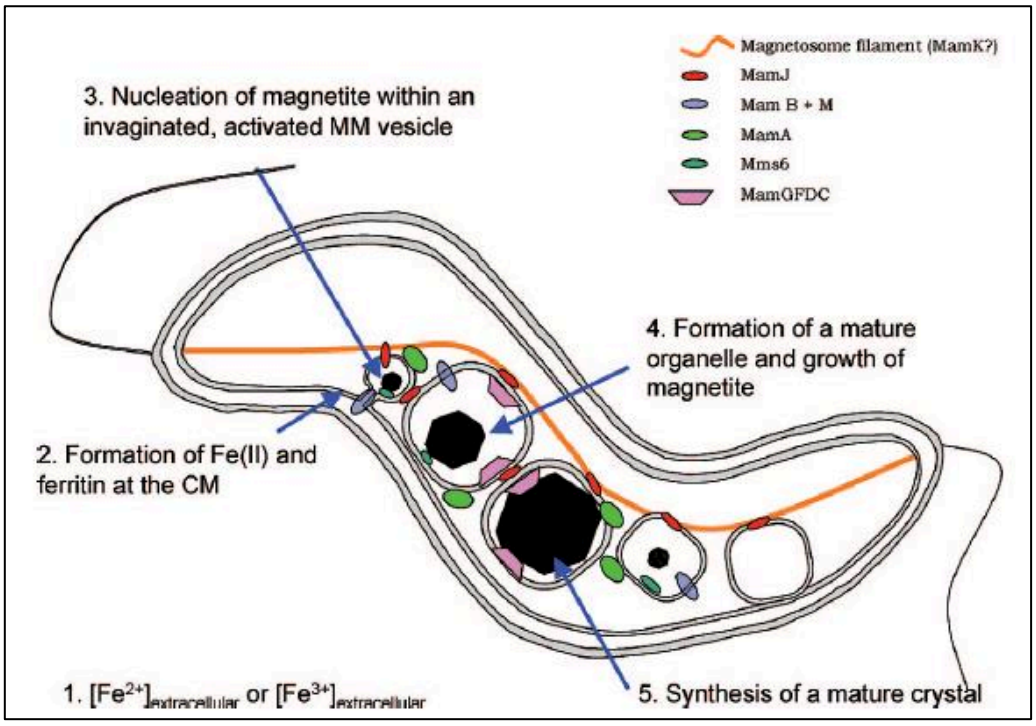

Figure 1.30: Role of various proteins involved in magnetosome formation, according to[107].

Some research teams have tried to use magnetosomes for various applications[110,111]. For example, magnetosomes can be fused with nanobodies to perform magnetic separation of targeted cells[90]. Magnetosomes could treat cancer via hyperthermia[112], or be modified for biosensing[113]. However, it is difficult to engineer magnetotactic bacteria for specific applications. They grow slowly. They require specific conditions of O_2 and nutrients[98]. They have a complicated genome. Thus a genetic modification on the magnetosomes to fuse them with a protein, to make them fluorescent or compatible with immunoassay for instance, is not a simple process. Nevertheless, by selecting magnetosome genes from *M. gryphiswaldense,* the team of D. Schüler has successfully triggered magnetosomes formation in a foreign strain: *Rhodospirillum rubrum*[114]. Even if this strain was relatively close to magnetoactic bacteria, this is a first step toward making other (more simple-to-handle) microorganisms magnetic!

Indeed, inspired by magnetotactic bacteria, other strategies have been investigated to confer magnetic properties to easier to handle microorganisms. Two main techniques can be applied. The first one can be the creation of a biohybrid. Magnetic properties can be given either by the conjugation of a magnetic particle to a bacterium, or by conjugating a magnetotactic bacteria to a non-living object (a drug-loaded vesicle for instance). The other strategy is to do genetic

modification to encode the formation of "magnetic" particles within easy-to-handle bacteria or yeast. In the end of this chapter, I will give few examples of both strategies.

1.4.c.ii) Magnetic biohybrids

Thus to make a magnetic biohybrid one strategy can be to attach a magnetic micro- or nanoparticle on a live and active bacterium. Thus, the biohybrids benefit from the bacterial properties (motility, fluorescence, drug secretion) and from magnetic guidance[21]. Magnetic particles can even target a tumor or be coated with an anticancer drug in the context of tumor therapy.

For instance, several microswimmers have been created by linking magnetic nanoparticles on a living microbe. By combining with biotin/streptavidin interaction between motile *Serratia marcescens* and superparamagnetic beads of 6 µm, a team was able to control their swimming using a magnetic field[115]. This kind of bacteria was used because it easily links to surface and is easy to cultivate, nevertheless it is pathogenic. Hence it has to be attenuated for eventual *in vivo* applications. With a spermatozoid instead of a motile bacterium, a magnetic biohybrid was created by trapping it in a magnetic microtube[116]. Contrary to spheric magnetic nanoparticles, the microtube does not break the cell membrane of the spermatozoid and is less toxic, resulting in a better success of creation of biohybrids during the conjugation step. With an external magnet, the authors could control the swimming direction of their biohybrid. The swimming of a eukaryotic cilliate, *Tetrahymena pyriformis,* has been controlled thanks to the internalization of ferromagnetic nanoparticles[117].

To go further, a study[118] has engineered magnetic biohybrids to make them deliver antitumor drugs *in vivo*. They stuck on a motile *E. coli* a poly-electrolyte monolayer microparticle containing doxorubicin, an anti-cancer drug, and magnetic nanoparticles (**Fig. 1.31**). As the distribution of nanoparticles is inhomogeneous in the microparticle, the biohybrid has a magnetic moment and its swimming motion can be controlled by external magnetic forces. With an *in vitro* assay on cell lines, the author showed that magnetic guidance was faster than chemotaxis to efficiently deliver doxorubicin to cancer cells.

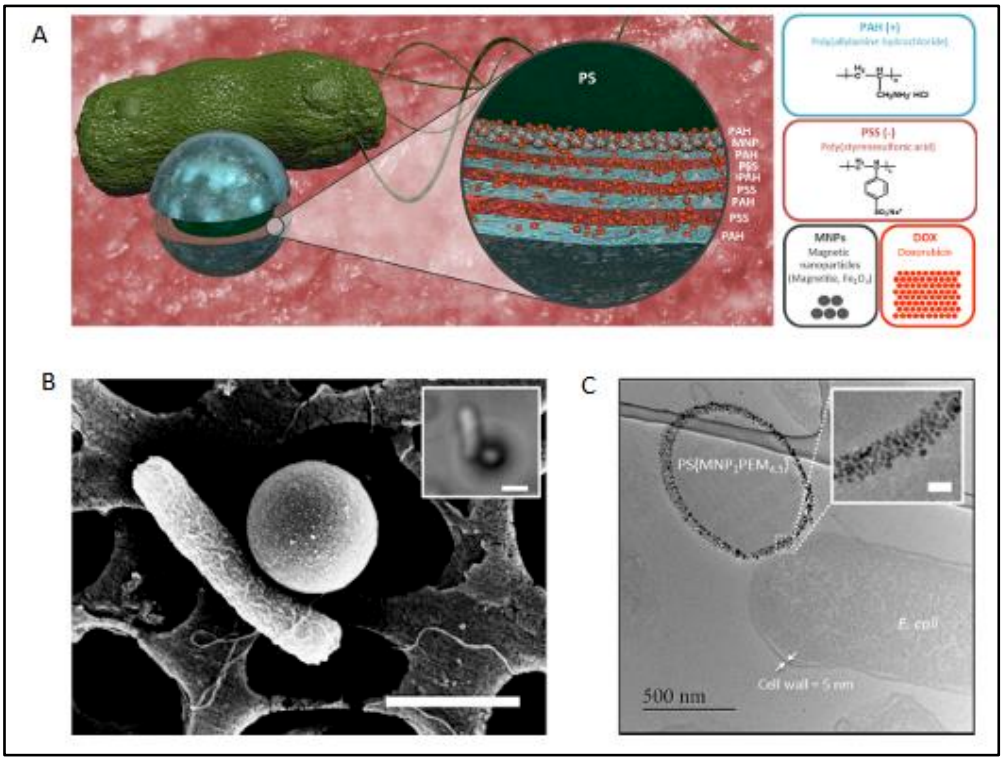

Figure 1.31: A magnetic biohybrid that can deliver doxorubicin to cell, extracted from[118]. (A) Schematic of the biohybrid: a motile *E. coli* is attached by non-covalent interaction to a positively charged 1 µm polystyrene microparticle that contains: layers of poly(allylamine hydrochloride), of poly(sodium 4-styrenesulfonate), magnetic nanoparticles and doxorubicin. **(B)** Scanning electron micrograph of the biohybrid, scale bar 1µm. The insert panel displays the optical image of the biohybrid, scale bar 1µm. **(C)** Transmission electron micrograph of a section of a biohybrid. The insert panel is a zoom on the magnetic nanoparticles, scale bar 50nm.

The reverse approach was also investigated for the creation of biohybrids: magnetotactic bacterium chemically modified with a cargo vesicle for instance. It has been done with *Magnetococcus marinus* (MC-1) linked to drug-loaded nanoliposomes and guided by magnetic forces to target tumors in mice[119]. Moreover, another team captured *M. gryphiswaldense* within a microtube which contained a drug (here ciprofloxacin). The so-formed biohybrids were able to deliver drugs to bacterial biofilm[120]. Thanks to the bacterial magnetic and motile properties, the swimming motion of the biohybrid was externally controlled with magnetic fields to reach the biofilm. The drug could be delivered in acidic conditions (due to the composition of the microtube), such as the ones found in *E. coli* biofilms. Thus their system ensures a local and controllable drug-delivery system (**Fig. 1.32**).

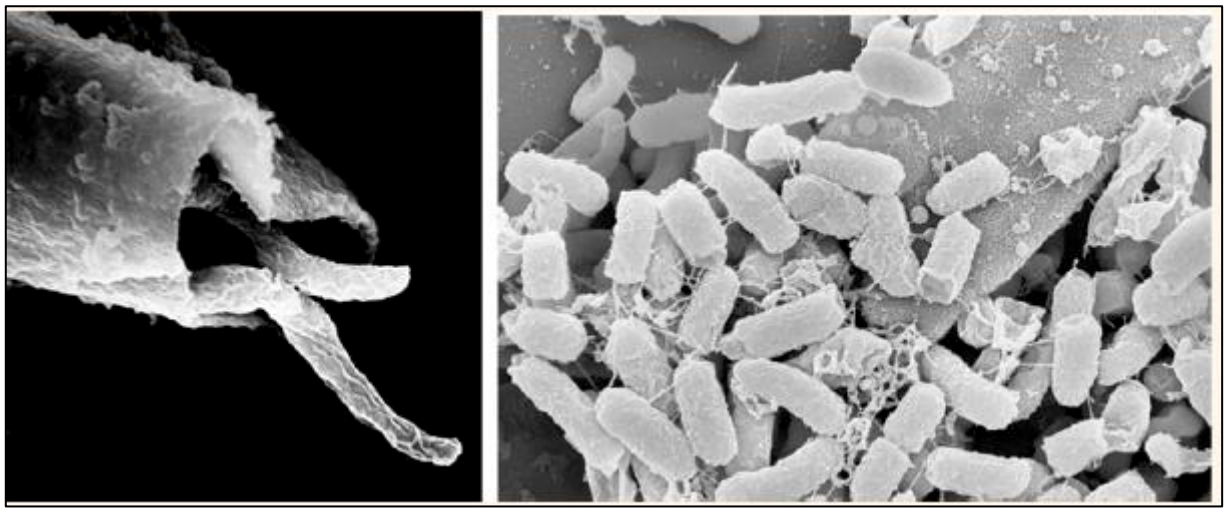

Figure 1.32: Scanning electron micrograph of a biohybrid made with magnetotactic bacteria, extracted from[120]. On **the left**: *M. gryphiswaldense* is entrapped in a silica microtube. On **the right**: the biohybrid is at the contact of an *E. coli* biofilm.

However magnetism is not only studied to modify or control the swimming of cells. Magnetic particles and especially magnetosomes are good contrast agents for MRI or can do hyperthermia in cells[112,121]. Thus, by biomimetism, magnetic biohybrids have been engineered to help for MRI as well. For instance, *Spirulina platensis* microalgae have been externally covered by Fe_3O_4 nanoparticles, thus leading to be monitored in the gut[122]. During this study the authors found that the algae could be toxic for cancer cells. However, its mechanism of action must be unveiled before using it as an imaging-guided therapeutic agent.

Mammalian cells can even become magnetic simply in contact of magnetic nanoparticles. A study[123] has revealed that incubated cells (mouse macrophage and HeLa) with maghemite nanoparticles resulted in their internalization via the endocytosis pathway. The resulting cells were magnetic enough to be sorted in a microfluidic chip: a sorting called magnetophoresis. With their micro-fluidic device, the authors have sorted cells depending of their level of magnetization, while keeping them biologically active and not damaged (**Fig. 1.33**).

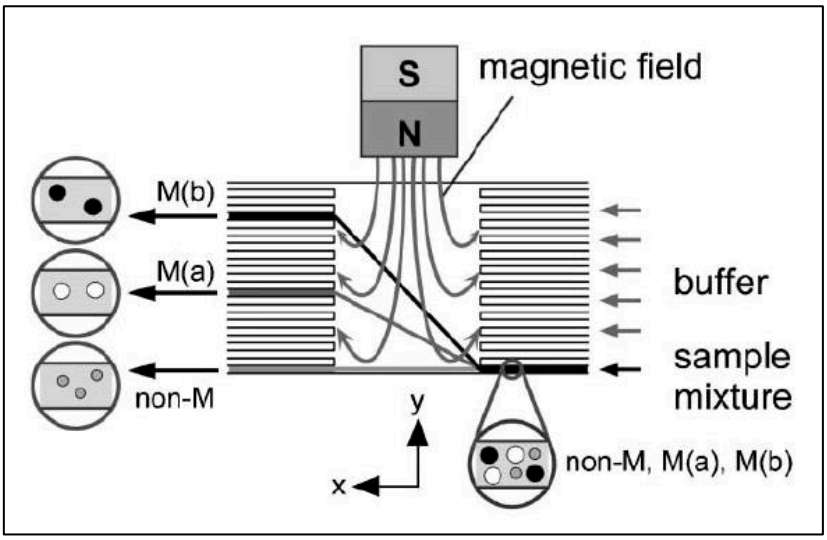

Figure 1.33: Schematic of the magnetophoresis microfluidic set up, extracted from[123]. A sample bearing non-magnetic and magnetic cells is introduced. The magnet leads to a deflection of magnetic cells (M(b) and M(a)): they go up and are sorted from the non-magnetic ones (non-M).

Yet, even if the use of biohybrids is promising, there are some limitations. First, fixing bacteria on nanoparticles or vesicles requires several steps and is time consuming. Then, not all the strains of bacteria, and all the cargos used in these studies are biocompatible and safe for an *in vivo* use. Therefore other strategies have been investigated to confer genetically-encoded magnetic properties to easy-to-handle microbes.

1.4.c.iii) Genetically encoded magnetic properties in microorganisms

As seen previously, molecular biology techniques can be used to confer magnetic properties to simple-to-handle organisms: to make them produce or contain in their cytoplasm ferrimagnetic, paramagnetic (or other types of magnetic) objects. Usually, the simplest way is to genetically encode iron-storage compartments into microorganisms so that they transform imported iron into stored iron oxides.

Most cells, and especially bacteria like *E. coli*, have storage protein to keep iron: proteins from the ferritin family. In fact, for bacteria, three proteins can store iron: ferritin A, bacterioferritin and Dps (DNA-protection during starvation)[124,125]. Ferritin is a 24-monomer protein, coded by only one gene, found in bacteria, archea and eukaryotic cells. It forms a 12 nm nanocage whose empty core is 8 nm large. It has a ferroxidase function and can import iron II and transform it *in vivo* into

iron oxides in presence of phosphates[126,127]. *In vitro* mineralization assays on ferritin[128] have revealed that it could store iron under a paramagnetic and even ferrimagnetic form (magnetite depending on pH or redox conditions), following the equation, for bacterial ferritin for instance:

$$\textbf{Eq}_1\ 2Fe^{2+} + 4H_2O \rightarrow 2\ FeOOH + 6H^+ + 2e^-$$

$$\textbf{Eq}_2\ O_2 + 2e^- + 2H^+ \rightarrow H_2O_2$$

$$\textbf{Eq}_3\ 2Fe^{2+} + O_2 + 4H_2O \rightarrow 2\ FeOOH + 4H^+ + H_2O_2$$

Thus *in vitro* mineralization of ferritins leads to the formation of monodispere iron oxide nanoparticles (as the size of particles is limited by the nanocage size) that can be functionalized. As the ferritin is coded by only one gene, the nanocage protein can be fused with other proteins of interest. Moreover, like magnetosomes which can be extracted and used for hyperthermia[112] or as great contrast agents in MRI[129], thanks to their pure magnetite phase, ferritins can also be extracted from microorganisms and have *in vivo* applications by themselves. This protein can be *in vitro* loaded with metals or drugs to monitor or treat disease. For example loaded human ferritin have an effect on the relaxation times in NMR and was proved to be uptaken by macrophages[130]. More generally, ferritin was well studied as a potential anticancer agent. It can be a nanomedical tool that safely encapsulates chemical drugs like cisplatin or doxorubicin, that delivers siRNA for cancer therapy, that stores magnetite or gadolinium for MRI of tumors or that can even trap photothermal agent for photothermal therapy[131]. The encapsulation can be done by changing the pH conditions that lead to the assembly/disassembly of the 24 monomers of ferritin forming the nanocage (**Fig. 1.34**)[132].

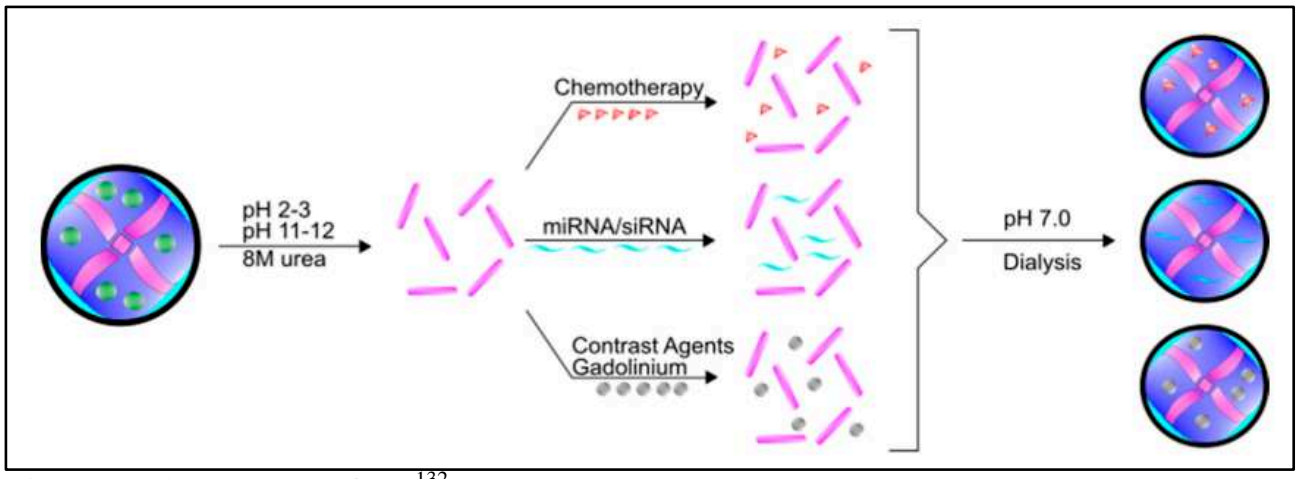

Figure 1.34, extracted from[132]. pH changes can induce disassembly of the ferritin. Other molecules can be put at the contact of the monomers. The nanocage assembles around them by turning back the pH to neutral conditions.

One particular interesting ferritin is the one form *P. furiosus* which can endure elevated temperature (60°C)[133], conditions apparently needed for the formation of magnetite in the core[134]. This ferritin is made of 24 monomers and can store iron in solid phase to detoxify cells[133] (**Fig. 1.35**).

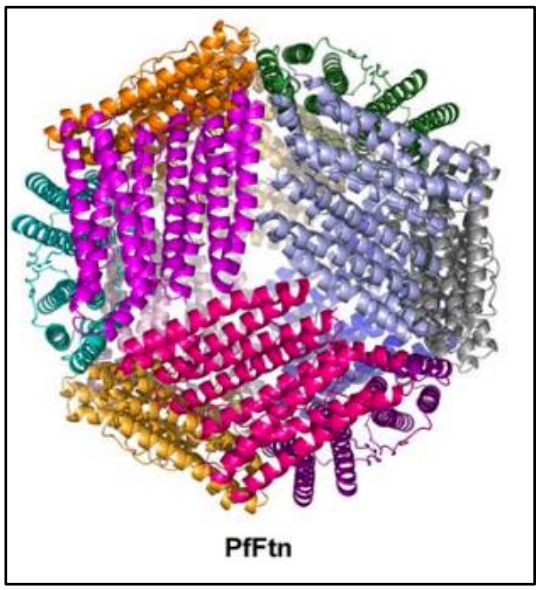

Figure 1.35: Crystal structure of ferritin from *P. furiosus*, extracted from[133]. The 24 monomers form a nanocage.

In the laboratory[135], previous worked have been made with extracted ferritin from *P. furiosus*. Using recombinant DNA techniques, the gene of ferritin was expressed in *E. coli.* After over-production of ferritins, the proteins were purified and mineralized *in vitro* under controlled

conditions (65°C, pH 8.5); the magnetic attraction of ferritins was tested using permanent magnets. In **figure 1.36** is displayed a transmission electron micrograph of the *in vitro* mineralized ferritins.

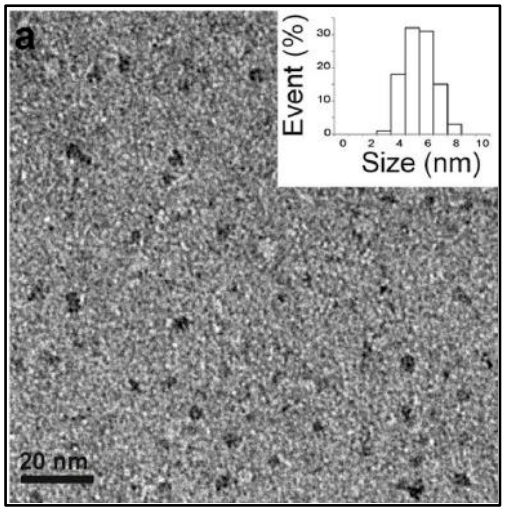

Figure 1.36: Transmission electron micrograph of mineralized ferritins, extracted from[135]. The iron oxides are visible in black.

Hence, ferritin was a natural candidate to create genetically encoded magnetic nanoparticles. Over-expression of ferritin was used as a strategy to try to develop microbes with magnetic properties. I will present several examples here.

First, the team of P. Silver[136] has discovered that yeasts, which do not have ferritins, store iron in their vacuoles. By changing their physiology (by adding iron II and iron III to the growing medium) yeasts could internalize iron, and phosphorous in their vacuoles. Magnetization assays revealed that the yeasts might have stored paramagnetic or superamagnetic material mixed with a few ferro-ferrimagnetic particles. They further cloned the ferritin genes inside yeasts to have an over-production of ferritin. Upon the same physiological conditions, upon iron addition, this resulted in an increase of magnetic signal by 2-3 times (concerning the magnetic susceptibility assays).

To continue with the idea of encoding ferritin into microorganisms to enhance the formation of magnetic crystals, P. Silver and coworkers used directed evolution to get "magnetic" bacteria[137]. They used a library of bacterial ferritin (FtnA) mutant in *E. coli*. They selected the best ferritin-over-expressing mutants: they applied several rounds of magnetic sorting in magnetic columns, in order to get the most "magnetic" strains. They confirmed their selection with magnetometry and found that the best mutants displayed a paramagnetic contribution. These mutant bacteria were attracted toward a magnet in liquid medium (**Fig. 1.37**). They also found that they were able to

grow with less defect in presence of toxic ions (Co, Ni, Cd, As), maybe because the iron sequestration into the ferritins led to the inclusion of toxic ions inside the mineral core, thus reducing the toxic effects.

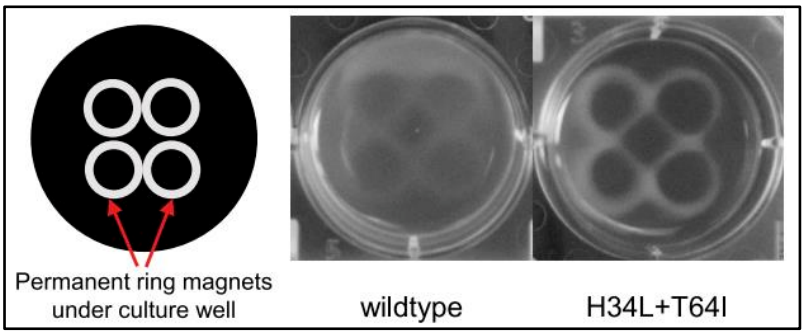

Figure 1.37: Magnetic *E. coli* attracted by permanent ring magnet, extracted from[137]. On the left-picture: wild type bacteria. On the right-picture: the mutant *E. coli* that presents magnetic properties.

Another study screened various mutant of ferritin (from *Pyrococcus furiosus*) to obtain magnetic sensing yeasts[138]. They generated a library of 10^7 ferritin mutants in yeast and selected the most paramagnetic ones (by directed evolution techniques). They sorted them with magnets placed around columns, and the selected mutants displayed a signal in MRI (they could be good contrast agent). Next, they engineered the ferritin to make them express streptavidin-tag. They added a gene coding for the expression of streptavidin tetramer. The gene was regulated by an inducible galactose promoter. When galactose was in the yeast environment, the tetramers of streptavidin were synthesized and linked to the ferritin nanocages. This resulted in an aggregation of ferritins, enhancing the T_2 relaxation rate and changing the contrast in MRI, the reporter signal (**Fig. 1.38**). Thus these magnetic yeasts were a kind of whole-cell biosensors for galactose presence.

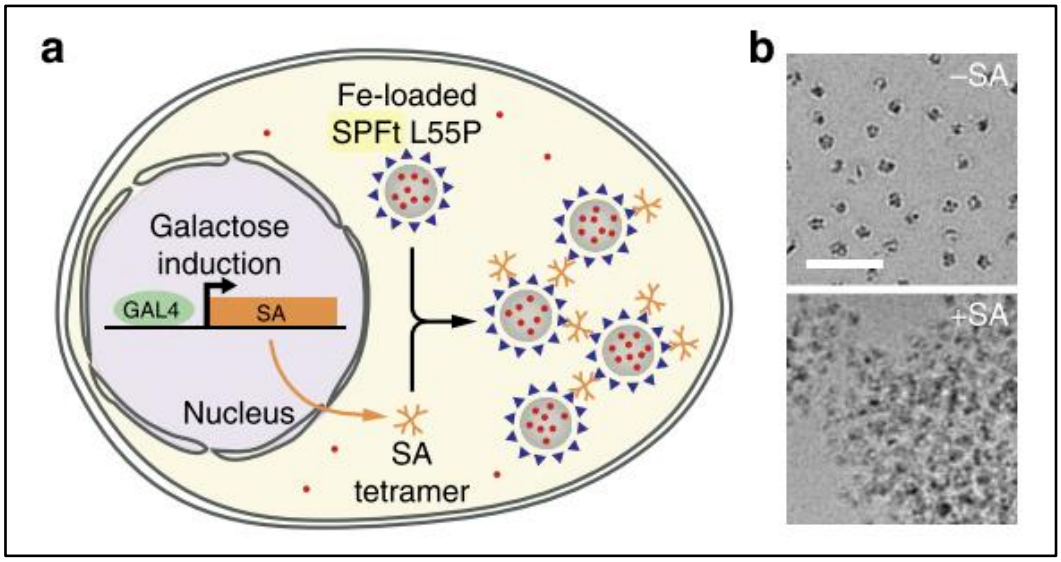

Figure 1.38: Engineered yeast that display mineralized ferritin, streptavidin tetramer upon galactose sensing, that could be biosensor, extracted from[138]. (A) The plasmid used in yeast. **(B)** Cryo-ectron micrograph displaying the aggregation that occurs in presence of streptavidin tetramers (SA).

Finally, other methods, which are not based on ferritin, are employed to give magnetic properties. A recent article[139] studied the possibility to get paramagnetic bacteria with a synthetic construct based on 3 genes: a ferrous ion transporter (to utpake iron from the medium), a ferroxidase, and a magnetite nucleating peptide (to help synthesize the magnetic crystals) (**Fig. 1.39**).

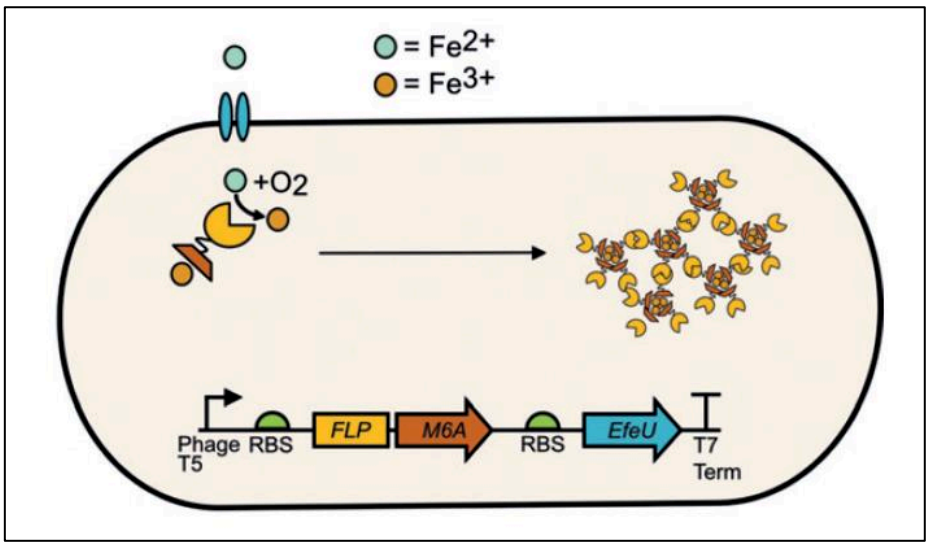

Figure 1.39: The genes used to create other types of paramagnetic *E. coli*, extracted from[139]. Iron II enters into bacteria thanks a ferrous iron transporter coded by *EfeU*. It is oxidized and incorporated in macromolecular structures with the ferroxidase, coded by *FLP*, and the magnetite nucleating peptide, coded by *M6A*.

They compared their construct with ferritin-expressing *E. coli*. When adding iron to their modified *E. coli* they created paramagnetic cells, which were attracted toward permanent magnets. Their bacteria were more paramagnetic that those with bacterial ferritin as checked by magnetometry measurements. That is why they qualified their system as "ultraparamagnetic". Finally, as the chassis was a *Nissle* strain, compatible with *in vivo* experiments in gut, they orally administered their *E. coli* to mice. They showed that the *E. coli* were visible on MRI, thanks to their effect on the T_2. They could even extract the magnetic bacteria from the feces (**Fig. 1.40**).

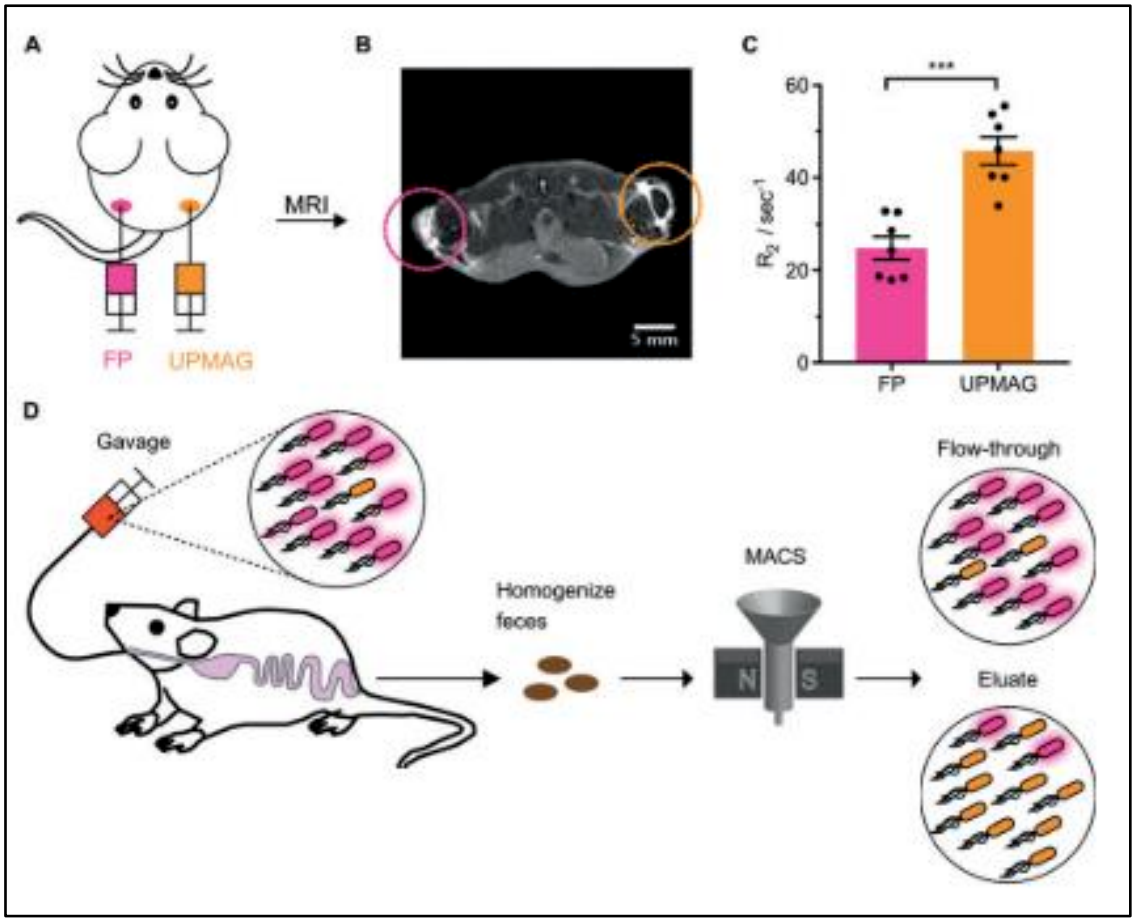

Figure 1.40: Ultraparamagnetic bacteria (UPMAG) administered to mice, as well as a fluorescent control (FP), extracted from[139]. (A) Schematic of an MRI assay: fluorescent bacteria or magnetic ones are injected in mice. **(B)** MRI in a mouse. **(C)** Relaxation rates obtained for FP and UPMAG in mice. **(D)** Experiment in mice. Fluorescent and magnetic bacteria are orally delivered into a mouse. The feces are collected and flowed through a column covered by a magnet. The flowthrough contained mainly fluorescent control bacteria whereas the eluates retained on the magnet got mostly the magnetic bacteria.

In fact, using paramagnetic bacteria in the perspective of *in vivo* therapeutic or sensing application could be of great interest, especially because magnetic microbes have an effect on the T_2 and could be good contrast agents. Another team used the same strain, *E. coli Nissle,* which

colonize preferentially tumor regions, and genetically transformed them to make them overexpress ferritin[140]. They obtained a better contrast for tumor regions in MRI with the help of these bacteria, after 24 hours, due to a natural incorporation of iron from cancer cells (tumor regions being iron-enriched areas).

1.5 – References

1. Waites, K. B. & Talkington, D. F. Mycoplasma pneumoniae and its role as a human pathogen. *Clin. Microbiol. Rev.* **17**, 697–728 (2004).
2. Schulz, H. N. *et al.* Dense populations of a giant sulfur bacterium in namibian shelf sediments. *Science (80-.).* **284**, 493–495 (1999).
3. Waksman, S. A., Joffre, J. S. Microorganisms concerned in the oxidation of sulfur in the soil: III. Media used for the isolation of sulfur bacteria from the soil. *J. Bacteriol.* **7**, 239–256 (1922).
4. Kado, C. I. Historical account on gaining insights on the mechanism of crown gall tumorigenesis induced by Agrobacterium tumefaciens. *Front. Microbiol.* **5**, 1–15 (2014).
5. Tory A., H. *et al.* Ongoing Transposon-Mediated Genome Reduction in the Luminous Bacterial Symbionts of Deep-Sea Ceratioid Anglerfishe. *Am. Soc. Microbiol.* **9**, 1–16 (2018).
6. Aita, B. C. *et al.* Biofiltration of H2S-rich biogas using Acidithiobacillus thiooxidans. *Clean Technol. Environ. Policy* **18**, 689–703 (2016).
7. Das, A. P., Sukla, L. B., Pradhan, N. & Nayak, S. Manganese biomining: A review. *Bioresour. Technol.* **102**, 7381–7387 (2011).
8. Hooykaas, P. J. J. & Schilperoort, R. A. Agrobacterium and plant genetic engineering. *Plant Mol. Biol.* **19**, 15–38 (1992).
9. Cameron, D. E., Bashor, C. J. & Collins, J. J. A brief history of synthetic biology. *Nat. Rev. Microbiol.* **12**, 381–390 (2014).
10. Jacob, F. & Monod, J. Genetic regulatory mechanisms in the synthesis of proteins. *J. Mol. Biol.* **3**, 318–356 (1961).
11. Cohen, S. N., Chang, A. C. Y., Boyer, H. W. & Helling, R. B. Construction of biologically functional bacterial plasmids in vitro. *Proc. Natl. Acad. Sci. U. S. A.* **70**, 3240–3244 (1973).
12. Bruggeman, F. J. & Westerhoff, H. V. The nature of systems biology. *Trends Microbiol.* **15**, 45–50 (2007).
13. Maung, N. W. & Smolke, C. D. Higher-order cellular information processing with synthetic RNA devices. *Science (80-.).* **322**, 456–460 (2008).
14. Elowitz, M. B. & Leibler, S. A synthetic oscillatory network of transcriptional regulators. *Nature* **403**, 335–338 (2000).
15. Gardner, T. S., Cantor, C. R. & Collins, J. J. Construction of a genetic toggle switch in Escherichia coli. *Nature* **403**, 339–342 (2000).
16. Stricker, J. *et al.* A fast, robust and tunable synthetic gene oscillator. *Nature* **456**, 516–519 (2008).

17. Nielsen, J. Metabolic engineering. *Appl. Microbiol. Biotechnol.* **55**, 263–283 (2001).
18. Packer, M. S. & Liu, D. R. Methods for the directed evolution of proteins. *Nat. Rev. Genet.* **16**, 379–394 (2015).
19. Chang, P. V., Prescher, J. A., Hangauer, M. J. & Bertozzi, C. R. Imaging cell surface glycans with bioorthogonal chemical reporters. *J. Am. Chem. Soc.* **129**, 8400–8401 (2007).
20. Laughlin, S. T., Baskin, J. M., Amacher, S. L. & Bertozzi, C. R. In Vivo Imaging of Membrane-Associated Glycans in Developing Zebrafish. *Science (80-.).* **320**, 664–667 (2008).
21. Stanton, M. M. & Sanchez, S. Pushing bacterial biohybrids to in vivo applications. *Trends Biotechnol.* **35**, 910–913 (2017).
22. El Karoui, M., Hoyos-Flight, M. & Fletcher, L. Future trends in synthetic biology—a report. *Front. Bioeng. Biotechnol.* **7**, 1–8 (2019).
23. Berg, P. *et al.* Potential Biohazards of Recombinant DNA Molecules. *Am. Assoc. Adv. Sci.* **185**, 303 (1974).
24. Bej, A. K., Perlin, M. H. & Atlas, R. M. Model suicide vector for containment of genetically engineered microorganisms. *Appl. Environ. Microbiol.* **54**, 2472–2477 (1988).
25. Rosano, G. L. & Ceccarelli, E. A. Recombinant protein expression in Escherichia coli: Advances and challenges. *Front. Microbiol.* **5**, 1–17 (2014).
26. Cleary, P. P. & Englesberg, E. Transcriptional control in the L-arabinose operon of Escherichia coli B/r. *J. Bacteriol.* **118**, 121–128 (1974).
27. Cho, S. A., Scharpf, S., Franko, M. & Vermeulen, C. W. Effect of iso-propyl-thio-β-D-galactoside concentration on the level of lac-operon induction in steady state Escherichia coli. *Biochem. Biophys. Res. Commun.* **128**, 1268–1273 (1985).
28. Schmitt, J., Hess, H. & Stunnenberg, H. G. Affinity purification of histidine-tagged proteins. *Mol. Biol. Rep.* **18**, 223–230 (1993).
29. Villaverde, A. & Carrio, M. M. Protein aggregation in recombinant bacteria: biological role of inclusion bodies. *Biotechnol. Lett.* **25**, 1385–1395 (2003).
30. Jang, B. & Ahn, Y. J. Enhanced recombinant insulin production in transgenic Escherichia coli that heterologously expresses carrot heat shock protein 70. *Biocatal. Agric. Biotechnol.* **20**, 101180 (2019).
31. Baeshen, N. A. *et al.* Cell factories for insulin production. *Microb. Cell Fact.* **13**, 1–9 (2014).
32. Hazelwood, L. A., Daran, J. M., Van Maris, A. J. A., Pronk, J. T. & Dickinson, J. R. The Ehrlich pathway for fusel alcohol production: A century of research on Saccharomyces cerevisiae metabolism. *Appl. Environ. Microbiol.* **74**, 2259–2266 (2008).
33. Atsumi, S., Hanai, T. & Liao, J. C. Non-fermentative pathways for synthesis of branched-

chain higher alcohols as biofuels. *Nature* **451**, 86–89 (2008).

34. Biggs, B. W. *et al.* Overcoming heterologous protein interdependency to optimize P450-mediated Taxol precursor synthesis in Escherichia coli. *Proc. Natl. Acad. Sci. U. S. A.* **113**, 3209–3214 (2016).
35. Paddon, C. J. & Keasling, J. D. Semi-synthetic artemisinin: A model for the use of synthetic biology in pharmaceutical development. *Nat. Rev. Microbiol.* **12**, 355–367 (2014).
36. Paddon, C. J. *et al.* High-level semi-synthetic production of the potent antimalarial artemisinin. *Nature* **496**, 528–532 (2013).
37. Tsouko, E. *et al.* Bacterial cellulose production from industrial waste and by-product streams. *Int. J. Mol. Sci.* **16**, 14832–14849 (2015).
38. Florea, M. *et al.* Engineering control of bacterial cellulose production using a genetic toolkit and a new celluloseproducing strain. *Proc. Natl. Acad. Sci. U. S. A.* **113**, E3431–E3440 (2016).
39. Klaus-Joerger, T., Joerger, R., Olsson, E. & Granqvist, C. G. Bacteria as workers in the living factory: Metal-accumulating bacteria and their potential for materials science. *Trends Biotechnol.* **19**, 15–20 (2001).
40. Sondi, I. & Salopek-Sondi, B. Silver nanoparticles as antimicrobial agent: A case study on E. coli as a model for Gram-negative bacteria. *J. Colloid Interface Sci.* **275**, 177–182 (2004).
41. Slawson, R. M., Lee, H. & Trevors, J. T. Bacterial interaction with silvers. 151–154 (1990).
42. Kowshik, M. *et al.* Extracellular synthesis of silver nanoparticles by a silver-tolerant yeast strain MKY3. *Nanotechnology* **14**, 95–100 (2002).
43. Gericke, M. & Pinches, A. Biological synthesis of metal nanoparticles. *Hydrometallurgy* **83**, 132–140 (2006).
44. Park, T. J., Lee, S. Y., Heo, N. S. & Seo, T. S. In vivo synthesis of diverse metal nanoparticles by recombinant escherichia coli. *Angew. Chemie - Int. Ed.* **49**, 7019–7024 (2010).
45. Van de Walle, A., Kolosnjaj-Tabi, J., Lalatonne, Y. & Wilhelm, C. Ever-Evolving Identity of Magnetic Nanoparticles within Human Cells: The Interplay of Endosomal Confinement, Degradation, Storage, and Neocrystallization. *Acc. Chem. Res.* (2020). doi:10.1021/acs.accounts.0c00355
46. Chang, H. J., Voyvodic, P. L., Zúñiga, A. & Bonnet, J. Microbially derived biosensors for diagnosis, monitoring and epidemiology. *Microb. Biotechnol.* **10**, 1031–1035 (2017).
47. Inda, M. E. & Lu, T. Microbes as Biosensors. *Annu. Rev. Microbiol.* **74**, 337–359 (2020).
48. Sørensen, S. J., Burmølle, M. & Hansen, L. H. Making bio-sense of toxicity: New developments in whole-cell biosensors. *Curr. Opin. Biotechnol.* **17**, 11–16 (2006).
49. Raut, N., O'Connor, G., Pasini, P. & Daunert, S. Engineered cells as biosensing systems in

biomedical analysis. *Anal. Bioanal. Chem.* **402**, 3147–3159 (2012).

50. Tauriainen, S., Karp, M., Chang, W. & Virta, M. Luminescent bacterial sensor for cadmium and lead. *Biosens. Bioelectron.* **13**, 931–938 (1998).
51. Park, M., Tsai, S. L. & Chen, W. Microbial biosensors: Engineered microorganisms as the sensing machinery. *Sensors* **13**, 5777–5795 (2013).
52. Waters, C. M. & Bassler, B. L. Quorum Sensing: Cell-to-Cell Communication in Bacteria. *Annu. Rev. Cell Dev. Biol.* **21**, 319–346 (2005).
53. Bassler, B. L. How bacteria talk to each other: Regulation of gene expression by quorum sensing. *Curr. Opin. Microbiol.* **2**, 582–587 (1999).
54. Ng, W.-L. & Bassler, B. L. Bacterial Quorum-Sensing Network Architectures. *Annu. Rev. Genet.* **43**, 197–222 (2009).
55. Choudhary, S. & Schmidt-Dannert, C. Applications of quorum sensing in biotechnology. *Appl. Microbiol. Biotechnol.* **86**, 1267–1279 (2010).
56. Kylilis, N., Tuza, Z. A., Stan, G. B. & Polizzi, K. M. Tools for engineering coordinated system behaviour in synthetic microbial consortia. *Nat. Commun.* **9**, (2018).
57. Struss, A., Pasini, P., Ensor, C. M., Raut, N. & Daunert, S. Paper strip whole cell biosensors: A portable test for the semiquantitative detection of bacterial quorum signaling molecules. *Anal. Chem.* **82**, 4457–4463 (2010).
58. Hsu, C. Y., Chen, B. K., Hu, R. H. & Chen, B. Sen. Systematic Design of a Quorum Sensing-Based Biosensor for Enhanced Detection of Metal Ion in Escherichia coli. *IEEE Trans. Biomed. Circuits Syst.* **10**, 593–601 (2016).
59. Kylilis, N. *et al.* Whole-cell biosensor with tunable limit of detection enables low-cost agglutination assays for medical diagnostic applications. *ACS Sensors* **4**, 370–378 (2019).
60. Forbes, N. S. Engineering the perfect (bacterial) cancer therapy. *Nat. Rev. Cancer* **10**, 785–794 (2010).
61. Danino, T. *et al.* Programmable probiotics for detection of cancer in urine. *Sci. Transl. Med.* **7**, (2015).
62. Mimee, M. *et al.* An ingestible bacterial-electronic system to monitor gastrointestinal health. *Science (80-.).* **360**, 915–918 (2018).
63. Yoo, J. W., Irvine, D. J., Discher, D. E. & Mitragotri, S. Bio-inspired, bioengineered and biomimetic drug delivery carriers. *Nat. Rev. Drug Discov.* **10**, 521–535 (2011).
64. Din, M. O. *et al.* Synchronized cycles of bacterial lysis for in vivo delivery. *Nature* **536**, 81–85 (2016).
65. Praveschotinunt, P. *et al.* Engineered E. coli Nissle 1917 for the delivery of matrix-tethered therapeutic domains to the gut. *Nat. Commun.* **10**, (2019).

66. Park, S. J. *et al.* New paradigm for tumor theranostic methodology using bacteria-based microrobot. *Sci. Rep.* **3**, 1–8 (2013).
67. Hosseinidoust, Z. *et al.* Bioengineered and biohybrid bacteria-based systems for drug delivery. *Adv. Drug Deliv. Rev.* **106**, 27–44 (2016).
68. Kojima, M., Zhang, Z., Nakajima, M., Ooe, K. & Fukuda, T. Construction and evaluation of bacteria-driven liposome. *Sensors Actuators, B Chem.* **183**, 395–400 (2013).
69. Alapan, Y. *et al.* Soft erythrocyte-based bacterial microswimmers for cargo delivery. *Sci. Robot.* **3**, (2018).
70. Buss, N., Yasa, O., Alapan, Y., Akolpoglu, M. B. & Sitti, M. Nanoerythrosome-functionalized biohybrid microswimmers Nanoerythrosome-functionalized biohybrid microswimmers. **026103**, (2020).
71. Gupta, S., Bram, E. E. & Weiss, R. Genetically programmable pathogen sense and destroy. *ACS Synth. Biol.* **2**, 715–723 (2013).
72. Saeidi, N. *et al.* Engineering microbes to sense and eradicate Pseudomonas aeruginosa, a human pathogen. *Mol. Syst. Biol.* **7**, 1–11 (2011).
73. Riglar, D. T. & Silver, P. A. Engineering bacteria for diagnostic and therapeutic applications. *Nat. Rev. Microbiol.* **16**, 214–225 (2018).
74. Williams, B. J., Anand, S. V., Rajagopalan, J. & Saif, M. T. A. A self-propelled biohybrid swimmer at low Reynolds number. *Nat. Commun.* **5**, 1–8 (2014).
75. Huang, H. W., Sakar, M. S., Petruska, A. J., Pané, S. & Nelson, B. J. Soft micromachines with programmable motility and morphology. *Nat. Commun.* **7**, 1–10 (2016).
76. Stanton, M. M. *et al.* Biohybrid Microtube Swimmers Driven by Single Captured Bacteria. *Small* **13**, 1–10 (2017).
77. Besemer, K. Biodiversity, community structure and function of biofilms in stream ecosystems. *Res. Microbiol.* **166**, 774–781 (2016).
78. Glass, D. S. & Riedel-Kruse, I. H. A Synthetic Bacterial Cell-Cell Adhesion Toolbox for Programming Multicellular Morphologies and Patterns. *Cell* **174**, 649–658 (2018).
79. Piñero-Lambea, C. *et al.* Programming controlled adhesion of E. coli to target surfaces, cells, and tumors with synthetic adhesins. *ACS Synth. Biol.* **4**, 463–473 (2014).
80. Lewis, D. D. *et al.* Engineered Stochastic Adhesion Between Microbes as a Protection Mechanism Against Environmental Stress. *Cell. Mol. Bioeng.* **11**, 367–382 (2018).
81. Isberg, R. R., Voorhis, D. L. & Falkow, S. Identification of invasin: A protein that allows enteric bacteria to penetrate cultured mammalian cells. *Cell* **50**, 769–778 (1987).
82. Isberg, R. R. & Falkow, S. A single genetic locus encoded by Yersinia pseudotuberculosis permits invasion of cultured animal cells by Escherichia coli K-12. *J. Chem. Inf. Model.* **317**,

262–264 (1985).

83. Anderson, J. C., Clarke, E. J., Arkin, A. P. & Voigt, C. A. Environmentally controlled invasion of cancer cells by engineered bacteria. *J. Mol. Biol.* **355**, 619–627 (2006).
84. Kong, W., Celik, V., Liao, C., Hua, Q. & Lu, T. Programming the group behaviors of bacterial communities with synthetic cellular communication. *Bioresour. Bioprocess.* **1**, 1–11 (2014).
85. Scott, S. R. *et al.* A stabilized microbial ecosystem of self-limiting bacteria using synthetic quorum-regulated lysis. *Nat. Microbiol.* **2**, (2017).
86. Boehm, C. R., Grant, P. K. & Haseloff, J. Programmed hierarchical patterning of bacterial populations. *Nat. Commun.* **9**, 1–10 (2018).
87. Kim, J. K. *et al.* Long-range temporal coordination of gene expression in synthetic microbial consortia. *Nat. Chem. Biol.* **15**, 1102–1109 (2019).
88. Karig, D. *et al.* Stochastic Turing patterns in a synthetic bacterial population. *Proc. Natl. Acad. Sci. U. S. A.* **115**, 6572–6577 (2018).
89. Ma, Y. *et al.* Synthetic mammalian signaling circuits for robust cell population control. 1–39 (2020).
90. Zheng, D. W. *et al.* Optically-controlled bacterial metabolite for cancer therapy. *Nat. Commun.* **9**, 1–12 (2018).
91. Shapiro, M. G. *et al.* Biogenic gas nanostructures as ultrasonic molecular reporters. *Nat. Nanotechnol.* **9**, 311–316 (2014).
92. Bourdeau, R. W. *et al.* Acoustic reporter genes for noninvasive imaging of microorganisms in mammalian hosts. *Nature* **553**, 86–90 (2018).
93. Hallali, N. Utilisation de nanoparticules magnétiques dans les traitements anti-tumoraux : Au-delà de l'hyperthermie magnétique. *PhD Manuscr.* I-4-I–14 (2017).
94. Bataille, A. Etude des propriétés physiques des lms de Fe3O4 épitaxiés et de la polarisation en spin à l ' interface Fe3O4 / γ-Al2O3. *PhD Manuscr.* 8–10 (2005).
95. Li, Q. *et al.* Correlation between particle size/domain structure and magnetic properties of highly crystalline Fe3O4 nanoparticles. *Sci. Rep.* **7**, 1–4 (2017).
96. Fortin, J. P. *et al.* Size-sorted anionic iron oxide nanomagnets as colloidal mediators for magnetic hyperthermia. *J. Am. Chem. Soc.* **129**, 2628–2635 (2007).
97. Putman, N. F. *et al.* Evidence for geomagnetic imprinting as a homing mechanism in pacific salmon. *Curr. Biol.* **23**, 312–316 (2013).
98. Blakemore, R. P., Maratea, D. & Wolfe, R. S. Isolation and pure culture of a freshwater magnetic spirillum in chemically defined medium. *J. Bacteriol.* **140**, 720–729 (1979).
99. Frankel, R. B. & Bazylinski, D. A. Magnetotaxis and magnetic particles in bacteria.

Hyperfine Interact. **90**, 135–142 (1994).

100. Xie, J., Chen, K. & Chen, X. Production, modification and bio-applications of magnetic nanoparticles gestated by magnetotactic bacteria. *Nano Res.* **2**, 261–278 (2009).
101. Fischer, A., Schmitz, M., Aichmayer, B., Fratzl, P. & Faivre, D. Structural purity of magnetite nanoparticles in magnetotactic bacteria. *J. R. Soc. Interface* **8**, 1011–1018 (2011).
102. Taoka, A., Umeyama, C. & Fukumori, Y. Identification of iron transporters expressed in the magnetotactic bacterium Magnetospirillum magnetotacticum. *Curr. Microbiol.* **58**, 177–181 (2008).
103. Schüler, D. Formation of magnetosomes in magnetotactic bacteria. *J. Mol. Microbiol. Biotechnol.* **1**, 79–86 (1999).
104. Frankel, R. B., Papaefthymiou, G. C., Blakemore, R. P. & O'Brien, W. Fe3O4 precipitation in magnetotactic bacteria. *BBA* **763**, 147–159 (1983).
105. Schuler, D. & Baeuerlein, E. Dynamics of iron uptake and Fe3O4 biomineralization during aerobic and microaerobic growth of Magnetospirillum gryphiswaldense. *J. Bacteriol.* **180**, 159–162 (1998).
106. Baumgartner, J. *et al.* Magnetotactic bacteria form magnetite from a phosphate-rich ferric hydroxide via nanometric ferric (oxyhydr)oxide intermediates. *Proc. Natl. Acad. Sci. U. S. A.* **110**, 14883–14888 (2013).
107. Faivre, D. & Schüler, D. Magnetotactic bacteria and magnetosomes. *Chem. Rev.* **108**, 4875–4898 (2008).
108. Lohße, A. *et al.* Genetic dissection of the mamAB and mms6 operons reveals a gene set essential for magnetosome biogenesis in magnetospirillum gryphiswaldense. *J. Bacteriol.* **196**, 2658–2669 (2014).
109. Scheffel, A. *et al.* An acidic protein aligns magnetosomes along a filamentous structure in magnetotactic bacteria. *Nature* **440**, 110–114 (2006).
110. Vargas, G. *et al.* Applications of magnetotactic bacteria, magnetosomes and magnetosome crystals in biotechnology and nanotechnology: mini-review. *Molecules* **23**, 1–25 (2018).
111. Jacob, J. J. & Suthindhiran, K. Magnetotactic bacteria and magnetosomes – Scope and challenges. *Mater. Sci. Eng. C* **68**, 919–928 (2016).
112. Alphandéry, E., Faure, S., Seksek, O., Guyot, F. & Chebbi, I. Chains of magnetosomes extracted from AMB-1 magnetotactic bacteria for application in alternative magnetic field cancer therapy. *ACS Nano* **5**, 6279–6296 (2011).
113. Roda, A. *et al.* Bioengineered bioluminescent magnetotactic bacteria as a powerful tool for chip-based whole-cell biosensors. *Lab Chip* **13**, 4881–4889 (2013).
114. Kolinko, I. *et al.* Biosynthesis of magnetic nanostructures in a foreign organism by transfer

of bacterial magnetosome gene clusters. *Nat. Nanotechnol.* **9**, 193–197 (2014).

115. Carlsen, R. W., Edwards, M. R., Zhuang, J., Pacoret, C. & Sitti, M. Magnetic steering control of multi-cellular bio-hybrid microswimmers. *Lab Chip* **14**, 3850–3859 (2014).
116. Magdanz, V., Sanchez, S. & Schmidt, O. G. Development of a sperm-flagella driven micro-bio-robot. *Adv. Mater.* **25**, 6581–6588 (2013).
117. Kim, D. H., Cheang, U. K., Khidai, L., Byun, D. & Kim, M. J. Artificial magnetotactic motion control of Tetrahymena pyriformis using ferromagnetic nanoparticles: A tool for fabrication of microbiorobots. *Appl. Phys. Lett.* **97**, (2010).
118. Park, B. W., Zhuang, J., Yasa, O. & Sitti, M. Multifunctional Bacteria-Driven Microswimmers for Targeted Active Drug Delivery. *ACS Nano* **11**, 8910–8923 (2017).
119. Felfoul, O. *et al.* Magneto-aerotactic bacteria deliver drug-containing nanoliposomes to tumour hypoxic regions. *Nat. Nanotechnol.* **11**, 941–947 (2016).
120. Stanton, M. M. *et al.* Magnetotactic Bacteria Powered Biohybrids Target E. coli Biofilms. *ACS Nano* **11**, 9968–9978 (2017).
121. Chen, C. *et al.* Bacterial magnetic nanoparticles for photothermal therapy of cancer under the guidance of MRI. *Biomaterials* **104**, 352–360 (2016).
122. Yan, X. *et al.* Multifunctional biohybrid magnetite microrobots for imaging-guided therapy. *Sci. Robot.* **2**, 1–15 (2017).
123. Pamme, N. & Wilhelm, C. Continuous sorting of magnetic cells via on-chip free-flow magnetophoresis. *Lab Chip* **6**, 974–980 (2006).
124. He, D. & Marles-Wright, J. Ferritin family proteins and their use in bionanotechnology. *N. Biotechnol.* **32**, 651–657 (2015).
125. Arosio, P., Elia, L. & Poli, M. Ferritin, cellular iron storage and regulation. *IUBMB Life* **69**, 414–422 (2017).
126. Hilton, R. J., Andros, N. D. & Watt, R. K. The ferroxidase center is essential for ferritin iron loading in the presence of phosphate and minimizes side reactions that form Fe(III)-phosphate colloids. *BioMetals* **25**, 259–273 (2012).
127. Honarmand Ebrahimi, K., Bill, E., Hagedoorn, P. L. & Hagen, W. R. The catalytic center of ferritin regulates iron storage via Fe(II)-Fe(III) displacement. *Nat. Chem. Biol.* **8**, 941–948 (2012).
128. Le Brun, N. E., Crow, A., Murphy, M. E. P., Mauk, A. G. & Moore, G. R. Iron core mineralisation in prokaryotic ferritins. *Biochim. Biophys. Acta - Gen. Subj.* **1800**, 732–744 (2010).
129. Hu, L. L. *et al.* Comparison of the 1H NMR relaxation enhancement produced by bacterial magnetosomes and synthetic iron oxide nanoparticles for potential use as MR molecular

probes. *IEEE Trans. Appl. Supercond.* **20**, 822–825 (2010).

130. Uchida, M. *et al.* A human ferritin iron oxide nano-composite magnetic resonance contrast agent. *Magn. Reson. Med.* **60**, 1073–1081 (2008).
131. Truffi, M. *et al.* Ferritin nanocages: A biological platform for drug delivery, imaging and theranostics in cancer. *Pharmacol. Res.* **107**, 57–65 (2016).
132. Chiou, B. & Connor, J. R. Emerging and dynamic biomedical uses of ferritin. *Pharmaceuticals* **11**, (2018).
133. Tatur, J., Hagen, W. R. & Matias, P. M. Crystal structure of the ferritin from the hyperthermophilic archaeal anaerobe Pyrococcus furiosus. *J. Biol. Inorg. Chem.* **12**, 615–630 (2007).
134. Xue, L., Deng, D. & Sun, J. Magnetoferritin: Process, Prospects, and Their Biomedical Applications. *Int. J. Mol. Sci.* **20**, (2019).
135. Ducasse, R. *et al.* Programmed Self-Assembly of a Biochemical and Magnetic Scaffold to Trigger and Manipulate Microtubule Structures. *Sci. Rep.* **7**, 1–11 (2017).
136. Nishida, K. & Silver, P. A. Induction of biogenic magnetization and redox control by a component of the target of rapamycin complex 1 signaling pathway. *PLoS Biol.* **10**, (2012).
137. Liu, X. *et al.* Engineering Genetically-Encoded Mineralization and Magnetism via Directed Evolution. *Sci. Rep.* **6**, 1–10 (2016).
138. Matsumoto, Y., Chen, R., Anikeeva, P. & Jasanoff, A. Engineering intracellular biomineralization and biosensing by a magnetic protein. *Nat. Commun.* **6**, (2015).
139. Ramesh, P. *et al.* Ultraparamagnetic Cells Formed through Intracellular Oxidation and Chelation of Paramagnetic Iron. *Angew. Chemie - Int. Ed.* **57**, 12385–12389 (2018).
140. Hill, P. J. *et al.* Magnetic resonance imaging of tumors colonized with bacterial ferritin-expressing Escherichia coli. *PLoS One* **6**, (2011).

[i] https://bch.cbd.int/protocol/
[ii] https://www.gene.com/stories/cloning-insulin
[iii] http://www.leederconsulting.com/toxicology_services_microtox.html

Chapter 2: Engineering *E. coli* for magnetic control and the spatial localization of functions

This section is based on the following article:

Engineering *E. coli* for magnetic control and the spatial localization of functions

Mary Aubry, Wei-An Wang, Yohan Guyodo, Eugénia Delacou, Jean Michel Guignier, Olivier Espeli, Alice Lebreton, François Guyot, Zoher Gueroui

Accepted in *ACS Synthetic Biology*

doi: https://doi.org/10.1021/acssynbio.0c00286

Content

2.1 - Genetic and chemical modifications to magnetize *Escherichia Coli*

With genetic or chemical modifications, as seen in the previous chapters, different properties can be engineered into microorganisms. As magnetic interactions can be contactless, remote controlled, and can deeply penetrate into thick materials, there is a strong interest in using magnetism. Indeed, having magnetic bacteria can give many advantages: bacterial position could be controlled via magnetic forces, bacteria could have a signature in magnetic resonance imaging (MRI), bacteria could be sorted, concentrated, localized in space. As seen in the previous chapter, there are few examples of magnetization of a naturally diamagnetic microorganism by over-expression of iron-storage ferritins or iron-binding proteins inside their cytoplasm and by supplementation in iron the growth medium. These studies showed that mineralized cells contained iron oxide deposits, can be detected using MRI, and can be magnetically sorted.

Yet, if we want to use magnetic microorganisms for biotechnological applications, several questions need to be addressed. It is important to know how magnetic properties are transmitted during cell division or if mineralized microorganisms can be transformed for achieving defined biochemical functions while being magnetically manipulated.

Here, we focused on these genetic and chemical approaches to give *E. coli* magnetic properties. In the following introduction, I will describe in more details our strategy, our experimental flow and the main questions we wanted to address.

2.1.a - Our strategy to obtain magnetic *Escherichia coli*

Our strategy to produce iron-rich inclusions in bacteria relied on a two-step process consisting first in overexpressing fluorescently-labelled ferritins and then supplying Fe (II) to the growth medium to biomineralize the bacteria (**Figure 2.1**).

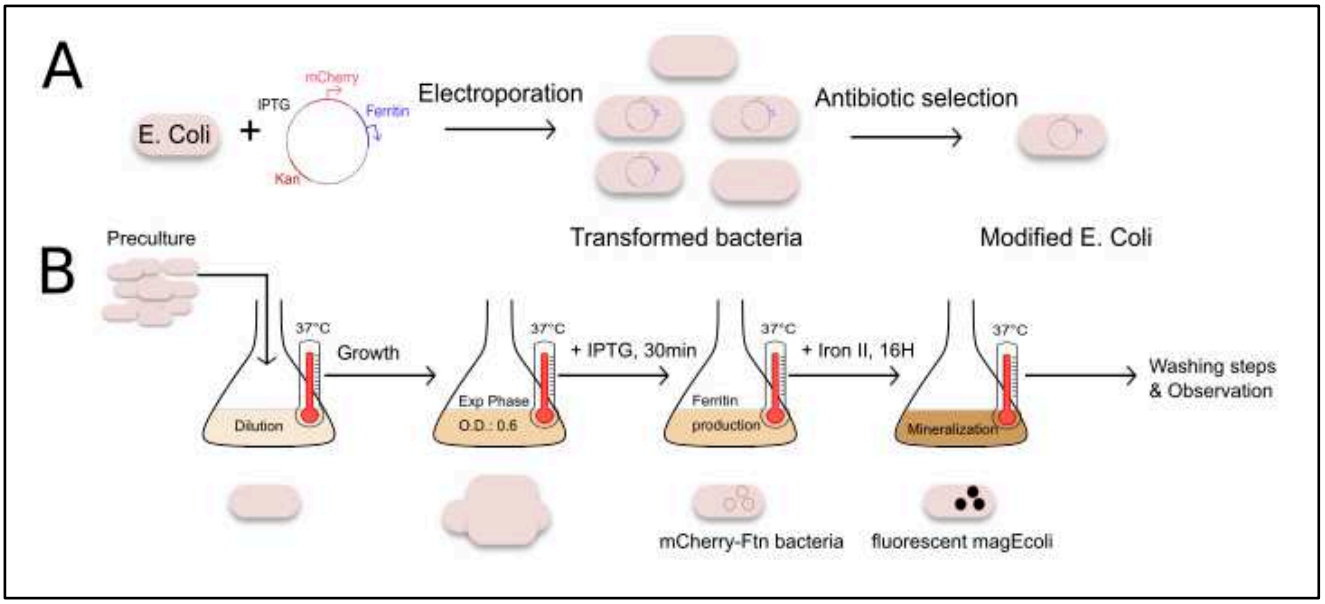

Figure 2.1: Protocol developed to create magnetic *E. coli.* (A) Genetic modifications of the bacteria. Molecular cloning has been performed to obtain a plasmid that bears the gene of ferritin from *P. furiosus*, fused with a fluorescent protein in N-terminal. Via electroporation the plasmid is inserted in *E. coli* and antibiotic selection allows us to maintain the expression of the *ferritin* gene. **(B)** Chemical modification. Modified bacteria are grown in presence of iron II in order to fill the nanocage with magnetic iron oxides.

We chose:

- ***E. coli* as the living organism**: it is robust (it can grow in aerobic or even anaerobic conditions), well-known, and easy-to-handle (with a fast doubling time of around 20 minutes). Thus biochemical and genetic modifications can be performed easily.
- **Ferritin from *P. furiosus* as the iron-storage protein.** *In vitro* assays showed that superparamagnetic nanoparticles like magnetite or maghemite (ferrimagnetic materials) can be synthesized inside the ferritin nanocage[1,2]. Therefore it is a good candidate for *in situ* mineralization. However, *in vivo* biomineralization conditions are different from those *in vitro*. The pH, oxygen fugacity, and temperature are controlled by the bacteria. Thus we are more likely to have a paramagnetic oxide or a superparamagnetic one (like an antiferromagnetic ferrihydrite-like structure) inside the ferritin nanocage instead of pure magnetite. To make the bacteria over-express ferritin, we inserted the *ferritin* gene into a plasmid. This ferritin comes from an archaeon that can live at high temperature[3,4,5] and can store around 2 700 atoms of iron per nanocage[6].
- **mCherry or GFP, fused with *ferritin* gene, to track the level of ferritin production.** We fused the fluorescent protein at the N-terminal extremity of each ferritin monomer. According to the crystal structure of ferritin, the N-terminal extremity points to the exterior of the nanocage during its auto-assembly. Furthermore, previous work performed in the

laboratory showed that mCherry-ferritin or GFP-ferritin led to a monodisperse nanocage which could be mineralized *in vitro*[7].

- **Iron II (Mohr Salt) as the iron source added after induction to biomineralize:** based on the studies of *P. Silver*[8] we decided to add free iron into the growing medium of *E. coli* to induce a biomineralization. Iron III being un-solubilized, we decided to only add iron II. Since the ferritin production was controlled by an IPTG inducible promoter, we decided to add iron 30 minutes after IPTG addition (in order to let bacteria produce some ferritins first)
- **37°C and aerobic conditions:** it is the physiologic conditions of bacterial growth.

2.1.b – Main questions to address

Once we have settled our protocol of biomineralization, several questions rose (**Figure 2.2**).

First, we know that iron can have a negative impact on living cells (oxidative stress due to Fenton effect for example), thus we wondered what the consequences of our mineralization protocol on bacterial growth were. **Can bacteria still grow in presence of iron?** Does ferritin protect bacteria from iron toxicity?

Then, the major questions were related to magnetism. Was our protocol of biomineralization successful? Does over-produced ferritin succeeded in storing iron under a "magnetic" form? **What was the structure of the iron oxides? Their chemical composition? Their structure? Their magnetic properties? Can we attract bacteria with magnetic forces?**

Next, further questions appeared based on the physiology of bacteria themselves. Are the bacteria still alive after biomineralization? Can they grow again and divide? What happens to magnetic properties if they divide? **How magnetic properties are shared between daughter cells?**

Finally, in the idea of using magnetic bacteria for biotechnological applications, we wanted to perform proof-of-concept experiments.

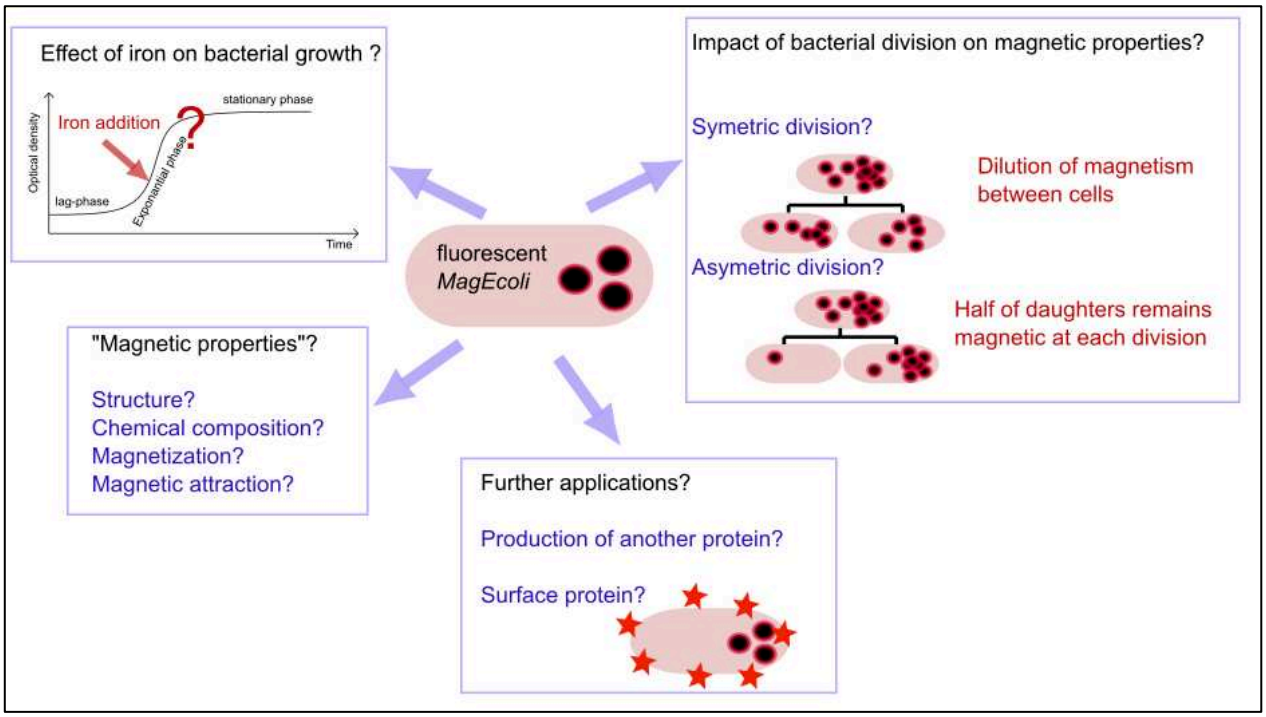

Figure 2.2: Representation of the scientific questions we wanted to address in this chapter. After genetic and chemical modification, we obtain a bacterium, called *MagEcoli*. The first steps are to characterize this system before trying to use it in any proof-of-concept experiment.

2.1.c - Preliminary answer: Effect of iron on bacterial growth during biomineralization

To become magnetic, the modified *E. coli* has to internalize a large amount of iron, in order to create iron oxides in the ferritins. Here the typical concentration of iron II in the growing medium during biomineralization was set to 1 to 4 mM. It is a high dose which might be toxic for bacteria!

For all cells, iron is a vital element that is involved in numerous processes[9]: like DNA repair via iron-requiring proteins[10], or energy production for bacteria. Iron ions can enter in bacteria through various pathways: active ones with specific receptors, siderophores or heam-proteins for instance[11] (see **Fig. 2.3** for the 3 main pathways in Gram-negative bacteria like *E. coli*). Nevertheless, at high dose it can be toxic for bacteria[11–14]. For example, it is responsible for a Fenton effect that triggers oxidative stress in cells mediated by ROS (Reactive Oxygen Species)[15]. To note, different techniques measure the stress in bacteria. Genetic reporters can be designed[16], heat shock proteins[17,18] can be dosed, as well as polyphosphates[19] as they represent a marker of stress. To avoid iron toxicity, its homeostasis is tightly regulated in bacteria by proteins like *fur*[20].

Ferritin can also be a way for bacteria to detoxify its cytoplasm in iron ions, by storing them at the center of the nanocage, under a solid form[11,21,22].

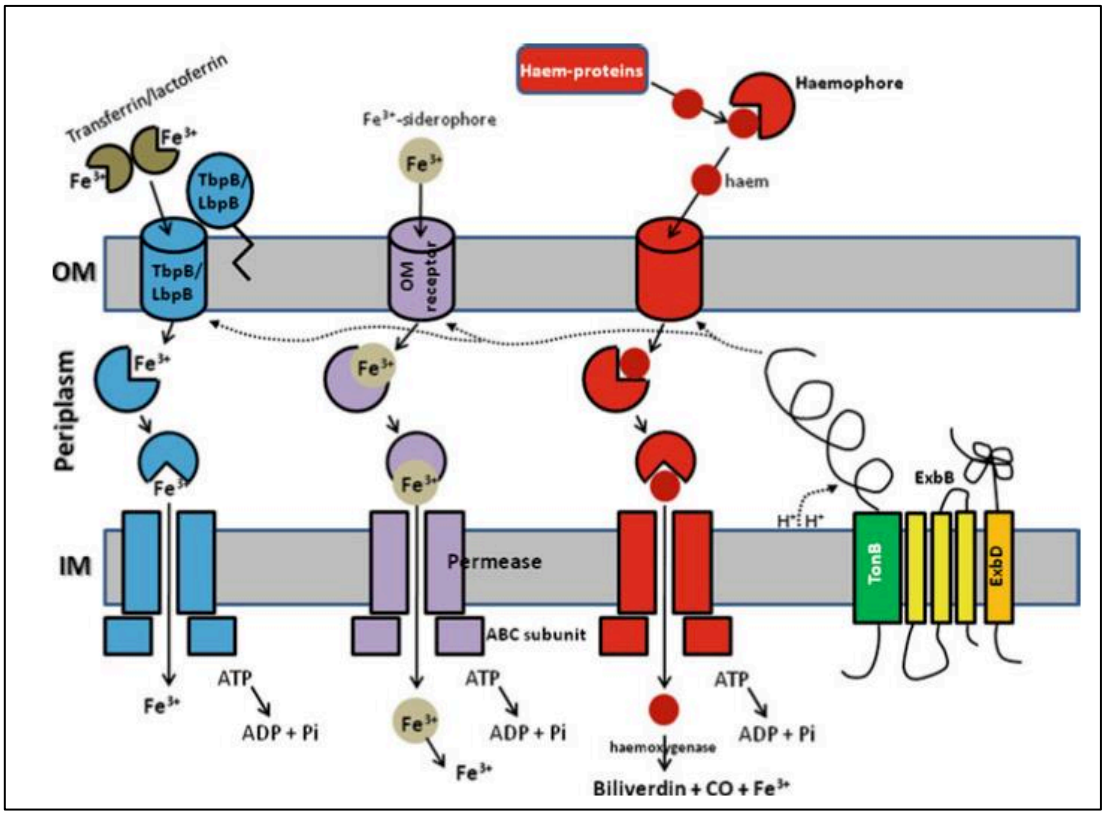

Figure 2.3: The main pathways used by gram-negative bacteria to import iron, extracted from[11].

To examine the impact of iron II on our bacteria, we decided to monitor their growth curve. A normal growth curve of bacteria is constituted of a lag time, followed by an exponential phase and ended by a stationary phase. When bacteria are stressed by the environment or a chemical, their growth speed diminish as well as the Optical Density (O.D.) of their stationary phase. Thus, to monitor the effect of biomineralization on *E. coli* and the advantages of having ferritins on iron-induced toxicity, we observed the growth of bacteria during biomineralization. One of our assays consisted in exposing over-expressing ferritins *E. coli* or *E. coli* that lack endogenous ferritin with different concentrations of iron II (0 to 4 mM) (**Fig. 2.4**). In both cases, bacteria with high concentration of iron (3 or 4 mM) have a lower growth rate. Strikingly, they have a steady state that is situated in lower O.D. This is in agreement with the toxicity provoked by iron in cytoplasm. If we look at the **Figure 2.4**, we can see that the O.D. of bacteria without ferritin at 4 mM totally decreases after 10 hours. This means that without ferritins *E. coli* are more sensitive to iron-induced toxicity. One hypothesis could be that ferritin can indeed detoxify the cytoplasm of free iron II and

reduce the production of reactive oxygen species. To confirm this, it would have been great to observe if there is actually more ROS without ferritin expression.

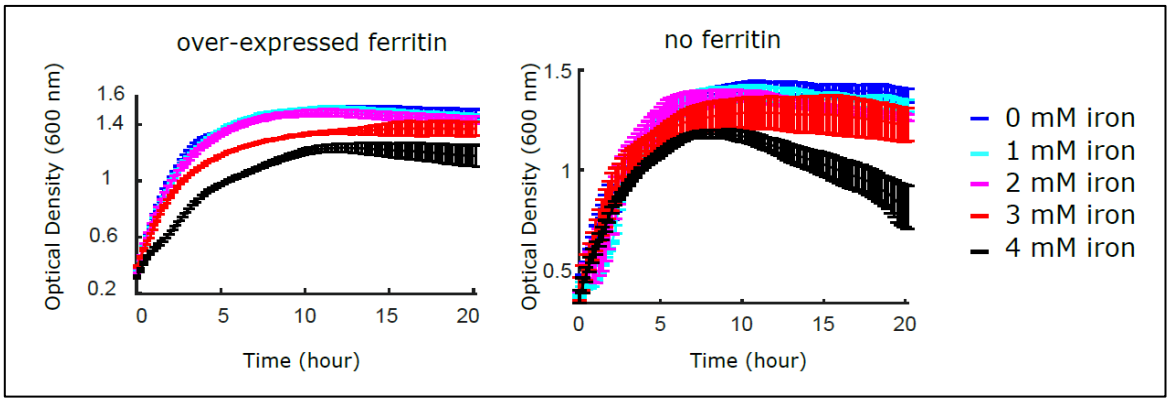

Figure 2.4: growth curves of *E. coli* in presence of various quantities of iron II. On the **left panel:** growth curves of over-expressing ferritin, *E. coli* MG1655 with a constitutive promoter. On the **right panel:** growth curve of *E. coli* MG1655 genetically modified to lack endogenous ferritin.

Methods for this assay:
To make bacteria overproduce ferritin, E. coli MG1655 were transformed with a plasmid coding for mCherry fused with ferritin from P. furiosus under a constitutive promoter. To have E. coli that lack ferritin, MG1655 strain with a delta fur mutation were transformed with a plasmid coding for a GFP fused with Halotag, under a prototer inducible by IPTG. To obtain growth curves, precultures of bacteria were diluted 1/50^{e} in the morning in LB with antibiotics and 500 µM IPTG when needed. Bacteria were placed at 37°C 220rpm to grow until they reach an O.D. of 0.4. Next, a fresh solution of Mohr salt was added to obtain a final concentration of 0 to 4 mM. 200 µL of bacteria were transferred in wells of a 96-well plate, in triplicate. O.D. was monitored using a TECAN at 37°C and under agitation every ten minutes.

Altogether, we can assume that ferritin helps to detoxify bacteria in presence of an excess of iron II (**Fig. 2.5**). In the following article, we will recapitulate the main strategy to create *MagEcoli*, we will examine the main characteristics of magnetic bacteria and perform two proof-of-concept experiments.

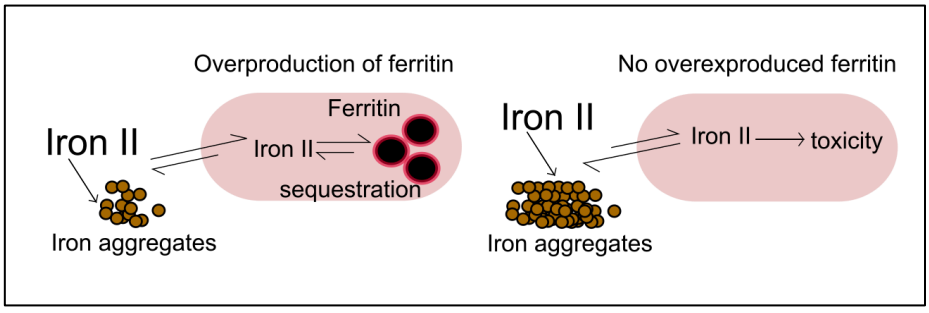

Figure 2.5: Schematic representation of a simple-hypothesis of iron-sequestration by ferritin in modified *E. coli*. The iron is internalized by ferritins, reducing its toxicity.

2.2 – Article & Supplementary Information

ACS SyntheticBiology

pubs.acs.org/synthbio Research Article

Engineering *E. coli* for Magnetic Control and the Spatial Localization of Functions

Mary Aubry, Wei-An Wang, Yohan Guyodo, Eugénia Delacou, Jean-Michel Guignier, Olivier Espeli, Alice Lebreton, François Guyot, and Zoher Gueroui*

Cite This: https://dx.doi.org/10.1021/acssynbio.0c00286 Read Online

ACCESS | Metrics & More | Article Recommendations | Supporting Information

ABSTRACT: The fast-developing field of synthetic biology enables broad applications of programmed microorganisms including the development of whole-cell biosensors, delivery vehicles for therapeutics, or diagnostic agents. However, the lack of spatial control required for localizing microbial functions could limit their use and induce their dilution leading to ineffective action or dissemination. To overcome this limitation, the integration of magnetic properties into living systems enables a contact-less and orthogonal method for spatiotemporal control. Here, we generated a magnetic-sensing *Escherichia coli* by driving the formation of iron-rich bodies into bacteria. We found that these bacteria could be spatially controlled by magnetic forces and sustained cell growth and division, by transmitting asymmetrically their magnetic properties to one daughter cell. We combined the spatial control of bacteria with genetically encoded-adhesion properties to achieve the magnetic capture of specific target bacteria as well as the spatial modulation of human cell invasions.

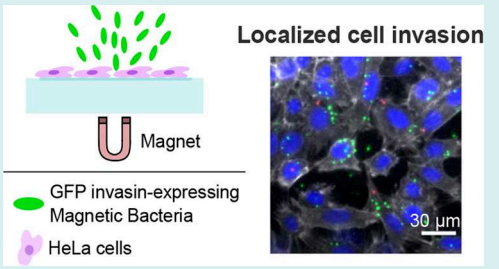

By programming and harnessing the cellular behavior of living organisms, synthetic biology tools enable broad applications ranging from basic biology to health and environment issues. Synthetic circuits have been developed for *in vitro* and *in vivo* diagnostics,[1] to produce novel material,[2,3] or to direct the assembly of synthetic multicellular systems.[4,5] For instance, programmed as whole-cell biosensors bacteria can report on environmental changes, detect specific molecules,[6,7] or monitor and diagnose diseases.[8−13] Bacteria can be further modified to act on their environment as illustrated by their use to target pathogenic bacteria[14,15] or cancer cells.[16−19]

Programming cells to be sensitive to nonbiochemical stimuli, such as acoustic or magnetic waves, could expand their capacity to probe or act on their environment.[20] For instance, the integration of magnetic properties into living organisms could enable their spatial manipulation by magnetic forces, and their use as contrast agents for magnetic resonance imaging or as heat generator.[21−27] As future perspectives, the magnetic localization of programmed bacteria may overcome their spatial dissemination driving to ineffective action, because of their dilution, or to biosafety issues. In this context, several strategies have been established to produce and use magnetic-sensing bacteria. First, magnetotactic bacteria are among the few living systems known to exploit magnetism by using their unique intracellular organelles, the magnetosomes,[28] to swim along the Earth's magnetic field. Despite several attempts to use magnetotactic bacteria,[29] they remained difficult to harness[30] and to manipulate genetically. One second strategy consisted in building bacterial biohybrid systems either using magnetotactic bacteria carrying cargo-particles,[31,32] or reciprocally, using a magnetic field to control the orientation of motile bacteria linked to magnetic beads.[33,34] A third approach aimed to magnetize naturally diamagnetic microorganisms or eukaryotic cells by overexpressing iron-storage ferritins or iron-binding proteins inside their cytoplasm. These bacteria could serve as containers favoring the formation of iron-oxide deposits when cells were fed with iron.[35−40] These studies showed that mineralized cells containing iron oxide deposits can be detected using NMR and can be magnetically sorted. However, to envision biotechnological applications using mineralized cells, several important challenges still need to be achieved. Among primary questions, knowing how magnetic properties are transmitted during cell division or whether magnetized cells are amenable for achieving defined biochemical functions while being magnetically manipulated are essential elements that have not yet been solved.

To address such questions, we engineered and characterized *MagEcoli*, that are iron-mineralized *Escherichia coli* bacteria expressing the iron-storage ferritin. We used *MagEcoli* to demonstrate that mineralized bacteria can be programmed to perform specific biochemical functions with spatiotemporal

Received: May 29, 2020
Published: September 14, 2020

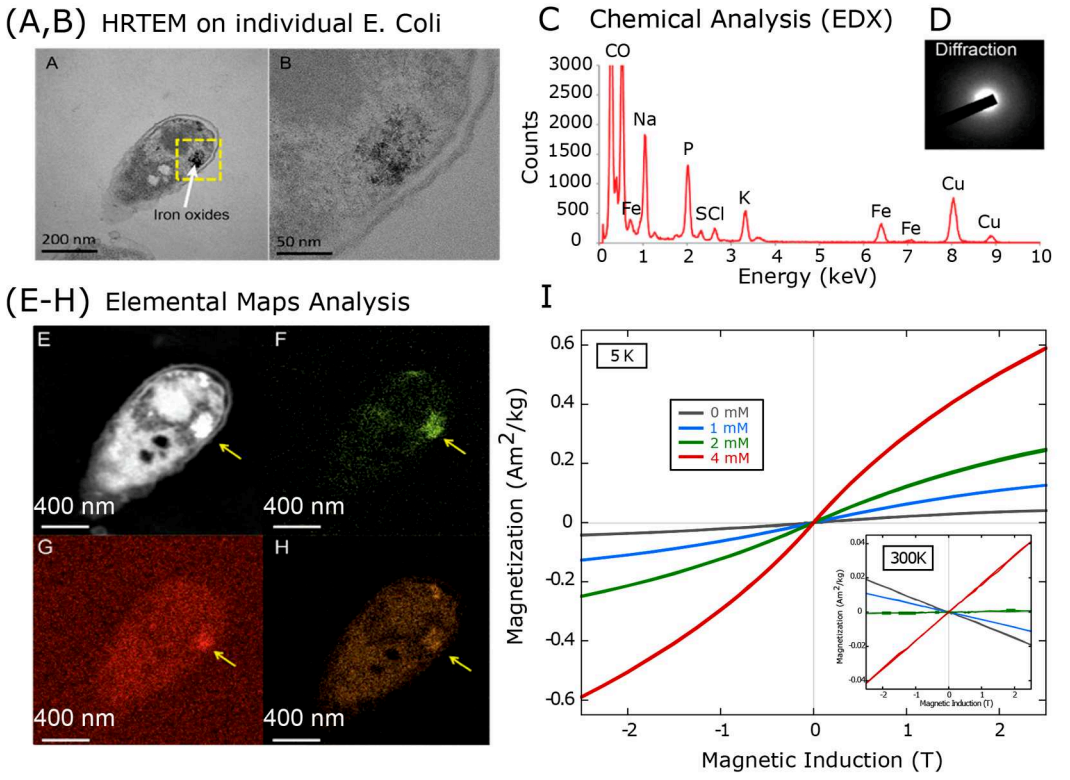

Figure 1. Structural and chemical characterization of *MagEcoli* bacteria. (A,B) TEM images of a cross sectioned mineralized mCherry-ferritin expressing *E. coli* strain. (C) Energy dispersive X-ray spectroscopy spectra of the electron-dense deposit (yellow area). (D) Electron diffraction pattern of nanoparticles. (E-H) Elemental mapping of a mineralized cross-section of mCherry-ferritin expressing *E. coli* strain. (E) STEM image. (F−H) Each panel represents the detection of a different element: iron (F), oxygen (G), phosphorus (H). (I) Magnetization curves of mineralized *E. coli* for different concentration of iron supplementation: 0 mM (black), 1 mM (blue), 2 mM (green), 4 mM (red). Measurements were performed at 5 and 300 K (inset) on a MPMS, with magnetic inductions cycling between +2.5T, −2.5T, and +2.5T.

control using magnetic forces. First, we performed structural and magnetic characterization of *MagEcoli* and found that they contained iron oxide-enriched bodies conferring magnetic properties. Next, we showed that *MagEcoli* could be spatially manipulated when exposed to magnetic forces, with an efficiency that increased with iron loading. Moreover, *MagEcoli* divided and transmitted asymmetrically iron oxide ferritin-enriched bodies during division, thus avoiding the dilution of the magnetic properties during population growth. Finally, we combined the spatial control of *MagEcoli*, modified with genetically encoded-adhesion properties displayed on their outer membrane, to achieve the magnetic capture of specific target cells as well as the spatial modulation of human cell invasions.

RESULTS

Genetic and Chemical Modifications to Obtain a Magnetic *Escherichia coli*. We aimed to induce the formation of iron-bearing particles within *Escherichia coli* cytoplasm to provide magnetic properties to the bacteria. Our strategy to produce iron-rich inclusions in bacteria relied on a two-step process consisting first in overexpressing fluorescently labeled ferritins and then supplying Fe(II) to the growth medium to biomineralize the bacteria. We chose the heterologous production of the iron-storage ferritins derived from *Pyroccocus Furiosus*.[41] Increasing Fe(II) concentration from 0 to 4 mM resulted in reducing bacteria growth and the plateau value of their stationary phase (Figure S1). After 16 h of iron biomineralization, bacteria were washed and then characterized at the nanometer scale using transmission electron microscopy (TEM) images of cross sectioned mineralized *E. coli*. TEM images showed accumulation of a large electron-dense-deposit often localized at the extremity of the bacteria (Figure 1A). The intracellular clusters were formed by the aggregation of small nanoparticles (∼3−5 nm, Figure 1B), which was consistent with the cavity size of ferritin nanocages (8 nm inner diameter). The iron-rich clusters, quasi-spherical in shape and 100−300 nm in diameter, were localized in the cytosol of the bacteria. The electron diffraction pattern of the iron clusters showed that the nanoparticles were either amorphous or poorly crystallized (Figure 1D). Their analysis by energy dispersive X-ray spectroscopy in scanning transmission electron microscopy (STEM) on 60 nm thick cross sections of *Escherichia coli* overexpressing ferritin proteins revealed iron, phosphorus, and oxygen (Figure 1C,E−H). This was confirmed by analyzing the minerals inside entire bacteria using cryo-TEM (Figure S2A). As control, we imaged mineralized GFP-expressing *E. coli* which did not overexpress ferritins, and no-electron dense deposits were observed in those bacteria (Figure S2B). In those conditions, only extracellular precipitates were observed suggesting that the overexpression of ferritins was necessary to induce the formation of intracellular iron oxide nanoparticles (Figure S2C).

Further quantitative characterization of the bacteria magnetic properties was achieved through the use of a magnetic properties measurement system (MPMS). The cells were subjected to a measurement of their mass-normalized

https://dx.doi.org/10.1021/acssynbio.0c00286
ACS Synth. Biol. XXXX, XXX, XXX−XXX

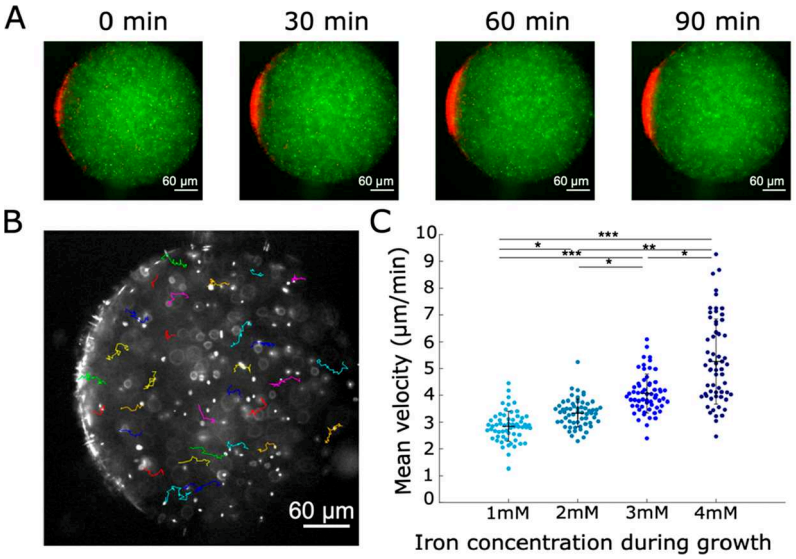

Figure 2. Biomineralized bacteria can be micromanipulated through space with a magnetic field. (A) Representative time lapse epifluorescence acquisition of the magnetic localization of *MagEcoli*^{mCherry} in a confined environment upon magnetic force application. *MagEcoli*^{mCherry} were homogeneously mixed with nonmagnetic *E. coli*^{GFP} at an early time point. The magnet was positioned on the left. Time points at 0, 30, 60, 90 min after starting acquisition, color merged. (B) Representation of trajectories as a function of time of *MagEcoli*^{mCherry} mineralized with 2 mM of iron II. Magnet on the left. (C) Histogram of bacterial speed during magnetophoresis experiments as a function of iron concentration during biomineralization. For each condition, the mean ± standard deviation is displayed, for two independent experiments. NS means there is no significant difference between the two distributions, one star means p-value < 10^{-5}, two stars mean p-value < 10^{-10}, three stars mean p-value < 10^{-15}.

magnetization at 5 and 300 K in magnetic inductions ranging between −2.5 and 2.5T (Figure 1I). At room temperature (i.e., 300 K), all samples exhibit a linear magnetization-versus-field behavior. The slope of the magnetization curve is negative for the sample without iron supplementation, which is inherent to the diamagnetic nature of most biological materials. Iron supplementation resulted in the addition of another linear component of positive slope, likely of paramagnetic nature. The maximum magnetization (in 2.5T) was increased by 0.01, 0.02, and 0.06 Am^2/kg for the 1, 2, and 4 mM Fe supplementations, respectively. The gain of magnetic susceptibility due to iron biomineralization is more evident when measuring at low temperature, as paramagnetism and other magnetic properties (ferro-, ferri-, antiferro-magnetism) increase in magnitude as temperature decreases, while diamagnetism remains constant. Measurements preformed at 5 K clearly display this magnetic enhancement. Compared to the zero-supplementation sample, maximum values of the magnetization increased by 0.09, 0.21, and 0.55 Am^2/kg for the 1, 2, and 4 mM Fe(II) supplementations, respectively. Altogether, those data highlight that magnetic *E. coli* contain iron minerals ferritin-enriched bodies conferring magnetic properties (referred as *MagEcoli* hereafter).

Spatial Manipulation and Localization of Bacteria upon Magnetic Forces. To assess the possibility to spatially manipulate *MagEcoli*, we performed magnetophoretic experiments, which consist in observing the motion of nonmotile bacteria submitted to magnetic forces. A mixture of biomineralized bacteria expressing mCherry-ferritin (*MagEcoli*^{mCherry}) and nonmineralized ones, expressing emGFP-ferritin (*E. coli*^{GFP}) were diluted in a minimal medium with a density adjusted to prevent bacterial sedimentation. The mixture was then confined into water-in-oil droplets to minimize hydrodynamic flow perturbations and facilitate observation. Once formed, the bacteria droplets were injected into a capillary next to a permanent magnet generating a gradient of about 10 T·m^{-1}. Time-lapse observations showed that within a few minutes the *MagEcoli*^{mCherry} began to move in a direction oriented toward the magnet, whereas nonmineralized ones displayed no net motion (Figure 2A). Moving bacteria eventually accumulated on the edge of the droplet as illustrated by the strong enhancement of mCherry signal intensity (Figure 2A, Figure S3A−C, Movies S1, and S2). During this process, *E. coli*^{GFP} remained uniformly distributed within the droplet. After 90 min all magnetic bacteria were attracted (Figure 2A, Figure S3). To quantify the mobility of the *MagEcoli*, we tracked single bacterial trajectories within the droplet and computed their speed (Figure 2B). This procedure was performed for respectively 1, 2, 3, and 4 mM Fe(II) added during the biomineralization step. For instance, single bacteria that were mineralized with 4 mM iron displayed a directed motion toward the magnet position with a mean speed of about 5 $\mu m \cdot min^{-1}$ ± 2 $\mu m \cdot min^{-1}$ (mean ± standard deviation) (Figure 2C). These mean speed values were also strongly correlated to the magnetic enhancement values deduced from MPMS measurements. This asymmetrical magnetic concentration procedure can be applied to force the colocalization of two bacterial populations, as exemplified in Figure S4 where *MagEcoli*^{GFP} and *MagEcoli*^{mCherry} were strongly concentrated within the same area at the vicinity of the magnet.

Altogether, these data showed that *MagEcoli* can be spatially manipulated upon magnetic forces, with an efficiency that increases with the concentration of iron added during the biomineralization step. The magnetic concentration process is very specific of the state of biomineralization of the bacteria and did not affect nonmagnetized bacteria diffusing in the mixture, allowing the performance of basic operations such as magnetic separation and magnetic mixing (Figure 2A and Figure S4).

https://dx.doi.org/10.1021/acssynbio.0c00286
ACS Synth. Biol. XXXX, XXX, XXX−XXX

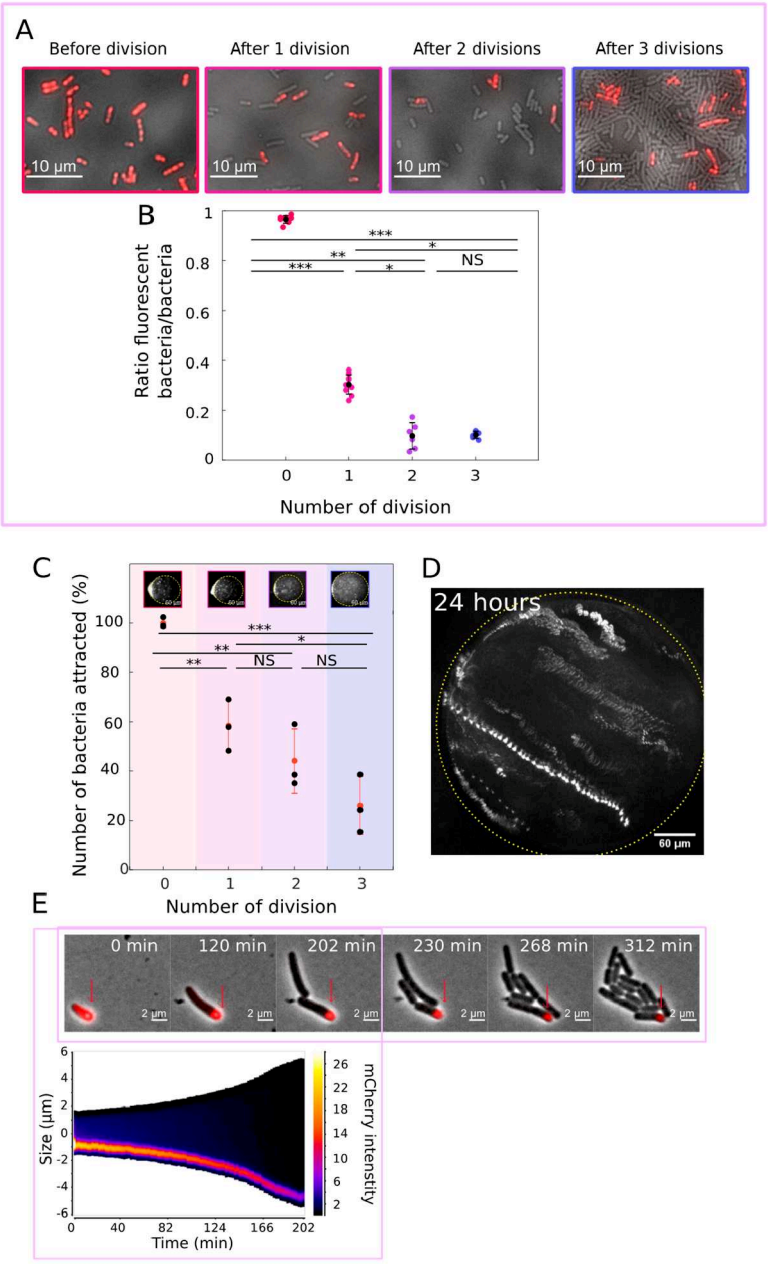

Figure 3. Evolution of the magnetic properties of *MagEcoli* as a function of cell division. (A) Superimposition of mCherry fluorescence and bright field images of mineralized bacteria after 0, 1, 2, and 3 divisions. (B) Quantification of the evolution as a function of cell division of the ratio of bacteria remaining magnetic compared to the total number of growing bacteria (1000 bacteria, two different experiments performed at different days). Each point represents a ratio computed from a microscopic observation. The mean ± standard deviation are displayed. NS means there is no significant difference between the two distributions, one star means p-value < 10^{-5}, two stars mean p-value < 10^{-10}, three stars mean p-value < 10^{-15}. (C) Upper panel: Representative magnetophoresis images of the accumulation of *MagEcoli* after 0, 1, 2, and 3 divisions. Images were taken 90 min after starting the accumulation; magnet is on the left, scale bar, 60 μm. Graph: Quantification of the number of bacteria attracted toward the magnet for the corresponding experiment. For each condition, the mean ± standard deviation is displayed for three independent experiments. NS means there is no significant difference between the two distributions, one star means p-value < 0.1, two stars mean p-value < 0.01, three stars mean p-value < 0.001. (D) Projection of bacterial trajectories integrated on 50 min of bacteria still containing mineralized ferritins after 24 h of new growth. Magnet on the bottom left. (E) Time-lapse images of live fluorescence microscopy images (merged images of phase contrast and mCherry channels, level of mCherry adjusted for each image). Time points at 0, 120, 202, 230, 268, and 312 min. Lower panel: Kymograph of the dividing bacteria displayed on top.

How Magnetic Properties of *MagEcoli* Propagate through Cell Division? Obtaining magnetized bacteria that can sustain cell division is of primary importance for basic understanding, and also to envision applications requiring magnetic manipulations of metabolically active bacteria as well as long-term operations. We examined the transmission of magnetic properties after cell division by combining microscopy observations and magnetophoresis.

First, after overnight mineralization, *MagEcoli*^{mCherry} were diluted and let grow into fresh LB medium lacking iron supply. We observed ferritin-enriched bodies within bacteria at various growth stages: before new growth, and after 1, 2, and 3

https://dx.doi.org/10.1021/acssynbio.0c00286
ACS Synth. Biol. XXXX, XXX, XXX−XXX

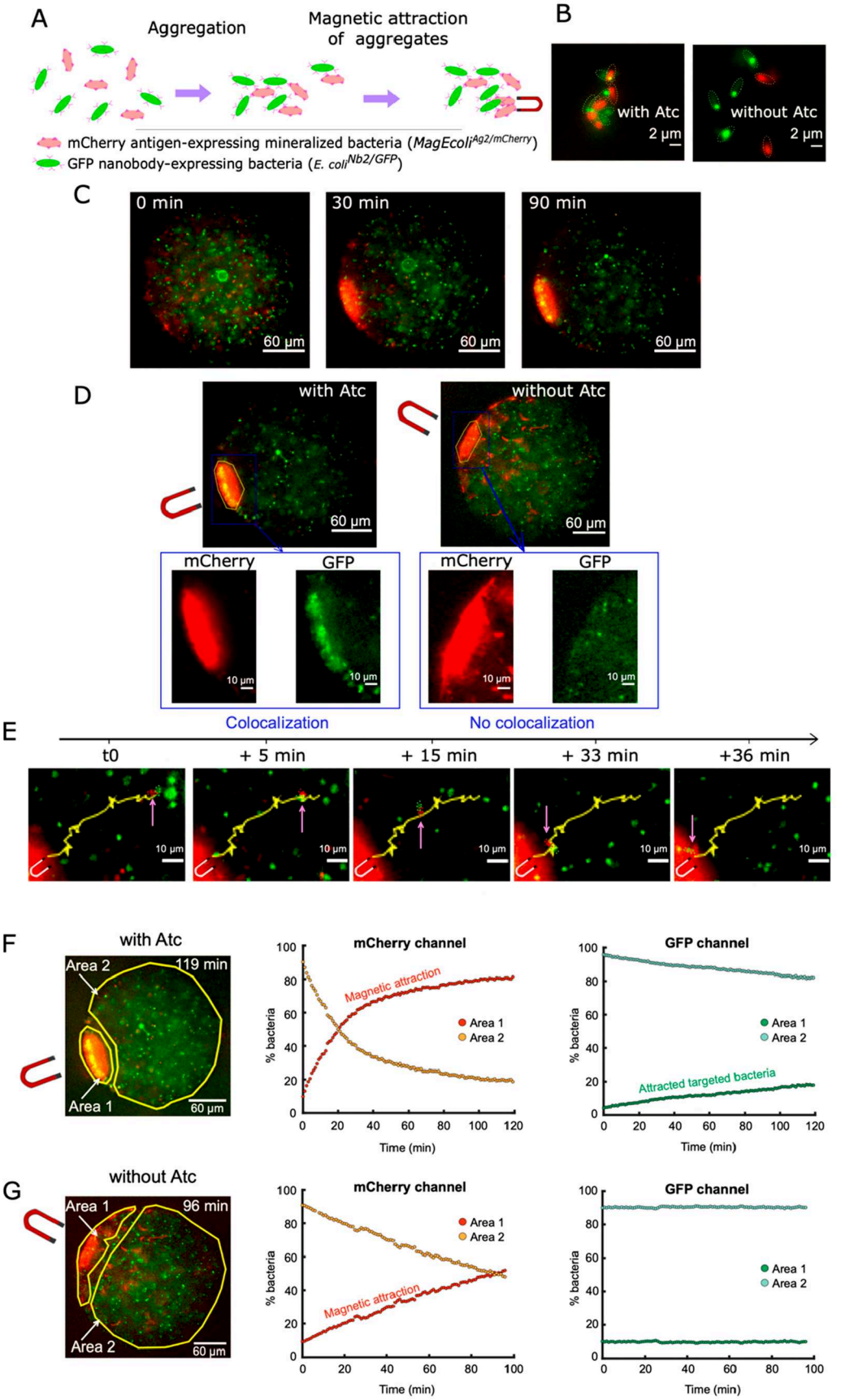

Figure 4. Capture and spatial attraction of targeted bacteria by antigen/antibody recognition. (A) Scheme of the assay of the capture and spatial attraction of targeted bacteria by antigen/antibody recognition. GFP nanobody-expressing bacteria (*E. coli*$^{Nb2/GFP}$) can adhere to mCherry antigen-expressing mineralized *E. coli* (*MagEcoli*$^{Ag2/mCherry}$). (B) On the left panel: aggregation of antigen-presenting *MagEcoli* (mCherry) with nanobody-

https://dx.doi.org/10.1021/acssynbio.0c00286
ACS Synth. Biol. XXXX, XXX, XXX−XXX

Figure 4. continued

presenting *E. coli* (GFP), in the presence of anhydrotetracycline (Atc). On the right panel: control performed without anhydrotetracycline. Epifluorescence observations. Merged images. Scale bar, 2 μm. (C) Time lapse images of magnetic accumulation of antigen-producing *MagEcoli* (mCherry) adhering to nanobody-producing *E. coli* (GFP). Images at 0 min, 30 and 90 min upon magnetic field application. Merged images. Scale bar, 60 μm. (D) Images of magnetic accumulation of aggregates in the presence (left) or in the absence (right) of anhydrotetracycline. Merged images. Scale bar 60 μm. Below: zoom of the accumulation of magnetic bacteria. Colorized images. Extracted from the movie in panel C. Scale bar, 10 μm. (E) Time-lapse images showing the trajectory two adhering bacteria (*MagEcoli*$^{Ag2/mCherry}$ and *E. coli*$^{Nb2/GFP}$) over time. Extracted from the movie in panels C and D. Merged images. Scale bar, 10 μm. (F) Quantification of the number of bacteria attracted in the presence of anhydrotetracycline using the data extracted from the time-lapse of the panel D (left). Left panel: The two regions of interest used for the quantification are highlighted in yellow. Merged channel. Middle panel: plot of the intensity of fluorescence of *MagEcoli*$^{Ag2/mCherry}$ next to the magnet (area 1, red) and far from the magnet (area 2, orange), as a function of time. Right panel: plot of the intensity of fluorescence of *E. coli*$^{Nb2/GFP}$ next to the magnet (area 1, dark green) and far from the magnet (area 2, light green), as a function of time. (G) Quantification of the number of bacteria attracted in the absence of anhydrotetracycline using the data extracted from the time-lapse of panel D (Right). Left panel: The two regions of interest used for the quantification are highlighted in yellow. Merged channel. Middle panel: plot of the intensity of fluorescence of *MagEcoli*$^{Ag2/mCherry}$ next to the magnet (area 1, red) and far from the magnet (area 2, orange), as a function of time. Right panel: plot of the intensity of fluorescence of *E. coli*$^{Nb2/GFP}$ next to the magnet (area 1, dark green) and far from the magnet (area 2, light green), as a function of time.

divisions, respectively. As the bacteria grew in the absence of IPTG, mCherry fluorescence was directly correlated with the presence of ferritins expressed by the mother bacteria, which allowed us to monitor iron oxide enriched bodies (Figure 3A). Before division, almost 100% of bacteria displayed heterogeneous mCherry fluorescence accumulation (Figure 3A). At this stage, we found bright fluorescent bodies localized at one or at both bacterial poles and coexisting with a diffuse fluorescence distributed within the cell body. These observations were in agreement with TEM acquisitions (Figure 1A). When observing bacteria at a later stage of growth, the number of fluorescent bacteria decreased compared to nonfluorescent ones. After the first division, 30% of the observed bacteria continued to display a fluorescent accumulation, whereas in contrast, the remaining bacteria showed a weak or no fluorescence signal (Figure 3A). The fluorescent bacteria represent about 10% of the total bacteria after the third division, suggesting that bacteria asymmetrically transmitted their ferritin-enriched bodies to daughter cells (Figure 3A).

This asymmetric cell division model was also confirmed by monitoring the process of division using live microscopy (Figure 3E, Movie S3). *MagEcoli*^{mCherry} that divided after biomineralization conserved their large bright inclusion bodies at the pole, leading to the transmission of the major part of mCherry-ferritin to one daughter cell only (Figure S5).

Furthermore, after 24 h of growth following the end of biomineralization, the remaining fluorescent bacteria moved as fast as the mineralized bacteria that had not undergone cell division (5 μm·min^{-1} ± 3 μm·min^{-1}, 15 tracked trajectories, three different assays, (Figure 3D)). We next quantified the evolution as a function of cell division of the ratio of bacteria remaining magnetic compared to the total number of growing bacteria. Mineralized mother bacteria were grown in a medium supplemented with IPTG to allow all newborn bacteria (magnetic and nonmagnetic) to be monitored by fluorescence. The ratio of attraction toward the magnet of magnetic versus nonmagnetic bacteria drops from 100 to 58, 44, and, 26% after the first three division steps (Figure 3C).

Altogether, these data showed that *MagEcoli* were still able to grow and divide. Only newborn bacteria maintaining iron oxide ferritin-enriched bodies inherited magnetic properties. This asymmetric division process avoids the dilution of the magnetic properties during population growth.

***MagEcoli* with Genetically Encoded-Adhesion Properties for Spatial Control of Cell Capture and Cell Invasion.** Engineering the adhesion properties of cells offers multiple applications ranging from programming tissues, living materials, and cell signaling to designing whole-cell biosensors to detect specific analytes.[2−6,16,18] To envision applications combining the spatial control of bacteria and adhesion, we extended the capacity of *MagEcoli* to perform two distinct specific functions: the capture of specific bacteria and the invasion of human cells.

To capture, manipulate, or sort in space specific target bacteria, we have implemented in *MagEcoli* a genetically encoded surface-displaying adhesin system developed for controlling cell−cell adhesion.[5] This modular system displays on bacteria outer membrane nanobodies or antigens.[5] *MagEcoli* were transformed to produce on their outer membrane Ag2, an antigen based on a cell surface-bound adhesin and encoded as a single fusion protein designed to bind Nb2 nanobody-presenting bacteria[5] (Figure 4A). Expression of Nb2 and Ag2 was under control of anhydrotetracycline addition. When Ag2-producing *MagEcoli* (*MagEcoli*$^{Ag2/mCherry}$) were mixed with Nb2-producing bacteria (*E. coli*$^{Nb2/GFP}$), we could observe multicellular aggregates formed by a few tens of cells with the same morphological patterns as previously demonstrated (Figure 4B, left panel and Figure S6). This indicated that the mineralization of bacteria did not preclude their adhesive properties. In the absence of anhydrotetracycline, no aggregation was observed confirming the specificity of the adhesion system (Figure 4B, right panel). To assess the capacity to capture and spatially manipulate target bacteria using *MagEcoli*, we mixed *MagEcoli*$^{Ag2/mCherry}$ with *E. coli*$^{Nb2/GFP}$ in droplets and applied a permanent magnetic field as explained above (Figure 4A). Remarkably, at the vicinity of the magnet, the concentration of *E. coli*$^{Nb2/GFP}$ was observed concomitantly with the one of *MagEcoli*$^{Ag2/mCherry}$ (Figure 4C,D). After about 30 min of attraction, we observed an increase in GFP as well as mCherry intensity at the vicinity of the magnet, indicating that *E. coli*$^{Nb2/GFP}$ were dragged along the magnetic gradient by the *MagEcoli*$^{Ag2/mCherry}$. Moreover, no attraction was observed in the absence of anhydrotetracycline and the attraction of *MagEcoli*$^{Ag2/mCherry}$ left the position of *E. coli*$^{Nb2/GFP}$ unaltered (Figure 4D). With a closer look at the magnetophoresis experiments, we observed long-range transport of *E. coli*$^{Nb2/GFP}$ by *MagEcoli*$^{Ag2/mCherry}$ along the magnetic force axis, indicating that enrichment by target cells was powered by *MagEcoli* transportation (Figure 4E). Next, we computed the fraction of accumulated *E. coli*$^{Nb2/GFP}$ while attracting *MagEcoli*$^{Ag2/mCherry}$, and found that 80% of *MagEcoli*$^{Ag2/mCherry}$ and 20% of *E. coli*$^{Nb2/GFP}$ were attracted

https://dx.doi.org/10.1021/acssynbio.0c00286
ACS Synth. Biol. XXXX, XXX, XXX−XXX

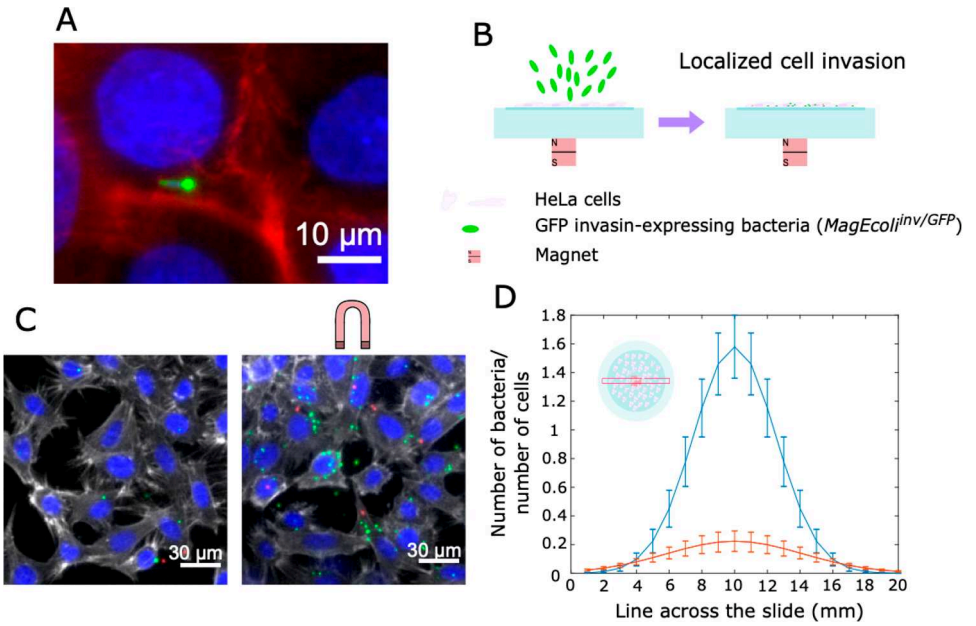

Figure 5. Magnetic localization of bacterial infection of HeLa cells. (A) Epifluorescence images of *MagEcoli*$^{inv/GFP}$ inside a Lovo cell. In blue, nucleus of human cells (LoVo) and bacterial DNA; in red, actin; in green, ferritin of *MagEcoli*$^{inv/GFP}$. (B) Scheme of the setup used to localize invasion of HeLa Cells by magnetic invasive bacteria. *MagEcoli*$^{inv/GFP}$ are placed on a culture dish covered with Hela Cells. (C) Epifluorescence images of invasion of Hela cells by *MagEcoli*$^{inv/GFP}$. In blue, nucleus of HeLa cells; in gray, actin; in green, *MagEcoli*$^{inv/GFP}$; in red, *E. coli*$^{inv/mCherry}$. (D) Number of bacteria that invaded one HeLa Cell. In blue, the mean of the number of *MagEcoli*$^{inv/GFP}$ for 4 different zones of observation on the same sample; in red, the respective number of *E. coli*$^{inv/mCherry}$. The *x*-axis represents the zone of observation, in millimeters. Data are normalized by the number of nucleus of cells counted on each field of observation, and a Gaussian fit was applied on the data for each zone of observation.

after 120 min, indicating an efficiency of capture of about 25% (Figure 4F,G). Altogether these data showed that *MagEcoli* can be programmed to capture and transport specific bacteria upon magnetic field application.

We next devised an assay to monitor the spatial localization of *MagEcoli* programmed to invade human cells. First, we expressed in *MagEcoli* the gene encoding *Yersinia pseudotuberculosis* invasin, an adhesive protein that is known to allow the invasion of cultured animal cells by otherwise noninvasive enterobacteria.[42] We verified that *MagEcoli*$^{inv/GFP}$ (*MagEcoli* expressing invasin) were able to specifically recognize and invade human cells (Figure 5A and Figure S7). The invasiveness of *MagEcoli*$^{inv/GFP}$ toward HeLa cells was quantified by gentamicin protection assay (Figure S7): extracellular bacteria are killed by the antibiotic, while intracellular bacteria are protected due to the impermeability of host cells plasma membranes. Plating serial dilutions of cell lysates on LB-agar plates following 1 h of gentamicin treatment thus enables an estimation of the number of internalized bacteria. We found that the internalization of *MagEcoli*$^{inv/GFP}$ into HeLa cells did not differ significantly from that of the same bacteria that had been grown in the absence of iron (Figure S7), arguing that mineralization of invasive *E. coli* did not impair their ability to invade human cells. To demonstrate the magnetic localization of cell invasion, we placed a magnet under a dish containing HeLa cells in contact with *MagEcoli*$^{inv/GFP}$ for 4 h (Figure 5B). After gentamicin treatment, cells were fixed and stained to image *MagEcoli*, actin filaments, and the cell nucleus. Strikingly, cells adhering in the vicinity of the magnetic field contained a larger number of *MagEcoli* in their cytoplasm than cells adhering far from the magnet. Moreover, the density of bacteria per cells increased with the gradient of magnetic field to reach about 8-fold of the bacteria density measured in absence of magnetic forces (Figure 5C,D). Altogether, these data demonstrate our ability to target *MagEcoli* invasion to a specific zone with a magnetic field.

DISCUSSION

We demonstrate the spatial control of engineered bacteria mediated by magnetic forces and programmed to achieve specific tasks using modified surface-adhesion properties. Magnetic bacteria were engineered using two-step processes, consisting first in the production of the iron storage ferritin in *E. coli*, and second, in growing these bacteria in an iron-rich medium. Iron mineralization of ferritin-expressing bacteria resulted in the formation of amorphous iron oxide minerals enriched with iron, oxygen, and phosphorus. These *MagEcoli* bacteria display paramagnetic properties that increase with the amount of iron supplemented during bacteria growth. In contrast, biomineralized bacteria that did not overexpress ferritins were not exhibiting any detectable intracellular iron oxide particles, but showed extracellular iron deposits. MPMS measurements showed that biomineralized control *E. coli* displayed a diamagnetic signal, suggesting that the paramagnetic contribution of *MagEcoli* is mainly due to intracellular iron oxide minerals. These data suggest a model in which ferritin-expressing *E. coli* hyperaccumulate iron metals that form iron-oxide minerals stored into ferritin-enriched bodies, with chemical and crystal structures that are constrained by the physical−chemical state of the *E. coli* cytoplasma in terms of pH/redox conditions.

We next demonstrate that *MagEcoli* can be concentrated using magnetic forces to generate spatial heterogeneity in bacterial concentration. For instance, when confined in a millimeter-size confined environment, *MagEcoli* could be physically separated from a nonmagnetic bacteria population

https://dx.doi.org/10.1021/acssynbio.0c00286
ACS Synth. Biol. XXXX, XXX, XXX−XXX

or, in contrast, forced to mix together with a second magnetic bacterial strain in a specific area.

To investigate how cell division could impact the magnetic properties of *MagEcoli*, we studied how ferritin-enriched bodies and magnetic properties propagated when bacteria divided. We found that *MagEcoli* transmitted asymmetrically their ferritin-enriched bodies to only one daughter cell. The proportion of attracted magnetic bacteria by the magnet dropped concomitantly with the cell division number to reach about 10% after three divisions. This corroborates a model for which the main magnetic properties were inherited by one daughter cell, consequently resulting in the maintenance of a constant population of *MagEcoli* in regard to a growing nonmagnetic population of bacteria. Interestingly, this mechanism limits the dilution of the magnetic properties, which would in contrast be expected if mineralized ferritin bodies would equally be distributed between the two daughter cells.

One essential aspect when envisioning applications of *MagEcoli* was to assess how these bacteria could be further programmed to perform specific biochemical functions. By expressing genetically encoded surface adhesion proteins, we studied the spatial localization of *MagEcoli* programmed to recognize and adhere to specific bacteria or to invade a mammalian host. We first demonstrated the spatial manipulation of *MagEcoli* acting as a surface-displaying antigen to adhere specifically to nonmagnetic nanobody-displaying bacteria. We found that *MagEcoli* can capture and transport target bacteria along a magnetic force axis to eventually drive their accumulation. Such properties illustrate potential perspectives for biotechnological purposes as *MagEcoli* could be programmed and magnetically manipulated to transport cargos, for patterning living materials, or as whole-cell biosensors for *in vitro* or *in vivo* diagnostic. In a second application, we demonstrated the spatial modulation of cell invasion in a magnetic field by programming *MagEcoli* to invade human cells. The magneto-localization of infection could provide a novel tool for basic studies of host−pathogen interactions. One horizon consists in the spatiotemporal control of bacteria programmed as delivery vehicles to release cytotoxic molecules into cancer cells.

MATERIALS AND METHODS

Chemicals. Kanamycin, chloramphenicol, ampicillin, spectinomycin, Mohr's Salt, LB broth, M9 broth, glycerol, agar, sucrose, IPTG, mineral oil, PBS, and anhydrotetracycline were purchased from Sigma-Aldrich. Arlacel P135 was purchased from CRODA; Optiprep was purchased from StemCell. Vitrex was purchased from VWR.

DNA Plasmids and Strains. The list of the plasmids used in this study are reported in Table S1. The *Pyrococcus furiosus* ferritins were fused at their N-terminal to mCherry or Emerald GFP (EmGFP) and were cloned into pet28, pGBM4. The ability of *E. coli* to be internalized into epithelial cells was granted by the pRI203 plasmid allowing the expression of the invasin gene from *Yersinia pseudotuberculosis* (*inv*) in a pBR325 vector.

Models. *E. coli* bacteria were purchased at Merck for Rosetta (DE3)pLysS, at New England Biolabs for BL21 and dH10β. *E. coli* MG1655 come from Blattner et al., 1997. HeLa cell lines come from ATCC (CCl-2) as well as LoVo cell line (CCL-229).

Transformation. All plasmids were incorporated into electro-competent bacteria (Rosetta or MG1655) via electroporation.

Biomineralization Protocol. Plasmids used for biomineralization and their corresponding antibiotics are listed in Table S1. Stock solutions of antibiotics were made at 1000× kanamycin (50 mg/mL in water), ampicillin (100 mg/mL in water), chloramphenicol (34 mg/mL in ethanol), and spectinomycin (100 mg/mL in water) and stored at −20 °C. Antibiotics were diluted to the LB medium and added at every step of bacterial culture or biomineralization.

As a source of iron II, Mohr salt was used and kept under inert condition. At each step of iron addition, a fresh solution of Mohr salt was made in water at a concentration of 100 mM. This solution was immediately added to the bacteria and kept no longer than 10 min.

Bacteria were grown overnight in LB medium with the corresponding antibiotics (Table S1) until they reached the steady state (precultures). The next day, they were diluted and grown into fresh LB medium with antibiotics at 37 °C for approximately 2 h, until they reached an optical density at 600 nm between 0.4 and 0.6; 500 μM of IPTG was added into the medium when growing bacteria transformed with the specific plasmids (Table S1). Bacteria were incubated at 37 °C for 30 min. Next, Fe(II) was added to the bacteria to a final concentration of 1 to 4 mM. Bacteria were grown overnight at 37 °C (about 16 h ± 10%). The next morning, bacterial O.D. at 600 nm was measured. Correction from the absorption of iron was performed using a blank measured with LB containing Fe(II) at 0 to 4 mM. Finally, bacteria were washed after centrifugation to remove iron oxide residues from the LB and placed into the desired buffer (free from antibiotics, for observation or further experiments).

Growth Curve. Overproducing mCherry-ferritin *E. coli* were grown overnight in LB medium supplemented with kanamycin (50 μg/mL) and chloramphenicol (34 μg/mL), until they reached the steady state (precultures). The next day, bacteria were diluted 1:50 in fresh LB supplemented with kanamycin (50 μg/mL), chloramphenicol (34 μg/mL), and 500 μM of IPTG; 200 μL of bacteria were deposited into a 96 μL-well microplate (in triplicate for each condition). Measurements were taken at 600 nm with a plate reader (TECAN) each 10 min for 20 h. After 2 h, when bacteria reached an OD of about 0.3−0.4, Fe(II) was supplemented in the medium to reach a final concentration of 0, 2, 3, and 4 mM. As a source of iron, Mohr salt, stored under inert conditions, was freshly made in water at a stock concentration of 100 mM. A blank of LB mixed with Fe(II) at 0, 2, 3, and 4 mM was taken into account to subtract the O.D. due to iron precipitation over time.

Ultrathin Section Transmission Electron Microscopy. *E. coli* cells were fixed for 2 h in 2% glutaraldehyde in 0.1 M Sörensen phosphate buffer and washed with iso-osmolar phosphate buffer. Afterward the samples were fixed for 1 h with 1% of osmium tetroxide and washed with iso-osmolar phosphate buffer. After repeated washing, the samples were dehydrated through an ethanol series and embedded in epoxy resin (ERL 42O6) in beem capsules, which polymerized at 55 °C for 48 h. Ultrathin sections were obtained using a diatome diamond knife in a Leica UCT ultramicrotome and deposited onto a 300 mesh carbon-coated grid. TEM images were obtained on a Jeol 2100 F microscope. This machine, operating at 200 kV, is equipped with a field emission gun,

https://dx.doi.org/10.1021/acssynbio.0c00286
ACS Synth. Biol. XXXX, XXX, XXX−XXX

an ultrahigh resolution pole piece, and an ultrathin window JEOL detector.

Cryo-Transmission Electron Microscopy (Cryo-TEM) Images. A drop of bacteria solution was deposited on a "quantifoil" (Quantifoil Micro Tools GmbH, Germany) carbon membrane. The excess of liquid on the membrane was absorbed with a filter paper and the membrane was quench-frozen quickly in liquid ethane to form a thin vitreous ice film. Once placed in a Gatan 626 cryo-holder cooled with liquid nitrogen, the samples were transferred in the microscope and observed at low temperature (−180 °C). Cryo-TEM images were recorded on an ultrascan 2k × 2k CCD camera (Gatan, USA), using a LaB_6 JEOL JEM2100 (JEOL, Japan) cryo-microscope operating at 200 kV with a JEOL low dose system (minimum dose system, MDS) to protect the thin ice film from any irradiation before imaging and reduce the irradiation during the image capture.

Magnetic Characterization. Magnetic characterization of the samples was performed using Quantum Design incorporated Magnetic Properties Measurements System (MPMS-XL 5 evercool). The MPMS allows low temperature measurements of magnetic moments and magnetic susceptibility down to 2K. Prior to measurements, dry powdered samples were placed in gelatin capsules and inserted in 5 mm in diameter nonmagnetic plastic straws. Measured magnetic moments were mass normalized in order to calculate magnetizations, allowing comparisons between samples.

Magnetophoresis Setup. For the magnetophoresis experiments, freshly mineralized bacteria were washed twice in antibiotic free M9 medium. Next, bacteria were concentrated to an optical density of approximately 6, when not mentioned. For O.D. measurements, the blank was made of M9 medium. Then bacteria were diluted 10 times with M9 supplemented with sucrose (500 mg of sucrose for 700 μL of M9), to prevent sedimentation. A water-in-oil emulsion was formed by mixing up 99 μL of mineral oil supplemented with a block copolymer at 0.4 g/L (ArlacelP135) and 1 μL of bacteria. The emulsion was inserted into a capillary (1 mm of diameter) fixed on a microscopic slide (32 × 40 mm). The capillary was sealed with Vitrex, and a neodymium magnet was placed at one side (cubic magnet NdFeB 3 mm, Supermagnet), the N−S axis being perpendicular to the capillary's direction. Observations were made using epifluorescence microscopy.

Study of the Transmission of Magnetism as a Function of Cell Division with Magnetophoresis. *MagEcoli* (4 mM of Fe(II)) were diluted to an optical density of around 0.1 into fresh LB medium. Depending on the context, 500 μM of IPTG and kanamycin were added to induce the constant production of mCherry-ferritin during growth. Once the bacteria reached the desired optical density (corresponding to 1, 2, or 3 divisions), magnetophoresis tests were performed with bacteria washed twice and concentrated into M9 medium.

Observation of Bacteria as a Function of Cell Division. To perform visualization of bacteria during cell division, mineralized bacteria (2 mM of Fe(II)) were washed in LB medium and then diluted into a fresh LB medium (kanamycin) to 0.1 O.D. Bacteria grow at 37 °C under agitation. For single-cell observation, bacteria at the desired optical density were washed and concentrated into M9 medium. They were spread on an agarose pad (2% agarose LB) and observed by fluorescence microscopy.

Live Observation of Single Dividing Bacteria. *MagEcoli* (2 mM of Fe(II) and 0 mM of Fe(II) for the control without iron) were washed in LB medium and then spread under an agarose pad (1% agar LB). Time-lapse microscopy was performed using a confocal spinning disk (W1 Yokogawa) on an inverted Zeiss Axio Imager microscope at 63× magnification controlled by Metamorph (Molecular Imaging) and a CMOS camera (Hamamatsu). Metamorph autofocus control was used at each time point on the phase contrast signal. Images were acquired every 2 min for 5 h at 37 °C. Four positions were observed simultaneously for each experiment, with 20−50 cells per position.

Magnetic capture by *MagEcoli*. Ag2-producing *MagEcoli* ($MagEcoli^{Ag2/mCherry}$): MG1655 bacteria were cotransformed with both pDSG419 and pGBM4_mCherry-ferritin plasmids, and then mineralized with 4 mM or Fe(II) in the presence of 100 ng/mL of anhydrotetracycline and antibiotics. Nb2-producing bacteria ($E.\ coli^{Nb2/GFP}$): MG1655 were cotransformed with pDSG375 and pGBM4-GFP-Ferritin plasmids and were diluted in LB with 100 ng/mL of anhydrotetracycline and antibiotics for overnight preculture. The next day, both populations of bacteria were washed twice with antibiotic free M9 medium. The two strains were mixed in M9 medium at a density of around 0.4 (for aggregates visualization) or into M9 medium supplemented with sucrose (500 mg of sucrose for 700 μL of M9) at a density of around 0.4 (for immediate test of magnetophoresis). Adhesion experiments were made at a ratio of bacteria of 1:1. After several hours, the mixes in M9 let at room temperature were observed in glass chip chambers to monitor aggregation. On the same day, a first set of control experiments were performed with nonadhering bacteria using $MagEcoli^{Ag2/mCherry}$ and $E.\ coli^{Nb2/GFP}$ that were grown without anhydrotetracycline. A second set of control experiments was performed with adherent but nonmagnetic bacteria using $E.\ coli^{Ag2/mCherry}$ and $E.\ coli^{Nb2/GFP}$ (without iron addition). Observation was performed using epifluorescence acquisitions.

Assessment of Cell Invasion by Gentamicin Protection. LoVo cells were grown in monolayers in 24-well plates in D-MEM medium containing 10% fetal bovine serum (FBS) until they reached a density of 1×10^5 cell per well. $MagEcoli^{inv/GFP}$ consisted in mineralized BL21 (4 mM Fe(II)) cotransformed with the pRI203 plasmid expressing *Yersinia pseudotuberculosis inv* gene and the pet28-GFP-ferritin plasmid. $E.\ coli^{inv/GFP}$ consisted in BL21 cotransformed with the pRI203 plasmid expressing *Yersinia pseudotuberculosis inv* gene and the pet28-GFP-ferritin plasmid and that were not mineralized. Both $MagEcoli^{inv/GFP}$ and $E.\ coli^{inv/GFP}$ were pelleted by centrifugation at 6000*g*, then washed with prewarmed PBS and diluted in D-MEM without serum containing 20% Optiprep (to prevent sedimentation) to an optical density of 0.1. Cell culture wells were washed once with 500 μL of prewarmed D-MEM, then 200 μL of each inoculum was dispensed onto the cell culture monolayers, and the cultures were left to incubate for 4 h at 37 °C under 5% CO_2 atmosphere. The multiplicity of infection (MOI) was estimated by plating serial dilutions of each inoculum on LB-agar plates and was found to be in the range of 100 for both conditions. After 4 h, the inoculum was washed away with 500 μL of prewarmed D-MEM containing 40 μg/mL of gentamicin, then replaced with D-MEM containing 10% FBS and 40 μg/mL of gentamicin for 1 h. This incubation allows the complete killing of extracellular bacteria by gentamicin, while intracellular bacteria are protected from the antibiotic by

https://dx.doi.org/10.1021/acssynbio.0c00286
ACS Synth. Biol. XXXX, XXX, XXX−XXX

the plasma membrane. After 1 h, cell monolayers were washed with 500 μL of prewarmed PBS, then lysed by adding 200 μL of 4 °C sterile water to each well. Serial dilutions of cell lysates were plated on LB-agar plates to quantify the number of intracellular bacteria in each well. Data are provided as the percentage of the inoculum having entered cells and represent the results of double counting from six different wells per condition in a representative experiment out of three independent experiments.

Spatial Modulation of Cell Invasion by *MagEcoli*. Experiments were performed with *MagEcoli*$^{inv/GFP}$ and as control with *E. coli*$^{inv/mCherry}$. Bacteria were washed with PBS just after overnight growth and were diluted in PBS + 20% Optiprep (to prevent sedimentation) to an optical density of 0.02. On each cell chamber containing confluent HeLa cells, 2 mL of a mixture of *MagEcoli*$^{inv/GFP}$ and *E. coli*$^{inv/mCherry}$ in PBS were added. Each chamber was placed above a NdFeB magnet (cubic 5 mm, Supermagnet) in an incubator providing a constant temperature of 37 °C and carbon dioxide supply, for 4 h. After incubation, the PBS was removed and the chambers were filled with 2 mL of DMEM and gentamicin (40 μg/mL). Immediately, it was replaced by 2 mL of DMEM with gentamicin (40 μg/mL) and FBS 10%. The system was allowed to stand for 1 h at 37 °C to kill all extracellular bacteria. Then, after washing with PBS, cells were fixed with paraformaldehyde (PFA), 4%. After being washed with PBS, cells were permeabilized with PBS and Triton 0.5% and stained with DAPI and Alexa Fluor 647 Phalloidin for 1 h. Another strain was tested as represented on the images of Figure 5A: *MagEcoli*$^{inv/GFP}$ were added to Lovo cells for 1 h of infection.

Microscopy Observations. Magnetophoresis experiments were observed using a IX81 (Olympus) epifluorescence microscope equipped with an EM-CCD camera (electron multiplying CCD, C9100-13 or C9100-02, Hamamatsu, Corporation), a LED for illumination (Spectra X, Lumencor), and with ×10, ×20, ×60 oil objectives. Microscopes were controlled by MicroManager or SimplePCI software.

Data Analysis. Image analyses were made using Fiji. A running Z projector plug-in was used to observe superimposed trajectories in the magnetophoresis assays. For tracking the bacteria position, 60 trajectories were analyzed for each biomineralization condition (1 to 4 mM Fe(II)) using Excel and Matlab. Experiments were performed twice for each concentration of iron on different samples.

To quantify the number of bacteria under the agar-gel, a cell-counter plug-in was used on composite images (merged bright field and mCherry). The assay of bacterial growth was duplicated on a different day. For each division of each assay, we counted around 1000 bacteria. The 1000 bacteria counted came from a different field on the slide.

For Figure 3C, to quantify the ratio of attraction toward the magnet of magnetic versus nonmagnetic bacteria as a function of cell division, we measured the intensity of the region of interest corresponding to fluorescent bacteria accumulating at the vicinity of the droplet 90 min after starting magnetophoresis. This value was normalized by the intensity on the whole droplet at an initial time (right after starting magnetophoresis). Measurements were performed on three different conditions acquired for different biomineralization experiments (three movies).

For Figure S3, Figure 4F,G, to quantify the number of bacteria in both areas, we measured the intensity in the region of interest at each minute. We normalized this value by the intensity of the whole droplet at the initial time (right after starting the magnetophoresis). We subtracted the background in the measurements. We normalized the data by assuming that the sum of bacteria in both areas was equal to 100%.

To quantify the number of bacteria invading HeLa cells, we counted the number of nucleus and bacteria on binary-transformed images (after applying a manual threshold). Analyses were performed on four different areas crossing the cell chamber on the same representative sample, and a Gaussian fit was applied for each zone of observation.

For the movie of dividing bacteria (Movie S3), the bleaching of mCherry fluorescence was corrected with the FIJI plug-in "bleach correction", using the simple ratio method and a background intensity level of 110.

Statistical Analysis. Data treatment and graphic generations were performed with Excel (Microsoft) and MATLAB (Mathworks). For Figure 2C, Figure 3B, and Figure 3C, a Student's t test (parametric test to compare two observed means) was performed with the ttest2 function with Matlab. Error bars always show the standard deviation (SD). For Figure S7, the values were obtained for 12 technical replicates from representative invasion assays among three independent experiments; their means and standard deviations were plotted. The probability p of rejection of the null hypothesis was assessed using a two-tailed Student's t-test.

■ ASSOCIATED CONTENT

Supporting Information

The Supporting Information is available free of charge at https://pubs.acs.org/doi/10.1021/acssynbio.0c00286.

List of the plasmids used in the study; further characterizations of *MagEcoli*, other magnetophoresis characterization (PDF)

Magnetophoresis experiments movie of *MagEcoli* (AVI)

Magnetophoresis experiments division movie of *MagEcoli* (AVI)

Division of single *MagEcoli* (AVI)

Data for two proof-of-concept assays (XLSX)

■ AUTHOR INFORMATION

Corresponding Author

Zoher Gueroui − *P.A.S.T.E.U.R., Department of Chemistry, École Normale Supérieure, PSL University, Sorbonne Université, CNRS, 75005 Paris, France;* orcid.org/0000-0003-1819-5427; Email: zoher.gueroui@ens.fr

Authors

Mary Aubry − *P.A.S.T.E.U.R., Department of Chemistry, École Normale Supérieure, PSL University, Sorbonne Université, CNRS, 75005 Paris, France*

Wei-An Wang − *P.A.S.T.E.U.R., Department of Chemistry, École Normale Supérieure, PSL University, Sorbonne Université, CNRS, 75005 Paris, France; IMPMC, Muséum National d'Histoire Naturelle, Sorbonne Université, UMR CNRS 7590, Paris 75005, France*

Yohan Guyodo − *Université de Paris, Institut de Physique du Globe de Paris, CNRS, Paris F-75005, France*

Eugénia Delacou − *P.A.S.T.E.U.R., Department of Chemistry, École Normale Supérieure, PSL University, Sorbonne Université, CNRS, 75005 Paris, France*

https://dx.doi.org/10.1021/acssynbio.0c00286
ACS Synth. Biol. XXXX, XXX, XXX−XXX

Jean-Michel Guignier − *IMPMC, Muséum National d'Histoire Naturelle, Sorbonne Université, UMR CNRS 7590, Paris 75005, France*
Olivier Espeli − *CIRB-Collège de France, CNRS-UMR7241, INSERM U1050, PSL Research University, Paris 75005, France*
Alice Lebreton − *Institut de biologie de l'ENS (IBENS), Département de biologie, École Normale Supérieure, CNRS, INSERM, PSL University, Paris 75005, France; INRAE, IBENS, Paris 75005, France*
François Guyot − *IMPMC, Muséum National d'Histoire Naturelle, Sorbonne Université, UMR CNRS 7590, Paris 75005, France; Institut Universitaire de France (IUF), France*

Complete contact information is available at: https://pubs.acs.org/10.1021/acssynbio.0c00286

Author Contributions

M.A., F.G., and Z.G. conceived the project and analyzed results of the study. M.A. carried out and analyzed most of the experiments. W.A.W. contributed to the initial design of the magnetophoresis experiments. W.A.W., J.M.G., and F.G. carried out and analyzed the TEM and energy dispersive X-ray spectroscopy experiments. Y.G. carried out and analyzed the MPMS data. M.A. and O.E. carried out live microscopy of bacteria division. A.L. carried out the assessment of cell invasion by gentamicin protection assay. M.A. and A.L. performed the spatial modulation of cell invasion. M.A. and E.D. performed the magnetic capture assay. M.A. and Z.G. wrote the manuscript, and all authors were involved in revising it critically for important intellectual content.

Notes

The authors declare the following competing financial interest(s): M.A., W.A.W., F.G., and Z.G. filed a provisional patent, EP19188019.4, Magnetic Bacteria, Non-Therapeutic and Therapeutic Uses ThereoF, on the 24 July 2019.

■ ACKNOWLEDGMENTS

This work was supported by the ANR (ANR-16-CE09−0002-Nanoheaters), the CNRS, and Ecole Normale Supérieure. The authors acknowledge Ludovic Jullien, Guillaume Morin, and the members of the Biophysical Chemistry group of the École normale supérieure for fruitful discussion. We thank Chakib Djediat (MNHN) for help with TEM sample preparation.

■ REFERENCES

(1) Slomovic, S., Pardee, K., and Collins, J. J. (2015) Synthetic Biology Devices for in Vitro and in Vivo Diagnostics. *Proc. Natl. Acad. Sci. U. S. A. 112*, 14429.
(2) Nguyen, P. Q., Botyanszki, Z., Tay, P. K. R., and Joshi, N. S. (2014) Programmable Biofilm-Based Materials from Engineered Curli Nanofibres. *Nat. Commun.*, No. 4945, DOI: 10.1038/ncomms5945.
(3) Chen, A. Y., Deng, Z., Billings, A. N., Seker, U. O. S., Lu, M. Y., Citorik, R. J., Zakeri, B., and Lu, T. K. (2014) Synthesis and Patterning of Tunable Multiscale Materials with Engineered Cells. *Nat. Mater. 13*, 515.
(4) Toda, S., Blauch, L. R., Tang, S. K. Y., Morsut, L., and Lim, W. A. (2018) Programming Self-Organizing Multicellular Structures with Synthetic Cell-Cell Signaling. *Science (Washington, DC, U. S.) 361* (6398), 156−162.
(5) Glass, D. S., and Riedel-Kruse, I. H. (2018) A Synthetic Bacterial Cell-Cell Adhesion Toolbox for Programming Multicellular Morphologies and Patterns. *Cell 174* (3), 649−658.e16.
(6) Kylilis, N., Riangrungroj, P., Lai, H. E., Salema, V., Fernández, L. Á., Stan, G. B. V., Freemont, P. S., and Polizzi, K. M. (2019) Whole-Cell Biosensor with Tunable Limit of Detection Enables Low-Cost Agglutination Assays for Medical Diagnostic Applications. *ACS Sensors 4* (2), 370−378.
(7) Van Der Meer, J. R., and Belkin, S. (2010) Where Microbiology Meets Microengineering: Design and Applications of Reporter Bacteria. *Nat. Rev. Microbiol. 8*, 511.
(8) Mimee, M., Nadeau, P., Hayward, A., Carim, S., Flanagan, S., Jerger, L., Collins, J., McDonnell, S., Swartwout, R., Citorik, R. J., Bulović, V., Langer, R., Traverso, G., Chandrakasan, A. P., and Lu, T. K. (2018) An Ingestible Bacterial-Electronic System to Monitor Gastrointestinal Health. *Science (Washington, DC, U. S.) 360*, 915.
(9) Riglar, D. T., Giessen, T. W., Baym, M., Kerns, S. J., Niederhuber, M. J., Bronson, R. T., Kotula, J. W., Gerber, G. K., Way, J. C., and Silver, P. A. (2017) Engineered Bacteria Can Function in the Mammalian Gut Long-Term as Live Diagnostics of Inflammation. *Nat. Biotechnol. 35*, 653.
(10) Riglar, D. T., and Silver, P. A. (2018) Engineering Bacteria for Diagnostic and Therapeutic Applications. *Nat. Rev. Microbiol. 16* (4), 214−225.
(11) Daeffler, K. N., Galley, J. D., Sheth, R. U., Ortiz-Velez, L. C., Bibb, C. O., Shroyer, N. F., Britton, R. A., and Tabor, J. J. (2017) Engineering Bacterial Thiosulfate and Tetrathionate Sensors for Detecting Gut Inflammation. *Mol. Syst. Biol. 13*, 923.
(12) Certain, L. K., Way, J. C., Pezone, M. J., and Collins, J. J. (2017) Using Engineered Bacteria to Characterize Infection Dynamics and Antibiotic Effects In Vivo. *Cell Host Microbe 22*, 263.
(13) Mimee, M., Tucker, A. C., Voigt, C. A., and Lu, T. K. (2015) Programming a Human Commensal Bacterium, Bacteroides Thetaiotaomicron, to Sense and Respond to Stimuli in the Murine Gut Microbiota. *Cell Syst. 1*, 62.
(14) Gupta, S., Bram, E. E., and Weiss, R. (2013) Genetically Programmable Pathogen Sense and Destroy. *ACS Synth. Biol. 2* (12), 715−723.
(15) Hwang, I. Y., Koh, E., Wong, A., March, J. C., Bentley, W. E., Lee, Y. S., and Chang, M. W. (2017) Engineered Probiotic Escherichia Coli Can Eliminate and Prevent Pseudomonas Aeruginosa Gut Infection in Animal Models. *Nat. Commun. 8*, 1−11.
(16) Anderson, J. C., Clarke, E. J., Arkin, A. P., and Voigt, C. A. (2006) Environmentally Controlled Invasion of Cancer Cells by Engineered Bacteria. *J. Mol. Biol. 355* (4), 619−627.
(17) Din, M. O., Danino, T., Prindle, A., Skalak, M., Selimkhanov, J., Allen, K., Julio, E., Atolia, E., Tsimring, L. S., Bhatia, S. N., and Hasty, J. (2016) Synchronized Cycles of Bacterial Lysis for in Vivo Delivery. *Nature 536* (7614), 81−85.
(18) Piñero-Lambea, C., Bodelón, G., Fernández-Periáñez, R., Cuesta, A. M., Álvarez-Vallina, L., and Fernández, L. Á. (2015) Programming Controlled Adhesion of E. Coli to Target Surfaces, Cells, and Tumors with Synthetic Adhesins. *ACS Synth. Biol. 4* (4), 463−473.
(19) Danino, T., Prindle, A., Kwong, G. A., Skalak, M., Li, H., Allen, K., Hasty, J., and Bhatia, S. N. (2015) Programmable Probiotics for Detection of Cancer in Urine. *Sci. Transl. Med. 7* (289), 289ra84.
(20) Piraner, D. I., Farhadi, A., Davis, H. C., Wu, D., Maresca, D., Szablowski, J. O., and Shapiro, M. G. (2017) Going Deeper: Biomolecular Tools for Acoustic and Magnetic Imaging and Control of Cellular Function. *Biochemistry 56*, 5202.
(21) Mannix, R. J., Kumar, S., Cassiola, F., Montoya-Zavala, M., Feinstein, E., Prentiss, M., and Ingber, D. E. (2008) Nanomagnetic Actuation of Receptor-Mediated Signal Transduction. *Nat. Nanotechnol. 3*, 36−40.
(22) Li, T. L., Wang, Z., You, H., Ong, Q., Varanasi, V. J., Dong, M., Lu, B., Paşca, S. P., and Cui, B. (2019) Engineering a Genetically Encoded Magnetic Protein Crystal. *Nano Lett. 19*, 6955.
(23) Liße, D., Monzel, C., Vicario, C., Manzi, J., Maurin, I., Coppey, M., Piehler, J., and Dahan, M. (2017) Engineered Ferritin for Magnetogenetic Manipulation of Proteins and Organelles Inside Living Cells. *Adv. Mater. 29* (42), 1−7.
(24) Rao, S., Chen, R., LaRocca, A. A., Christiansen, M. G., Senko, A. W., Shi, C. H., Chiang, P. H., Varnavides, G., Xue, J., Zhou, Y.,

Park, S., Ding, R., Moon, J., Feng, G., and Anikeeva, P. (2019) Remotely Controlled Chemomagnetic Modulation of Targeted Neural Circuits. *Nat. Nanotechnol. 14*, 967.
(25) Hoffmann, C., Mazari, E., Lallet, S., Le Borgne, R., Marchi, V., Gosse, C., and Gueroui, Z. (2013) Spatiotemporal Control of Microtubule Nucleation and Assembly Using Magnetic Nanoparticles. *Nat. Nanotechnol. 8*, 199−205.
(26) Du, V., Luciani, N., Richard, S., Mary, G., Gay, C., Mazuel, F., Reffay, M., Menasché, P., Agbulut, O., and Wilhelm, C. (2017) A 3D Magnetic Tissue Stretcher for Remote Mechanical Control of Embryonic Stem Cell Differentiation. *Nat. Commun.*, 400 DOI: 10.1038/s41467-017-00543-2.
(27) Van de Walle, A., Sangnier, A. P., Abou-Hassan, A., Curcio, A., Hémadi, M., Menguy, N., Lalatonne, Y., Luciani, N., and Wilhelm, C. (2019) Biosynthesis of Magnetic Nanoparticles from Nanodegradation Products Revealed in Human Stem Cells. *Proc. Natl. Acad. Sci. U. S. A. 116*, 4044.
(28) Arakaki, A., Nakazawa, H., Nemoto, M., Mori, T., and Matsunaga, T. (2008) Formation of Magnetite by Bacteria and Its Application. *J. R. Soc., Interface 5* (26), 977−999.
(29) Roda, A., Cevenini, L., Borg, S., Michelini, E., Calabretta, M. M., and Schüler, D. (2013) Bioengineered Bioluminescent Magnetotactic Bacteria as a Powerful Tool for Chip-Based Whole-Cell Biosensors. *Lab Chip 13* (24), 4881−4889.
(30) Xie, J., Chen, K., and Chen, X. (2009) Production, Modification and Bio-Applications of Magnetic Nanoparticles Gestated by Magnetotactic Bacteria. *Nano Res. 2* (4), 261−278.
(31) Stanton, M. M., Park, B. W., Vilela, D., Bente, K., Faivre, D., Sitti, M., and Sánchez, S. (2017) Magnetotactic Bacteria Powered Biohybrids Target E. Coli Biofilms. *ACS Nano 11* (10), 9968−9978.
(32) Felfoul, O., Mohammadi, M., Taherkhani, S., de Lanauze, D., Zhong Xu, Y., Loghin, D., Essa, S., Jancik, S., Houle, D., Lafleur, M., Gaboury, L., Tabrizian, M., Kaou, N., Atkin, M., Vuong, T., Batist, G., Beauchemin, N., Radzioch, D., and Martel, S. (2016) Magneto-Aerotactic Bacteria Deliver Drug-Containing Nanoliposomes to Tumour Hypoxic Regions. *Nat. Nanotechnol. 11* (11), 941−947.
(33) Alapan, Y., Yasa, O., Schauer, O., Giltinan, J., Tabak, A. F., Sourjik, V., and Sitti, M. (2018) Soft Erythrocyte-Based Bacterial Microswimmers for Cargo Delivery. *Sci. Robot. 3* (17), No. eaar4423.
(34) Stanton, M. M., Park, B. W., Miguel-López, A., Ma, X., Sitti, M., and Sánchez, S. (2017) Biohybrid Microtube Swimmers Driven by Single Captured Bacteria. *Small 13* (19), 1−10.
(35) Matsumoto, Y., Chen, R., Anikeeva, P., and Jasanoff, A. (2015) Engineering Intracellular Biomineralization and Biosensing by a Magnetic Protein. *Nat. Commun. 6*, 8721 DOI: 10.1038/ncomms9721.
(36) Nishida, K., and Silver, P. A. (2012) Induction of Biogenic Magnetization and Redox Control by a Component of the Target of Rapamycin Complex 1 Signaling Pathway. *PLoS Biol. 10* (2), e1001269.
(37) Lee, J.-H., Roh, Y., and Hur, H.-G. (2008) Microbial Production and Characterization of Superparamagnetic Magnetite Nanoparticles by Shewanella Sp. HN-41. *J. Microbiol. Biotechnol. 18* (9), 1572−1577.
(38) Ramesh, P., Hwang, S. J., Davis, H. C., Lee-Gosselin, A., Bharadwaj, V., English, M. A., Sheng, J., Iyer, V., and Shapiro, M. G. (2018) Ultraparamagnetic Cells Formed through Intracellular Oxidation and Chelation of Paramagnetic Iron. *Angew. Chem., Int. Ed. 57*, 12385.
(39) Liu, X., Lopez, P. A., Giessen, T. W., Giles, M., Way, J. C., and Silver, P. A. (2016) Engineering Genetically-Encoded Mineralization and Magnetism via Directed Evolution. *Sci. Rep. 6*, 1−10.
(40) Lau, Y. H., Giessen, T. W., Altenburg, W. J., and Silver, P. A. (2018) Prokaryotic Nanocompartments Form Synthetic Organelles in a Eukaryote. *Nat. Commun. 9* (1), 1311 DOI: 10.1038/s41467-018-03768-x.
(41) Tatur, J., Hagedoorn, P. L., Overeijnder, M. L., and Hagen, W. R. (2006) A Highly Thermostable Ferritin from the Hyperthermophilic Archaeal Anaerobe Pyrococcus Furiosus. *Extremophiles 10* (2), 139−148.
(42) Isberg, R. R., Voorhis, D. L., and Falkow, S. (1987) Identification of Invasin: A Protein That Allows Enteric Bacteria to Penetrate Cultured Mammalian Cells. *Cell 50* (5), 769−778.

https://dx.doi.org/10.1021/acssynbio.0c00286
ACS Synth. Biol. XXXX, XXX, XXX−XXX

Supplementary Information for
Engineering *E. coli* for magnetic control and the spatial localization of functions

Mary Aubry[1], Wei-An Wang[1,2], Yohan Guyodo[3], Eugénia Delacou[1], Jean-Michel Guignier[2], Olivier Espeli[4], Alice Lebreton[5,6], François Guyot[2,7], Zoher Gueroui[1*]

[1] PASTEUR, Department of Chemistry, École Normale Supérieure, PSL University, Sorbonne Université, CNRS, 75005 Paris, France.

[2] IMPMC, Muséum National d'Histoire Naturelle, Sorbonne Université, UMR CNRS 7590, 75005 Paris, France.

[3] Université de Paris, Institut de physique du globe de Paris, CNRS, F-75005 Paris, France.

[4] CIRB-Collège de France, CNRS-UMR724, INSERM U1050, PSL Research University, Paris, France.

[5] Institut de biologie de l'ENS (IBENS), Département de biologie, École normale supérieure, CNRS, INSERM, PSL University, 75005 Paris, France.

[6] INRAE, IBENS, 75005 Paris, France.

[7] Institut Universitaire de France (IUF).

*Corresponding author. Email: zoher.gueroui@ens.fr

Table S1. List of plasmids used in this study.

Plasmid	Gene expression	Resistance	Source
pET28_mCherrry-ferritin	ferritin fused with mCherry	Kanamycin	From this study
pET28_GFP-ferritin	ferritin fused with EmGFP	Kanamycin	From this study
pGBM4_mCherrry-ferritin	ferritin fused with mCherry	Spectinomycin	From this study
pGBM4_GFP-ferritin	ferritin fused with EmGFP	Spectinomycin	From this study
pDSG375[a]	Nb2 production	Kanamycin	(*5*)
pDS419[a]	Ag2 production	Kanamycin	(*5*)
pRI203[b]	*Yersinia pseudotuberculosis inv* gene	Ampicillin Chloramphenicol	(*42*)

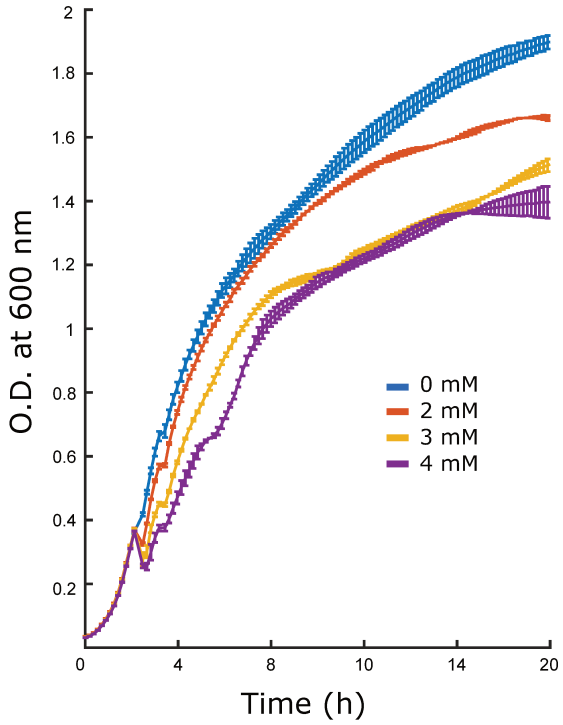

Figure S1. Growth curve of *E. coli* mineralized with 0, 2, 3 or 4 mM of Fe(II). The Optical Density at 600 nm for each condition of Fe(II) added is displayed as a function of time. In blue 0 mM, in red 2 mM, in yellow 3 mM, in purple 4 mM.

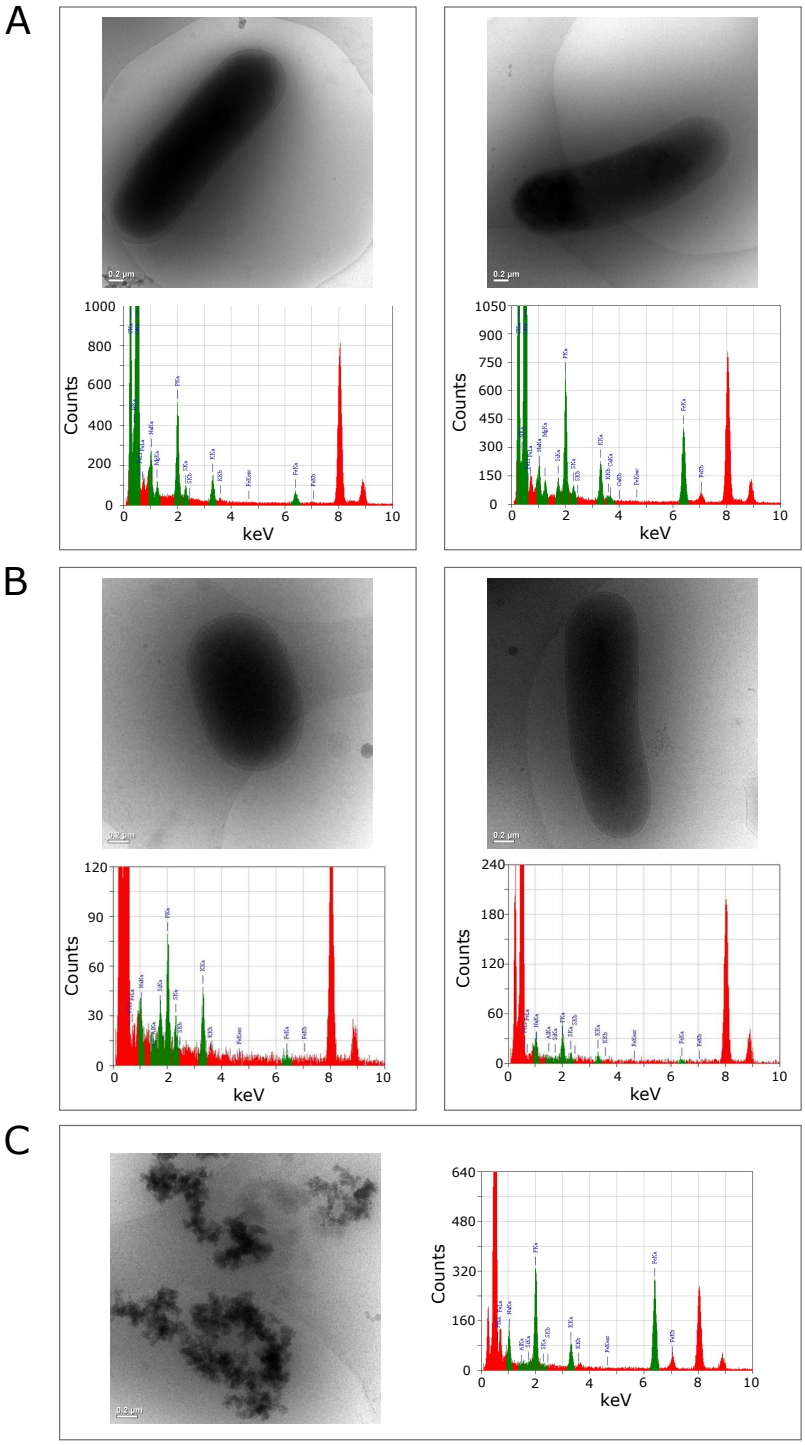

Figure S2. Cryo-TEM observations of *MagEcoli* and *E. coli* bacteria after biomineralization. (**A**) *MagEcoli* mineralized with 2 mM Fe(II) (**Right panel**) or 4 mM Fe(II) (**Left panel**). On the **top panel**: high resolution cryo-TEM images. Scale bar, 0.2µm. On the **bottom panel**: energy dispersive X-ray spectroscopy spectra for the bacterial cytoplasm. (**B**) Control *E. coli* that does not overproduce ferritin in presence of 2 mM Fe(II) (**Right panel**) or 4 mM Fe(II) (**Left panel**). On the **top panel**: high resolution

cryo-TEM images. Scale bar, 0.2µm. On the **bottom panel**: energy dispersive X-ray spectroscopy spectra for the bacterial cytoplasm. (**C**) Extracellular aggregates generated in the medium of control *E. coli* that does not overproduce ferritin in the presence of 4 mM Fe(II). On the **top panel**: high resolution cryo-TEM images. Scale bar, 0.2µm. On the **bottom panel**: energy dispersive X-ray spectroscopy spectra for the aggregate.

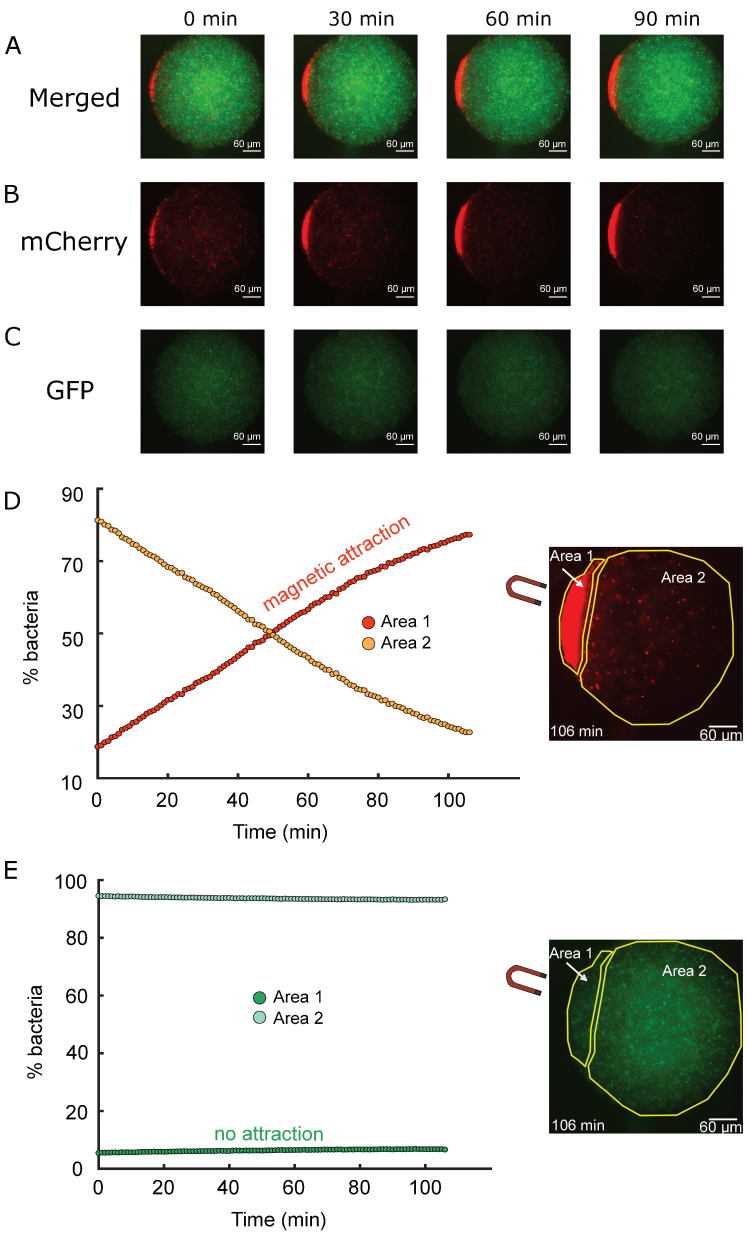

Figure S3. Quantification of the magnetic localization of *MagEcoli*^{mCherry} and *E. coli*^{GFP} from data displayed on Figure 2. *MagEcoli*^{mCherry} were homogenously mixed with non-magnetic *E.coli*^{GFP} at early time point. The magnet was positioned on the left. Time points at 0, 30, 60, 90 min after starting acquisition. **(A)** Data corresponding to the one displayed in Figure 2A. Color merged. **(B)** mCherry channel, colorized images. **(C)** GFP channel, colorized images. **(D)** Quantification of the number of *MagEcoli*^{mCherry} attracted toward the magnet as a function of time using the data extracted from the time-lapse reported on the Figure S3A. **Left:** Intensity of *MagEcoli*^{mCherry} measured in the area next to the magnet (area 1, red) and far from the magnet (area 2, orange), as a function of time. **Right**: The two regions of interest used for the quantification are highlighted in yellow. mCherry channel, colorized image. **(E)** Quantification of the number of *E. coli*^{GFP} attracted toward the magnet as a function of time. **Left:** Intensity of *E. coli*^{GFP} measured in the area next to the magnet (area 1, dark green) and far from the magnet (area 2, light green), as a function of time. **Right**: The two regions of interest used for the

quantification are highlighted in yellow. GFP channel, colorized image. For these curves, the intensity was normalized assuming that the sum of the number of bacteria in the two areas corresponds to 100%.

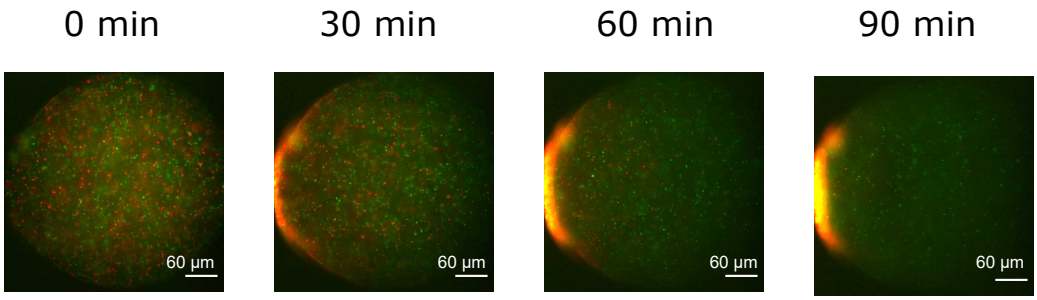

Figure S4. Representative time lapse fluorescence acquisition of the magnetic localization of *MagEcoli*^{mCherry} and *MagEcoli*^{GFP} in a confined environment upon magnetic force application. *MagEcoli*^{mCherry} were homogenously mixed with *MagEcoli*^{GFP} at early time point. The magnet was positioned on the left. Time points at 0, 30, 60, 90 min after starting acquisition. Color merged.

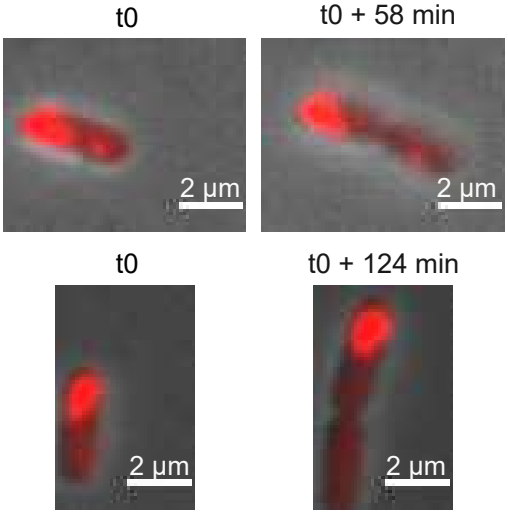

Figure S5. Mineralized bacteria before and after division. Superimposition of mCherry fluorescence and bright field images. The images of bacteria are extracted from time-lapse images of live fluorescence microscopy images as described in the Figure 3.

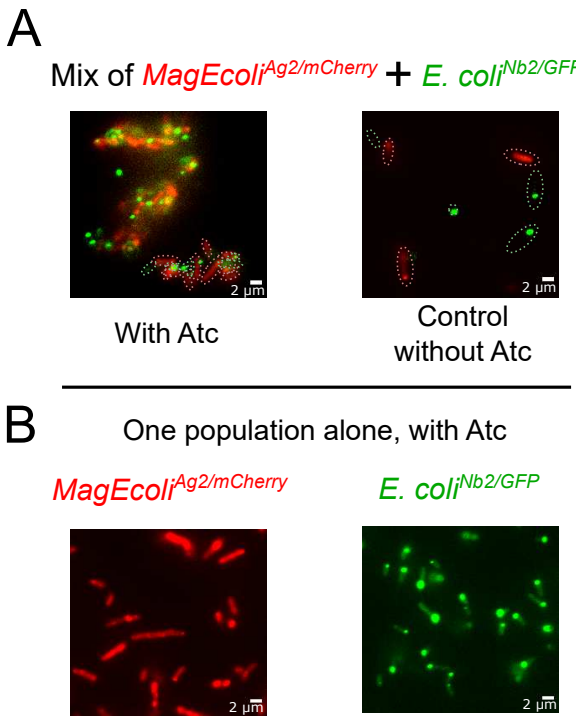

Figure S6. Fluorescence images of aggregates of *MagEcoli*$^{Ag2/mCherry}$ and *E. coli*$^{Nb2/GFP}$. Fluorescence observations. Scale bar, 2 µm. **(A)** The two populations are mixed. On the **left panel**: aggregates of *MagEcoli*$^{Ag2/\text{mCherry}}$ and *E. coli*$^{Nb2/GFP}$ in presence of anhydrotetracycline (Atc). On the **right panel**: control performed without anhydrotetracycline. Merged images of mCherry and GFP channels. **(B)** Auto-aggregation behavior of *MagEcoli*$^{Ag2/\text{mCherry}}$ and *E. coli*$^{Nb2/GFP}$ alone, in presence of anhydrotetracycline. On the **left panel**: *MagEcoli*$^{Ag2/\text{mCherry}}$. mCherry channel, colorized image. On the **right panel**: *E. coli*$^{Nb2/GFP}$. GFP channel, colorized image.

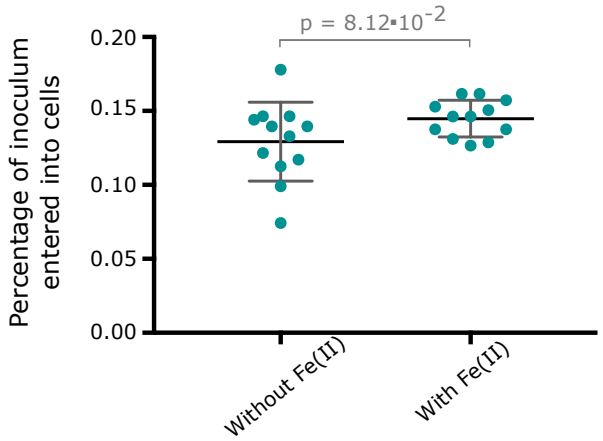

Figure S7. The biomineralization of invasive *MagEcoli* does not impede their internalization into epithelial cells. LoVo cells were infected for 4 h with *E. coli*$^{inv/GFP}$ expressing the invasin gene from *Y. pseudotuberculosis* and the ferritin-GFP fusion, that had been grown in medium containing either no Fe(II) (*E. coli*$^{inv/GFP}$*, left*) or 4 mM of Fe(II) (*MagEcoli*$^{inv/GFP}$, *right*). After gentamicin treatment for 1 h, the percentage of the inoculum having entered was assessed by plating serial dilutions of cell lysates. The values obtained for 12 technical replicates from a representative invasion assays among three independent experiments, their means and standard deviations were plotted. The probability *p* of rejection of the null hypothesis was assessed using a two-tailed Student's *t*-test.

Legends for Movies

Movie S1. Magnetophoresis experiments of *MagEcoli*^{mCherry} (2 mM of Fe(II)). Magnet was placed on the left. An image was taken every minute. Scale bar, 60 μm.

Movie S2. Magnetophoresis experiments of *MagEcoli*^{mCherry} (4 mM of Fe(II)). Magnet was placed on the left. An image was taken every minute. Scale bar, 60 μm.

Movie S3. Live fluorescence imaging of the division of single *MagEcoli*^{mCherry} over time. Merged movie of mCherry and contrast phase channel. An image was taken every two minutes. Scale bar, 2 μm.

2.3 - Annex

2.3.a – Iron dosage in *MagEcoli* after biomineralization

This part has been done in collaboration with Wei-An Wang that performed the chemical dosages.

As we added different concentrations of iron II during biomineralization, we wanted to know how many irons were really internalized by the *MagEcoli*. To have quantitative results, we chemically dosed the concentration of iron of mineralized bacteria. To do so, we followed a protocol of chemical dosage using phenantroline absoprtion adapted from the guidebook "Standard Methods for Water and Wastewater Analysis", APHA 1992.

We found that for a sample of mineralized *E. coli* at an O.D. of around 1:

- A **2 mM biomineralization** ends up in an iron concentration of 2 mM in the bacteria.
- A **4 mM biomineralization** ends up in an iron concentration of 3 mM in the bacteria.

Using an approximation: 1nM of iron correspond to 1 iron per bacteria (as the volume of bacteria could be 2 μm^3 = 2 fL, using the Avogadro number), we can say that we have around:

for 2mM biomineralization:

$$\boldsymbol{iron_{bacteria} = 2 \,.\, 10^6\, iron/bacteria}$$

And for **4mM biomineralization**:

$$\boldsymbol{iron_{bacteria} = 3 \,.\, 10^6\, iron/bacteria}$$

Previous lab work of purification of ferritin from bacterial culture showed us that we have around 0.016 µM of nanocage of ferritin per liter of culture. We can assume that the purification is made at saturation so for an O.D. of around 2 so for 2.10^9 bacteria/mL.

Hence we can calculate the number of ferritin nanocage per bacteria in this condition:

$$\boldsymbol{Ftn_{bacteria} = \frac{[Ftn].N_{avogadro}}{[bacteria]}}$$

$$Ftn_{bacteria} = \frac{1.6 \,.\, 10^{-8} \,.\, 6.022 \,.\, 10^{23}}{2.\, 10^{12}}$$

$$\boldsymbol{Ftn_{bacteria} \sim 5\,000\, ferritin/bacteria}$$

Now we can try to see how many atoms of iron are in the ferritins of *MagEcoli* for these two conditions: $\boldsymbol{Iron_{Ftn}} = \frac{\boldsymbol{iron_{bacteria}}}{\boldsymbol{Ftn_{bacteria}}}$

We find:

For 2mM biomineralization: $\boldsymbol{Iron_{Ftn}} \sim \boldsymbol{400\ iron/ferritine}$

For 4mM biomineralization: $\boldsymbol{Iron_{Ftn}} \sim \boldsymbol{600\ iron/ferritine}$

These numbers are **lower** than the actual storage capacity of ferritin (2 700 atoms of iron *in vitro* for a ferritin from *P. furiosus*[6]). It can be explained by different factors.

First our conditions of *in vivo* mineralization are different from an *in vitro* one. The temperature, pH, redox potential are controlled by the bacteria. Maybe in our conditions, less iron ions might have entered into the ferritins. Besides, a study of Hilton et. al[23] confirmed that, in presence of oxygen and phosphate like we have, the ferritins are less loaded with iron.

Furthermore, *E. coli* are living organisms and can regulate iron homeostasis. So a portion of the externally added iron II might have been expulsed from the bacteria. This is in agreement with our experimental observations: during biomineralization an iron deposit is formed in the tube!

Nevertheless, our result was in agreement with the data given for "ultraparamagnetic bacteria"[24]. Indeed, the authors have found a concentration of around 3fg of iron per bacteria, which corresponds to 10^7 atoms of iron per bacteria. They have dosed more iron, but in their case, on one hand, their magnetic properties seemed to be higher than ours (**see annex 2.3.c**). On the other hand, they may have underestimated their number of bacteria by basing their measures on colony forming unit and not O.D. like we did.

2.3.b – Magnetophoresis assay: set up explanations and comparisons

As performed in the article, to test the magnetic attraction of *MagEcoli*, we used a simple set up of magnetophoresis. We encapsulated freshly mineralized and washed bacteria in water-in-oil droplets. This has the purpose to confine the bacteria in a small observation chamber, and to reduce all hydrodynamic flows that could disturb magnetic attraction. Then the emulsion was inserted in a capillary (later sealed) and a magnet was placed at the extremity. Epifluorescence observation was made on droplets of around 200-600 µm diameter. If bacteria are attracted their Brownian motion is disturbed by the magnetic forces: magnetic forces dragged the bacteria and counterbalance viscosity.

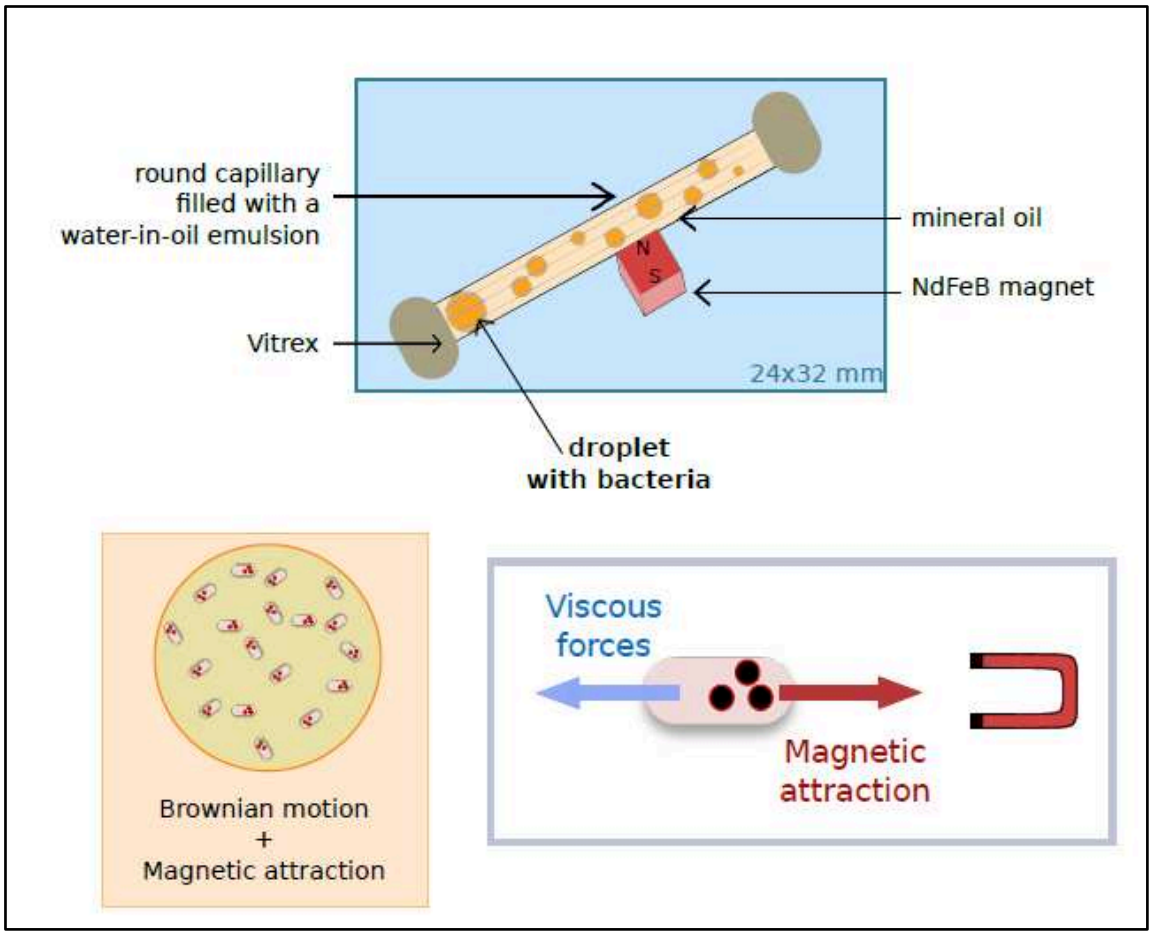

Figure 2.6: schematic representation of the magnetophoresis assays. At **the top**: an emulsion of bacteria is inserted in a round capillary. A magnet is placed, the North/Sud axis being perpendicular to the capillary direction. A camera is placed under the coverslip for microscopic observations. At **the bottom**: bacteria are trapped in droplets supplemented with sucrose or Optiprep to fight sedimentation. When bacteria are magnetic, magnetic forces attract the bacteria and counterbalance viscous forces; making their trajectory less dominated by the Brownian motion.

From these magnetophoresis assays, we extracted magnetic attraction velocities. We found a maximal speed for 4 mM-mineralized bacteria of 5 $\mu m.min^{-1} \pm 2\ \mu m.min^{-1}$. We know that magnetic

attraction counterbalances viscous forces in this low Reynolds regime. Hence we can deduce the magnetic forces acting on bacteria, via the Stokes Law:

$$F_{magnetic} = F_{viscous}$$

$$F_{magnetic} = 6\pi\eta r v$$

With η the dynamic viscosity of 40 %sucrose in water at 20°C = 6.22.10^{-3} Pa.s
With r the typical length of bacteria = around 1 µm
With the speed of bacteria = 5 µm.min^{-1}

Finally, we found a magnetic force of approximatively equal to:

$$\boldsymbol{F_{magnetic} = 10^{-14}\, N = 10\, fN}$$

From this data, we want to find the magnetic moment of a single *MagEcoli*. According to previous work from the lab with *in vitro* mineralized ferritin[7], in this condition of magnetophoresis, the magnetic force can be approximated with formula:

$$\boldsymbol{F_{magnetic} = m_{MagEcoli} \cdot \frac{dB}{dx}}$$

with $m_{MagEcoli}$ the magnetic moment of a MagEcoli

with dB/dx the gradient of magnetic forces induced by the magnet = 100 T/m maximum

So we can deduce and approximate a magnetic moment of *MagEcoli*:

$$\boldsymbol{m_{magecoli} = 10^{-16}\, Am^2}$$

The magnetic moment for *in vitro* mineralized ferritin found by previous laboratory work[7] was around:

$$\boldsymbol{m_{ftn\ in\ vitro} = 10^{-19}\, Am^2}$$

We can try to see if we find back this result, even if we know that conditions of *in vitro* mineralization are different (so the crystal phase might be better *in vitro*)!

We previously calculated that we have around **5 000 ferritins per bacteria**.
Thus, we can calculate the magnetic moment for each ferritin in *MagEcoli*:

$$m_{ftn\ in\ MagEcoli} = \frac{m_{MagEcoli}}{number\_ftn_{bacteria}}$$

$$m_{ftn\ in\ MagEcoli} = \frac{10^{-16}}{5000}$$

$$\boldsymbol{m_{ftn\ in\ MagEcoli} = 2.10^{-20}\ Am^2}$$

This result is **5 times lower** from the one found for *in vitro* mineralized ferritin. This may be due to many parameters. First the phase of iron oxides synthesized in ferritin *in vivo* is different from an *in vitro* synthesis. Indeed, the conditions of *in vivo* mineralization are not adjusted to aim a maghemite or magnetite phase, as they are regulated by the physiology of *E. coli* (pH, redox, temperature…). The number of irons stored in ferritin can also be lower for *in vivo* biomineralization because fluxes regulate iron concentration in the cytoplasm, and iron can interact *in vivo* with other partners making it less available for ferritins compared to *in vitro* mineralization. Besides, the gradient of magnetic field depends on the distance between the edge of the magnet and our droplet, it can be lower in our set up of magnetophoresis.

2.3.c – Comments on the magnetic properties of *MagEcoli* based on magnetometry assays

In the article, with the help of Yohan Guyodo, we conducted magnetometry tests in an attempt to characterize the structure of iron oxides inside *MagEcoli* (**Fig. 2.7**). This allowed us to compare it to magnetometry assays performed on other magnetic bacteria. For instance, the ferritin-overproducing bacteria of P. Silver[8] or the "ultraparamagnetic" bacteria[24] have been tested with magnetometry (**Fig. 2.7**).

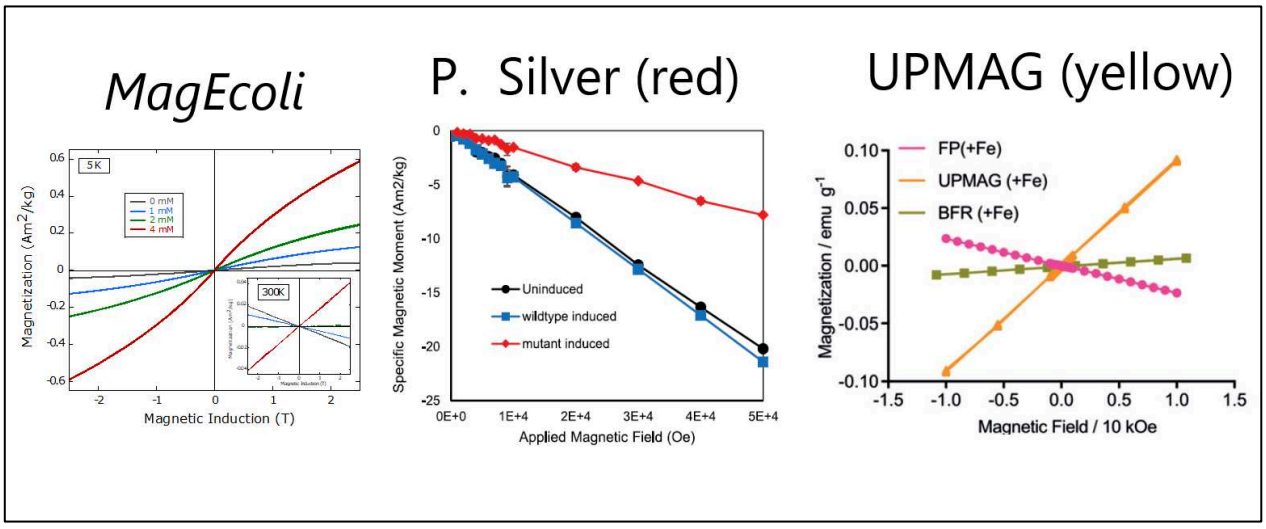

Figure 2.7: Magnetometry curves used to measure magnetic moments of mineralized *E. coli*. On **the left**: Curves for our *MagEcoli*, extracted from the article. In **the middle**: Curves for ferritin over-producing *E. coli* in red, extracted from[8]. On **the right**: Curves for "ultraparamagnetic bacteria" in yellow, extracted from[24].

If we look at our results, we have a positive slope for bacteria mineralized at 4 mM at 300K and for 0, 2 or 4 mM at 5K. It means that the diamagnetic composition of bacteria is counterbalanced by a positive magnetic contribution (paramagnetic, ferrimagnetic or antiferromagnetic…). The signal appears paramagnetic as no hysteresis was measured. Therefore, stoichiometric magnetite is unlikely present, as it is ferrimagnetic and would likely display hysteresis at 5K. This might fit with either a paramagnetic crystal or a highly disordered crystal with different phases (amorphous, ferrihydrite which is antiferromagnetic….), hence different contributions. We expected to have a ferrihydrite-like structure with some degree of phosphate inclusions, but VSM could not confirm it. Indeed, pure or slightly substituted ferrihydrite, while being antiferromagnetic displays some hysteresis at low temperature. Perhaps in our case the amount of phosphorus, while not necessarily affecting the global structure, may drastically reduce

super-exchange interactions between iron ions and thus affect magnetic ordering. A diluted ferrihydrite magnetite signal could be also difficult to observe. In any case, our iron oxides might be made of different phases and several magnetic contributions might counterbalance the diamagnetic effect, when the slope is positive.

Now, if we compare it to the work of P. Silver[8], we can see that their magnetization curves have negative slopes. In their case the diamagnetic contribution of organic matter is thus not counterbalanced by the mineralized ferritin. Considering that the temperature is not specified, we shall assume these were taken at room temperature. In our case, the room temperature data display a negative slope for the 0 and 1 mM sample, and a positive slope for the 2 and 4 mM biomineralization samples. We might argue that we obtained samples with better magnetic properties, yet a comparison is difficult since our data are a 100 times smaller in magnitude (at 300 K our highest contribution is 0.04 Am^2/kg for 2.5 T whereas their highest magnetic moment for their best mutant is around -4 Am^2/kg at 2.5 T). Such high negative value is however puzzling. Indeed, most diamagnetic materials possess magnetic susceptibility values in the -10^{-9} or -10^{-8} ranges, leading to magnetizations (in 2.5 T) in the 10^{-1} or 10^{-2} ranges. Either their sample holder is diamagnetic and fairly heavy compared to the samples, or there was a problem with their mass normalization or unit conversion. Considering the relative variations in magnetization, their data point to the presence of a positive component, which at 2.5 T represents 50% of the original signal for uninduced bacteria. This difference is close to the one we obtained between the 0 mM and 1 mM of iron added during biomineralization samples.

The data for "ultraparamagnetic bacteria"[24] have a magnitude that is similar to ours. At 30 K, their bacteria have a magnetic moment of around 0.14 Am^2/kg at 1 T, whereas ours have a magnetic moment of about 0.3 Am^2/kg at 5K and 1 T. Because their data were taken at 30 K and ours at 5 K, these cannot be compared directly. Authors of this study also measured the magnetic susceptibility as a function of temperature below 300 K. From these data, we can extrapolate a value of more than 0.4 Am^2/kg. Most importantly taking into account the large increase in susceptibility of any paramagnetic component, their samples would likely have a positive magnetization at 5 K (as it is the case for their BFR sample). Using the same argument, our sample would show low or negative magnetizations at 30 K (and does at 300 K). Both reasoning lead us to rationally assume that they produced bacteria with slightly higher magnetic moments. Besides, in the methods, they said they have avoided any contact with ferromagnetic materials for the sample preparation (such as the spatula) to avoid any contamination. This might explain why we, on the contrary, got a positive slope for non-mineralized *E. coli:* maybe a contamination. However, the shape of magnetization curve of our 0 mM sample is the same as those of iron-supplied samples. Furthermore, any

ferromagnetic contamination would lead to the presence of a small opening of the magnetization curve below 0.5T. A ferromagnetic contamination would be surprising!

If we compare our magnetization curves with SPIONs (superparamagnetic chemically synthesized iron oxides), we can see that our mass magnetization is much lower. A recent study[25], for example, has made different SQUID measurements of SPIONs with various phases (mix of magnetite, maghemite, goethite, ferrihydrite). We can compare their value at 300K. They found magnetization curves with positive slopes, with, except for the non-spinel samples, saturation below 1 T (significantly lower than our maximum field which did not saturate our samples). For the spinel samples, saturation mass magnetizations vary from 29 Am^2/kg (for a mix goethite/magnetite) to 64 Am^2/kg (for a mix of goethite/magnetite/maghemite). Ferrihydrite samples have the lowest magnetizations with a maximum value of 1.4 Am^2/kg for 300 K and 5 T. This value is nevertheless still higher than ours. In their study, they also found open hysteresis curves at low temperature, contrarily to ours. This is a signature for ferrimagnetism at 10 K for a mix of magnetite/maghemite, for instance. For their ferrihydrite sample, the hysteresis is almost inexistent, even at 10K, which is interesting with respect to the possible presence of ferrihydrite in our samples. Considering the shape and maximum values of their magnetization curves, a small amount of a similar mineral in our samples (about 10%) would likely not provide a measurable hysteresis, while providing the observed values of magnetization.

For magnetotactic bacteria, an assay[26] made at 300 K for *M. gryphiswaldense MG*, *M. magnetotacticum MS1,* and *M. magneticum AMB1* showed hysteresis (in agreement with magnetite signature), with coercivity values between 15 and 40mT, and mass magnetizations largely above 50 Am^2/kg at 0.1 T for each strain. It is even larger than both the previous value of SPIONs and our *MagEcoli*, as would be expected for magnetite (Ms = 92 Am^2/kg at 300K) embedded in dry organic matter[27].

Nevertheless, with the results of the articles and the magnetometry tests, we did not succeed in observing iron repartition in the individual ferritins inside the *MagEcoli.* We still do not know how iron atoms are distributed within the ferritins. TEM with a better resolution might help us to visualize the ferritin nanocage inside the inclusion bodies of bacteria and to look if iron is well in the protein core and not at the outside of ferritins. In the same way, the data did not determine precisely the phase of the iron oxides in bacteria. Other experiments based on X-ray absorption spectroscopy, XANES (X-ray Absorption Near Edge Structure) coupled with EXAFS (Extended X-Ray Absorption Fine Structure), are scheduled with Guillaume Morin and will give the Fe (II) / Fe (III) ratio and local structure of the biomineralized ferritins.

2.4 - References

1. Bulte, J. W. M. *et al.* Magnetoferritin: Characterization of a novel superparamagnetic MR contrast agent. *J. Magn. Reson. Imaging* **4**, 497–505 (1994).
2. Uchida, M. *et al.* Targeting of cancer cells with ferrimagnetic ferritin cage nanoparticles. *J. Am. Chem. Soc.* **128**, 16626–16633 (2006).
3. Kengen, S. W. M. 'Pyrococcus furiosus, 30 years on'. *Microb. Biotechnol.* **10**, 1441–1444 (2017).
4. Fiala, G. & Stetter, K. O. Pyrococcus furiosus sp. nov. represents a novel genus of marine heterotrophic archaebacteria growing optimally at 100°C. *Arch. Microbiol.* **145**, 56–61 (1986).
5. Tatur, J., Hagen, W. R. & Matias, P. M. Crystal structure of the ferritin from the hyperthermophilic archaeal anaerobe Pyrococcus furiosus. *J. Biol. Inorg. Chem.* **12**, 615–630 (2007).
6. Tatur, J., Hagedoorn, P. L., Overeijnder, M. L. & Hagen, W. R. A highly thermostable ferritin from the hyperthermophilic archaeal anaerobe Pyrococcus furiosus. *Extremophiles* **10**, 139–148 (2006).
7. Ducasse, R. *et al.* Programmed Self-Assembly of a Biochemical and Magnetic Scaffold to Trigger and Manipulate Microtubule Structures. *Sci. Rep.* **7**, 1–11 (2017).
8. Liu, X. *et al.* Engineering Genetically-Encoded Mineralization and Magnetism via Directed Evolution. *Sci. Rep.* **6**, 1–10 (2016).
9. Zhang, C. Essential functions of iron-requiring proteins in DNA replication, repair and cell cycle control. *Protein Cell* **5**, 750–760 (2014).
10. Rudolf, J., Makrantoni, V., Ingledew, W. J., Stark, M. J. R. & White, M. F. The DNA Repair Helicases XPD and FancJ Have Essential Iron-Sulfur Domains. *Mol. Cell* **23**, 801–808 (2006).
11. Banci, L. *Metallomics and the cell*. *Metal Ions in Life Sciences* **12**, (2013).
12. Nikaido, H. Molecular Basis of Bacterial Outer Membrane Permeability Revisited. *Microbiol. Mol. Biol. Rev.* **67**, 593–656 (2003).
13. Fardeau, S. *et al.* Bacterial iron uptake : a promising solution against multidrug resistant bacteria. *Sci. against Microb. Pathog. Commun. Curr. Res. Technol. Adv.* 695–705 (2011).
14. Andrews, S. C., Robinson, A. K. & Rodríguez-Quiñones, F. Bacterial iron homeostasis. *FEMS Microbiol. Rev.* **27**, 215–237 (2003).
15. Dixon, S. J. & Stockwell, B. R. The role of iron and reactive oxygen species in cell death. *Nat. Chem. Biol.* **10**, 9–17 (2014).

16. Hever, N. & Belkin, S. A dual-color bacterial reporter strain for the detection of toxic and genotoxic effects. *Eng. Life Sci.* **6**, 319–323 (2006).
17. Hightower, L. E. Heat shock, stress proteins, chaperones, and proteotoxicity. *Cell* **66**, 191–197 (1991).
18. Van Dyk, T. K. *et al.* Rapid and sensitive pollutant detection by induction of heat shock gene- bioluminescence gene fusions. *Appl. Environ. Microbiol.* **60**, 1414–1420 (1994).
19. Gray, M. J. & Jakob, U. Oxidative Stress Protection by Polyphosphate - New Roles for an Old Player. *Curr. Opin. Microbiol.* **24**, 1–6 (2015).
20. Escolar, L., Pérez-Martín, J. & De Lorenzo, V. Opening the iron box: Transcriptional metalloregulation by the fur protein. *J. Bacteriol.* **181**, 6223–6229 (1999).
21. Arosio, P., Elia, L. & Poli, M. Ferritin, cellular iron storage and regulation. *IUBMB Life* **69**, 414–422 (2017).
22. Chiancone, E., Ceci, P., Ilari, A., Ribacchi, F. & Stefanini, S. Iron and proteins for iron storage and detoxification. *BioMetals* **17**, 197–202 (2004).
23. Hilton, R. J., Andros, N. D. & Watt, R. K. The ferroxidase center is essential for ferritin iron loading in the presence of phosphate and minimizes side reactions that form Fe(III)-phosphate colloids. *BioMetals* **25**, 259–273 (2012).
24. Ramesh, P. *et al.* Ultraparamagnetic Cells Formed through Intracellular Oxidation and Chelation of Paramagnetic Iron. *Angewandte Chemie - International Edition* (2018). doi:10.1002/anie.201805042
25. Matos, J. C., Clara Gonçalves, M., Pereira, L. C. J., Vieira, B. J. C. & Waerenborgh, J. C. SPIONS prepared in air through improved synthesis methodology: The influence of γ-Fe2O3/Fe3O4 ratio and coating composition on magnetic properties. *Nanomaterials* **9**, (2019).
26. Staniland, S. *et al.* Controlled cobalt doping of magnetosomes in vivo. *Nat. Nanotechnol.* **3**, 158–162 (2008).
27. Harrison, R. J., Dunin-Borkowski, R. E., Kasama, T., Simpson, E. T. & Feinberg, J. M. Magnetic Properties of Rocks and Minerals. In T. J. Ahrens (Ed.), Handbook of Physical Constants. *Am. Geophys. Union.* **3**, 189–204 (1995).

Chapter 3: Engineering *E. coli* for magnetic control of quorum sensing communication and detection

This section is based on the following article in preparation for submission:

Magnetic whole *E. coli* biosensor programmed to detect AHL

Mary Aubry, Zoher Gueroui

Content

3.1 – Motivation: *MagEcoli* programmed to deliver or sense small molecules. Impact of the magnetic localization on quorum sensing-based communication

In this chapter, we examined how *MagEcoli* can be used to magnetically concentrate bacteria programmed to deliver or sense small molecules diffusing in the environment. We focused on quorum sensing, a mode of communication between bacteria that produce and respond to autoinducers (as AHL families). Such small molecules can diffuse in the environment and trigger gene expression of bacteria upon specific binding to a regulatory DNA circuit (**Chapter 1**). As simple bacterial communication system, we used two populations of *E. coli*: *E. coli* programmed to secrete AHL molecules in the environment, called *senders*, and *E. coli* modified with an AHL-dependent plasmid expression system which produces a red fluorescent protein (RFP), called *sensors*.

Our first goal was to investigate how the magnetic accumulation of AHL-secreting bacteria could induce a localized pattern of bacterial population detecting AHL (**Fig. 3.1**). Conversely, our second goal examined the magnetic accumulation of AHL-sensing bacteria, and asked if localization of sensing-bacteria may increase the detection of molecules for biosensing and diagnostic purposes. As quorum sensing may depend strongly on local concentration of bacteria, our assay could be a first step toward the spatial control of bacterial community.

In the following sections, we are providing additional backgrounds regarding quorum sensing, examples of reconstitution of quorum sensing using synthetic circuits, and a brief description of the assay used in our study.

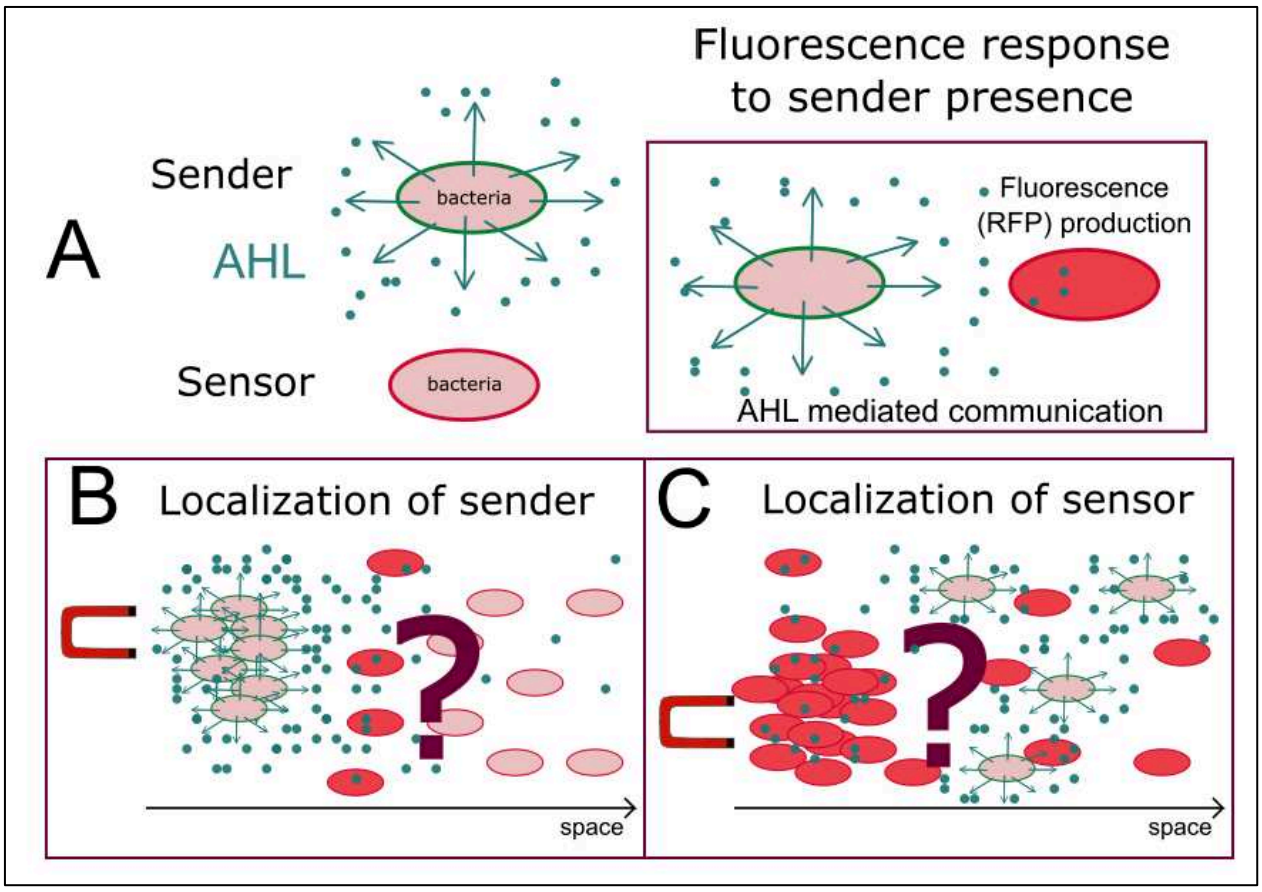

Figure 3.1: Schematic representation of our goal here: studying the effect of localization on bacterial communication. (A) The system used here: AHL-producing *E. coli* (*sender*) that can induce the production of RFP by an AHL-detecting *E. coli* (*sensor*). **(B)** We wanted to assess how magnetic accumulation of AHL-secreting bacteria could induce a localized pattern of AHL-detecting bacteria. **(C)** Conversely we examined the effect of magnetic localization of AHL-sensing bacteria on the detection signal (RFP production).

3.1.a –Quorum sensing communication depends on multiple factors in addition to cell density

3.1.a.i) Background regarding parameters controlling quorum sensing

As seen in the 1st chapter, quorum sensing is a mode of bacterial communication that allows a population to trigger a gene expression when they are numerous enough. To do so, bacteria, and even pathogenic ones, secrete autoinducers. Autoinducers can be molecules of acyl

homoserine lactone families for Gram-negative bacteria or peptides for Gram-positive ones. They trigger the expression of a gene that is linked to a specific phenotype: production of antibiotic, formation of biofilm, luminescence for instance. During quorum sensing, at low cell density, there is not enough autoinducers to trigger the gene. When bacteria reach a defined quorum, at high cell density, the gene is activated and the new phenotype occurs[1,2,3,4].

As autoinducers are secreted outside the bacteria, their local concentration can be disturbed by outer conditions. For example if autoinducers flow away from the bacterial population, the phenotype switch will be impacted[5]. Thus, we can logically assume that local variations of the environment have an additional impact on the microbial behavior. To regulate quorum sensing and diminish the environmental dependency, coordination strategies and diverse genetic pathways have appeared. We can cite the human pathogen *P. aeruginosa* that secretes not one but four principal autoinducers[6] (**Fig. 3.2**). This bacterium has evolved and ended with a more complicated quorum sensing circuit than *V. fisheri (V. fischeri* was discovered in 1994[7] in luminescent fish and its quorum sensing mechanism is controlled by only one pair of genes: *luxI/luxR)*. There are also *V. cholera,* a pathogen responsible for the cholera colonizing guts, and *V. harveyi,* a marine pathogen. They have a similar genetic architecture that relies on a two-channel system with membrane receptors[8]. Besides, it has been found in the early 2000s that *V. cholera* might response to a 3rd and maybe a 4th signaling component[9]. A recent study has confirmed that there are at least four parallel channels[10]. In this case, having multiple autoinducers might help these pathogenic bacteria to resist to fluctuant autoinducer concentrations in the environment and to better colonize the gut[11].

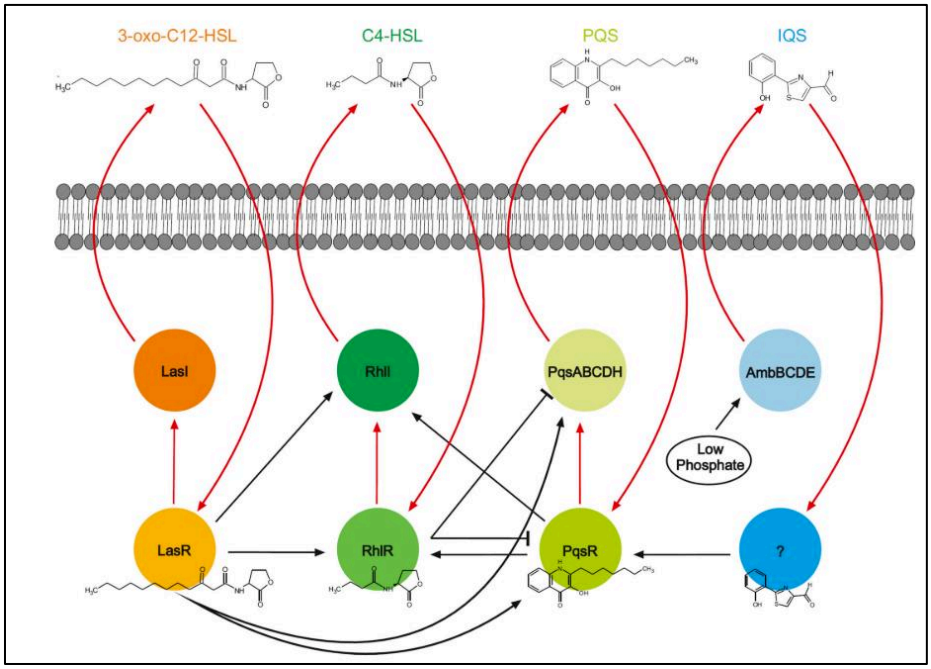

Figure 3.2: Example of a quorum sensing circuits: *P. aeruginosa,* extracted from[12]. Four autoinducers are secreted via various genes. They can interact with each other and this makes the genetic circuits of quorum sensing more complex.

In addition to physical events such as flows, the behavior of a group of bacteria also depends on its close bacterial neighbors. Indeed, some microorganisms can disturb quorum sensing communication of a strain via quorum quenching. Quorum quenching is a way to inhibit quorum sensing by acting at different levels: on the autoinducer itself or on the genes involved in quorum sensing (the one for autoinducer secretion or the one for autoinducer sensing)[13]. For instance two AHL molecules, N-decanoyl HSL and N-(3-oxo)tetradecanoyl-HSL, can substitute to N-hexanoyl-HSL in the quorum sensing circuit of *Chromobacterium violaceum* and reduce the production of violacein[14]. Moreover, a team has found that 24 on 166 isolated strains of marine bacteria can inhibit the violacein production by reducing AHL activity[15]. Microorganisms can use quorum quenching to regulate the virulence or population number of other strains. Even mammalian cells can do it, maybe as a way to inhibit microbial infections[16].

Finally, quorum sensing depends also on the geometry, the structure, of the environment. The phenotypes does not express the same way when bacteria are trapped in a cavity than when they are in a large area for instance[17] (**Fig. 3.3**). As a matter of fact, to prevent autoinducers loss via dilution or hydrodynamic flows, some bacteria create biofilm. In this specific structure, the

bacteria at the base are far from the outside and the secreted autoinducers remained trapped in the biofilm. With biofilm, bacteria can fight the disappearance of inducers due to external flows[18,19] (**Fig. 3.3**).

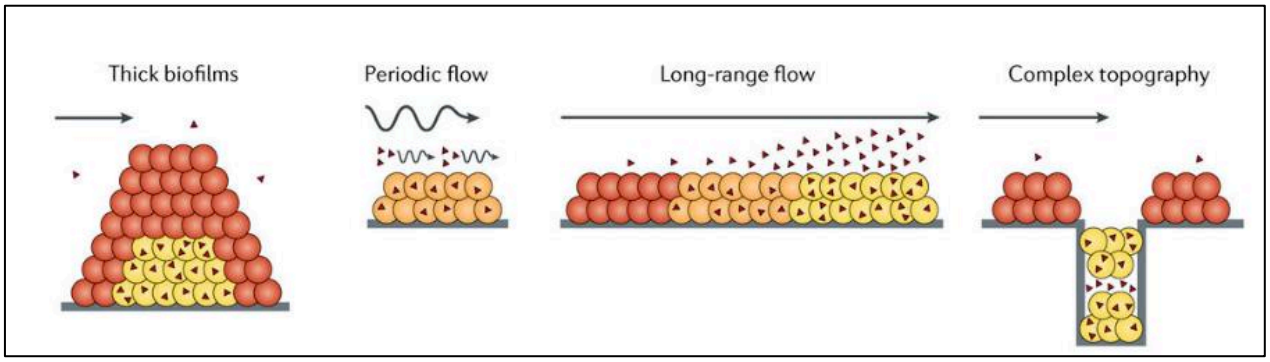

Figure 3.3: Behavior of a population of bacteria under flow, extracted from[17]. In yellow bacteria have adopted a "high density quorum sensing behavior", in orange "partial effect of inducers", in red bacteria behave as if they were at low cell density. Depending on the flow (arrow) and the geometry, the behavior of a population can be totally different.

3.1.a.ii) Reconstitution of quorum sensing in controlled geometries and using synthetic circuits

As environmental conditions can change the behavior of bacteria, some teams have created microfluidic tools to study quorum sensing in controlled conditions. For instance, to understand the unknown interaction of C8HSL with 3OC6HSL during quorum sensing for *V. fischeri*, a bacterium that uses both autoinducers, a team has designed a microfluidic set-up[20] in which a flow of C8HSL at various concentrations goes by bacteria. With their device they had understood that the two AHL molecules have a competitive behavior, at least at high cell density. Another team has used a water-in-oil-in-water emulsion to perform a double encapsulation of bacteria[21] and to study the quorum sensing behavior apparition in it.

Other teams have used encapsulation to study the effect of bacterial aggregation or autoinducer concentration on quorum sensing expression. In a study, scientists have looked at the impact of bacterial geometry and biofilm on quorum sensing[22]. They have encapsulated *Vibrio*

harveyi in hydrogels to precisely control the amount of bacteria studied. The trapped microorganisms formed different structures: “free cells”, “small and large aggregates”. They have found that fluorescence production via quorum sensing was enhanced when bacteria were aggregated and especially in large group of cells. This may be due to a lower diffusion of autoinducers in aggregates or less positive feedback (more autoinducers trigger the fluorescence gene instead). For bacteria confined at very low cell density in droplets (one or two bacteria per droplet), a study on *P. aeruginosa*[23] showed that quorum sensing initiation can be very different from a clone to another and generally begins once the bacterium divide. Their result highlighted that quorum sensing is not necessarily a group behavior. Under specific conditions, here extreme confinements of cells in droplets, it can be activated by one bacterium after several hours (**Fig. 3.4**). It only depends on the amount of autoinducers present in the medium.

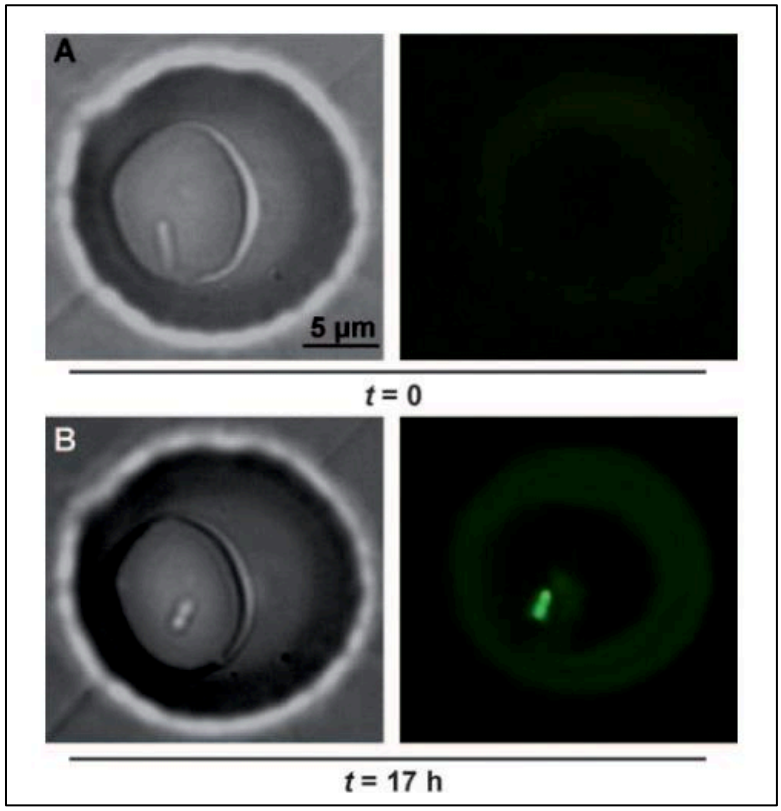

Figure 3.4: A droplet containing a *Pseudomonas aeruginosa*, extracted from[23]. Bright field on the left, fluorescence channel on the right. (A) Initial time **(B)** After 17 hours of encapsulation. The bacterium displays green fluorescence. It indicates quorum sensing activation that normally occurs at high cell density.

Furthermore, the team of Simmel has investigated bacterial communication mediated by AHL diffusion between droplets. In a first study[24], they used two populations of bacteria: the *senders* which produce and secrete AHL and the *sensors* which can trigger a gene upon AHL detection. By encapsulating separately both populations in water-in-oil droplets, they have shown that AHL diffuse through the oil and can trigger the *sensors*'s gene after a few hours (**Fig. 3.5**). They went even further in a second article[25], by encapsulating *sensors* separately from "cell free expression" system (AHL *senders*) in droplets organized in one direction. They have shown that their 1D set-up can be a way to locally activate gene expression in droplets (**Fig. 3.5**). By compartmenting bacteria in different droplets, they reveal that their system could be applied to force the communication between populations of bacteria that usually cannot live in the same culture medium.

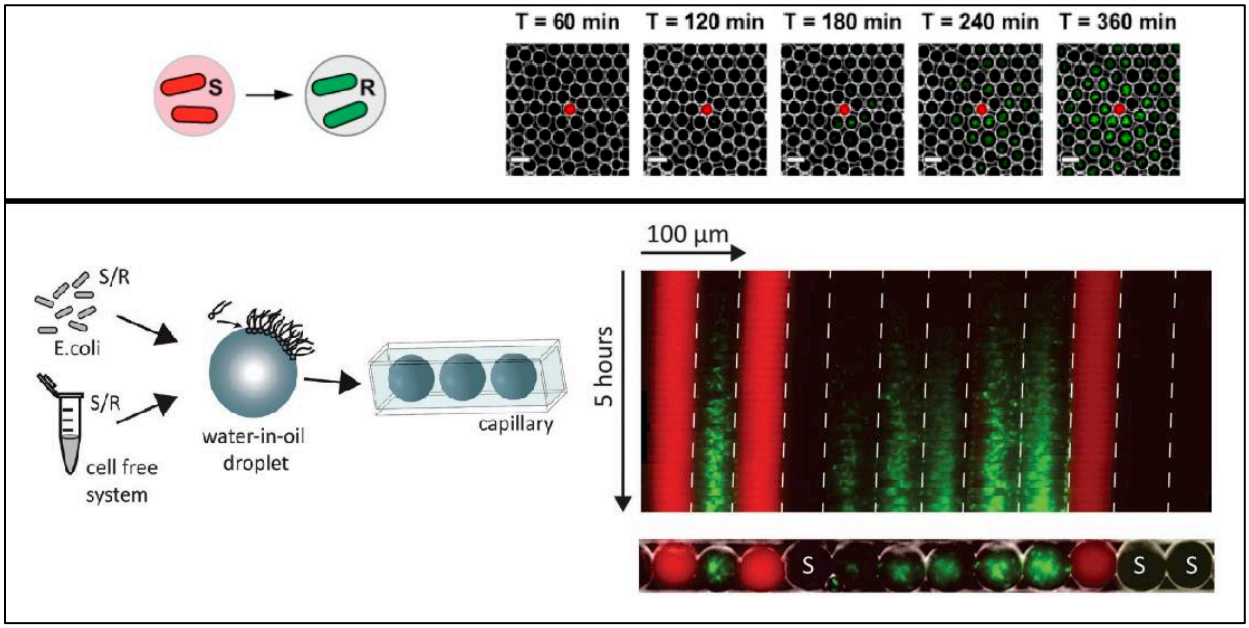

Figure 3.5: The set-up developed by the team of Simmel to study quorum sensing communication in emulsion, extracted from[24,25]. AHL and IPTG can diffuse through oil and activate *sensors* bacteria. Top panel: *Sender* and *sensor* bacteria are encapsulated in distinct droplets as depicted on **the left**. On **the right**, images of droplets at different time points. In red the *senders*, in green the *sensors* once they have expressed their AHL-dependent gene. **Bottom panel:** On **the left**, the set-up used in the second study. Bacteria or cell free systems are trapped in droplets inserted in a capillary in order to have a 1D arrangement. On **the right**, kymograph of fluorescence images of an assay of 5 hours. Droplets can either contain IPTG (in red), or cell free extract *senders* of AHL (no color) or *sensors* (in green after gene activation by both AHL and IPTG).

3.1.b – Our experimental set up to study quorum sensing

To examine quorum sensing, we decided to use a simple system based on two populations of bacteria: AHL-producing *E. coli* (*senders*) and AHL-detecting *E. coli* (*sensors*). The *senders* and *sensors* can communicate via AHL secretion and sensing, as drawn in **Figure 3.6**. The plasmids enable bacteria to produce (*sender*) or sense (*sensor*) by fluorescence an AHL molecule via the *luxI/luxR* genes: **N-(β-Ketocaproyl)-L-homoserine lactone (3OC6HSL)**[26,27].

To localize the *senders* or *sensors*, we decided to use magnetic forces. In the following parts we will study the effect of **(i)** having a *magnetic sender*, **(ii)** then a *magnetic sensor* on the communication. For these assay we co-transformed the *E. coli* with the plasmid coding for overproduction of GFP-ferritin and one of the two plasmids involved in quorum sensing. By applying our protocol of biomineralization with 4 mM of iron II, we obtained either *magnetic senders*, called *MagEcoli*^{senders}, or *magnetic sensors*, later referred as *MagEcoli*^{sensors}.

In order to get rid of external disturbances, we decided to confine bacteria in droplets, also because it is compatible with our experiment of magnetophoresis. We can simply use this set-up on *magnetic senders* or *magnetic sensors* to see the impact of magnetic concentration. We know that having bacteria in water-in-oil emulsion prevents large hydrodynamic flows and autoinducers loss, even though AHL partially diffuse through oil. Moreover, this configuration lets us visualize almost individual bacteria (**Fig. 3.6**).

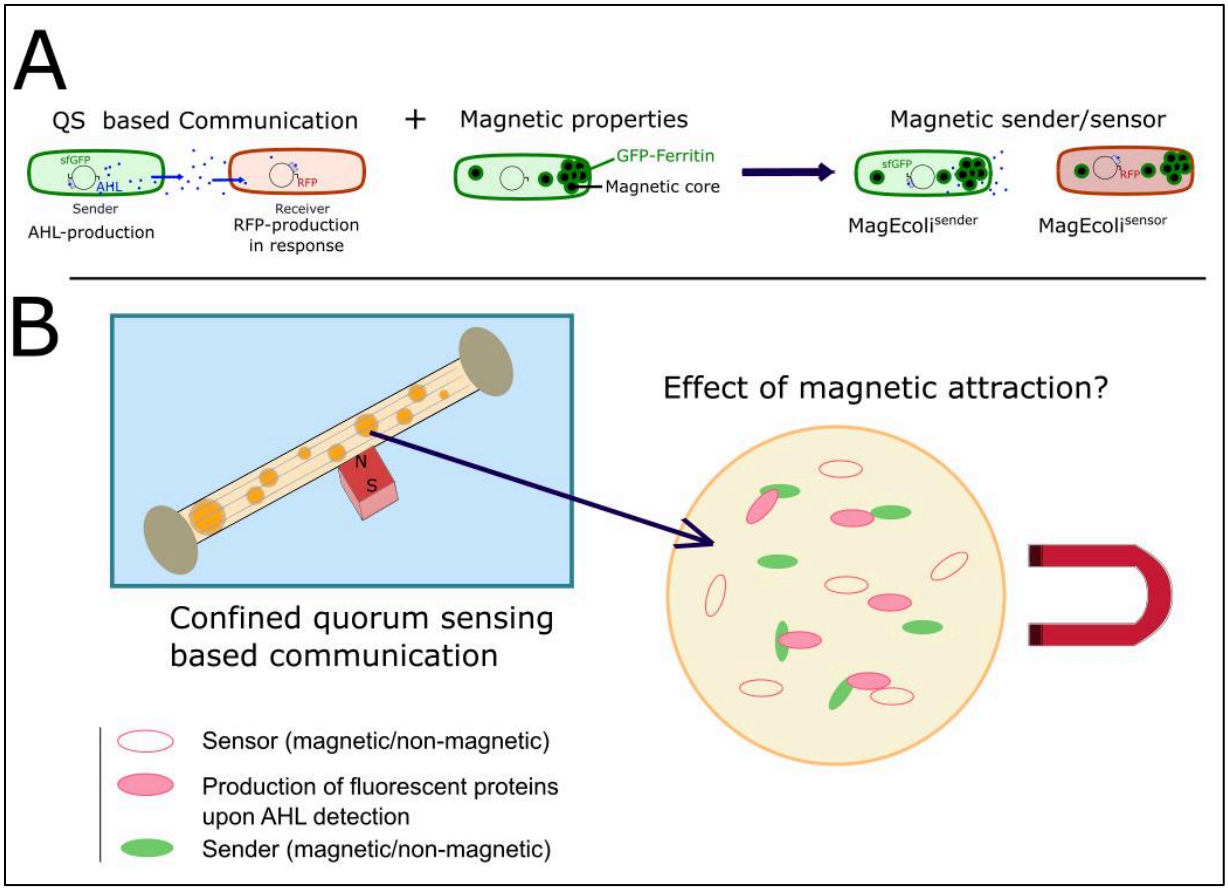

Figure 3.6: Schematic on the experiments made in this chapter. (A) Two plasmids from[27]and[28] mediate a communication between two populations of *E. coli*. A *sender* plasmid allows bacteria to overproduce sfGFP and to secrete 3OC6HSL. The *sensor* plasmid allows bacteria to express RFP upon induction via 3OC6HSL. We can additionally modify *E. coli* with a plasmid described in the 2nd chapter to make them over-produce GFP-Ferritin. With a process of biomineralization, ferritins are loaded with iron oxide and become magnetic (*MagEcoli*). Finally both properties can be combined in order to obtain a *MagEcoli*^{sender} or a *MagEcoli*^{sensor}. **(B)** The set-up of magnetophoresis used to study quorum sensing communication with bacteria that could display magnetic properties.

3.1.c – Challenges: impact of magnetic localization on AHL-based communication

So, in the following part, we will try, using *MagEcoli* which were transformed to have a role in quorum sensing communication, to determine if magnetism could be a useful tool to act on bacterial interactions (**Fig. 3.7**).

If the *senders* are magnetic, we wanted to know if localizing by magnetic forces the source of AHL is sufficient to induce a local sensing. **Does magnetic concentration of *senders* induce a localized gene expression for *sensors*?**

If the *sensors* are magnetic, we wanted to see if localizing the *sensors* could be a way to improve the level of detection. As concentration of fluorescent bacteria induces a local increase of fluorescence, we wanted to know if localizing the *sensors*, if they respond to AHL by fluorescence, could help us to detect lower amount of AHL. **Does concentrating *sensors* change the signal expression and quantification?**

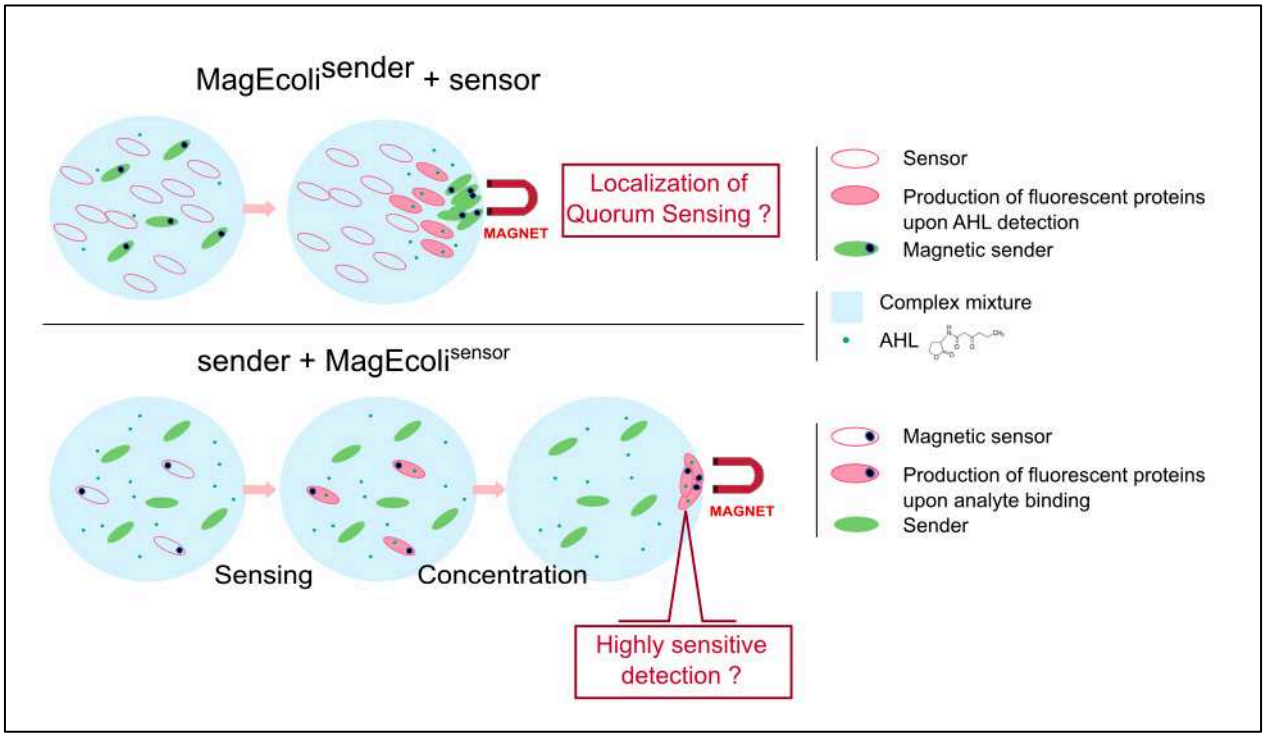

Figure 3.7: Magnetic properties to concentrate *sender* and *sensing* bacteria in space. At **the top** we wonder the consequences of having localized *MagEcoli*^{senders}. At **the bottom** we wonder the consequences of having localized *MagEcoli*^{sensors}.

3.2 - Magnetic localization of AHL *senders*

We studied the following configuration: *MagEcoli*^{senders} mixed with *sensors* (*E. coli*^{sensors}) in a liquid droplet. We investigated whether biomineralization altered the secreting functions of the *magnetic senders*, and the effect on detection when *senders* are localized by magnetic forces.

3.2.a - Results

3.2.a.i) Effect of ferritin over-expression and biomineralization on AHL secretion

Our *sender E. coli* consisted in AHL-producing bacteria (transformed with the plasmid pTD103luxIsfGFP[26] and a GFP-Ferritin expressing plasmid). Our *sensing E. coli* consisted in AHL-detecting bacteria (transformed with the plasmid pLux01[27]) (**Fig. 3.8A**). Using non-mineralized bacteria, we verified that the two plasmids could induce quorum sensing in our set-up, even in presence of an overproduction of GFP-Ferritin (**Fig. 3.8B**). Using our protocol of biomineralization on *senders* (4 mM iron (II)) which resulted in obtaining *MagEcoli*^{senders}, we also found that their magnetic localization resulted in RFP production as found in non-mineralized state (**Fig. 3.8B**).

This assay indicates that *MagEcoli*^{senders} keep their magnetic properties and are metabolically active enough to produce an AHL signals.

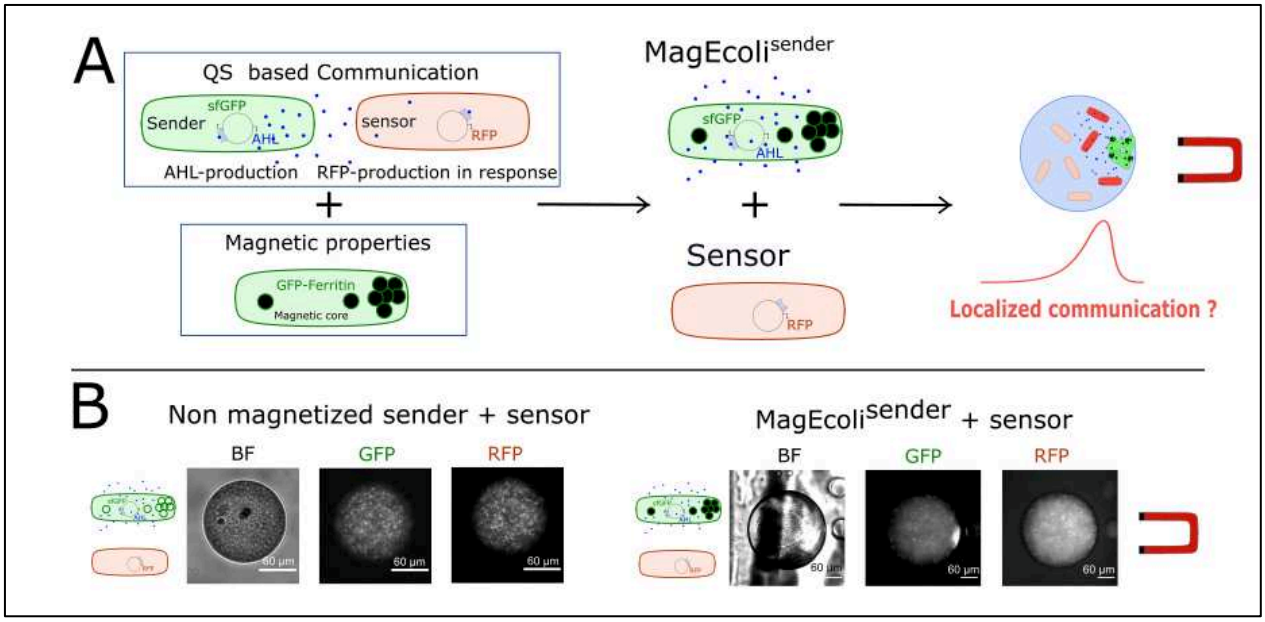

Figure 3.8: Representation of the assay. *MagEcoli*^{senders} and *sensors* are mixed in a droplet. (A) Schematic of the experiment. *E. coli* are genetically modified to communicate via 3OC6HSL. The *senders* are green fluorescent and secrete 3OC6HSL. The *sensors* can become red fluorescent upon the induction via 3OC6HSL. Via genetic and chemical modifications, the *senders* become magnetic and can be localized next to a magnet in a droplet. **(B)** Epifluorescence microscopy images of the experiments. On the **left panel**: non mineralized *senders* (bearing empty GFP-ferritins) are mixed with *sensors* for 2 hours and encapsulated in a droplet. On the **right panel**: *MagEcoli*^{sender} are mixed with *sensors* in droplets for around 2 hours with a magnet at the extremity. Bright field, GFP and RFP channel images are displayed. Scale bar, 60 µm.

3.2.a.ii) Magnetic attraction in liquid droplets to localize sensing by *sensors*?

To understand if localizing the source of AHL could be a way to spatially constrain the detection signal in space, we monitored the influence of concentrated *MagEcoli*^{senders} on sensing bacteria. We mixed the two populations in LB supplemented with Optiprep (to prevent sedimentation). We used our set up of magnetophoresis and observed both magnetic attraction and quorum sensing communication occurring in droplets via live fluorescence microscopy. At the beginning, *MagEcoli*^{senders} were uniformly distributed in the droplet (GFP channels) and the *sensors* could not be visualized in RFP channel (**Fig. 3.9A**). Over-time we observed a progressive accumulation of *MagEcoli*^{senders} toward the magnet and a uniformly increase of RFP fluorescence in the droplet (**Fig. 3.9A&B**). After 100 minutes of magnetophoresis, *MagEcoli*^{senders} (GFP) were localized next to the magnet, whereas the signal and position of *sensors* (RFP) was

homogenously distributed in the droplet (**Fig 3.9A&B**). We did not observe any localized production of RFP next to the magnet.

If we look closer at the red and green intensity in areas next and far from the magnet, we can see that, over-time, next to the magnet, there is a raise of RFP signal (AHL detection) and GFP signal (magnetic attraction). However, far from the magnet there is a loss of GFP signal (in agreement with magnetic attraction) but a raise of RFP signal (**Fig. 3.9B**). This quantification clearly indicates that RFP production is not confined by magnetic localization of senders. This is explained by the quick diffusion of AHL in the liquid medium. This small molecule has a size of around **72.5 Å²** [i]. We can estimate its diffusion coefficient in water as an approximation (as the viscosity in Optiprep is unknown):

D = $\frac{kT}{6\,\pi a \mu}$, with *a* the length of 3O6HSL and μ the dynamic viscosity of water at 20°C,

D = $\frac{1.38*10^{-23}*293.15}{6*3.14*\sqrt{72.5*10^{-20}}*1.002*10^{-3}}$ = 2.52 10^{-10} $m^2.s^{-1}$

We obtained around **252 µm².s⁻¹**. The radius of the droplets are around 200 – 800 µm. In few seconds the AHL produced has the time to go all around the droplet! If we take into account the fact that RFP needs several minutes to be produced and maturated (for instance mCherry needs 15 minutes[29]), AHL has the time to diffuse everywhere before any red fluorescence production, even if the *senders* are localized at an extremity ! The magnetic localization of *senders* cannot give satisfactory results in term of containment of quorum sensing activation by *sensors*.

If we still want to induce a local activation of *sensors* (next to the *senders*), we have to introduce a "sink" for AHL, which would degrade the autoinducer while it is being produced and help to decrease its concentration in the droplet. For instance we could add in the droplet a bacterial strain that would degrade AHL (via lactonase for example) or we could equip our *sensors* with a lactonase enzyme. If we suppose that k_0 is the degradation frequency, the length of AHL diffusion will be $\sqrt{\frac{D}{k_0}}$ with D the diffusion coefficient, if we adapt the formula described by Kholodenko for phosphoprotein gradients[30]. If the degradation of AHL is fast enough, we could reduce its diffusion!

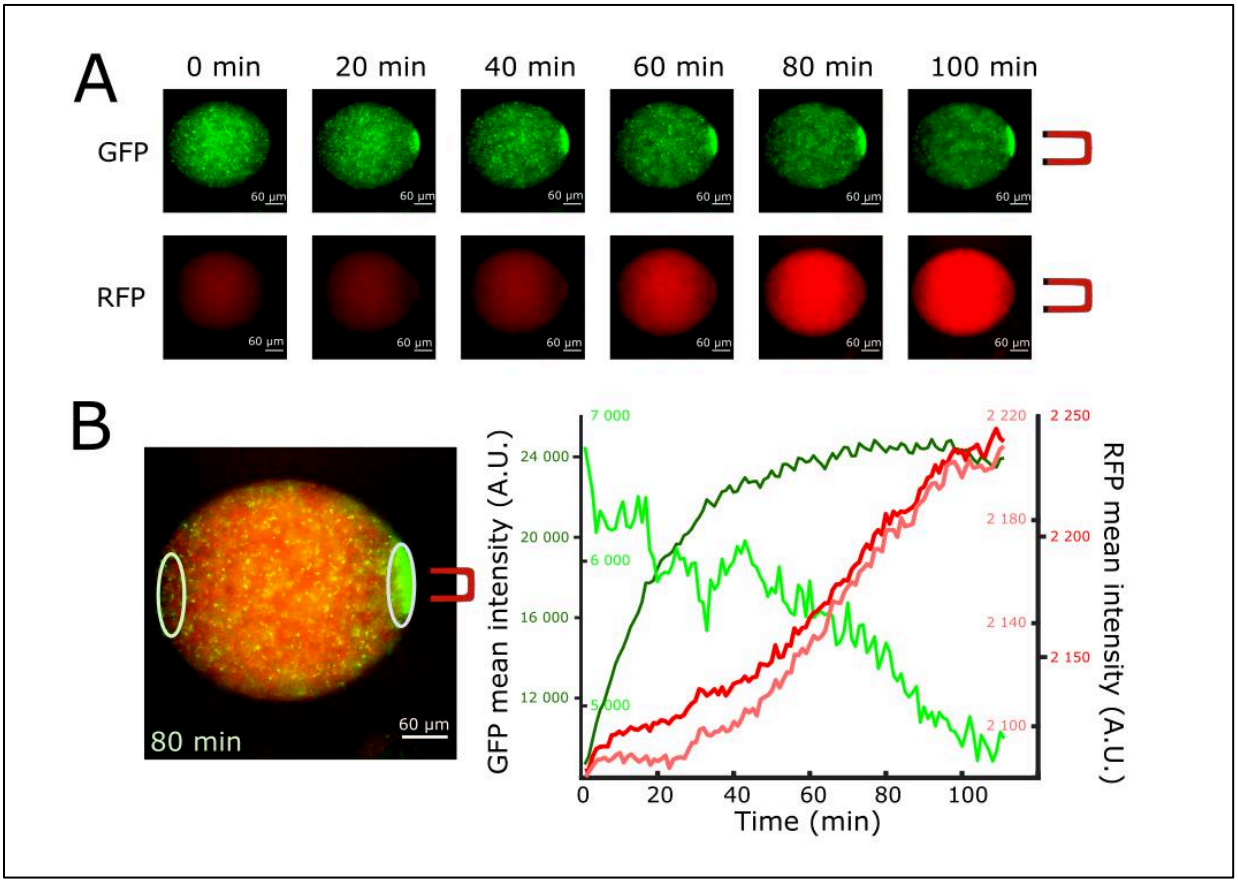

Figure 3.9: Magnetophoresis on *MagEcoli*^{senders} and *sensors*. (A) Time lapse images of a droplet containing magnetic *senders* and *sensors*. The magnet is placed on the right. Colorized images in GFP and RFP channel. Scale bar, 60 µm. **(B)** On **the left:** Merged image at 80 minutes of the droplet in **(A)** with magnetic *senders* and *sensors*. The magnet is placed on the right. Two areas are highlighted in white: closed to the magnet and far from the magnet, used for further quantification. Scale bar, 60 µm. On **the right**: plot of green and red fluorescence intensity at a function of time, in the area next to the magnet and far from the magnet. In dark green, GFP intensity next to the magnet. In light green, GFP intensity far from the magnet. In dark red, RFP intensity next to the magnet. In pink, RFP far from the magnet.

3.2.a.iii) Magnetic localization on solid medium to constrain the sensing?

As AHL fast diffusion in liquid media precludes any effect of the localization of magnetic *senders* at submillimeter scales, we examined another geometry consisting in depositing localized *senders* on solid agar medium. This will provide two additional features: a larger amount of bacteria growing into solid agar and the possibility to detect gradient of AHL concentration on larger space-scale (centimeter). Our assay consisted in extracting *MagEcoli*^{senders} from a liquid

medium by magnetic forces and transferring them via contact printing on a solid surface already covered by an homogenous population of *sensors* (**Fig. 3.10A**). After 24 hours, in most of assays, we could detect a gradient of RFP intensity localized around the contact zone between the gel and the magnet. Using a solid medium was a way to activate a spatial pattern of RFP production (**Fig. 3.10B**). On solid surface, several parameters can influence RFP distribution: a large amount of *sensors* next to the magnet that can uptake produced AHL for RFP production (and locally reduce its availability), a more complex diffusion of AHL in this viscous matrix mixing agar-gel and bacteria (even though the dimension of AHL are certainly smaller than the 1.5% agar gel mesh size). This result was in agreement with the simulation and experiment made in similar conditions[31]: the activation of *sensors* around *senders* has a size of several millimeters.

Control experiments performed with non-biomineralized sender bacteria displayed a less intense gradient of RFP producing bacteria (**Fig. 3.10B**). This is probably due to the non-specific adsorption of sender bacteria on the magnet surface.

As a perspective and in the context of diagnostic and pathogen detection in complex medium, we could think of first extracting the pathogens with nanobody-expressing magnetic bacteria (as shown for the Ag2/Nb2 application in the 2nd chapter), and then transfering the pathogens on a solid surface (gel or paper for instance) covered by sensor bacteria.

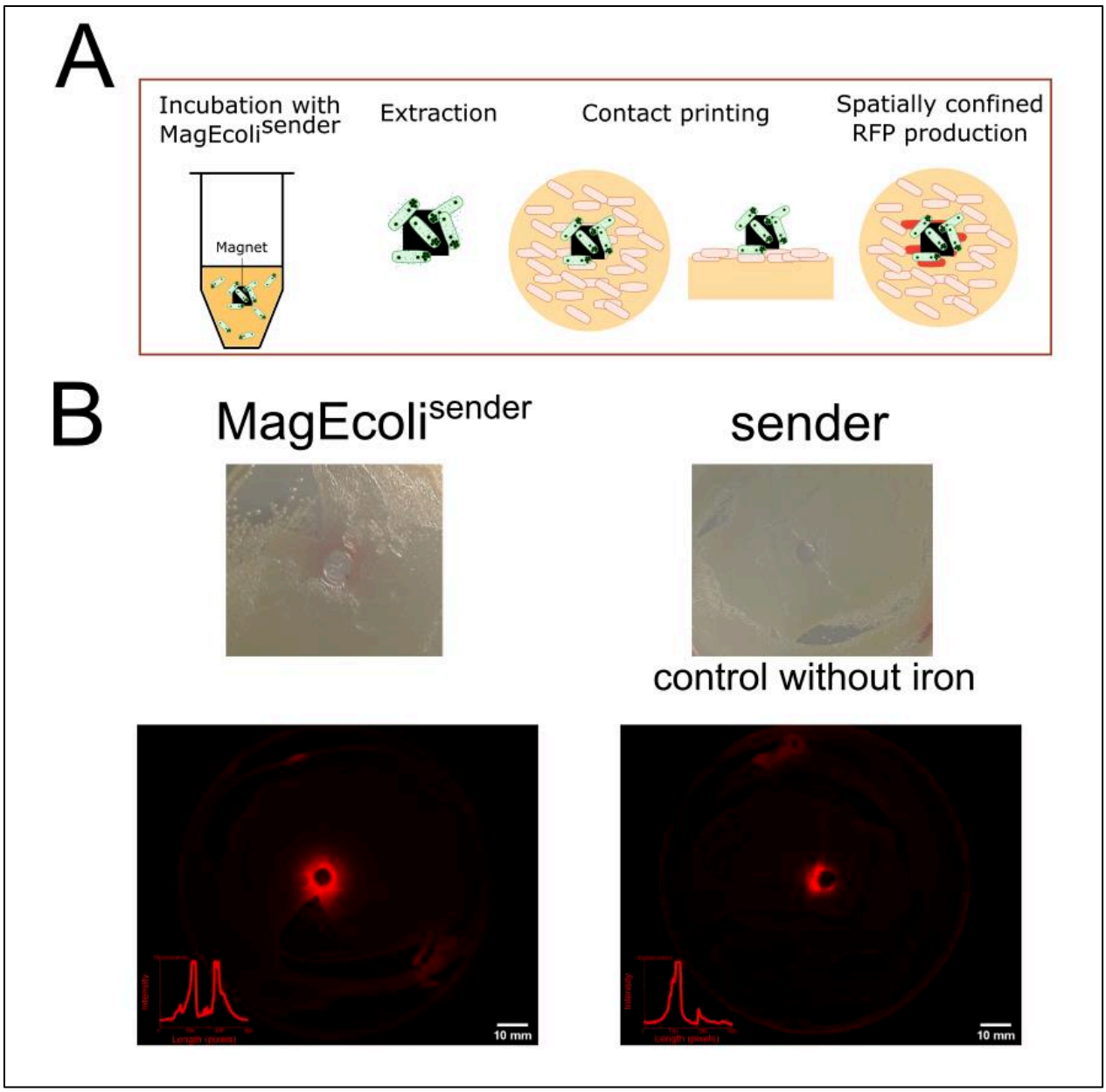

Figure 3.10: Assay of magnetic printing. (A) Schematic representation of the experiments. *Senders* are incubated for 2 hours with a waterproof Teflon-coated magnet under agitation to extract *MagEcoli*^{senders}. Next the magnet is deposited on an agar plate covered with *sensors.* After 24 hours of incubation at 37°C, the *sensors* in presence of magnetic *senders* have produced RFP visible on eye. **(B)** Pictures of the plate with the red fluorescent ring, visible on eye at **the top**, or with 546 nm illumination and 0.5 s of exposure time at **the bottom**. On **the left panel:** magnetic *senders* were attracted by the magnet. On **the left panel:** non-biomineralized *senders* were adsorbed on the magnet, control experiment. Scale bar, 10 mm. In **the inset:** plot profile of the red fluorescence intensity across the magnet. The measures are made on along a same line of 300 pixels crossing the magnet printing for the two conditions. In both conditions the RFP intensity saturates but the gradients of fluorescence have different length.

3.3 – Magnetic localization of AHL *sensors*

3.3.a – Context: whole-cell biosensors for quorum sensing pathogens

Quorum sensing is also used amongst pathogens like Gram-negative bacteria[1,32]. Thus, biosensors based on AHL-sensing are studied to detect quorum sensing communicating pathogen (**Chapter 1**). Sensing the autoinducers in the medium is a way to efficiently spot the quorum sensing pathogens presence. This technique has many advantages. AHL is specific to one kind of bacteria, is secreted by alive, active and pathogenic strain and could be sensed in a few hours. It can be detected by HPLC measurements, but it requires the chromatographic equipment, and steps of purification to enter into the columns[14]. An inexpensive and fast alternative is provided by whole-cell biosensors. By modifying bacteria with plasmids that respond to AHL either by bioluminescence or by the production of fluorescence molecules, quorum sensing pathogens can be found easily with optical detection. Optical or colorimetric response offers detection via a non-destructive pathway and can be done *in situ*. Many teams of scientists have investigated this type of biosensors, based on luminescence, fluorescence, violacein secretion... One team has combined thin layer chromatography to identify the AHL molecules detected by biosensors in sputum samples[33], another has tried to detect AHL in stool stample[34]. A strain has even been engineered to sense and kill pathogenic bacteria[35,36]. Teams of scientists obtained a level of detection of AHL in liquid samples between the micromolar and nanomolar range[34] (even picomolar range for the most performing ones[37]). In a recent study, scientists have developed a paper-based kit to detect AHL: it contained bacterial sensors that secreted B-galactosidase in response to AHL. As this molecules turn blue in contact to XGaI, they could have obtained an AHL sensitivity of 10 nM after 90 minutes to AHL on paper[38].

3.3.b – Article & Supplementary Information

The following article is in preparation for submission and gathers exploratory experiments. Complementary assays still need to be performed.

Magnetic whole *E.coli* biosensor programmed to detect AHL

Mary Aubry and Zoher Gueroui

Abstract

Whole-cell biosensors that respond to targeted chemicals could provide numerous advantages such as flexibility and low-cost of production. As example, bacteria programmed with synthetic circuits designed to respond to specific molecules could detect pathogenic bacteria by delivering an optical or colorimetric signal. For now, there is a need to improve whole-cell biosensors in order to have a fast and highly sensitive detection. In this context, we implemented magnetic properties into *Escherichia coli* which can detect AHL, a small molecule that mediates the communication among bacteria through the quorum sensing system. We studied the detection of AHL by magnetic-sensing *E. coli* and evaluated the detection by magnetic *E. coli* biosensors.

Introduction

Microorganisms can be engineered to perform various tasks with potential impacts in basic science, health, as well as material science. For instance their use as whole-cell biosensors that respond to targeted chemicals could provide numerous advantages such as flexibility and low-cost of production. Generally whole-cell sensors are composed of a sensing module, often a protein targeting a ligand or an environmentally responsive plasmid, that, in presence of the analytes, drive the host cells to produce a measureable signal such as fluorescence[1–4]. This strategy showed that they could be used to detect pathogens, pollutants, hormones in complex samples (biological samples[5], food[6], air[7]…). Thus whole-cell biosensors are likely to engage the current challenges of quantitative and real-time detection for diagnostic tests as well as *in situ* and non-invasive diagnostics in living organisms[8,9].

In order to expand the use of biosensors, we designed a magnetic whole-cell biosensor enabling the detection of analytes as well as the manipulation and concentration of the host cells by magnetic forces. Having a magnetic sensor can be advantageous. They can be manipulated in space, concentrated or even extracted from complex samples enabling a better read-out or sensitivity[10,11]. Here, we examined *E. coli* programmed to detect a specific-type of AHL, 3OC6HSL, a small molecule that mediates a communication among Gram-negative bacteria called quorum sensing[12]. *E. coli* was modified with an AHL-dependent plasmid expression system which produces a red fluorescent protein (RFP)[13]. We first studied the detection of AHL at the single bacterial level in a liquid medium by measuring the production of RFP. We worked in droplets to avoid hydrodynamic flows. This had the advantages of isolating the bacteria from the environment, and avoiding signal dilution[14,15,16]. Next by combining AHL biosensing capability with a magnetic-sensing *E. coli*, we assessed if we could build a magnetic whole-cell biosensor. We examined the AHL sensing at the single bacterial level and in liquid medium by attracting the biosensors confined in droplets using magnetic forces. This resulted in fold increase in the biosensor concentration next to the magnet and eventually the detected signal. With our assays, we managed to detect AHL at a concentration of 10 nM in less than 2 hours.

Results

Detection of single bacterial response to AHL in liquid droplets

We inserted a plasmid[13] coding for the production of Red Fluorescence Protein (RFP) upon N-(β-Ketocaproyl)-L-homoserine lactone (3OC6HSL) addition in *E. coli,* later referred as *E. coli*^{sensor} (**Fig. 1A**). As we wanted to visualize bacteria at all time, even in absence of 3OC6HSL, we labeled the *E. coli* with green fluorescence by making them overproduce GFP-ferritins in their cytoplasm (**Fig. 1A**).

First, we assessed the detection of AHL in liquid medium. To prevent hydrodynamic flows that could wash away 3OC6HSL and disturb the sensing, we worked in confined environment. We trapped the *E. coli*^{sensor} in sub-millimetric water-in-oil droplets with 3OC6HSL and we observed the bacteria with epifluorescence microscopy. For 100 nM of AHL, at initial time, bacteria were only visible in green fluorescence, due to GFP-ferritin over-expression. Then, after 80 minutes, the intensity of RFP increased and individual biosensors could be distinguished (**Fig. 1C**). The-lag-time in appearance of RFP was certainly due to the long maturation time of the protein (50 min 90% of RFP to become mature).

To go further, we quantified the RFP apparition as a function of time. Since RFP production resulted in the neat apparition of red bacterial bodies, we calculated a signal/noise ratio as a function of time. To do so, we monitored RFP fluorescence in a defined region (of 96 µm x 96 µm) at the center of the droplet (**Fig. 1C, lower panel**). By plotting a signal/noise ratio in this area, we noticed an increase over time concomitantly with the apparition of red-fluorescent bacterial bodies (**Fig. 1D**). In absence of AHL and as expected, we did not observe any increase of signal/noise ratio (**Fig. 1D**). This approach seemed well-suitable to study AHL detection. To see its limit on this same example, we reduced the region of interest while keeping a satisfying signal/noise ratio (**Fig. S1**). We tested various areas, from 96 µm x 96 µm to 2 µm x 2 µm (**Fig. S1A**) and we were able to detect a signal for areas wider than 4 µm x 4 µm (**Fig. S1B&C**). However, this detection method worked for *sensors* that were individually identified, *e.g.* that were relatively diluted in droplets; as an example we could not detect 100 nM of AHL for a bacterial density superior to 10 (**Fig. S2**). To further explore the limit of detection of this approach, we examined a lower level of AHL (10 nM) and successfully detected the RFP production by individual bacteria (**Fig. S3**).

Altogether, these data indicate that encapsulated *E. coli* biosensors detect 10 nM of synthetic AHL in 2 hours.

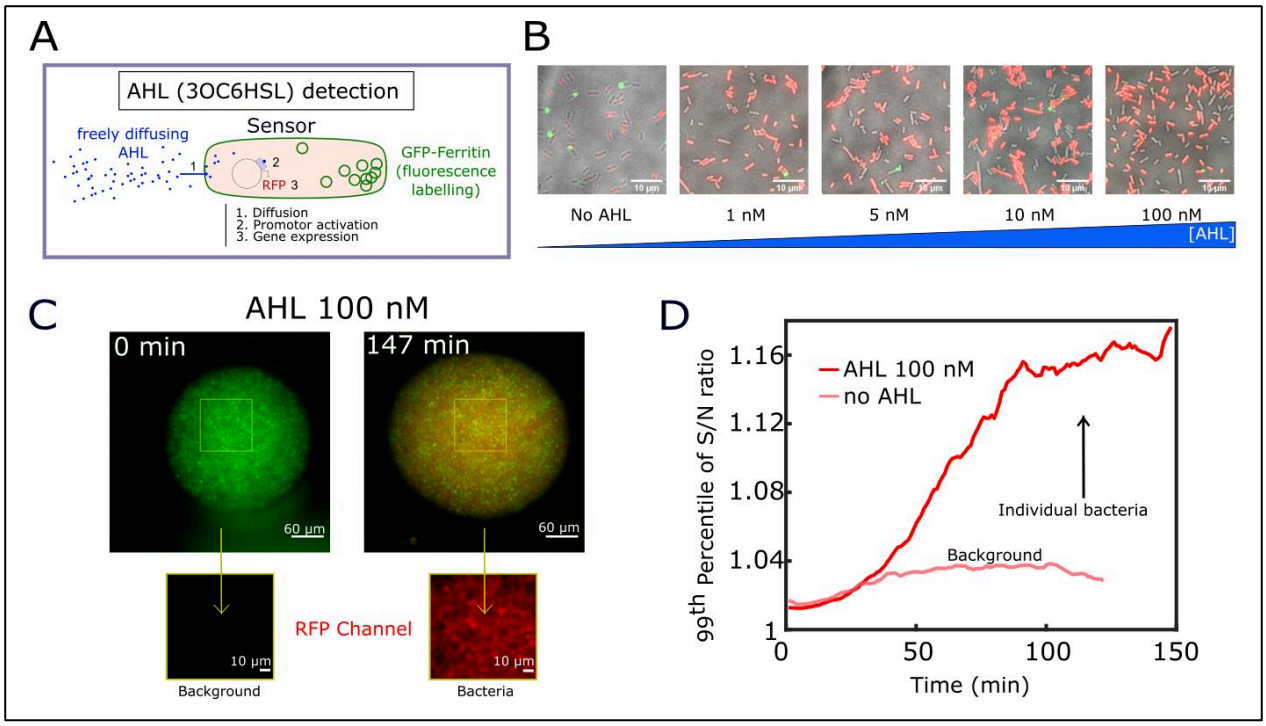

Figure 1: Detection of synthetic AHL by *E. coli*^{sensors}. (A) Schematic of the *sensor* used in this study. The *sensors* are *E. coli* which overproduce GFP-ferritin for visualization in green fluorescence. They have a plasmid that allows the production of RFP in response to 3OC6HSL presence. **(B)** Observation of *E. coli*^{sensors} after 2 hours in contact with AHL at various concentrations: 0 to 100 nM. Merged images of bright field, RFP and GFP channels. Scale bar, 10 µm. **(C)** Detection of bacterial body apparition in red fluorescence over time for an experiment of *sensors* encapsulated at an optical density of 5 with 100 nM of AHL. **Upper panel** Images at 0 (first acquisition) and 147 min (final acquisition). Merged GFP and RFP channels. Scale bar, 60µm. The area used for quantification is highlighted by the yellow square. **Lower panel:** Zoom of the yellow square area inside the droplet at 0 and 147 min, in RFP channel. Colorized images. Scale bar, 10µm. **(D)** Plot of the 99th percentile of signal upon noise ratio, following our method of detection in the square at the center of the droplet, as a function of time. In red, for the assay displayed at (C). In pink, for the negative control (without AHL), performed the same day, at the same bacterial concentration.

Magnetic whole-cell biosensor

Next we implemented magnetic properties to our *E. coli* in order to build a magnetic whole-cell biosensor as a first step to concentrate or sort sensing bacteria using external controls. The process to obtain magnetic bacteria with sensing properties consisted in co-expressing the *sensor* and the GFP-ferritin plasmids in *E. coli* in medium supplemented with iron (II)[17]. This process of iron biomineralization led, after over-night culture, to bacteria containing iron oxide-enriched bodies and conferring magnetic properties to *E. coli*, later referred as *MagEcoli*^{sensor} (**Fig. 2A**). To examine if the sensing properties of the *MagEcoli*^{sensors} were not precluded by the biomineralization step, we mixed the bacteria with synthetic 3OC6HSL (10 µM) for 2 hours and observed them on

agarose pad. As seen, *MagEcoli*^{sensors} produced red fluorescent protein in response to AHL (**Fig. S4**). Whereas all bacteria exhibited homogenous red fluorescence, only a fraction displayed a strong green fluorescence corresponding to ferritin with enriched iron-oxides accumulation.

Next, we tested the detection of AHL in liquid medium by *MagEcoli*^{sensors} in presence of a magnetic field (**Fig. 2A**). We confined *MagEcoli*^{sensors} with 3OC6HSL (100 µM) into millimetric emulsion droplets and deposited the droplets at the vicinity of a permanent magnet generating a gradient of about 100 $T.m^{-1}$. At initial time, epifluorescence observations showed a green fluorescent signal distributed uniformly in the droplet (**Fig. 2B**). Time-lapse observation showed that GFP expressing-*MagEcoli*^{sensors} started accumulating next to the magnet after few minutes, and that a majority of the bacteria were attracted in about 30 minutes **(Mov. S1, Fig. 2B, Fig. 2C upper panel)**. In addition, the quantification of the mean and integrated fluorescence intensity of RFP computed alongside the droplet's diameter revealed the local production of RFP after 45 minutes, which continuously increased during the acquisition time (**Mov. S1, Fig. 2B, Fig. 2C, lower panel**). We could also distinguish the appearance of red bacterial bodies homogenously distributed within the droplet that were not attracted. This result could be explained by the asymmetric division of *MagEcoli*^{sensors} that had occurred during the magnetophoresis assays: when *MagEcoli*^{sensors} divided in the droplet, only one daughter cell inherited the magnetic properties and was attracted toward the magnet[17].

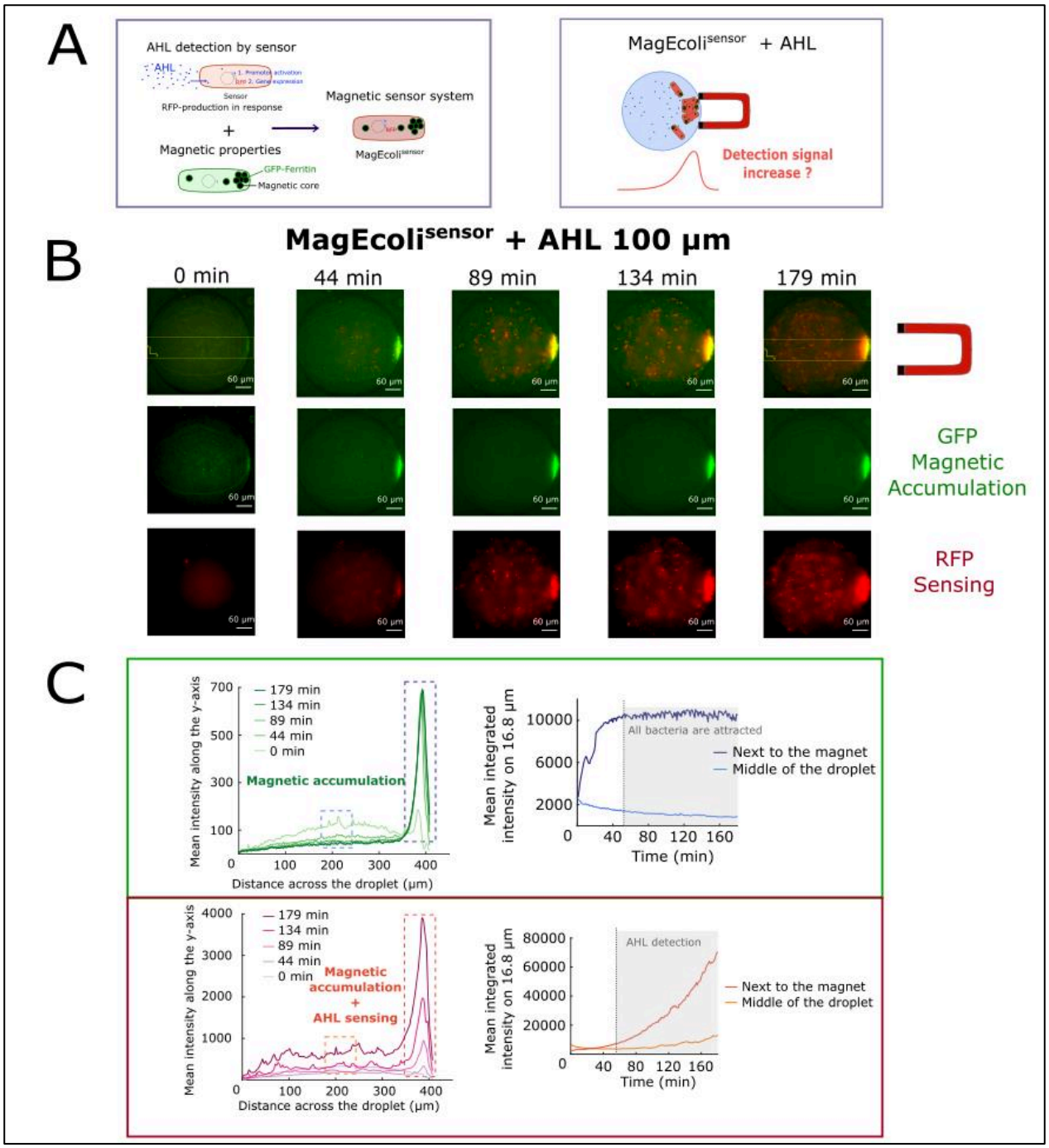

Figure 2: Assay of detection of AHL by the magnetic biosensors. (A) On the left: Schematic of the genetically engineered *E. coli* used in this study. With a set of 2 plasmids and our protocol of biomineralization, bacteria can sense 3OC6HSL presence and acquire magnetic properties. **On the right:** Representation of the hypothesis tested in this study: does a magnetic localization increase the *sensor* signal? **(B)** Assay of attraction of magnetic biosensor with 100 µM of synthetic AHL. Time-lapse images. **From top to bottom:** Merged, GFP and RFP colorized images. The magnet is on the right. Scale bar, 60 µm. **(C) At the top:** Mean intensity of green fluorescence over time across the droplet. On the right, integration over time of the mean intensity in the region next to the magnet and at the middle of the droplet (delimited by the yellow rectangle at (B)). **At the bottom:** Mean intensity of red fluorescence over time across the droplet. On the right, integration over time of the mean intensity in the region next to the magnet and at the middle of the droplet (delimited by the yellow rectangle at (B)).

We next examined the response of our *MagEcoli*^{sensor} to a second population of *E. coli* that produces and releases AHL in the environment and simultaneously over-expresses sfGFP, referred as *senders*[18] (**Fig. 3A & S5**). With this condition green fluorescence was distributed in all the droplets corresponding with both *senders* and *MagEcoli*^{sensors} signal. We found qualitatively a similar behavior with a detection of AHL by RFP production in 80 minutes, in the whole droplet and especially next to the magnet, due to magnetic attraction of *MagEcoli*^{sensors} (**Fig. 3B**), as reported in **Fig. 3C**.

Altogether, these data indicate that magnetic attraction increases the detected signal.

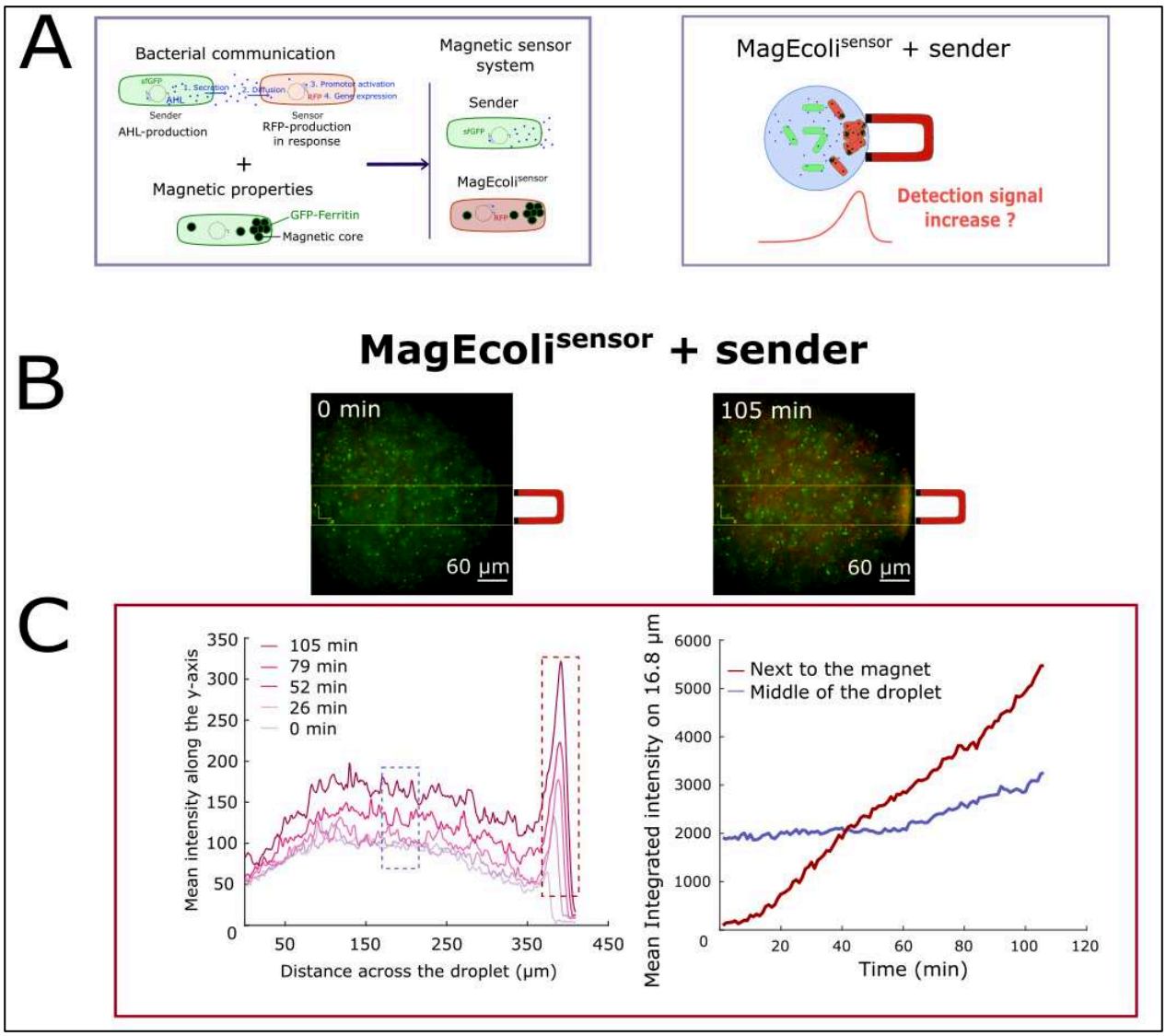

Figure 3: Assay of detection of *senders* by the magnetic biosensors. (A) On the left: Schematic of the genetically engineered *E. coli* used in this study. With a set of 2 plasmids and our protocol of biomineralization, bacteria can either send or sense 3OC6HSL presence and the *sensors* can acquire magnetic properties. **On the right:** Representation of the hypothesis tested in this study: does a magnetic localization of *sensors* increase the fluorescence signal? **(B)** Images of fluorescence signal over time for senders mixed with magnetic *sensors*, at 0 and 105 min. Merged RFP and GFP channels, magnet on the right. Scale bar, 60 µm. **(C)** Mean intensity of red fluorescence over time

across the droplet. On the right, integration over time of the mean intensity in the region next to the magnet and at the middle of the droplet (delimited by the yellow rectangles at (B)).

Improving the speed and yield of magnetic attraction (using iron oxide precipitation)

We saw that bacterial division of *MagEcoli*^{sensors} into a magnetic and a non-magnetic population precluded the concentration of the overall sensing *E. coli* next to the magnet. With the idea of increasing both the speed and the yield of attraction of biosensors toward the magnet, we adopted an alternative strategy. Contrary to our previous protocol, freshly prepared Fe^{2+} (2 mM) solution was directly mixed with non-mineralized *E. coli*^{sensors} and synthetic AHL (10 nM) in the droplets. In this condition, iron ions started to destabilize into colloidal iron oxides that could interact with the bacterial outer-membrane. Upon magnetic field application, this resulted in a strong accumulation of the majority of bacteria within 15 min, with all biosensors accumulated after about 80 min (**Movie S2 & Fig. 4A upper panel & Fig. S6**). Contrarily to the previous assays, quantification showed that all biosensors were attracted before RFP production and no red fluorescence intensity was monitored in the middle of the droplet (**Fig. 4B and 4C**). Concerning the area next to the magnet, a peak appeared and kept growing even after attraction of all biosensors at 80 minutes, indicating a production of RFP. Finally, we tried to lower the quantity of 3OC6HSL in the droplet to see if the sensitivity could be improved. 1 nM of AHL could not be detected: the fluorescence profile next to the magnet was similar to the one obtained for the control condition.

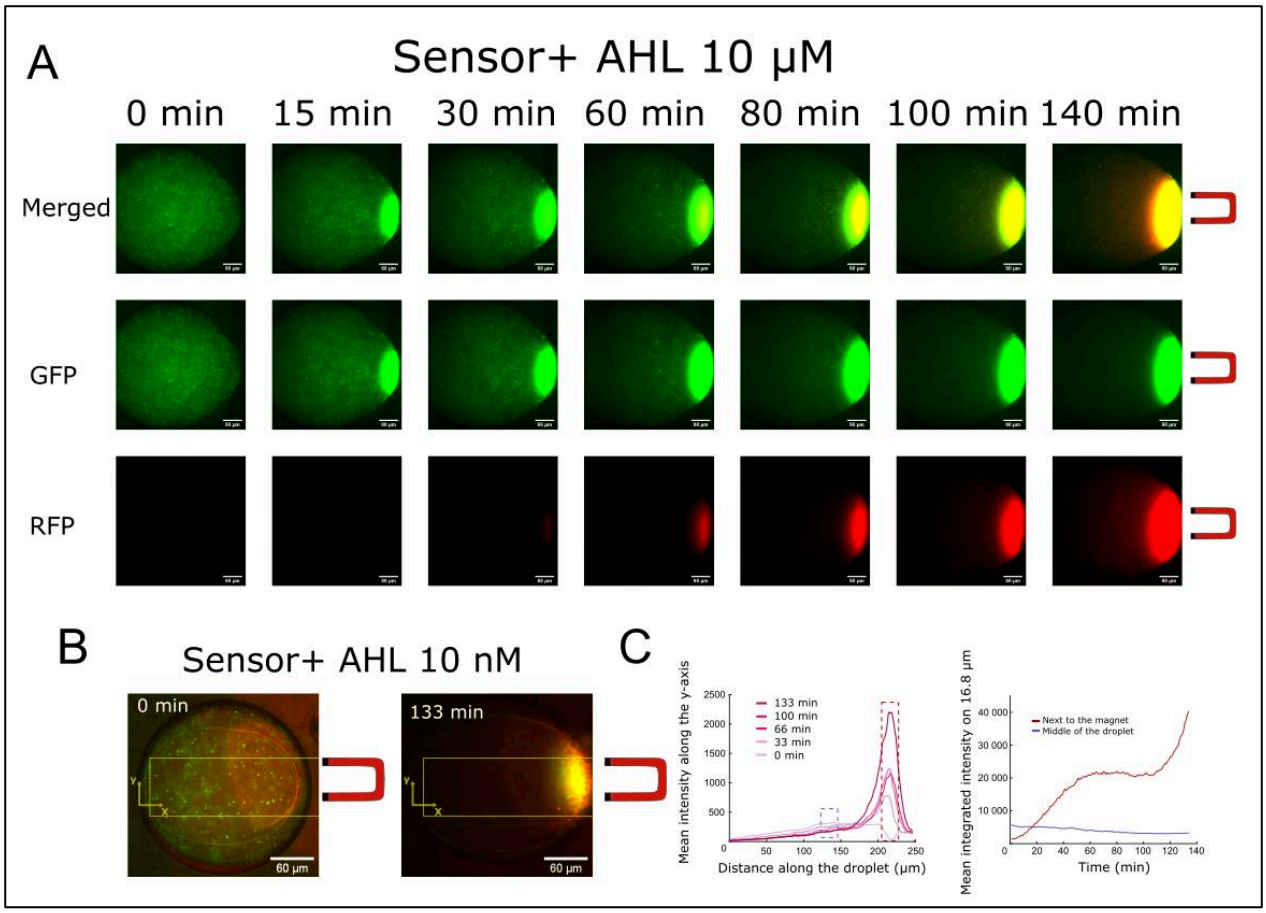

Figure 4: Detection of RFP signal of *sensors* in presence of AHL with magnetic concentration due to iron addition in the droplet. (A) Time lapse images of *sensors* mixed with 10 µM of 3OC6HSL and 2 mM of iron II attracted by the magnet. The magnet is on the right. **First row**: merged images of RFP and GFP channels. **Second row:** GFP channel, colorized images. **Third row:** RFP channel, colorized images. Scale bar, 60 µm. **(B)** Images of fluorescence signal for *sensors* mixed with 10 nM of 3OC6HSL and 2 mM of iron II at 0 and 133 min. Merged RFP and GFP channels, magnet on the right. Scale bar, 60 µm. **(C)** Mean intensity of red fluorescence over time across the droplet. On the right, integration over time of the mean intensity in the region next to the magnet and at the middle of the droplet (delimited by the yellow rectangles).

Discussion

We demonstrated that mineralized *E. coli* can be used as magnetic whole-cell biosensors to detect small chemical molecules. First, using AHL-responsive bacteria that drive the host cells to produce fluorescent proteins, we quantified the temporal evolution of RFP production within individual bacteria upon AHL addition. With our assay, we detected 10 nM of AHL in less than 2 hours which is in agreement with other quorum-sensing based biosensor assays found in the literature[19–22]. We can find a detection level of 1 nM of AHL for the best biosensors[23].

Next we found that the mineralization process of these *E. coli* sensors, that was used for obtaining magnetic *E. coli*, did not impede their capacity for producing fluorescent proteins in an AHL-dependent manner.

Finally, we showed that signal detection could be improved when *MagEcoli*^{sensors} were concentrated by magnetic forces in confined chambers. Beyond these proof-of-concept experiments that validate the concept of magnetic whole-cell biosensor, our approach could benefit from several improvements. First, the detection time could be strongly reduced if we use a fast folding fluorescent reporter system such as sfGFP. Secondly, to improve the speed and yield of magnetic attraction we could use higher magnetic forces by using dedicated assay as magnetic tips that locally enhance the gradient of magnetic field (up to 10^4 $T.m^{-1}$) and thus magnetic forces. An alternative approach described here was to use iron oxide precipitation on non-mineralized bacteria, which resulted on a faster attraction and localization of bacterial sensors. This approach is simpler but drive to non-specific attraction of all bio-based elements, including our bacteria. Besides, we could also use drugs to prevent bacterial division during the assay and reduce the loss of magnetic properties among the population of *MagEcoli*^{sensors}. We could also change the oil composing the continuous phase of the emulsion to reduce AHL diffusion (as proved by Simmel et. al for fluorocarbon oil[14]). Lastly, using improved environmental-responsive plasmids[24] will help increasing the biosensing characteristics: specificity, protein leakage in absence of chemical stimuli that increases noise or false positive (as a feedback loop or a logic gate for instance[25]).

As perspectives, our work could be developed for pathogen detection. As quorum sensing is used by pathogens[26], *MagEcoli*^{sensors} could be employed to detect or identify pathogens in complex media (food, biological samples) or even *in vivo*[27]. Moreover as AHL molecules are usually specific to one kind of bacteria, we could multiplex the detection by modifying *MagEcoli* to detect a library of AHL with more complex genetic circuits[28].

Material and Methods

Chemicals

Kanamycin, Chloramphenicol, Mohr's Salt, LB broth, Glycerol, Agar, IPTG, DMSO and Mineral oil were purchased from SIGMA-ALDRICH®. Arlacel P135 was purchased from CRODA®; Optiprep™ was purchased from StemCell®. Vitrex® was purchased from VWR®.

AHL was purchased from Bertin and kept at -20°C at 20 mM in DMSO.

DNA plasmids and strains

The list of the plasmids used in this study is reported in **Table S1**. The *Pyrococcus Furiosus* ferritins were fused at their N-terminal to Emerald GFP (EmGFP) and were cloned into a pet28 derivative.

Models

E. coli bacteria were purchased at New England Biolabs for BL21 and dH10β. *E. coli* MG1655 come from Blattner et al., 1997.

Transformation:

All plasmids were incorporated into electro-competent bacteria via electroporation.

BL21 were the *sensor* strains and MG1655 the *sender* strains (see **Table S1** for list of plasmids).

Biomineralization protocol of sensors

Stock solution of antibiotics were made at 1000X: kanamycin (50mg/mL in water) and chloramphenicol (34mg/mL in ethanol) and stored at -20°C. Antibiotics were diluted to the LB medium and added at every step of bacterial culture or biomineralization.

As a source of iron II, Mohr salt was used and kept under inert condition. At each step of iron addition, a fresh solution of Mohr salt was made in water at a concentration of 100 mM. This solution was immediately added to the bacteria and no kept longer than 10 minutes.

Sensors were grown overnight in LB medium with kanamycin and chloramphenicol until they reached the steady state (precultures). The next day, they were diluted and grown into fresh LB medium with the same antibiotics at 37 °C under agitation for approximately 2 hours, until they reached an optical density at 600 nm between 0.4-0.6. 500µM of IPTG was added into the medium. Bacteria were incubated at 37°C under agitation for 30 min. Next, Fe (II) was added to the bacteria to a final concentration of 4 mM. Bacteria were grown overnight at 37°C (about 16 hours ± 10%). The next morning, bacterial O.D. at 600 nm was measured. Correction from the absorption of iron

was performed using a blank measured with LB containing Fe (II) at 0 to 4 mM. Finally, bacteria were washed after centrifugation to remove iron oxide residues from the LB and fresh LB free from antibiotics.

Observation of AHL detection in droplets

To observe the detection of AHL by the biosensors (*E. coli*^{sensor} or *MagEcoli*^{sensor}), we used the following protocol before launching each movie.

Precultures of biosensors in LB supplemented with IPTG, Kanamycin and Chloramphenicol or mineralized sensors were taking out from 37°C in the morning, and placed at room temperature. The O.D. was measured (the blank was made from LB with 0 or 4 mM of iron depending on the conditions). The samples were washed twice in antibiotic and IPTG-free LB medium.

Then O.D. was measured again (blank made with LB) to dilute properly the biosensors at the desired O.D. in LB with 20% of Optiprep (to prevent bacterial sedimentation). When not mentioned we aimed to put the biosensors at a final O.D. of 0.3-0.6 in droplets.

When needed, AHL, *sender* bacteria, or DMSO were added to the bacteria. For AHL, the stock solution was diluted with water to a 100X concentration; in order to mix 1 µL of AHL and 99µL of biosensors. For *senders*, precultures of *senders* in LB with kanamycin followed the same washing same step in the morning. Then a mix between *senders* and biosensors was made in order to have a final O.D. of 0.3 to 0.6 of *senders* in the droplets with 20% of Optiprep.

For the control without AHL or *senders*, we added 1% of DMSO in the mix (in LB + Optiprep).

Next a water-in-oil emulsion was formed by mixing up 99 µL of mineral oil supplemented with a block copolymer at 0.4 g/L (ArlacelP135) and 1 µL of bacteria. The emulsion was inserted into a capillary (1mm of diameter) fixed on a microscopic slide (32x40 mm). The capillary was sealed with Vitrex®.

When *MagEcoli*^{sensor} were used, a neodymium magnet was placed at one side (cubic magnet NdFeB 3 mm, Supermagnet), the N-S axis being perpendicular to the capillary's direction. Observations were made using epifluorescence microscopy at 37°C.

For the *in vitro* magnetization, iron II, from a fresh solution of Mohr Salt, kept under inert gas, was added to the mix bacteria and AHL in LB + Optiprep. 2µL of a 100 mM of Mohr Salt (iron II diluted in sterile water) was added to 98 µL of the mix, making the final concentration in iron of 2 mM. The emulsion and the movie for magnetophoresis were immediately made.

Observation of biosensors on a solid medium

To observe magnetic or non-magnetic biosensors in contact of different concentrations of AHL, we used the following protocol.

Precultures of *E.coli*^{sensor} in LB supplemented with IPTG, Kanamycin and Chloramphenicol or *MagEcoli*^{sensor} were taking out from 37°C in the morning, and placed at room temperature. For the study displayed in **Fig. 1B**, *E.coli*^{sensor} were previously diluted 1/100^{e} and placed at 37°C under agitation for 2 hours to reach an O.D. of 0.5. For both types of samples, magnetic and non-magnetic biosensors, the O.D. was measured (the blank was made from LB with 0 or 4 mM of iron depending on the conditions). The samples were washed twice in antibiotic and IPTG free LB medium and diluted or concentrated at a final O.D. of 0.4. In the meantime, serial dilutions of an AHL stock solution (20 mM in DMSO) were made in water to reach the desired concentrations. Next 99 µL of washed biosensors (*E. coli*^{sensor} or *MagEcoli*^{sensor}) were mixed with 1 µL of the AHL solutions. The samples were put at 37°C for 2 hours.

For observations, 9 µL of bacteria were deposited on a LB agar pad (2% agarose) and observed by epifluorescence microscopy.

Microscopy observations

Magnetophoresis experiments were observed using IX81 (Olympus) epifluorescence microscope equipped with an EM-CCD camera (electron multiplying CCD, C9100-13 or C9100-02, Hamamatsu, Corporation), a LED for illumination (Spectra X, Lumencor), and with x10, x20, or 60x oil objectives. Microscopes were controlled by MicroManager or SimplePCI software.

Data analysis

All movies were observed on Fiji. Composite images, area selections for quantification were also made on Fiji.

2 different methods were developed to quantify the level of RFP produced by bacteria in droplets.

For the first one that consisted in measuring the fluorescence level of *E. coli*^{sensors}, the squared area was selected at the center of the droplet using FIJI. Data treatments and plots generation were made using Matlab. Signal and noise images were calculated using the imfilter function (that averages the original image on the 3x3 or 101x101 surrounding pixels for the signal and noise respectively). Then the function pctile was used to calculate the 99th percentile at each time. The percentile was plotted after smoothing the data using movmean.

To integrate the RFP intensity alongside the droplets, we selected an area of 80 µm height which crosses the whole droplet and a background area of 40 µm x 40 µm using Fji. Data treatments and plots generation were made using Matlab. The mean function was used to calculate the mean intensity of the background (in 2 dimension) and of the area of interest (along the height). Next the background was substracted from the 1D signal. The intensity signal was plotted after smoothing the data using movmean. To integrate the intenstity in the area in the middle of the droplet and next

to the magnet, we first used the function findpeak to find the extreme peak (we verified its location by hand to see if it was spotted in the right area). We used trapz to integrate the signal on pixels around the peak and the middle of the signal.

Images can be used twice for different quantifications.

For instance, for the observation on solid medium, the sample used for **Fig. 1B**, the condition without AHL, came from the same batch of experiment as the one used for **Fig. S4**.

For the movies in liquid medium some movies can be used in time-lapse and for quantifications:

- **Movie S1** corresponds to **Fig. 2B**.
- **Movie S2** corresponds to **Fig. 4A**.
- **Fig. S6** corresponds to **Fig. 2B** and **Fig. 4A.**
- The same movie is used for whole images and quantification in **Fig. 1CD**, **Fig. S1AB**, and some plot and time-lapse images in **Fig. S2AB.**
- The same movie is used for quantification in **Fig. 1D, Fig. S1C** and a plot in **Fig. S2C**.
- The time-lapse images of **Fig. S2A** are plotted in **Fig. S2B**.

Data availability

All data are available from the corresponding author upon request.

References

(1) Sørensen, S. J.; Burmølle, M.; Hansen, L. H. Making Bio-Sense of Toxicity: New Developments in Whole-Cell Biosensors. *Curr. Opin. Biotechnol.* **2006**, *17* (1), 11–16. https://doi.org/10.1016/j.copbio.2005.12.007.

(2) Chang, H. J.; Voyvodic, P. L.; Zúñiga, A.; Bonnet, J. Microbially Derived Biosensors for Diagnosis, Monitoring and Epidemiology. *Microb. Biotechnol.* **2017**, *10* (5), 1031–1035. https://doi.org/10.1111/1751-7915.12791.

(3) Inda, M. E.; Lu, T. Microbes as Biosensors. *Annu. Rev. Microbiol.* **2020**, *74* (1), 337–359. https://doi.org/10.1146/annurev-micro-022620-081059.

(4) Park, M.; Tsai, S. L.; Chen, W. Microbial Biosensors: Engineered Microorganisms as the Sensing Machinery. *Sensors* **2013**, *13* (5), 5777–5795. https://doi.org/10.3390/s130505777.

(5) Raut, N.; O'Connor, G.; Pasini, P.; Daunert, S. Engineered Cells as Biosensing Systems in Biomedical Analysis. *Anal. Bioanal. Chem.* **2012**, *402* (10), 3147–3159. https://doi.org/10.1007/s00216-012-5756-6.

(6) Velusamy, V.; Arshak, K.; Korostynska, O.; Oliwa, K.; Adley, C. An Overview of Foodborne Pathogen Detection: In the Perspective of Biosensors. *Biotechnol. Adv.* **2010**, *28* (2), 232–254. https://doi.org/10.1016/j.biotechadv.2009.12.004.

(7) Ibacache-Quiroga, C.; Romo, N.; Díaz-Viciedo, R.; Dinamarca, M. A. Detection and Control of Indoor Airborne Pathogenic Bacteria by Biosensors Based on Quorum Sensing Chemical Language: Bio-Tools, Connectivity Apps and Intelligent Intelligent Buildings. *Biosensing Technol. Detect. Pathog. Prospect. W. Rapid Anal. Rijeka InTech* **2018**, 73–87.

(8) Mimee, M.; Nadeau, P.; Hayward, A.; Carim, S.; Flanagan, S.; Jerger, L.; Collins, J.; Mcdonnell, S.; Swartwout, R.; Citorik, R. J.; Bulovi, V.; Langer, R.; Traverso, G.; Chandrakasan, A. P.; Lu, T. K. An Ingestible Bacterial Electronic System to Monitor Gastrointestinal Health. *Science (80-.).* **2018**, *360* (6391), 915–918. https://doi.org/10.1126/science.aas9315.An.

(9) Danino, T.; Prindle, A.; Kwong, G. A.; Skalak, M.; Li, H.; Allen, K.; Hasty, J.; Bhatia, S. N. Programmable Probiotics for Detection of Cancer in Urine. *Sci. Transl. Med.* **2015**, *7* (289). https://doi.org/10.1126/scitranslmed.aaa3519.

(10) Kretzer, J. W.; Schmelcher, M.; Loessner, M. J. Ultrasensitive and Fast Diagnostics of Viable Listeria Cells by CBD Magnetic Separation Combined with A511::LuxAB Detection. *Viruses* **2018**, *10* (11). https://doi.org/10.3390/v10110626.

(11) Gu, H.; Xu, K.; Xu, C.; Xu, B. Biofunctional Magnetic Nanoparticles for Protein Separation and Pathogen Detection. *Chem. Commun.* **2006**, No. 9, 941–949. https://doi.org/10.1039/b514130c.

(12) Waters, C. M.; Bassler, B. L. Quorum Sensing: Cell-to-Cell Communication in Bacteria. *Annu. Rev. Cell Dev. Biol.* **2005**, *21* (1), 319–346. https://doi.org/10.1146/annurev.cellbio.21.012704.131001.

(13) Florea, M.; Hagemann, H.; Santosa, G.; Abbott, J.; Micklem, C. N.; Spencer-Milnes, X.; De Arroyo Garcia, L.; Paschou, D.; Lazenbatt, C.; Kong, D.; Chughtai, H.; Jensen, K.; Freemont, P. S.; Kitney, R.; Reeve, B.; Ellis, T. Engineering Control of Bacterial Cellulose Production Using a Genetic Toolkit and a New Celluloseproducing Strain. *Proc. Natl. Acad. Sci. U. S. A.* **2016**, *113* (24), E3431–E3440. https://doi.org/10.1073/pnas.1522985113.

(14) Weitz, M.; Mückl, A.; Kapsner, K.; Berg, R.; Meyer, A.; Simmel, F. C. Communication and Computation by Bacteria Compartmentalized within Microemulsion Droplets. *J. Am. Chem. Soc.* **2014**, *136* (1), 72–75. https://doi.org/10.1021/ja411132w.

(15) Schwarz-Schilling, M.; Aufinger, L.; Mückl, A.; Simmel, F. C. Chemical Communication between Bacteria and Cell-Free Gene Expression Systems within Linear Chains of Emulsion Droplets. *Integr. Biol. (United Kingdom)* **2016**, *8* (4), 564–570. https://doi.org/10.1039/c5ib00301f.

(16) Trantidou, T.; Dekker, L.; Polizzi, K.; Ces, O.; Elani, Y. Functionalizing Cell-Mimetic Giant Vesicles with Encapsulated Bacterial Biosensors. *Interface Focus* **2018**, *8* (5). https://doi.org/10.1098/rsfs.2018.0024.

(17) Aubry, M.; Wang, W.-A.; Guyodo, Y.; Delacou, E.; Guignier, J.-M.; Espeli, O.; Lebreton, A.; Guyot, F.; Gueroui, Z. Engineering E. Coli for Magnetic Control and the Spatial Localization of Functions . *ACS Synth. Biol.* **2020**. https://doi.org/10.1021/acssynbio.0c00286.

(18) Prindle, A.; Samayoa, P.; Razinkov, I.; Danino, T.; Tsimring, L. S.; Hasty, J. A Sensing Array of Radically Coupled Genetic 'Biopixels'. *Nature* **2012**, *481* (7379), 39–44. https://doi.org/10.1038/nature10722.

(19) Boehm, C. R.; Grant, P. K.; Haseloff, J. Programmed Hierarchical Patterning of Bacterial Populations. *Nat. Commun.* **2018**, *9* (1), 1–10. https://doi.org/10.1038/s41467-018-03069-3.

(20) Saeidi, N.; Wong, C. K.; Lo, T. M.; Nguyen, H. X.; Ling, H.; Leong, S. S. J.; Poh, C. L.; Chang, M. W. Engineering Microbes to Sense and Eradicate Pseudomonas Aeruginosa, a Human Pathogen. *Mol. Syst. Biol.* **2011**, *7* (521), 1–11. https://doi.org/10.1038/msb.2011.55.

(21) Gupta, S.; Bram, E. E.; Weiss, R. Genetically Programmable Pathogen Sense and Destroy. *ACS Synth. Biol.* **2013**, *2* (12), 715–723. https://doi.org/10.1021/sb4000417.

(22) Struss, A.; Pasini, P.; Ensor, C. M.; Raut, N.; Daunert, S. Paper Strip Whole Cell Biosensors: A Portable Test for the Semiquantitative Detection of Bacterial Quorum Signaling Molecules. *Anal. Chem.* **2010**, *82* (11), 4457–4463. https://doi.org/10.1021/ac100231a.

(23) Kumari, A.; Pasini, P.; Deo, S. K.; Flomenhoft, D.; Shashidhar, H.; Daunert, S. Biosensing

Systems for the Detection of Bacterial Quorum Signaling Molecules. *Anal. Chem.* **2006**, *78* (22), 7603–7609. https://doi.org/10.1021/ac061421n.

(24) Hicks, M.; Bachmann, T. T.; Wang, B. Synthetic Biology Enables Programmable Cell-Based Biosensors. *ChemPhysChem*. 2020, p 131. https://doi.org/10.1002/cphc.201901191.

(25) Wang, B.; Barahona, M.; Buck, M. A Modular Cell-Based Biosensor Using Engineered Genetic Logic Circuits to Detect and Integrate Multiple Environmental Signals. *Biosens. Bioelectron.* **2013**, *40* (1), 368–376. https://doi.org/10.1016/j.bios.2012.08.011.

(26) Kai Papenfort, B. B. Quorum-Sensing Signal-Response Systems in Gram-Negative Bacteria. *Nat Rev Microbiol.* **2014**, *9* (2), 91–108. https://doi.org/10.1038/nrmicro.2016.89.Quorum-Sensing.

(27) Charbonneau, M. R.; Isabella, V. M.; Li, N.; Kurtz, C. B. Developing a New Class of Engineered Live Bacterial Therapeutics to Treat Human Diseases. *Nat. Commun.* **2020**, 1–11. https://doi.org/10.1038/s41467-020-15508-1.

(28) Kylilis, N.; Tuza, Z. A.; Stan, G. B.; Polizzi, K. M. Tools for Engineering Coordinated System Behaviour in Synthetic Microbial Consortia. *Nat. Commun.* **2018**, *9* (1). https://doi.org/10.1038/s41467-018-05046-2.

Supplementary Information for:

Magnetic whole *E.coli* biosensor programmed to detect AHL

Mary Aubry, Zoher Gueroui

Table S1. List of plasmids used in this study.

Plasmid	Gene expression	Resistance	Strain	Source
pLux01	Sensor plasmid: RFP expression upon 3OC6HSL induction	Chloramphenicol	BL21	(13)
pET28_GFP-ferritin	ferritin fused with EmGFP	Kanamycin	BL21	From this study
pTD103LuxIsfGFP	Sender plasmid: secretion of 3OC6HSL	Kanamycin	MG1655	(18)

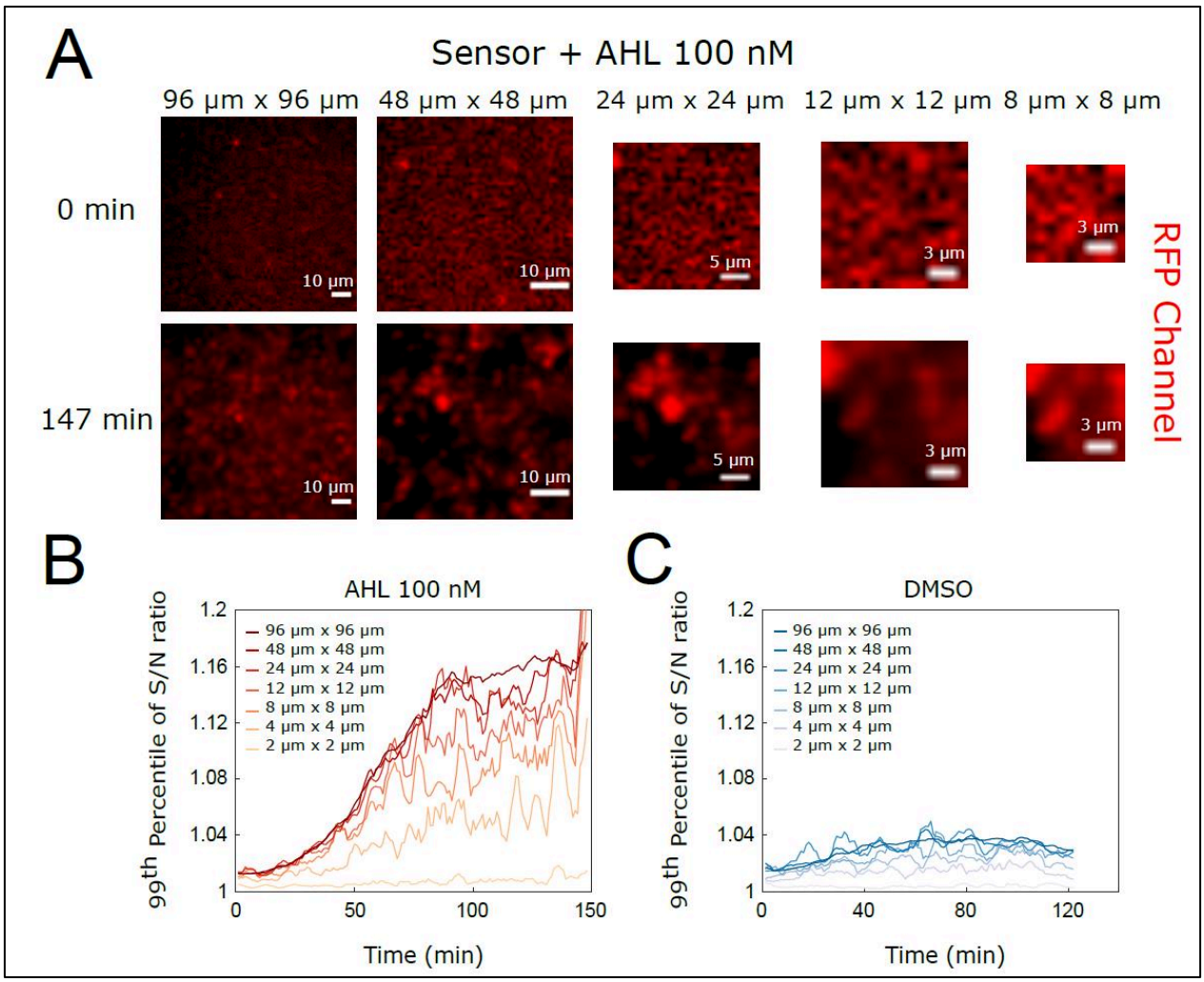

Figure S1: Detection of RFP signal in presence of 100 nM of AHL *E. coli*^{sensors}. (A) Various RFP colorized images of area selected for detection. The images are taken from the movie represented in Figure 1C, *sensors* at an O.D. of 5 and 100 nM of AHL. On the **top row**: images at 0 min. On the **bottom row**: images at the end time, 147 min. The selected areas have a size of 9216µm^2, 2304µm^2, 576µm^2, 144µm^2, 16µm^2. **(B)** Plots of the 99th percentile of signal/noise ratio, following our method of detection, as a function of time. The measures are taken at the center of droplet combining 100 nM of AHL and *sensors*, in the different sized squares. Each line corresponds to a square represented above. **(C)** Plots of the 99th percentile of signal upon noise ratio, following our method of detection, as a function of time. The measures are taken at the center of droplet with *sensors* alone, on a control movie without AHL made the same day, in the different sized squares.

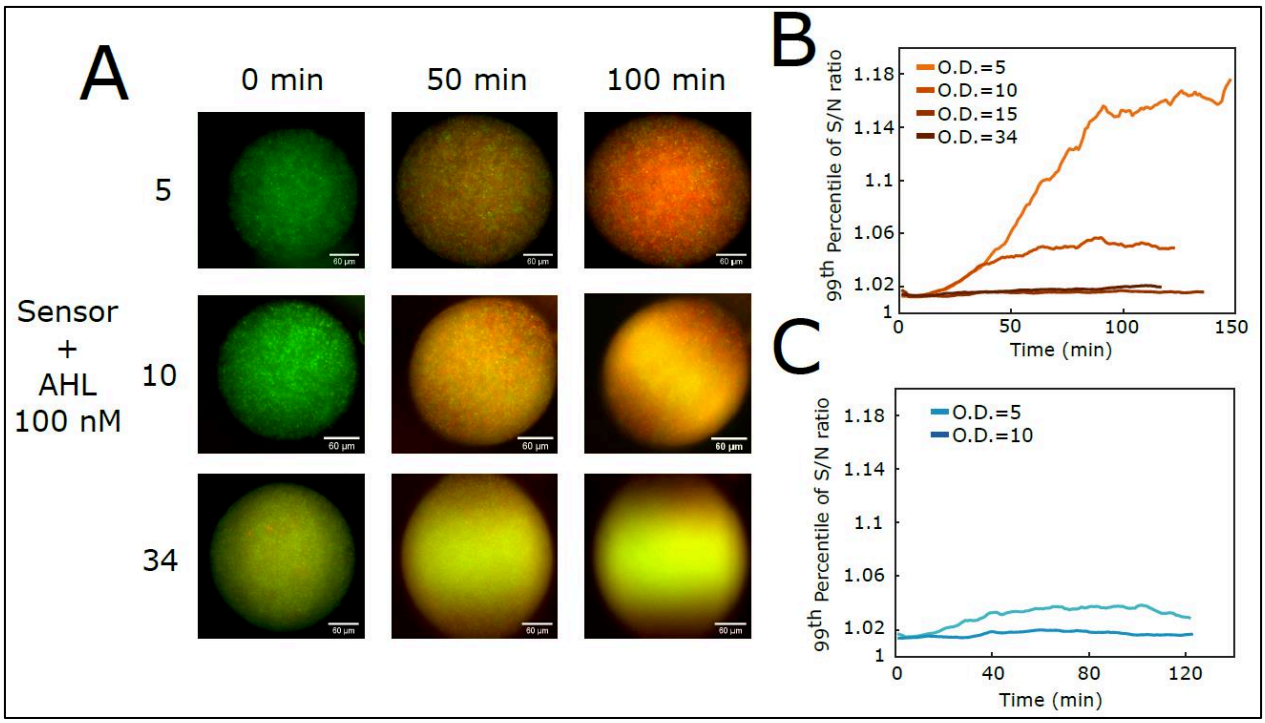

Figure S2: Detection of RFP signal in presence of 100 nM of AHL with various concentrations of *E. coli*^{sensors}. (**A**) Time-lapse images of droplets containing *E. coli*^{sensors} at different O.D. (5, 10 and 34) in presence of 3OC6HSL. Merged images of RFP and GFP channels, at 0, 50 and 100 min. Scale bar, 60 µm. **(B)** Plots of the 99th percentile of signal upon noise ratio, following our method of detection, as a function of time. The measures are taken in a same-sized square at the center of droplet combining 100 nM of AHL and *sensors*. Each line corresponds to one O.D. of *E. coli*^{sensors}. **(C)** Plot of the 99th percentile of signal upon noise ratio, following our method of detection, as a function of time. The measures are taken in a same-sized square at the center of droplet with *sensors* alone. Each line corresponds to one O.D. of *E. coli*^{sensors}. The measures are taken on control movies without AHL.

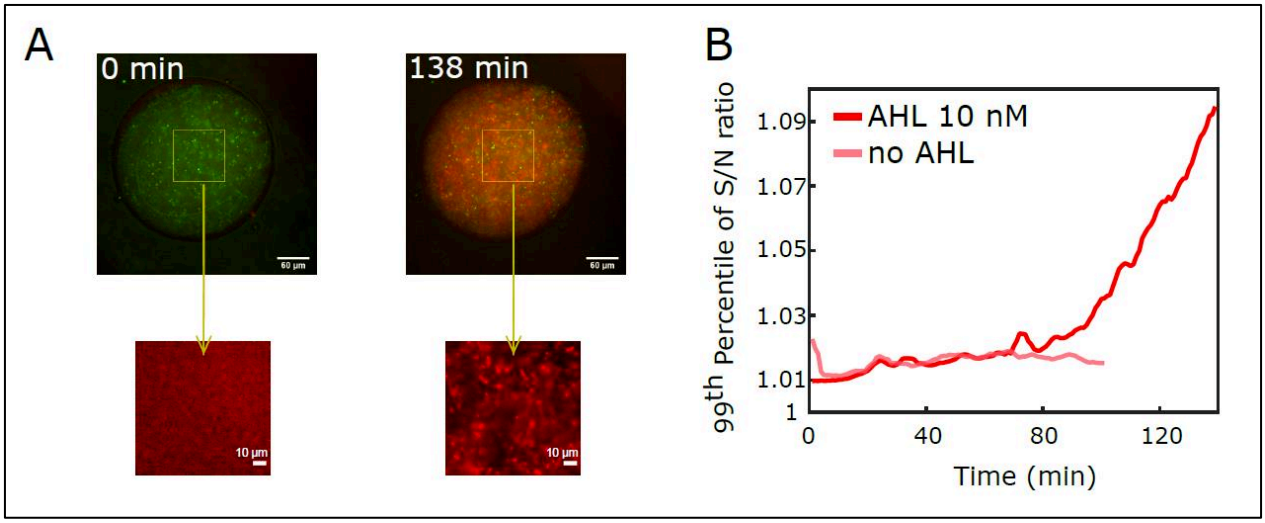

Figure S3: Detection of RFP signal produced by *E.coli*^{sensors} at an initial O.D. of 0.7 with 10 nM of synthetic AHL. (A) Upper panel: Fluorescence images of an assay with magnetic *sensors* and 10 nM of AHL at the first (noted 0 min) and final (noted 138 min) acquisition. Merged GFP and RFP channels. Scale bar, 60µm. **Lower panel**: Zoom at a region of the droplet at 0 and 138 min, in RFP channel. Colored images. Scale bar, 10µm. **(B)** Plots of the 99th percentile of signal upon noise ratio, following our method of detection in the square in the middle of the droplet, as a function of time. In red, for the assay displayed. In pink, for the negative control (without AHL), performed the same day.

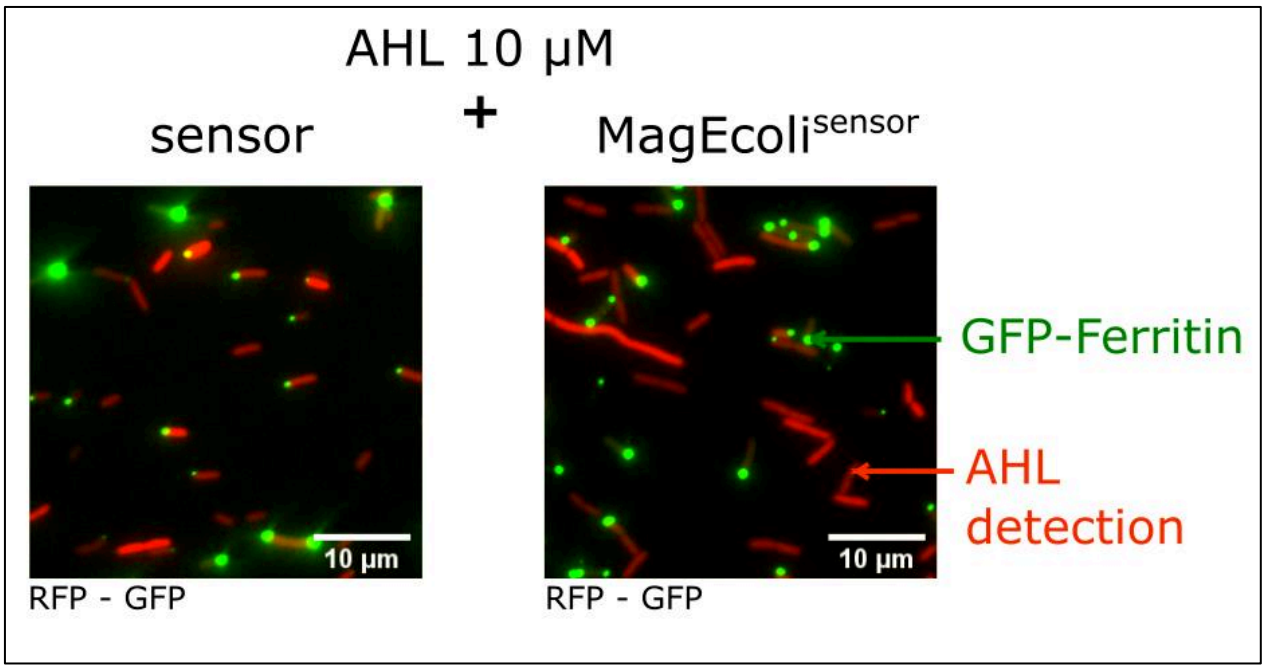

Figure S4: Observation of *sensors* after 2 hours in contact with 10 µM of AHL. On the **left panel**: *sensors* that are not magnetic. On the **right panel**: the *MagEcoli*^{sensors}, biomineralized with 4 mM of iron II. Merged images of RFP and GFP channel. RFP appears on the RFP channel. Ferritins appear on the GFP channel.

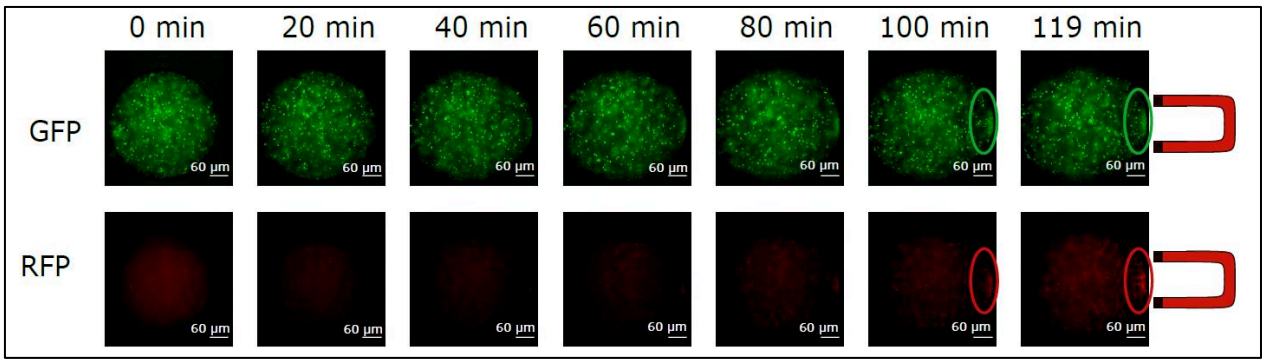

Figure S5: Time-lapse images of an assay of magnetophoresis with *senders* and magnetic *sensors*. Magnet is placed on the right. **On top**, the green channel reveals GFP fluorescence of *senders* and *sensors*. **At the bottom**, the red channel reveals the RFP fluorescence of *sensors*. Colorized images. Scale bar, 60 µm.

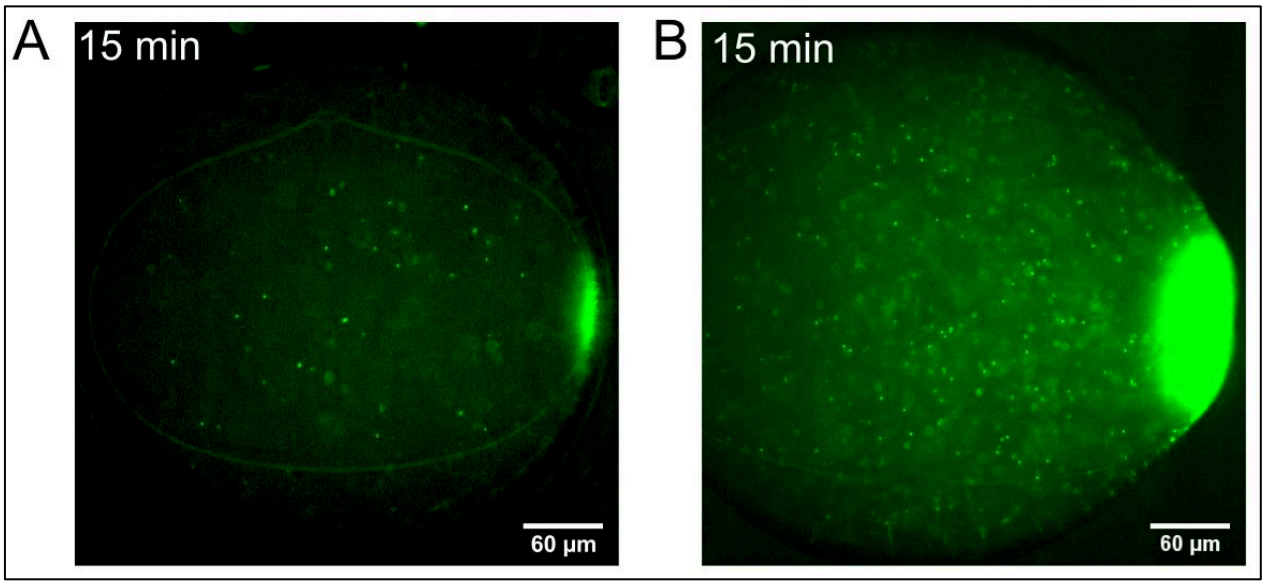

Figure S6: Fluorescent images after 45 minutes of attraction of *MagEcoli*^{sensors} from Fig. 2B and *sensors* mixed with iron II in the droplets from Fig. 4A. GFP channel, colorized images. Scale bar, 60 µm. **(A)** *MagEcoli*^{sensors}. **(B)** *Sensors* with 2 mM of iron II in the droplet.

Legends for Movies

Movie S1: Magnetophoresis experiments of *MagEcoli*^{sensors} in presence of 100 µM of 3OC6HSL. Magnet was placed on the right. An image was taken every minute. Scale bar, 60 µm.

Movie S2: Magnetophoresis experiments of *E. coli*^{sensors} in presence of 10 µM of 3OC6HSL and 2 mM of iron II. Magnet was placed on the right. An image was taken every minute. Scale bar, 60 µm.

3.4 - References

1. Bassler, B. L. How bacteria talk to each other: Regulation of gene expression by quorum sensing. *Curr. Opin. Microbiol.* **2**, 582–587 (1999).
2. Hooshangi, S. & Bentley, W. E. From unicellular properties to multicellular behavior: bacteria quorum sensing circuitry and applications. *Curr. Opin. Biotechnol.* **19**, 550–555 (2008).
3. Ng, W.-L. & Bassler, B. L. Bacterial Quorum-Sensing Network Architectures. *Annu. Rev. Genet.* **43**, 197–222 (2009).
4. Parker, C. T. & Sperandio, V. Cell-to-cell signalling during pathogenesis. *Cell. Microbiol.* **11**, 363–369 (2009).
5. Horswill, A. R., Stoodley, P., Stewart, P. S. & Parsek, M. R. The effect of the chemical, biological, and physical environment on quorum sensing in structured microbial communities. *Anal. Bioanal. Chem.* **387**, 371–380 (2007).
6. Ahator, S. Dela & Zhang, L. H. Small is mighty-chemical communication systems in Pseudomonas aeruginosa. *Annu. Rev. Microbiol.* **73**, 559–578 (2019).
7. Fuqua, W. C., Winans, S. C. & Greenberg, E. P. Quorum sensing in bacteria: The LuxR-LuxI family of cell density- responsive transcriptional regulators. *J. Bacteriol.* **176**, 269–275 (1994).
8. Cámara, M., Hardman, A., Williams, P. & Milton, D. Quorum sensing in Vibrio cholerae? *Nat. Genet.* **32**, 217–219 (2002).
9. Miller, M. B., Skorupski, K., Lenz, D. H., Taylor, R. K. & Bassler, B. L. Parallel quorum sensing systems converge to regulate virulence in Vibrio cholerae. *Cell* **110**, 303–314 (2002).
10. Jung, S. A., Hawver, L. A. & Ng, W. L. Parallel quorum sensing signaling pathways in Vibrio cholerae. *Curr. Genet.* **62**, 255–260 (2016).
11. Watve, S. *et al.* Parallel quorum-sensing system in Vibrio cholerae prevents signal interference inside the host. *PLoS Pathog.* **16**, 1–27 (2020).
12. Kai Papenfort, B. B. Quorum-Sensing Signal-Response Systems in Gram-Negative Bacteria. *Nat Rev Microbiol.* **9**, 91–108 (2014).
13. Uroz, S., Dessaux, Y. & Oger, P. Quorum sensing and quorum quenching: The Yin and Yang of bacterial communication. *ChemBioChem* **10**, 205–216 (2009).
14. McClean, K. H. *et al.* Quorum sensing and Chromobacterium violaceum: Exploitation of violacein production and inhibition for the detection of N-acylhomoserine lactones. *Microbiology* **143**, 3703–3711 (1997).
15. Romero, M., Martin-Cuadrado, A. B., Roca-Rivada, A., Cabello, A. M. & Otero, A. Quorum quenching in cultivable bacteria from dense marine coastal microbial communities. *FEMS Microbiol. Ecol.* **75**, 205–217 (2011).
16. Yang, F. *et al.* Quorum quenching enzyme activity is widely conserved in the sera of mammalian species. *FEBS Lett.* **579**, 3713–3717 (2005).
17. Mukherjee, S. & Bassler, B. Bacterial quorum sensing in complex and dynamically changing environments. *Nat. Rev. Microbiol.* **176**, 139–148 (2019).
18. Kim, M. K., Ingremeau, F., Zhao, A., Bassler, B. L. & Stone, H. A. Local and global consequences of flow on bacterial quorum sensing. *Nat. Microbiol.* **1**, 1–12 (2016).
19. Emge, P. *et al.* Resilience of bacterial quorum sensing against fluid flow. *Sci. Rep.* **6**, 1–10 (2016).

20. Hagen, S. J., Pérez, P. D. & Weiss, J. T. Noise and Crosstalk in the Two Quorum Sensing Channels of Vibrio Fischeri. *BMC Syst. Biol.* **5**, 153 (2011).
21. Zhang, Y. *et al.* A programmable microenvironment for cellular studies via microfluidics-generated double emulsions Ying. *Biomaterials* **34**, 4564–4572 (2013).
22. Gao, M. *et al.* A crucial role for spatial distribution in bacterial quorum sensing. *Sci. Rep.* **6**, 1–10 (2016).
23. Boedicker, J. Q., Vincent, M. E. & Ismagilov, R. F. Microfluidic confinement of single cells of bacteria in small volumes initiates high-density behavior of quorum sensing and growth and reveals its variability. *Angew. Chemie - Int. Ed.* **48**, 5908–5911 (2009).
24. Weitz, M. *et al.* Communication and computation by bacteria compartmentalized within microemulsion droplets. *J. Am. Chem. Soc.* **136**, 72–75 (2014).
25. Schwarz-Schilling, M., Aufinger, L., Mückl, A. & Simmel, F. C. Chemical communication between bacteria and cell-free gene expression systems within linear chains of emulsion droplets. *Integr. Biol. (United Kingdom)* **8**, 564–570 (2016).
26. Prindle, A. *et al.* A sensing array of radically coupled genetic 'biopixels'. *Nature* **481**, 39–44 (2012).
27. Florea, M. *et al.* Engineering control of bacterial cellulose production using a genetic toolkit and a new celluloseproducing strain. *Proc. Natl. Acad. Sci. U. S. A.* **113**, E3431–E3440 (2016).
28. Boehm, C. R., Grant, P. K. & Haseloff, J. Programmed hierarchical patterning of bacterial populations. *Nat. Commun.* **9**, 1–10 (2018).
29. Shaner, N. C., Steinbach, P. A. & Tsien, R. Y. A guide to choosing fluorescent proteins. *Nat. Methods* **2**, 905–909 (2005).
30. Kholodenko, B. N. Cell-signalling dynamics in time and space. *Nat. Rev. Mol. Cell Biol.* **7**, 165–176 (2006).
31. Silva, K. P., Chellamuthu, P. & Boedicker, J. Q. Signal Destruction Tunes the Zone of Activation in Spatially Distributed Signaling Networks. *Biophys. J.* **112**, 1037–1044 (2017).
32. Waters, C. M. & Bassler, B. L. Quorum Sensing: Cell-to-Cell Communication in Bacteria. *Annu. Rev. Cell Dev. Biol.* **21**, 319–346 (2005).
33. Middleton, B. *et al.* Direct detection of N-acylhomoserine lactones in cystic fibrosis sputum. *FEMS Microbiol. Lett.* **207**, 1–7 (2002).
34. Kumari, A. *et al.* Biosensing systems for the detection of bacterial quorum signaling molecules. *Anal. Chem.* **78**, 7603–7609 (2006).
35. Saeidi, N. *et al.* Engineering microbes to sense and eradicate Pseudomonas aeruginosa, a human pathogen. *Mol. Syst. Biol.* **7**, 1–11 (2011).
36. Gupta, S., Bram, E. E. & Weiss, R. Genetically programmable pathogen sense and destroy. *ACS Synth. Biol.* **2**, 715–723 (2013).
37. Ibacache-Quiroga, C., Romo, N., Díaz-Viciedo, R. & Dinamarca, M. A. Detection and Control of Indoor Airborne Pathogenic Bacteria by Biosensors Based on Quorum Sensing Chemical Language: Bio-Tools, Connectivity Apps and Intelligent Intelligent Buildings. *Biosensing Technol. Detect. Pathog. Prospect. W. Rapid Anal. Rijeka InTech* 73–87 (2018).
38. Struss, A., Pasini, P., Ensor, C. M., Raut, N. & Daunert, S. Paper strip whole cell biosensors: A portable test for the semiquantitative detection of bacterial quorum signaling molecules. *Anal. Chem.* **82**, 4457–4463 (2010).

[i] https://pubchem.ncbi.nlm.nih.gov/compound/N-_3-Oxohexanoyl_-L-homoserine-lactone#section=Chemical-and-Physical-Properties

Chapter 4: Insight of possible applications of *MagEcoli* as an *in vivo* reporter

Content

4.1 - Introduction: Potential *in vivo* applications of ferritin-producing bacteria

As seen in the previous chapters, *MagEcoli* can be engineered to perform specific tasks such as the magnetic capture of bacteria, cell invasion and communication via quorum sensing. However, we can envision other types of applications and especially those aiming *in vivo* therapy and diagnostic of diseases. In this chapter, I will describe preliminary experiments conducted in laboratory that are proof-of-concepts and open the way for further investigations.

Here, we wanted to know if **(i)** *MagEcoli* survive in a living organism, **(ii)** *MagEcoli* keep their magnetic properties *in vivo*, **(iii)** *MagEcoli* can be used to monitor the position of bacteria *in vivo*, in the idea of using them as *in vivo* reporter (**Fig. 4.1**).

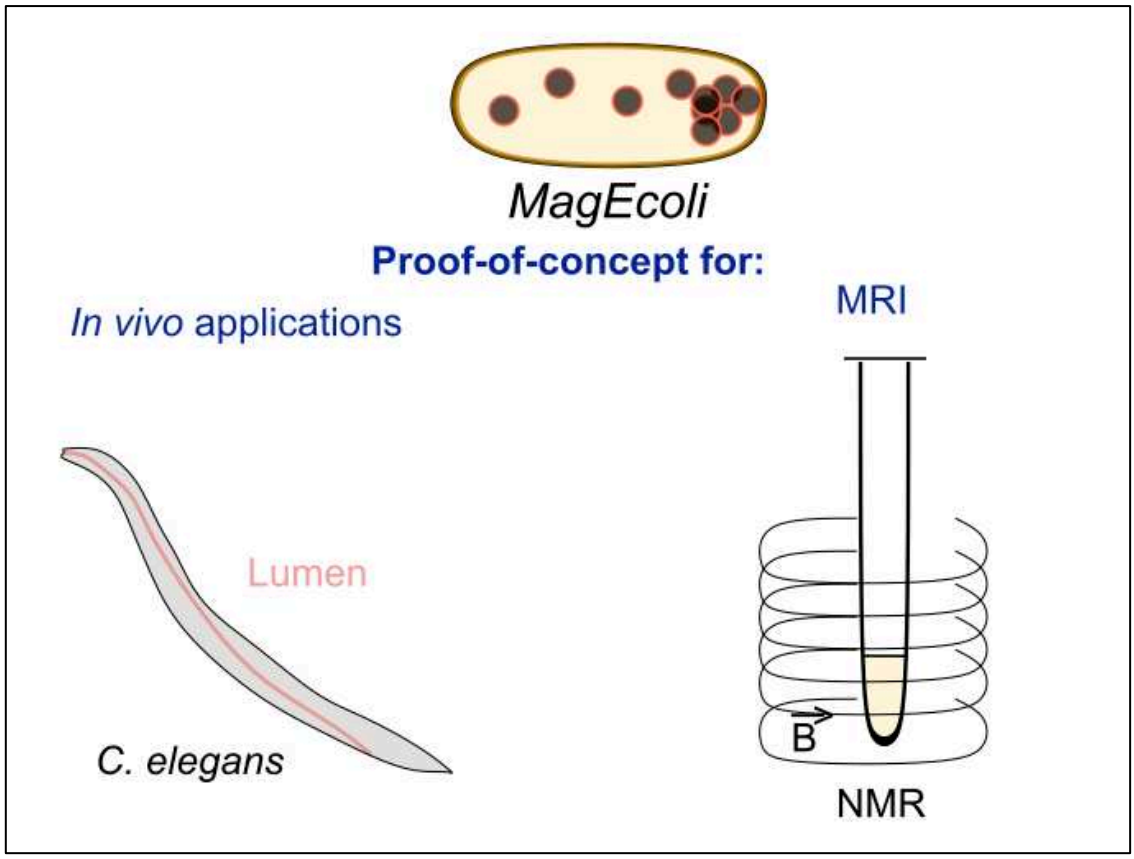

Figure 4.1: Motivations of the 4th chapter. We wanted to explore various future applications of our *MagEcoli*.

In this chapter, we explored various promising paths of applications. We wanted to see if our magnetic bacteria could be used for biotechnological purposes. We began to test if they can live and keep their magnetic properties *in vivo*. We assessed their resistance to the intestine of a simple

model organism: *Caenorhabditis elegans.* Then we measured by magnetic resonance imaging (MRI) the effect of *MagEcoli* on the relaxation times in order to see if they could be good reporter agents.

4.1.a - Magnetic bacteria as *in vivo* MRI contrast agents for *in situ* tracking

In addition to all the possible *in vivo* applications with reprogrammed microorganisms (detecting tumors[1] or inflammation[2], treating diseases[3–6]), taking advantage of the magnetic properties can help to improve their performances. Magnetic forces can do *in vivo* guidance (to better localize drug-delivery or sensing), collect microorganisms after their action (preventing spatial dissemination) and help to monitor their position with magnetic resonance imaging. Here, I will focus more on *in vivo* use of microorganisms as MRI reporters.

A recent and interesting example to begin with is the one developed by Ramesh et. al[7]. They orally administrated "ultraparamagnetic bacteria (UPMAG)" to mice. They managed to collect bacterial in the feces, with magnetic sorting; proving that their stay in the digestive tract did not altered their magnetic features. More interestingly, the position of bacteria in mice after subcutaneous injections was successfully observed by magnetic resonance imaging. Thanks to their paramagnetic iron oxides created in bacterial cytoplasm, bacteria appeared *in vivo* with MRI. Unfortunately, this example did not push further the application by programming the bacteria for a specific purpose (like drug-delivery or sensing). It would be great to combine both sides, such as sensing abilities and magnetic features. Here magnetic collection of excreted bacteria might improve the signal of the biosensors. On the other hand, we can imagine that one day we will be able to not only track but guide programmed magnetic bacteria through the gut like how we envision for the capsules for endoscopy[8,9].

As seen in the UPMAG example[7], bacteria with paramagnetic properties in their cytoplasm might be tracked by MRI, being contrast agent, *in vivo.* For MRI, two kinds of contrast agents exist: negative and positive ones. Depending on its constitution, a good contrast agent decreases the relaxation time T_2, thus leading to a negative contrast in T_2-weighted images (it appears darker on the pictures), or decreases the relaxation time T_1, inducing a faster return to equilibrium between two scans, hence leading to an increase of signal and a positive contrast in T_1-weighted images (it appears brighter on the pictures)[10].

Usually, for the contrast agents made of iron, the best common (negative) ones are SPIONs: chemically-synthesized superparamagnetic iron oxides nanoparticles. To have the highest R_2 ($1/T_2$) and thus the best contrast, scientists chemically controlled the particles' crystal phase, composition and size[11]. For the phase, paramagnetic crystal structures like magnetite are known to be good negative contrast agent since the early 90s and were investigated for further use *in vivo*[12,13]. Besides, magnetite is mostly used[11] as it has a lower T_2 than maghemite. Contrarily to our magnetic bacteria, SPIONs are too hydrophobic for direct *in vivo* applications: they have to be coated to enter into cells or to localize at the right spot, without using toxic transfection agents[11]. The coating strategies are numerous. For instance, to get soluble particles which could target cancer cells, scientists[14] have encapsulated SPIONs in albumin, later conjugated with folic acid. Another team[15] has coated SPIONs to positively charge it and found that they were stable in water, biocompatible and highly reducing the T_2. Furthermore, another example consisted of coated iron oxide nanocubes: thanks to their method, they reached a T_2 around 3-times lower than chemically-synthesized micrometer-sized iron oxide particles and commercial Feridex®[16].

Using (superpara or para)magnetic bacteria that trigger the desired area for imaging represent another good alternative. For instance, in 2011, a team has observed by MRI a tumor colonized by ferritin-overproducing *E. coli Nissle* strains[17]. They proceeded to *in vivo* tests by injecting bacteria in mice bearing brain tumors. They observed by luminescence an over-accumulation of bacteria next to the tumor (**Fig. 4.2**). After a day spent in the brain, the contact region between bacteria and tumor appeared clearly in MRI. This indicated that the bacteria were acting as contrast agents, even if they have not undergone a previous mineralization process. According to the study, ferritin-enriched bacteria were directly mineralized at the contact of the tumor during one day — tumor being known to be iron-rich areas. This confirmed the interest of using ferritin-producing bacteria for *in vivo* imaging. Following the same idea, a team has used a strain of magnetotactic bacteria, AMB-1 and has revealed that they can become positive MRI contrast agent under the correct iron diet[18].

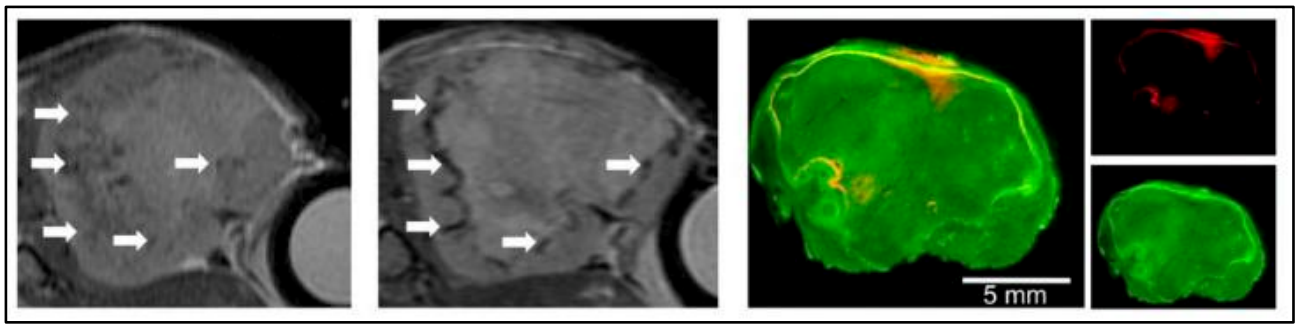

Figure 4.2: MRI (T_2) and immunofluorescence images of ferritin-expressing bacteria next to tumor in mice brain, extracted from[17]. On the **left**: Tumor area prior and 24 h after L-arabinose administration. The white arrows highlight the bacterial presence. On the **right**: Fluorescence imaging of the same tumor area. In red, bacteria; in green, actin.

A different strategy is to engineer eukaryotic cells to transform them as reporter agents. We can modify cells so that they express genes involved in the process of nucleation and growth of iron oxide particles. For instance, a team inspired by the magnetic properties of magnetotactic bacteria, have used as NMR reporters cells expressing one of their genes[19]. They identified and isolated the gene *MagA* that is partly responsible for the formation of magnetosomes. They transfected it in cells, injected the cells in mice, and showed that this gene was sufficient to create iron oxide in cells, with endogenous iron, inside the brain. With their method they could have a eukaryotic MRI reporter. Following this idea, another team has modified mice to express the heavy chain of human ferritin in their liver hepatocytes[20]. The authors have shown that after two years, with an iron-supplemented diet that did not affect the well-being of the animals, the liver could be visualized by MRI. With this idea of using ferritins, human cells[21], which expressed a chimeric ferritin (mixing light and heavy chains of human ferritin at a fixed ratio), were incubated with iron, and appeared to be monitored in MRI. To go further, another chimeric ferritin was expressed in cells: a peptide which can bind to magnetite during formation of magnetosomes was fused to a human ferritin[22]. The author maximized the NMR properties of ferritin, usually weak because of the ferrihydrite phase, by getting more iron internalized in ferritins and a different iron oxide phase. Finally a recent study[23] revealed that mesenchymal stem cells can become magnetic after being exposed to iron oxides nanoparticles. The degradation of internalized nanoparticles was followed by the storage of iron in ferritins, to avoid toxicity and leading to a remagnetization phenomenon. This article revealed that human cells are able to synthesize potential MRI-responsive iron oxides particles in presence of excess of iron without being genetically modified!

4.1.b - *C. elegans*: a model organism to examine host-bacteria interactions

For *in vivo* experiments, we chose to work on a simple model organism: *C. elegans.* The main reason is because this small nematode has a diet based on *E. coli*, and could be used to study gut microbiota. Besides, the millimeter-sized parasites, found in soil and rotten fruits, are bacterivorous, transparent, have easily sterilizable eggs and have a simple digestive tract. It might be a first step in our *in vivo* proof-of-concept assays, especially to investigate how our *MagEcoli* respond to being in a living organism. This might be a very first step toward applications on gut microbiota sensing for instance.

The easiest way to study gut effect on *MagEcoli* is to feed *C. elegans* with them. *C. elegans* ingests bacteria via their mouth. They digest them thanks to the grinder, an organ that lyses the bacteria, and thanks to a long linear cavity whose pH is acidic (**Fig. 4.3**). This digestion occurs in a few minutes, a time compatible with the short longevity of the nematodes[24]. An assay[25] have estimated a digestion time of around 2 minutes. To do so, they fed the nematodes with fluorescent microspheres mixed with *E. coli* and measured the fluorescence intensity after each expulsion event.

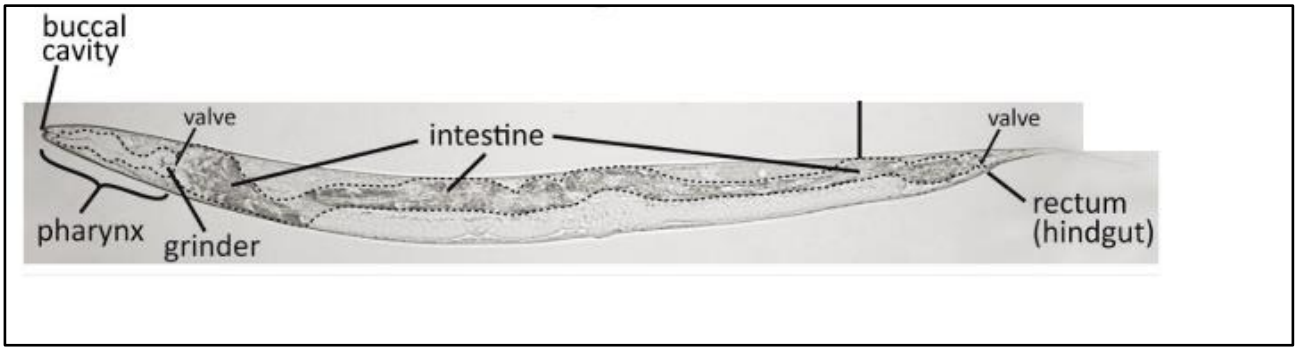

Figure 4.3: Digestive tract of an adult *C. elegans*, extracted from[24].

Recently, *C. elegans* have been particularly studied for host-microbiome interactions[26]. This organism is a model to study the molecular interactions between bacteria and the nematode, especially the effect on the immunity or life span. The nematodes have been exposed to various natural environments in order to study the effect of different populations of bacteria on the worm microbiota[27], the link between aging and intestinal bacterial proliferation[28], or to study host pathogens interactions like the resistance to bacterial infections thanks to its natural microbiome[29].

In the context of programmed bacteria, engineered probiotics have been tested into *C. elegans*[30]. In a recent study, the *Nissle* 1917 strain has been transformed to fight infections of the nematodes. They engineered the *E. coli* to kill the pathogenic *P. aeruginosa.* The authors then showed that the modified probiotics can protect *C. elegans* from *P. aeruginosa.* With fluorescence, they could visualize the ingestion of both populations of bacteria, and they measured the survival rate of the worms. With their probiotic the nematodes survived a few hours more (**Fig. 4.4 A**). Besides, a team has tested an another *Nissle* strain as an *in vivo* biosensor in *C. elegans*[31]. They designed *E. coli* with two plasmids that allowed constitutive mCherry expression and IPTG-inducible GFP expression. They fed the nematodes with the bacteria. With red fluorescence, they were able to monitor the presence of bacteria in the lumen. Upon external addition of IPTG in the environment, the bacteria also began to produce GFP fluorescence in the lumen proving that they worked *in vivo* as sensors (**Fig. 4.4 B**).

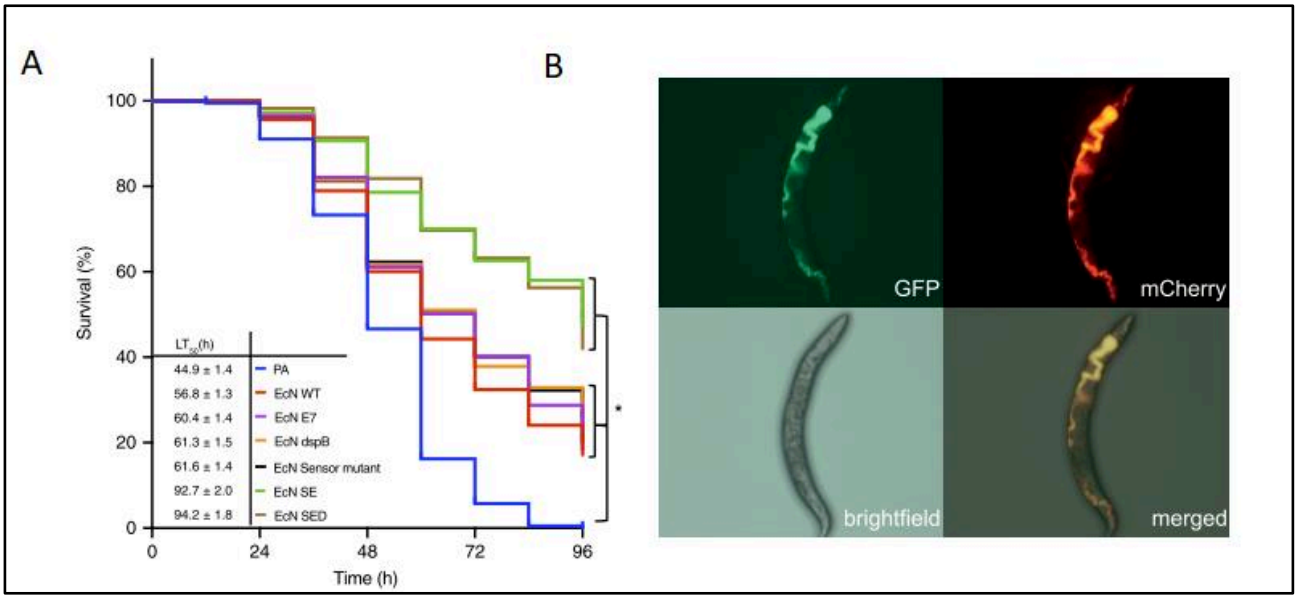

Figure 4.4: Example of results obtained with engineered probiotics in *C. elegans*. (A) Survival rate of nematodes infected with *P. aeruginosa*, in presence of a *Nissle* strain designed to kill the bacterial pathogen. In blue, after 96 hours with *P. aeruginosa,* all worms are dead. In green or brown, with the modified *Nissle,* around 40 % of nematodes are still alive after 96 hours. Extracted from[30]. **(B)** Microscopy images of *C. elegans* fed with an IPTG-biosensor. In presence of IPTG, the bacteria produce GFP in the lumen. Extracted from[31].

Thus, *C. elegans* seems to be a good candidate to study the effect of our *MagEcoli in vivo.* We could easily feed the nematodes with them. Since the nematodes are transparent, we could see with fluorescence their ingestion and their localization in the lumen. Moreover we could assess the test the magnetic properties of bacteria when they are *in vivo*.

4.2 - Results

4.2.a - Monitoring *MagEcoli* within *C. elegans* lumen

This part was done in collaboration with the team of Marie-Anne Felix, IBENS, ENS, for the experiments with C. elegans. The assays were performed with the help of Aurélien Richaud.

We fed *C. elegans* with our *MagEcoli* in order to **(i)** monitor the presence of magnetic bacteria in the lumen of *C. elegans,* **(ii)** to do magnetophoresis experiments on the worms, to check if incorporation in the digestive tract did not affect the magnetic properties. To do so we designed an experiment in which the nematodes were fed with *MagEcoli*, then treated with drugs and antibiotics to remove external *MagEcoli* and to reduce worm acitivity in order to avoid expulsion of *MagEcoli* from the lumen. Then a lysis of worm was applied to extract *MagEcoli* that were in the lumen and magnetophoresis was performed (**Fig. 4.5**).

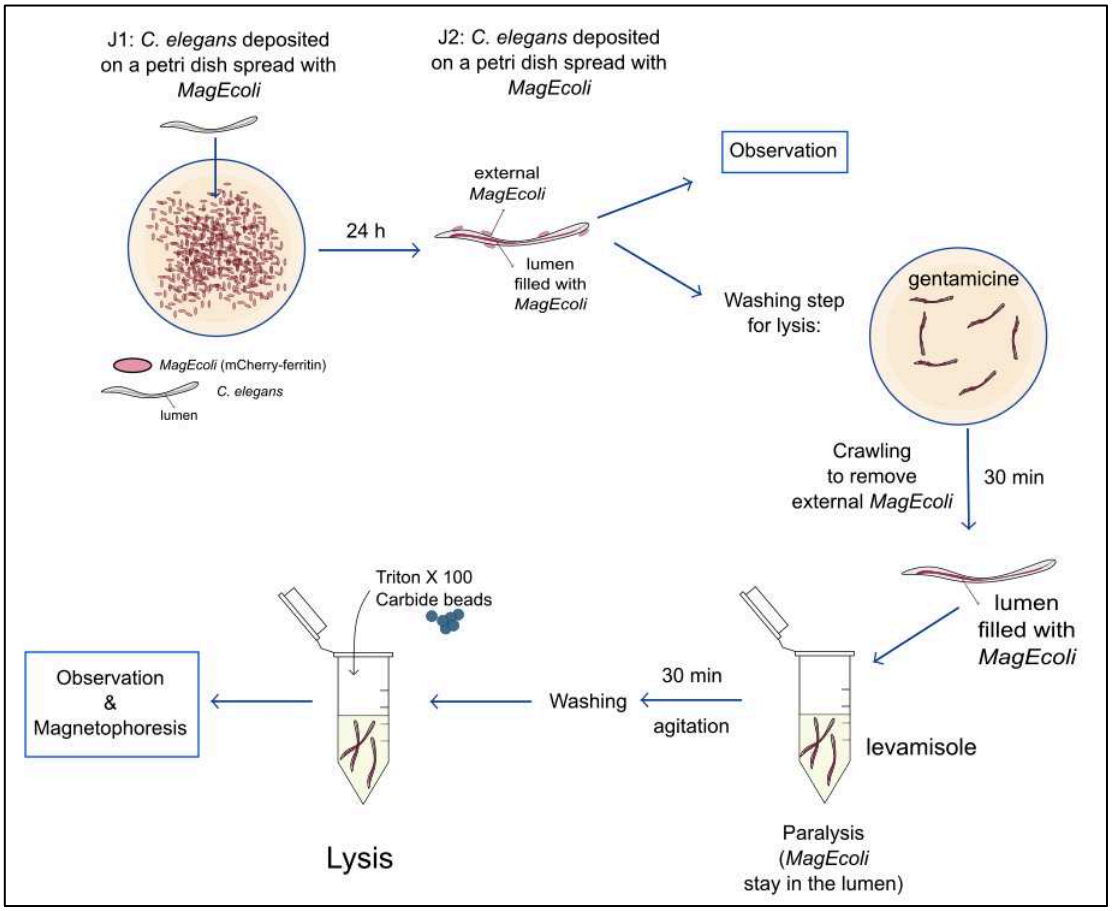

Figure 4.5: Schematic representation of the assay with *MagEcoli* and *C. elegans*. We wanted to select to observe intact *MagEcoli* in the lumen and then to lyse the nematodes and apply our set up of magnetophoresis to examine if bacteria were still magnetic.

This part presents exploratory experiments. The assays were made 2 or 3 times and were mainly qualitative results. Further experiments must be done in order to confirm the preliminary following results.

4.2.a.i) Selecting the right strain of *C. elegans*

The first step of our work was to choose the right strain of *C. elegans*. We wanted to have intact and living *E. coli* inside the worms. As they have a grinder at the entrance of their digestive tract to crush the bacteria (**Fig. 4.6**), we had to work with worms that did not lyse *E. coli* when they ate. Thus, we tested four strains and we selected the best one. We used the wild type *N2;* the natural strains discovered by Marie-Anne Felix JU1211 and JU282, and the genetically modified strain DA597. JU1211 and JU282 seemed to have *E. coli* colonizing their lumen, meaning that some bacteria were left intact after passing through their grinder; that is why we had chosen these strains. DA597 has a deletion in a gene coding for the grinder, so it was known to be grinder defective.

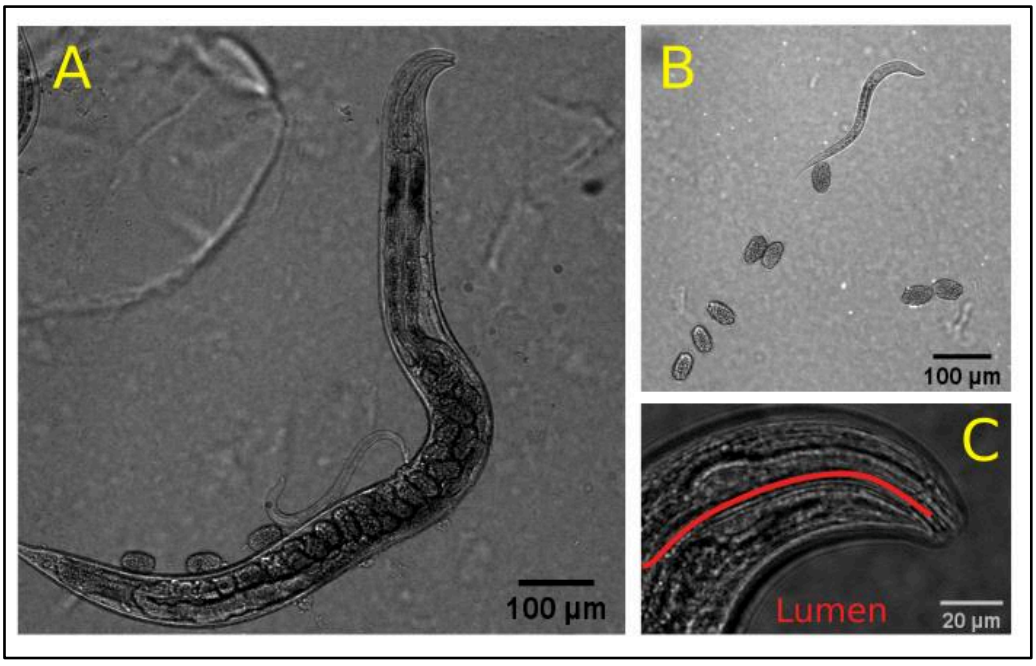

Figure 4.6: Bright field images of wild type *N2 C. elegans* fed with ferritin-producing *E. coli* at different life stages. (A) Adult worm. **(B)** L2 worm and eggs. **(C)** Zoom on the mouth of an adult *C. elegans*. The lumen is highlighted in red.

After a 24-hour incubation of *MagEcoli* or fluorescent ferritin-producing *E. coli* with worms, we observed with epifluorescence microscopy the lumen of the four strains. We noticed for the wild type, for JU1211 and for JU282, a diffuse red fluorescence in the lumen. Most of the time, we noticed a discrete red fluorescence just before the grinder corresponding to bacterial bodies and a

diffuse with almost no bacterial body just after it, in the lumen (**Fig. 4.7 B**). Whereas, for DA597, the fluorescence was less diffuse and let us distinguish bacterial bodies along the digestive tract (**Fig. 4.7 E**). This indicates that bacteria have been crushed by the lumen of N2, JU1211 and JU282 but left intact by DA597. We decided to perform our experiments with this last strain.

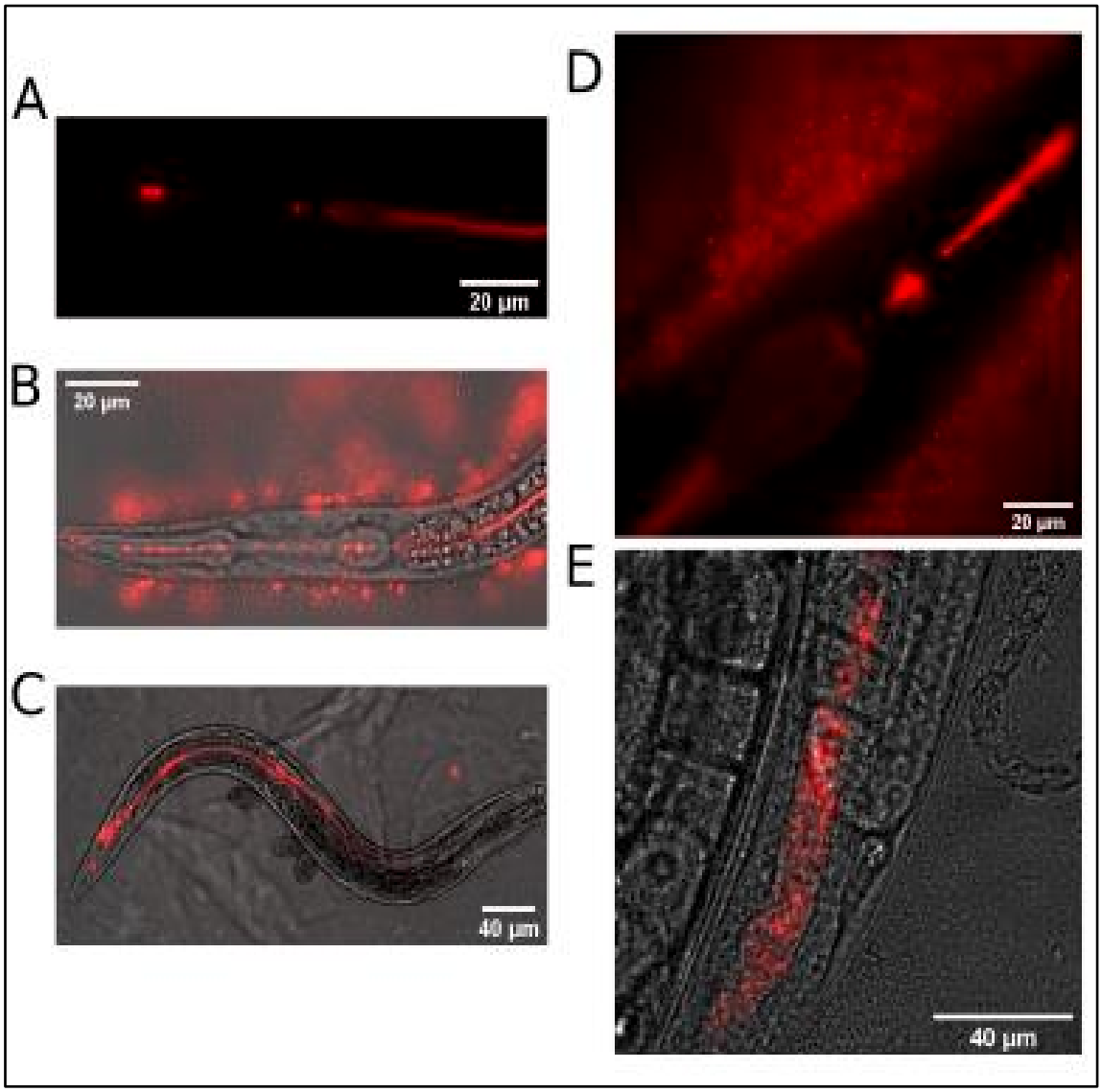

Figure 4.7: *MagEcoli* observed in different *C. elegans* strains. (A) mCherry images of wild type *N2*. Colorized image. **(B)** Merged images of Bright Field and mCherry channel of JU282. The intact bacteria are crushed when they pass through the grinder. **(C)** Merged images of Bright Field and mCherry channel of JU1211. Rare spots of red fluorescent can be seen. **(D)** mCherry images of JU282. Colorized images. The intact bacteria are crushed when they pass through the grinder. **(E)** Merged images of Bright Field and mCherry channel of DA597. The fluorescence is not diffused.

Altogether, the data proved that we have found a strain that left *MagEcoli* intact in the lumen. Most of the time, it is difficult for bacteria to pass the grinder of wild nematodes and to stay intact. That is why a grinder defective strain was the solution. Besides, fluorescence, as shown in a

study[32], is not sufficient to observe if bacteria in the lumen are alive: both intact bacteria and debris have the same signature in epifluorescence. Thereby, observing the shape of what seemed to be intact bacterial bodies in the intestine, was the first step for spotting living *MagEcoli in vivo.* We could have pushed further our investigations, by observing sections of *C. elegans* with transmission electronic microscopy (offering a better resolution), to confirm our choice. However, we had the confirmation of having intact *MagEcoli* inside DA597 by spreading the worm lysate on IPTG agar dish. We saw the formation of red fluorescent bacterial colonies, indicating that alive *MagEcoli* were present in the lysate, thus in the lumen, provided that all external bacteria have been previously removed from the worms.

4.2.a.ii) Lysis of *C. elegans* to get incubated *MagEcoli*

Once we could see by fluorescence the intact *MagEcoli* inside the lumen of *C. elegans*, we performed an assay to check if the bacteria remained magnetic. After a treatment with an antibiotic to remove external *E. coli* and a drug to paralyse worm digestive activity and prevent bacterial expulsion from the lumen, we chemically and mechanically lysed the *C. elegans* in order to extract the intestinal *MagEcoli* (see **Fig. 4.5**). Observation of the lysate showed individual fluorescent bacteria dispersed within a complex medium characteristic of cell extracts (**Fig. 4.8**). To note, we failed to observe a significant number of mCherry-ferritin overproducing *E. coli* (the condition without iron during biomineralization) in the lysate: the yield of bacterial extraction was weak compared to the conditions with *MagEcoli*. For now we have no convincing interpretation. Maybe supplementary assays will eventually led to the observation of non-mineralized bacteria after lysis.

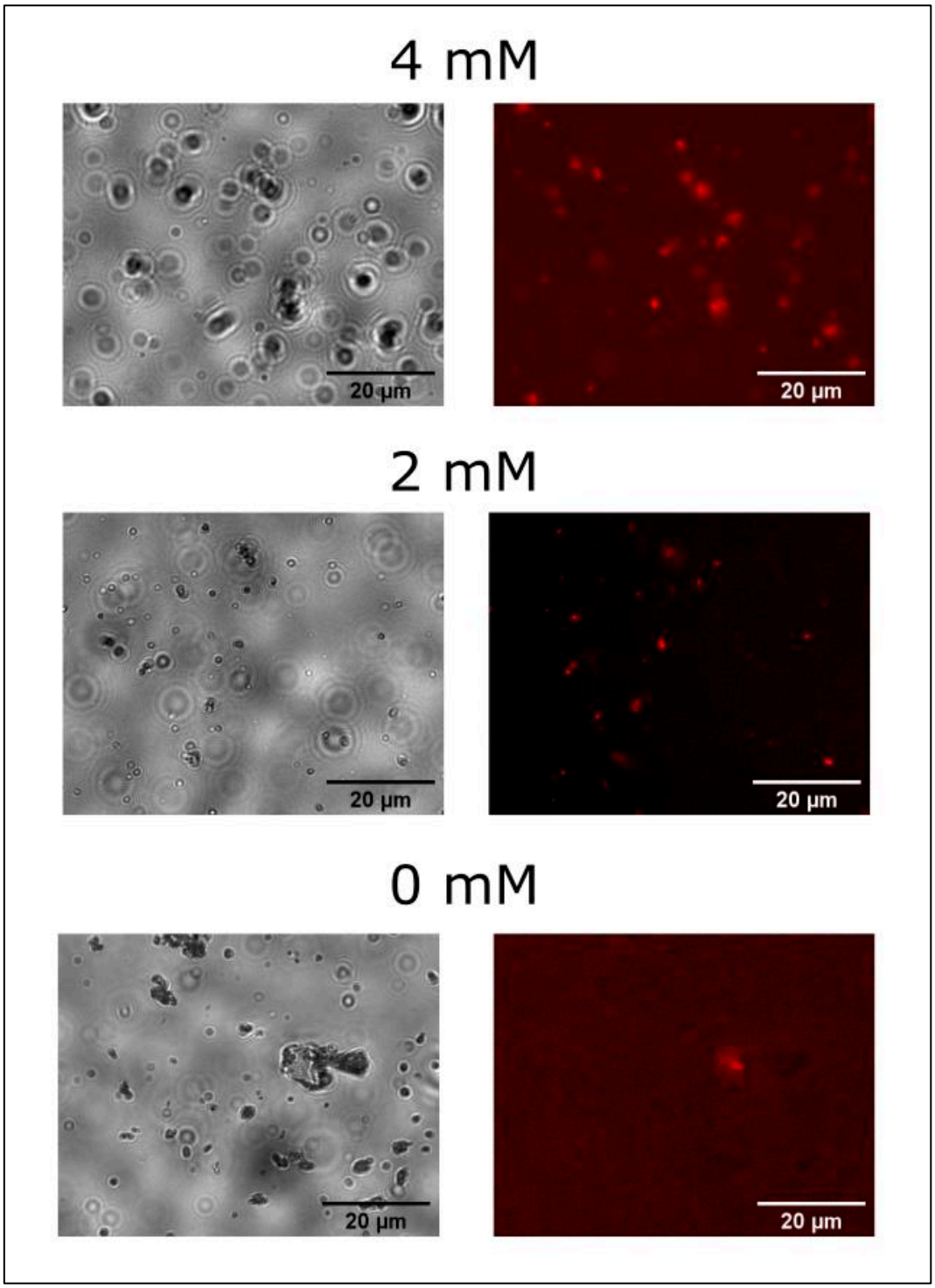

Figure 4.8: Microscopy image of lysate of DA597 fed with mCherry-ferritin overproducing *E. coli* mineralized with 0, 2 or 4 mM of iron. On **the left:** bright field. On **the right:** colorized mCherry channel. Scale bar, 20 µm.

4.2.a.iii) Magnetophoresis of *MagEcoli* present in the lysate

Then we applied our protocol of magnetophoresis on the lysate. With epifluorescence microscopy, we followed the trajectory of individual *MagEcoli* mineralized with 2 and 4 mM of iron (**Fig. 4.9**). If we superpose the trajectories over time, we can see that they longitudinally follow the direction of the magnetic gradients. This means that the bacteria were still attracted toward the magnet. As for the control, the non-mineralized *E. coli,* the red fluorescence of the lysate was not sufficient enough to monitor the trajectory of bacterial bodies. Other assays might help us to get more intact non-mineralized bacteria in the lysate and to perform the control. This would confirm the hypothesis of having kept the *MagEcoli* intact in the lumen and that the lysis was not altering the magnetic properties.

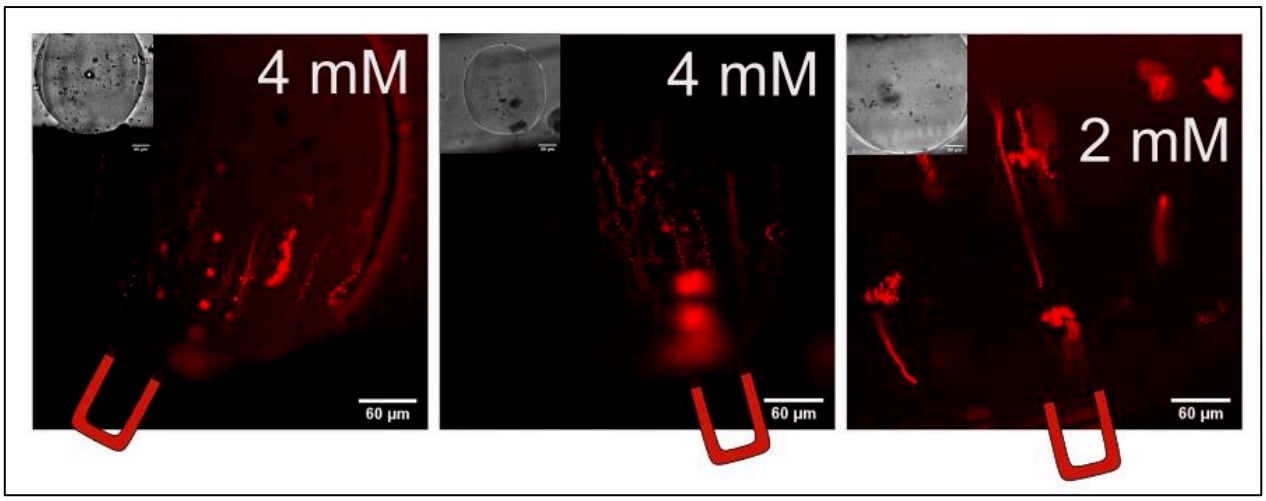

Figure 4.9: Computed trajectory of lysate of *DA597* and mineralized *E. coli*. Left & middle: Bacteria mineralized with 4 mM of iron II. **Right:** Bacteria mineralized with 2 mM of iron II. Colorized image of mCherry channel which superposes the trajectories of red-fluorescent bodies over time. On the left-top, images in bright field of the droplet at the beginning of the acquisition.

Thus, our data showed that we were able to feed a strain of *C. elegans* with *MagEcoli* and to examine by magnetophoresis extracted bacteria. We found that they remained magnetic after a 24-hour stay in the lumen. As a perspective, we could push further the applications. We could try to monitor bacterial presence in the nematodes by using magnetic resonance imaging, for example. We could also use our *MagEcoli* as *in vivo* magnetic biosensors. We could use them to sense the lumen microbiota and magnetically extract them to amplify the detection.

On the other hand, to better understand a potential toxicity induced by *MagEcoli* in nematodes, we could count the life span of *C. elegans* fed with magnetic bacteria. Indeed there is a

relationship between iron and the nematodes. According to studies, it seems that *C. elegans* need a diet rich in (bacterial) iron[33]. *C. elegans* lacking iron have a developmental delay. They can be rescued with iron supplemented at the mM range[34]. Thus, the nematodes might well tolerate iron-enriched bacteria. Moreover, a study showed us that *C. elegans* fed with 120-nanometer sized fluorescent nanodiamonds were not physiologically affected[35]. Nevertheless, in our case, as iron oxides are not inert, a life-span assay to assess toxicity of our *MagEcoli* might have been rewarding.

4.2.b - *In vitro* magnetic resonance imaging of *MagEcoli*

The NMR measurements were conducted by Philippe Pelupessy from the LBM, ENS. Like for the C. elegans assays, the following results are preliminary.

Here, we wanted to test *in vitro* the ability of *MagEcoli* to be used for potential live MRI. Indeed, the iron oxide crystals inside ferritin could be contrast agents. They could act as paramagnetic or superparamagnetic crystals and have an effect on the NMR relaxation times T_1 and T_2 [10]. Thus, we wanted to characterize our system and observe the effect on the two different relaxation times. To do so, we measured by MRI their effect on the relaxation times T_1, T_2 and T_2* (which acts similarly to T_2 but depends on the homogeneity of the bacterial environment), *in vitro*, in agarose solution.

4.2.b.i) *In vitro* measurement of *MagEcoli* response in MRI

We prepared different samples of 5 mm-NMR tubes filled with M9-agar and immobilized mineralized bacteria. We measured the T_1, T_2 and T_2* for different concentrations of bacteria in the tube (**Fig. 4.10 A**). We observed that our magnetic bacteria, when mineralized at 4mM, can be observed with MRI on axial and coronal sections of the tubes (**Fig. 4.10 B**). They seemed to have a strong effect on the T_2 (they decrease it). The T_2* was impacted in the same way as the T_2 by the bacteria. Here we decided to only display the results for R_2 ($1/T_2$) because **(i)** the effect was stronger than the one for T_1, and **(ii)** the T_2* depends on external factors in addition to the interaction between bacteria and M9-agar: it can be different from a sample to another due to a different distribution of bacteria in gel and other factors like the presence of air bubbles. While *MagEcoli* may give an excellent contrast *in vivo*, here T_2* is very dependent with the conditions of sample preparation, and less reliable.

Next, we studied the effect of iron concentration during mineralization on the relaxation times (**Fig. 4.10 C**). We measured the R_2 of *MagEcoli* mineralized at 0, 2 and 4 mM for an optical density of 2-3 inside the NMR tube. As displayed on the graph, the T_2 decreases when the concentration of iron rises. We also measured it for 2 mM-*MagEcoli* at an O.D. of around 1 in the tube and we found that the effect of T_2 was similar or slightly inferior for 2-time concentrated 2 mM-*MagEcoli.* This might indicates that bacterial concentration in the tube has not an impact as strong as iron concentration, for the range we are working with, at least. As a control, we measured the R_2 for bacteria that did not over-express ferritin but that followed the same protocol of mineralization with 0 or 2 mM of iron. They were at an O.D. of 1 in the tube. For the control at 0 mM, the T_2 was the same for non-mineralized *MagEcoli*, as expected. For 2 mM, the R_2 did not increase significantly and it was inferior to the ones measured for *MagEcoli* 2 mM at the same O.D. An additional measurements of LB supplemented with 4 mM of iron gave us an R_2 in the same range as the bacterial control. Altogether, these data indicates that *MagEcoli* have a distinct magnetic signatures that have an impact on the relaxation times T_2. Moreover, 4 mM-mineralized bacteria seemed to have the highest effect.

Then, we examined the link between R_2 and bacterial concentration in the sample (ranging for an O.D. from 0.2 to 10). As we saw that twice less concentrated *MagEcoli* in the tube seemed to have a smaller R_2, we studied the impact of bacterial O.D. on the R_2. To do so we prepared different samples of *MagEcoli* mineralized at 2 mM of iron mixed in M9-agar at various OD. The data are displayed in **Figure 4.10 D**. We can see that for low O.D., 0.2, the signal is weaker and similar to the control (LB with 4 mM of iron). However, at O.D. around 1, the R_2 clearly increases. Nevertheless, we did not observe a clear raise as we add more and more bacteria in the tube: the R_2 seems to fluctuate slightly around the value of 20 s^{-1}. The data have to be strengthened with triplicates to see if the fluctuation of T_2 is significant or is just experimental noise.

Finally, to confirm the use of 4 mM-mineralized *MagEcoli* as contrast agent, we prepared a sample in which the *MagEcoli* were not homogeneously distributed. The idea was to see if we could distinguish the regions enriched in bacteria from the rest of the sample. As displayed in **Fig. 4.10 E,** we observed a difference of $1/T_2$ intensity for the coronal section. We can observe on the image, the diffusion streaks generated by the bacteria quickly entrapped in the M9-agar. These showed us that our *MagEcoli* is a contrast agent *in vitro*.

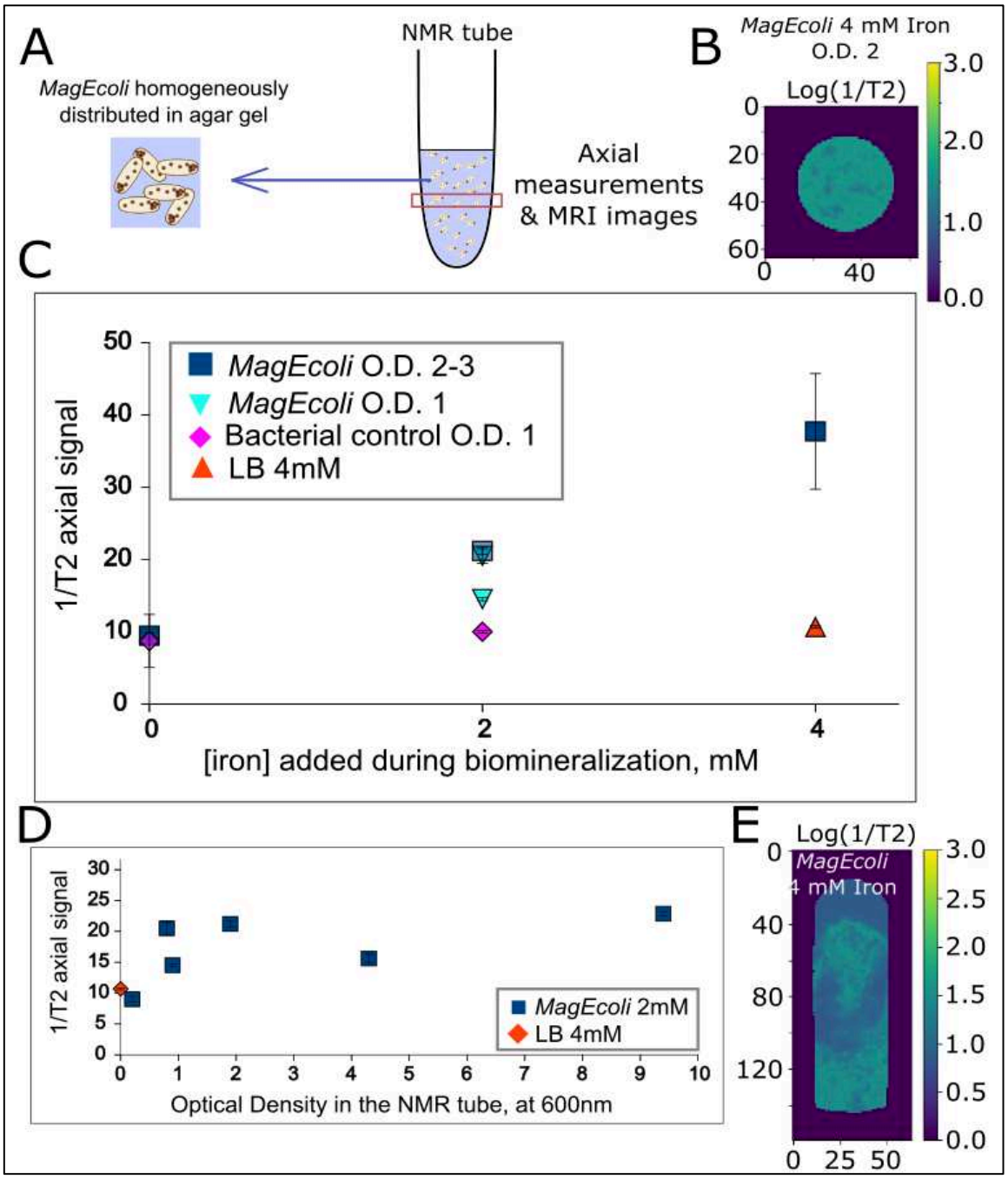

Figure 4.10: NMR measurements of *MagEcoli in vitro*. **(A)** The NMR tubes are filled with bacteria entrapped in an agar gel. Axial measurements of T_2, T_1 and T_2* are performed as well as MRI when needed. **(B)** Example of an axial image of *MagEcoli* mineralized with 4mM of iron II in the agar at an optical density of 2. The log values of $1/T_2$ are displayed. The axis represents the dimension of the axial section in millimeter. **(C)** The $1/T_2$ (in s^{-1}) is displayed as a function of the concentration of iron added during biomineralization of bacteria. In blue, with the square, are represented the data for the *MagEcoli* trapped at an O.D. of around 2-3 in the NMR tube; in light blue, with the triangle, the *MagEcoli* at an O.D. of around 1. The pink diamond stands for the $1/T_2$ measured with control bacteria, which do not overexpress ferritin, at an O.D. of around 1. The orange triangle is the signal for LB medium supplemented with 4 mM of iron. Each dot represents a sample. The error bars represent the dispersion of the relaxation rates over the sample. **(D)** The graph represents the $1/T_2$ (in s^{-1}) measured for *MagEcoli* mineralized with 2 mM of iron as a function of O.D. in the NMR tube. The square blue represents the data for the *MagEcoli* whereas the red diamond displays the $1/T_2$ measured for LB supplemented with 4 mM of iron. Each dot represents a sample. The error bar represent the dispersion of the relaxation rates over the sample.

(E) The MRI of *MagEcoli* mineralized at 4 mM of iron. The bacteria are not homogeneously distributed inside the agar. The log value of $1/T_2$ is displayed. The axis represents the dimension of the coronal section in millimeter.

4.2.b.ii) Comparison of the obtained T_2 with other iron oxides

All these data, and especially the fact that *MagEcoli* decreased the T_2, indicate that the bacteria could be negative contrast agent, the same way as chemically-synthesized iron oxide nanoparticles are used nowadays. The highest R_2 we reached was 37.7 s^{-1} for bacteria mineralized with 4 mM of iron at an O.D. of 2.

Our R_2 was slightly smaller than the ones found with expressed ferritin in cells: osteosarcoma cells[21], which produced a chimeric ferritin led to a R_2 of around 65 s^{-1}; in liver hepatocytes, over-produced ferritin led to a R_2 of 50 s^{-1} in mice fed with a high-iron diet[20]. If we look at examples of *in vivo* imaging of magnetic bacteria, we can find R_2 numbers to compare. First, for ferritin overproducing bacteria[17], the R_2 was around 30 s^{-1} and sufficient for MRI in brain tumor. In another study[7], "ultraparamagnetic bacteria" have a higher R_2 (around 50 s^{-1} at an O.D. of 10) that also gave a good contrast in MRI. **Thus our *MagEcoli* might have an effect on T_2 sufficient enough for *in vivo* imaging,** if we suppose that *in vivo* enough bacteria accumulate in the area to image.

Remarkably, in both articles, the authors also found a decrease of T_2 with concentration, an effect that has not been observed in our assay. This may be due to our concentration range that was too small. At higher O.D. we might have found an increase in the R_2 signal!

As perspectives for *in vivo* MRI assays, a preliminary experiment could be the MRI of *MagEcoli* inside *C. elegans*. Indeed we could examine by MRI if we get a signal from bacteria in the lumen. Are they numerous enough and magnetic enough to be contrast agent? This experiment is to put in the context of using probiotic strains for *in vivo* MRI of the intestine for diagnostic. For instance if our *MagEcoli* can stick to sick cells in the intestine, we could localize their presence by MRI in animal models.

However, **compared to SPIONs, our R_2 seems quite low**. The commercial ones have an R_2 of 166.71 $mM^{-1}.s^{-1}$ or 133 $mM^{-1}.s^{-1}$, depending on the studies[15,16] for Feridex®, or 230 $mM^{-1}.s^{-1}$ for Resovists®[36]. Coated SPIONs can even have higher R_2 : 728.23 $mM^{-1}.s^{-1}$ for the positively charged spion[15], 324 $mM^{-1}.s^{-1}$ for coated iron oxides nanocubes[16]. Magnetosomes themselves[36], as they are

made of magnetite perfectly controlled in size and shape, have an even higher R_2 1175 $mM^{-1}.s^{-1}$. This may be due to their pure phase. Indeed magnetite has a better signature than maghemite[37]. Thus our lower R_2 value is not surprising since the ferritins are not in the conditions to produce magnetite during the *in vivo* biomineralization.

To get better R_2 and contrast, we could try to enhance the effect on relaxation time T_2 of our *MagEcoli*. We could try to get a phase similar to magnetite, by changing the biomineralization parameters (controlling the pH, redox potential…). We could also change the protein scaffold to get bigger crystals, by using encapsulins (25-40 nm of diameter).

4.3 - Material and Methods

Chemicals

Kanamycin, Chloramphenicol, Mohr's Salt, LB broth, Glycerol, Agar, IPTG, and Mineral oil were purchased from SIGMA-ALDRICH®. Arlacel P135 was purchased from CRODA®. Vitrex® was purchased from VWR®.

Strains and plasmid

E. coli bacteria were purchased at Merck for Rosetta (DE3)pLysS. The plasmid and biomineralization used are the one described in chapter 2.

Feeding of *C. elegans*

100-200 µL of bacteria were spread at the center of fresh *C. elegans'* petri dish with kanamycin. A small agar cube with worms was transferred on the dish. *C. elegans* and bacteria were let in contact for 6-24 hours at 20°C, depending on the conditions of the experiment.
The worms were collected for observation or lysis in M9 medium.

Microscopy observation of single *C. elegans*

For the observation of *C. elegans* in fluorescence microscopy, the worms were taken out from the plate and put in an M9 medium containing sodium azide. The worms where then deposited on an M9-agar pad containing sodium azide spread on a coverslip. The observations were performed the same day. The epifluorescence microscopes used were the ones described in the previous chapter.

Lysis of *C. elegans* and magnetophoresis

After having fed the *C. elegans* with mineralized bacteria for 24 hours at 20°C, the worms were collected with M9 medium. We deposited the worm on agar dish enriched in gentamicine to remove the external bacteria that might have adhered to the *C. elegans*. We let the worms crawled in the dish for 30 minutes. Next we solubilized and collected the worms in M9 medium with 25 mM Levamisole (for immobilization) and 100 µg/mL gentamicine. We put the samples for 30 minutes under agitation at room temperature. We washed the *C. elegans* with M9 + 100µg/mL gentamicine first then M9 alone. We then proceeded to the lysis by putting the worms in PBS 1X with 0.1% Triton X100. We added carbide beads to mechanically lyse the worms with the vortex. We collected the supernatant and put it aside for magnetophoresis. We used the exact same set up as in chapter 2.

NMR sample preparation

We took the mineralized bacteria and washed them twice in M9 medium. We prepared an M9-agar gel by diluting 1% agarose in M9. When the M9-agar was hot, we mixed the pellet of washed bacteria and inserted in an NMR tube for measurements.

MRI experiments

The experiments have been done on a Bruker 800 MHz NMR spectrometer equipped with a micro-imaging probe with a 5mm resonator, and a Bruker Micro 2.5 gradient system with a maximum gradient strength of of 1.0 $T.m^{-1}$. The relaxation times have been determined with standard imaging sequences: T1, by varying the recovery time of a flash sequence, T2 and T2* by a multiple slice multi echo (MSME) and a single echo sequence, respectively. The acquisition and image processing has been done with the paravision program (version 6.01), while the extraction of the (position dependent) relaxation time has been done with in-house developed python programs.

4.4 - Annex

4.4.a - Extraction of *in vivo* mineralized ferritin from *MagEcoli*

For applications that requires non-living objects, by fear of GMOs dissemination, or *in vivo* bacterial mutation for instance, we can think about extracting the ferritins instead of using the whole-bacterium. In this configuration, bacteria serve only as living factories of genetically encoded nanoparticles. This biosynthesis has relative advantages toward chemical techniques: the biomineralization is entirely made by the bacteria and genetic modifications give us the possibility to easily add novel functions onto the ferritins. We can transform them genetically to fuse them with various proteins for fluorescence, protein-binding, or even labelling. In this last part, we tried to extract functionalized and bio-mineralized ferritins to see if the proteins still remained magnetic, and could be used by themselves.

4.4.a.i) Purification of mineralized ferritins

To engineer functionalized ferritins, we used a different plasmid that lead to the over-expression in *E. coli* of genetically encoded ferritins. Here, each monomer of ferritin is either fused with FKBP, mCherry and a Histidine-tag or fused with FRB, emGFP and a Histidine-tag. The Histidine-tag is here for collecting the proteins on Ni-NTA beads during purification by affinity. FRB and FKBP can homodimerize in the presence of rapamycin. So the resulting bacteria can produce fluorescent ferritin fused with FRB or FKBP (**Fig. 4.11**). We applied our protocol of biomineralization on the bacteria to mineralize the ferritins. After lysing and purifying, we collected the lysate.

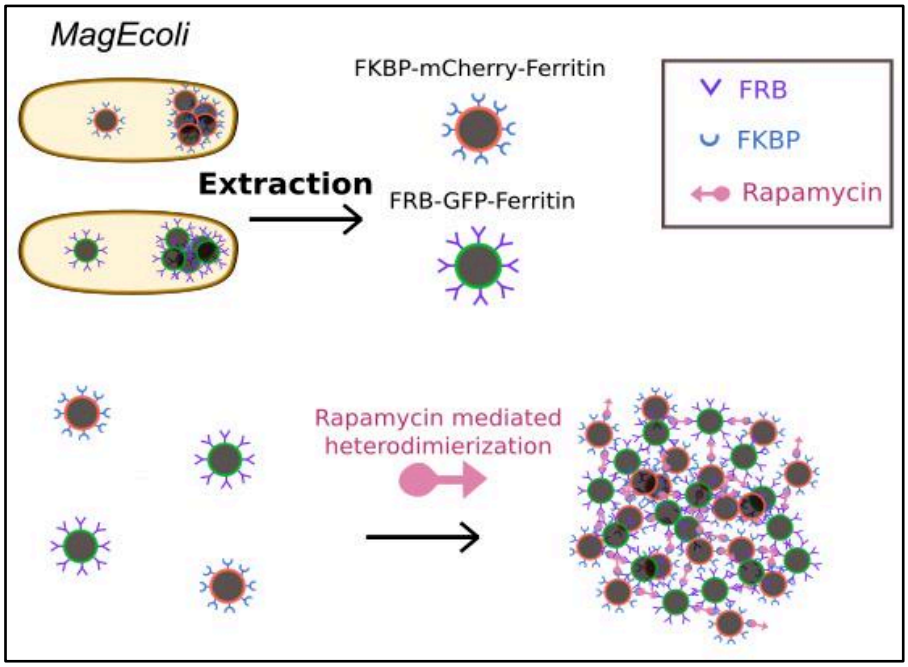

Figure 4.11: Principle of the assay. FRB-GFP-Ferritin or FKBP-mCherry-Ferritin bacteria are biomineralized and lysed. The ferritins are extracted, and can form magnetic clusters upon addition of rapamycin.

4.4.a.ii) Magnetophoresis of extracted ferritins

Then we tested the magnetism with our protocol of magnetophoresis. We mixed the two populations of ferritins. To be able to observe them on the microscope, we added rapamycin to induce the dimerization of FRB and FKBP, thus the formation of micrometric clusters of mineralized ferritins. We monitored the apparition of clusters in the fluorescent channel as expected (see **Fig. 4.12**). With the help of a tip fixed on a permanent magnet, we generated a magnetic field of 10^4 $T.m^{-1}$. In general, when clusters were formed, they were attracted toward the tip as soon as it approached the droplet, counterbalancing hydrodynamics fluxes (**Fig. 4.12**). This experiment showed us that *MagEcoli* might become factory for engineered magnetic nanoparticles. This assay should have been repeated other times, with a different batch of purified ferritin, to quantify its robustness, and for proper quantification.

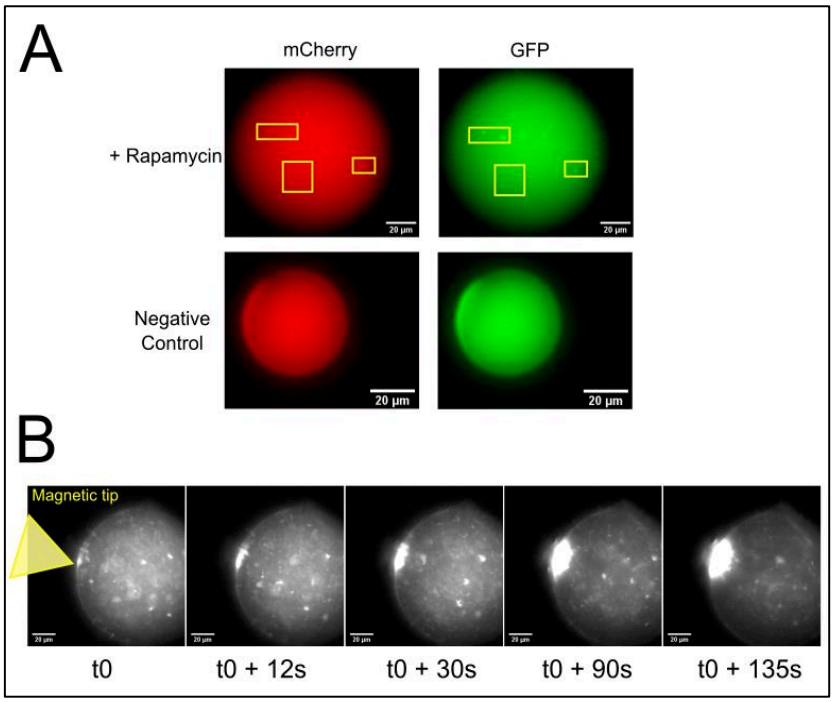

Figure 4.12: formation of clusters of ferritin and magnetophoresis assay. (A) Colorized fluorescence images of a droplet containing FRB-GFP-ferritins and FKBP-mCherry-ferritins with and without rapamycin. The clusters formed are highlighted in the yellow rectangles. **(B)** Time lapse images of an assay of magnetophoresis. FRB-GFP-ferritin and FKBP-mCherry-ferritin clusters are in the droplet and the magnetic tip is on the left. Scale bar, 20 µm. mCherry channel.

Altogether, these date prove that it is possible to extract magnetic ferritins from bacteria and to fuse it with other proteins of interest, here the FRB/FKBP complex, GFP and mCherry. Contrary to the whole bacterium, the modified ferritin is not alive and cannot produce molecules or proteins such as the one required for quorum sensing communication for instance. However, having an inert object can be interesting as it does not require biosafety measures such as the incorporation of a kill switch to prevent from the multiplication of the object in the environment.

However, in the case of an *in vivo* mineralization, like we did, the iron oxide synthesis is not controlled and limited by the bacterial biochemistry (in terms of temperatures, pH, redox potential) and did not lead to a pure magnetite phase for instance. An *in vitro* mineralization of extracted ferritins could be considered. A biological synthesis of functionalized ferritins could be followed by an *in vitro* mineralization, or even an encapsulation of drugs for local drug-delivery. Even if 8 nm-diameter nanoparticles, especially in the case of *in vivo* mineralization, can lead to a low effect on the relaxation time T_2, having the possibility to build bigger structures might be a strategy to have a better signal in MRI. This is an experiment to test.

4.4.a.iii) Methods

Strains and plasmid

E. coli bacteria were purchased at Merck for Rosetta (DE3)pLysS. For the extraction of ferritin, the two plasmids are pet28dut modified by the adding of His-FRB-GFP-Ftn_FKBP-mCherry-Ftn or His-FKBP-mCherry-Ftn_FRB-GFP-Ftn genes. These genes lead to the expression of FRB-GFP-Ferritin and FKBP-mCherry-Ferritin in different proportions.

Production and extraction of magnetic ferritins

Rosetta bacteria with the pet28duet plasmids were precultured overnight in LB medium with kanamycin and chloramphenicol at 37°C under agitation. The next morning, the precultures were diluted in fresh LB medium and antibiotics and let grow at 37°C under agitation to reach an optical density of 0,6 à 600nm. 500µM of IPTG was added as well as 1mM of iron II (Mohr's salt solution) and 1mM of iron III (iron acetate solution). The bacteria were put for 16 hours at 16°C under agitation. The following day, for protein purification, the bacteria were centrifuged at 4500 rpm for 30 minutes at 4°C. The pellet was washed with PBS buffer and re-suspended in the washing buffer: PBS1X with 10 mM of imidazole. For bacterial lysis, on ice, lyzozyme, 0.1% of Triton X100, 1 nM of AEBSF and protease inhibitor were added for 30 minutes. We next applied 30 cycles of sonication and mechanical lysis. After a 10-minute centrifugation at 10 000 rpm at 4°C, the supernatant was incubated for 2 hours at 4°C on Ni-NTA beads in the washing buffer for affinity purification. We washed with the same buffer the protein and beads on column and eluted with PBS 1X, 100mM EDTA, 250 mM imidazole and 5% glycerol. We dialyzed the ferritins to change the buffer for PBS 1X durnig 1 hour and overnight. We measured by Nanodrop, SDS page and Bradford assay the concentration of proteins in the fraction eluted. The ones with the higher concentrations were used for magnetophoresis. The samples were kept at 4°C in PBS buffer for use in the next days.

Magnetophoresis of extracted ferritins

We used an adapted protocol of the magnetophoresis described in Chapter 2. To visualize the mineralized and extracted ferritines, we began to induce the formation if clusters. We mixed the FKBP-mCherry-Ferritins with the FRB-GFP-Ferritins with 100 µM of rapamycin in PBS to trigger the heterodimerization of FRB and FKBP. We added BSA to prevent the adsorption on the droplet interface. We then formed the emulsion and we assessed the magnetic properties with a magnetized tip (radius of curvature of about 25 µM) adapted on the N-S axis of a NdFeB square magnet (3 mm).

We placed the tip next to the droplet thanks to a micromanipulator (Narishige), generating a gradient of magnetic field of about 10^4 T.m^{-1}.

4.5 - References

1. Danino, T. *et al.* Programmable probiotics for detection of cancer in urine. *Sci. Transl. Med.* **7**, (2015).
2. Riglar, D. T. *et al.* Engineered bacteria can function in the mammalian gut long-term as live diagnostics of inflammation. *Nat. Biotechnol.* **35**, 653–658 (2017).
3. Riglar, D. T. & Silver, P. A. Engineering bacteria for diagnostic and therapeutic applications. *Nat. Rev. Microbiol.* **16**, 214–225 (2018).
4. Hosseinidoust, Z. *et al.* Bioengineered and biohybrid bacteria-based systems for drug delivery. *Adv. Drug Deliv. Rev.* **106**, 27–44 (2016).
5. Forbes, N. S. Engineering the perfect (bacterial) cancer therapy. *Nat. Rev. Cancer* **10**, 785–794 (2010).
6. Ho, C. L. *et al.* Engineered commensal microbes for diet-mediated colorectal-cancer chemoprevention. *Nat. Biomed. Eng.* **2**, 27–37 (2018).
7. Ramesh, P. *et al.* Ultraparamagnetic Cells Formed through Intracellular Oxidation and Chelation of Paramagnetic Iron. *Angewandte Chemie - International Edition* (2018). doi:10.1002/anie.201805042
8. Shamsudhin, N. *et al.* Magnetically guided capsule endoscopy: *Med. Phys.* **44**, e91–e111 (2017).
9. Salerno, M. *et al.* A discrete-time localization method for capsule endoscopy based on on-board magnetic sensing. *Meas. Sci. Technol.* **23**, (2012).
10. Xiao, Y. D. *et al.* MRI contrast agents: Classification and application (Review). *Int. J. Mol. Med.* **38**, 1319–1326 (2016).
11. Li, L. *et al.* Superparamagnetic iron oxide nanoparticles as MRI contrast agents for non-invasive stem cell labeling and tracking. *Theranostics* **3**, 595–615 (2013).
12. Widder, D. J., Edelman, A., Lawrence, W. & Monda, L. Magnetite Albumin Suspension : A Superparamagnetic Oral. *Am. J. Roentgenol.* **149**, 839–843 (1987).
13. Bulte, J. W. M. *et al.* Specific MR imaging of human lymphocytes by monoclonal antibody-guided dextran-magnetite particles. *Magn. Reson. Med.* **25**, 148–157 (1992).
14. Ma, X. *et al.* Exploring a new SPION-based MRI contrast agent with excellent water-dispersibility, high specificity to cancer cells and strong MR imaging efficacy. *Colloids Surfaces B Biointerfaces* **126**, 44–49 (2015).
15. Kim, H. *et al.* A highly sensitive magnetite nanoparticle as a simple and rapid stem cell labelling agent for MRI tracking. *J. Mater. Chem.* **21**, 7742–7747 (2011).
16. Lee, N. *et al.* Magnetosome-like ferrimagnetic iron oxide nanocubes for highly sensitive MRI of single cells and transplanted pancreatic islets. *Proc. Natl. Acad. Sci. U. S. A.* **108**, 2662–2667 (2011).
17. Hill, P. J. *et al.* Magnetic resonance imaging of tumors colonized with bacterial ferritin-expressing Escherichia coli. *PLoS One* **6**, (2011).
18. Benoit, M. R. *et al.* Visualizing implanted tumors in mice with magnetic resonance imaging using magnetotactic bacteria. *Clin. Cancer Res.* **15**, 5170–5177 (2009).
19. Zurkiya, O., Chan, A. W. S. & Hu, X. MagA is sufficient for producing magnetic nanoparticles in mammalian cells, making it an MRI reporter. *Magn. Reson. Med.* **59**, 1225–1231 (2008).
20. Ziv, K. *et al.* Ferritin as a reporter gene for MRI: Chronic liver over expression of h-ferritin during dietary iron supplementation and aging. *NMR Biomed.* **23**, 523–531 (2010).
21. Iordanova, B., Robison, C. S. & Ahrens, E. T. Design and characterization of a chimeric ferritin with enhanced iron loading and transverse NMR relaxation rate. *J. Biol. Inorg. Chem.* **15**, 957–965 (2010).
22. Radoul, M. *et al.* Genetic manipulation of iron biomineralization enhances MR relaxivity in a

ferritin-M6A chimeric complex. *Scientific Reports* **6**, (2016).
23. Van de Walle, A. *et al.* Biosynthesis of magnetic nanoparticles from nanodegradation products revealed in human stem cells. *Proc. Natl. Acad. Sci. U. S. A.* (2019). doi:10.1073/pnas.1816792116
24. Dimov, I. & Maduro, M. F. The C. elegans intestine: organogenesis, digestion, and physiology. *Cell Tissue Res.* **377**, 383–396 (2019).
25. Ghafouri, S. & McGhee, J. D. Bacterial residence time in the intestine of Caenorhabditis elegans. *Nematology* **9**, 87–91 (2007).
26. Gerbaba, T. K., Green-Harrison, L. & Buret, A. G. Modeling host-microbiome interactions in caenorhabditis elegans. *J. Nematol.* **49**, 348–356 (2017).
27. Berg, M. *et al.* Assembly of the Caenorhabditis elegans gut microbiota from diverse soil microbial environments. *ISME J.* **10**, 1998–2009 (2016).
28. Portal-Celhay, C., Bradley, E. R. & Blaser, M. J. Control of intestinal bacterial proliferation in regulation of lifespan in Caenorhabditis elegans. *BMC Microbiol.* **12**, (2012).
29. Kissoyan, K. A. B. *et al.* Natural C. elegans Microbiota Protects against Infection via Production of a Cyclic Lipopeptide of the Viscosin Group. *Curr. Biol.* **29**, 1030-1037.e5 (2019).
30. Hwang, I. Y. *et al.* Engineered probiotic Escherichia coli can eliminate and prevent Pseudomonas aeruginosa gut infection in animal models. *Nat. Commun.* **8**, 1–11 (2017).
31. Rutter, J. W. *et al.* Detecting Changes in the Caenorhabditis elegans Intestinal Environment Using an Engineered Bacterial Biosensor. *ACS Synth. Biol.* **8**, 2620–2628 (2019).
32. Hsiao, J. Y., Chen, C. Y., Yang, M. J. & Ho, H. C. Live and dead GFP-tagged bacteria showed indistinguishable fluorescence in Caenorhabditis elegans gut. *J. Microbiol.* **51**, 367–372 (2013).
33. Rajan, M. *et al.* NHR-14 loss of function couples intestinal iron uptake with innate immunity in C. elegans through PQM-1 signaling. *Elife* **8**, (2019).
34. Zhang, J. *et al.* A Delicate Balance between Bacterial Iron and Reactive Oxygen Species Supports Optimal C. elegans Development. *Cell Host Microbe* **26**, 400-411.e3 (2019).
35. Mohan, N., Chen, C. S., Hsieh, H. H., Wu, Y. C. & Chang, H. C. In vivo imaging and toxicity assessments of fluorescent nanodiamonds in caenorhabditis elegans. *Nano Lett.* **10**, 3692–3699 (2010).
36. Hu, L. L. *et al.* Comparison of the 1H NMR relaxation enhancement produced by bacterial magnetosomes and synthetic iron oxide nanoparticles for potential use as MR molecular probes. *IEEE Trans. Appl. Supercond.* **20**, 822–825 (2010).
37. Basti, H. *et al.* Catechol derivatives-coated Fe3O4 and γ-Fe2O3 nanoparticles as potential MRI contrast agents. *J. Colloid Interface Sci.* **341**, 248–254 (2010).

General conclusion and perspectives

Our goal was to integrate magnetic properties into *Escherichia coli* to enable a contact-less and orthogonal method for spatial control. We have generated a magnetic-sensing *E. coli* by driving the formation of iron-rich bodies into bacteria. The resulting bacteria (*MagEcoli)* presented iron oxides and phosphates deposits at their pole and displayed a paramagnetic signature. *MagEcoli* could be spatially controlled by magnetic forces and sustained cell growth and division, by transmitting asymmetrically their magnetic properties to one daughter cell. This mode of growth avoided a strong dilution and loss of magnetic properties over-time.

To examine whether magnetized bacteria were amenable for achieving defined bio-chemical functions while being magnetically manipulated, we performed several proof-of-concept experiments.

First, we genetically encoded adhesion properties on the outer membrane of *MagEcoli* to achieve the magnetic capture of specific target cells as well as the spatial modulation of human cell invasions.

Secondly, we programmed *MagEcoli* to deliver or sense small molecules in order to examine the impact of magnetic localization on quorum sensing-based communication. We showed that magnetic bacteria remained metabolically active enough to either send or sense a small mediator called AHL. While the magnetic localization of the AHL-sending *MagEcoli* in space was not sufficient to concentrate a sensing response at its vicinity, due to AHL diffusion, the concentration of magnetic AHL-sensors was sufficient to induce a local increase of detection signal.

Then, we performed exploratory experiments in the perspective of using *MagEcoli* for *in vivo* applications. We showed that *MagEcoli* are potential good candidates as contrast agents for MRI. Besides, preliminary tests revealed that bacteria remained magnetic after being 24 hours in the lumen of a strain of *Caenorhabditis elegans*, which is a pre-request to use *MagEcoli* as sensor or detector *in vivo.*

Finally, we showed that magnetic ferritin can be extracted from *E. coli*, which might be interesting for applications requiring bacteria as living factories of functionalized nanoparticles.

The perspectives of this work are multifold.

From a fundamental point of view, one exciting direction will be to assess if other magnetic structures could be synthetized in *E. coli* (magnetite, maghemite). Both kinetic (rate of iron oxidation) or thermodynamic considerations (modulation of redox potential and pH at the locus of biomineralization) are key parameters for the formation of magnetic nanoparticles. Thus, one first strategy could be to adapt our biomineralization protocol in order to turn *in vivo* the ferrihydrite-like phases we had synthetized in the apoferritins into well-crystallized magnetic ones. Here, we expected that using anoxic instead of aerobic conditions during biomineralization might allow the ferrihydrite precursors to be transformed into magnetite in presence of a cytoplasmic excess of Fe^{2+}. A second strategy could be the use of mutant strains to tune the global redox or pH homeostasis of the bacteria in order to favor the thermodynamic stability of magnetic nanophases. However, it is unclear that this could be done using *E. coli*, since it is difficult to control and to tune iron oxidation rates, redox and pH parameters. Alternatively, the use of larger compartments like encapsulin (size between 25-40 nm) could be of interest to increase the size of the synthetized iron oxides.

From a biotechnological perspective, improving magnetic properties will certainly facilitate the applications that could be implemented with our assay. *MagEcoli* technologies may be of interest for diagnostic performed ex-*vivo*, as whole-cell biosensors could provide numerous advantages such as flexibility and low-cost of production. In this context one need to consider important developments: dedicated gene circuits to increase specificity of the detection module, fast fluorescent or colorimetric reporters, and improved magnetic set-up for higher gradient of magnetic field. The development and use of *MagEcoli* technology *in vivo* could benefit from using other bacterial strains such as *E. coli* Nissle 1917, or Gram-positive probiotics that are currently developed as living therapeutics.

Résumé en français :

Production de bactéries magnétiques et leurs utilisations en biotechnologie

Contenu

Introduction :

La naissance du génie génétique jusqu'aux techniques actuelles de biologie synthétique ont rendu possible la modification d'un micro-organisme pour le rendre plus intelligent, c'est-à-dire pour qu'il soit doté de fonctions d'intérêts. On peut modifier un microbe pour qu'il devienne une usine à molécules ou à protéines (comme l'artémisinine[1,2] ou l'insuline[3] par exemple), pour qu'il réponde en temps réel à son environnement et le sonde (c'est le principe des biosenseurs[4]), ou même pour qu'il nous soigne (c'est l'objet de la thérapie génique[5–7]).

Le magnétisme est l'une des propriétés remarquables que l'on peut donner à un micro-organisme. D'abord parce qu'avoir un micro-organisme magnétique ouvre un grand champ d'applications : on peut facilement contrôler sa position dans l'espace et sa localisation, le concentrer en un point, l'extraire d'un milieu complexe mais aussi faire de l'hyperthermie[8] ou encore suivre sa position par imagerie de résonance magnétique (IRM)[9]. En outre le magnétisme à l'avantage de bien pénétrer les tissus biologiques et d'être orthogonal aux systèmes vivants : il ne perturbe pas leurs processus biologiques. On pourrait donc même imaginer utiliser un microbe magnétique pour du diagnostic ou de la thérapie, magnétiquement localisée et suivie, *in vivo* (**Fig. 1**).

L'objet du travail de thèse a été de conférer des propriétés magnétiques à des bactéries largement utilisées dans des laboratoires de biotechnologies : *Escherichia coli*. Après l'introduction dans la bactérie d'une protéine extraite d'une archée, la ferritine de *Pyrococcus furiosus*[10,11], nous avons développé un protocole chimique de biominéralisation des ferritines des *E. coli* pour rendre magnétique tout l'objet bactérien. Nous avons ensuite étudié nos bactéries et essayé de répondre à quelques questions fondamentales : Quelle est la structure et la composition chimique des ferritines minéralisées *in vivo* ? Les bactéries magnétiques sont-elles vivantes ? Capables de se diviser ? Sont-elles contrôlables par des forces magnétiques ? Peuvent-elles réaliser d'autres fonctions d'intérêt ? Une fois le système caractérisé, nous avons tenté de réaliser des applications biotechnologiques comme la capture et le tri magnétique de bactéries cibles, par reconnaissance anticorps/antigènes, et même l'invasion bactérienne de cellules mammifères magnétiquement localisée. Enfin, dans un contexte d'utilisation *in vivo*, comme toute première

étape, nous avons étudié la survie de nos bactéries et de leurs fonctions magnétiques dans le système digestif d'un organisme modèle, *Caenorhabditis elegans*[12].

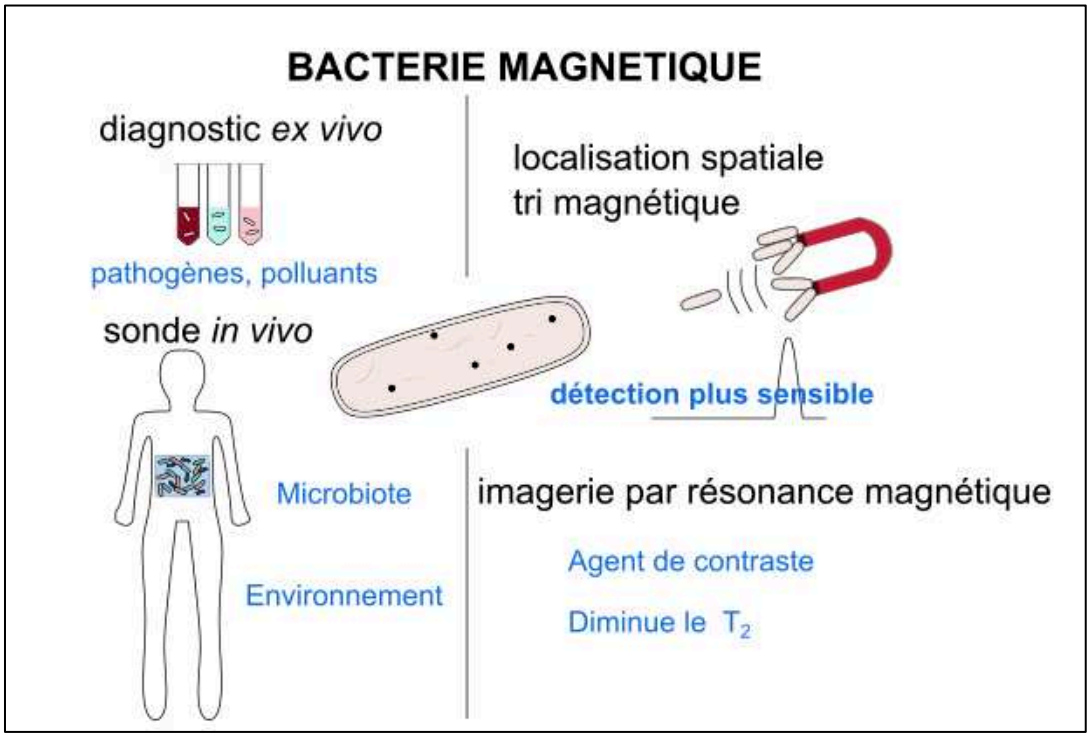

Figure 1 : Une bactérie magnétique peut avoir plusieurs applications. Elle peut être localisée dans l'espace par un aimant, ce qui pourrait par exemple augmenter le signal de détection dans le cadre de diagnostic *ex vivo.* Elle peut être suivie par IRM lors de thérapie ou de diagnostic *in vivo* si elle est en plus reprogrammée.

Résultats :

1. Biominéralisation de *E. coli* et première applications basées sur des modifications de propriétés de surface

Pour rendre des *E. coli* magnétiques, inspirés par les bactéries magnétotactiques[13,14] et les travaux d'évolution dirigée de Pamela Silver[15], nous avons modifié à la fois génétiquement et chimiquement des bactéries. D'abord, nous avons fait surproduire par *E. coli* une protéine naturellement capable de stocker du fer sous la forme d'oxyde : la ferritine. Nous avons fusionné cette ferritine avec une protéine fluorescence, mCherry ou GFP, pour suivre sa présence dans le cytoplasme bactérien par microscopie de fluorescence. Par l'ajout de sel de Mohr sur des cultures de ces bactéries modifiées, nous avons pu minéraliser *in vivo* les ferritines surproduites et obtenir des objets magnétiques.

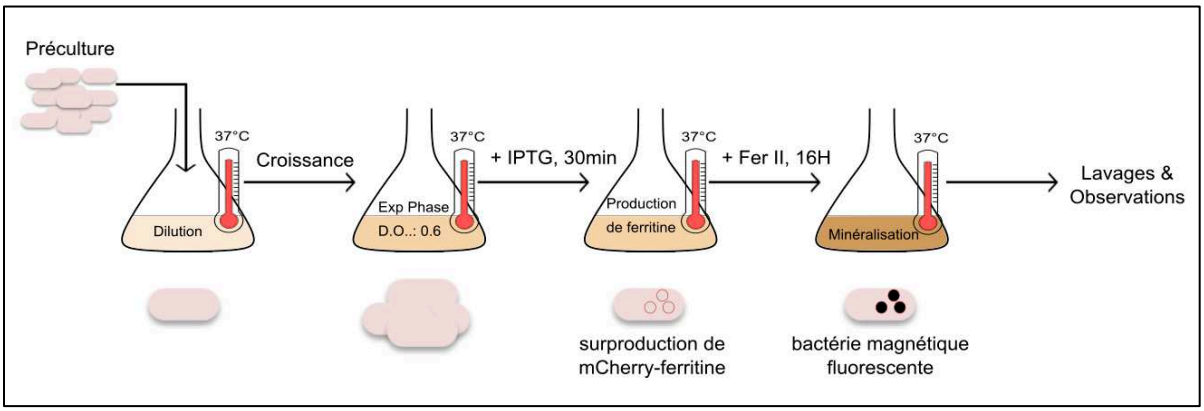

Figure 2 : Protocole de biominéralisation développé sur *E. coli*. Après 16h de contact avec du fer II, les *E. coli* obtenues sont fluorescentes et magnétiques.

Dans un premier temps, nous avons tenté de caractériser les bactéries magnétiques formées. Des images de microscopie électronique à transmission (MET) avec de la spectroscopie de rayon X à dispersion d'énergie, couplées à de la microscopie de fluorescence nous ont indiqué que les ferritines tout comme le fer se localisent à l'extrémité des bactéries (**Fig. 3**). Cela est sans doute causé par la formation de corps d'inclusion qui surviennent en général lors de production de protéines recombinantes. Malheureusement, nous n'avons pas pu visualiser les ferritines

individuelles. Cela laisse un doute quant à la localisation exacte du fer, des phosphates et des oxygènes : dans et/ou autour des ferritines ? Des tests antérieurs de minéralisation *in vitro* qui avaient montré que les nanocages de ferritines se remplissent d'oxyde de fer en présence de fer II, suggèrent fortement que la minéralisation s'est bien faite à l'intérieur des protéines.

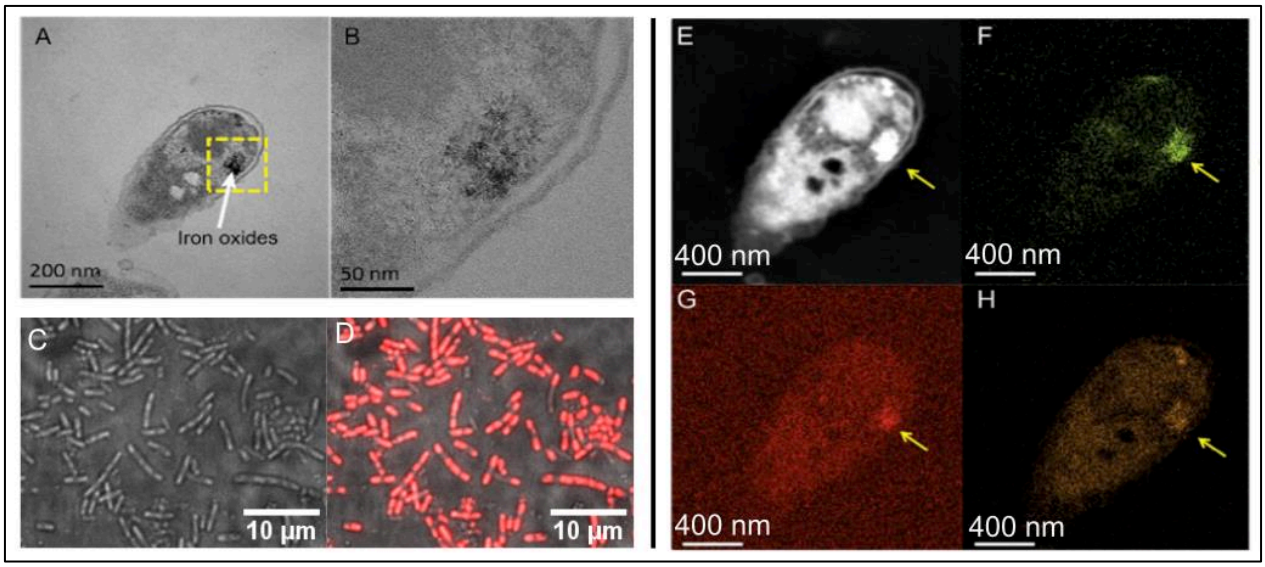

Figure 3 : Images de microscopie électronique à transmission ou de fluorescence des bactéries magnétiques. (A, B) Image MET d'une section de *E. coli* magnétiques. Une région riche en oxyde de fer est entourée en jaune, au pôle de la bactérie. **(C, D)** Images de microscopie d'épifluorescence d'*E. coli* magnétiques. **A gauche** le champ clair révèle les corps bactériens, **à droite** la superposition avec le canal de fluorescence rouge dévoile la présence des mCherry-ferritines dans les pôles bactériens. **(E – H**) Cartographies d'une section de bactérie minéralisée. **(E**) Images de microscopie électronique en transmission à balayage. **(F)** Détection de l'élément fer. **(G)** Détection de l'élément oxygène. **(H)** Détection de l'élément phosphore.

Ensuite, pour vérifier que les bactéries sont bien magnétiques, nous avons mis au point un protocole simple de magnétophorèse. Nous les avons encapsulées dans des gouttes de quelques centaines de micromètres de diamètre pour éviter toute perturbation due à des flux hydrodynamiques. Puis avec un aimant NdFeB placé à l'extrémité des gouttes, nous avons regardé leur attraction magnétique. Les bactéries, qui surproduisaient de la ferritine fluorescente, minéralisées avec 1 à 4 mM de fer II, étaient attirées par les forces magnétiques en quelques dizaines de minutes (**Fig. 4**). La magnétophorèse a dévoilé une véritable corrélation entre quantité de fer ajoutée lors de la biominéralisation et vitesse d'attraction magnétique : plus il y a de fer,

plus les bactéries sont attirées. Cela est sans doute dû au fait qu'à des quantités plus élevées en fer, les ferritines sont plus remplies en oxydes magnétiques ou alors plus de ferritines sont minéralisées.

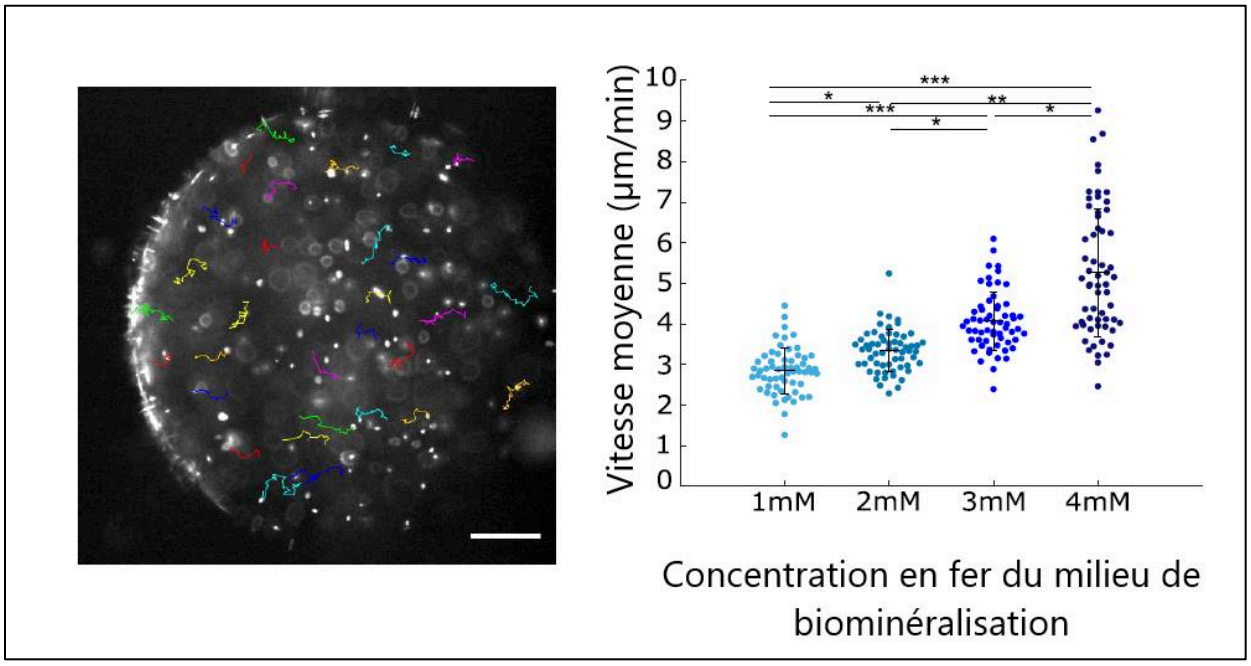

Figure 4 : Magnétophorèse de bactéries magnétiques. A gauche : Représentation des trajectoires de bactéries sur-exprimant la mCherry-ferritine et biominéralisées avec 2mM de fer II. L'aimant est à gauche. Echelle, 60 µm. **A droite :** Histogramme des vitesses d'attraction des bactéries magnétiques contre l'aimant en fonction de la quantité de fer ajoutée pendant la biominéralisation. La moyenne et la déviation standard sont affichées par la croix noire. Chaque point représente une bactérie et une trajectoire. * correspond à une p-value de 10^{-5}, ** de 10^{-10}, *** de 10^{-15}.

Une fois nos bactéries magnétiques formées et caractérisées, nous avons voulu voir si elles étaient toujours vivantes. Des bactéries magnétiques diluées dans un milieu nutritif, à 37°C, poussent à nouveau et se divisent. A partir de là, une question se pose quant au devenir de propriétés magnétiques au cours du temps. Comment le magnétisme se transmet d'une bactérie mère à ses filles ? Pour y répondre nous avons à la fois fait des tests de magnétophorèse sur des *E. coli* magnétiques après quelques divisions cellulaires et nous avons observé la division des bactéries magnétiques en temps réel, en microscopie de fluorescence pour bien suivre les ferritines. Nous avons vu qu'au cours du temps, la proportion de bactéries attirées par un aimant diminue, mais pas leur vitesse d'attraction. Cela suggérerait que les bactéries magnétiques ont

une division asymétrique : seulement une des deux filles récupère la majorité des ferritines, l'autre n'en hérite pas et reste purement diamagnétique. L'observation de division en temps réel a confirmé cette hypothèse : la ferritine étant majoritairement à l'un des pôles, en se divisant, une seule des deux bactéries filles hérite des propriétés magnétiques (**Fig. 5**). Au cours du temps, une portion de plus en plus faible de bactéries restera autant magnétique que la population initiale. Même si, plus la division avance plus la proportion de bactéries magnétiques sur le nombre total de descendantes est faible, cette division asymétrique a un avantage non négligeable. En effet, cela évite une dilution forte du magnétisme dans toutes les descendantes. La masse de ferritines magnétiques restant la même au cours du temps, une division symétrique aurait résulté en une perte totale du magnétisme en quelques heures. Même après 24h, nous avons toujours pu attirer quelques bactéries contre un aimant !

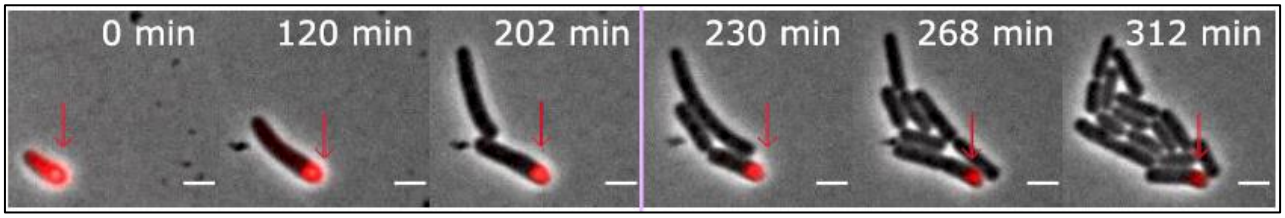

Figure 5 : Images de microscopie de fluorescence (superposition du champ clair et du canal de fluorescence rouge) prises successivement et qui montrent la division d'une *E. coli* magnétique. Echelle, 2 µm.

Enfin, nous avons voulu voir si les *E. coli* magnétiques pouvaient être programmées pour des applications simples. Nous les avons modifiées génétiquement pour qu'elles expriment à leur surface des protéines. D'abord, grâce à un set de plasmides[16], nous avons pu leur faire présenter à leur membrane soit des antigènes soit les anticorps correspondants. Nous avons montré, toujours avec notre montage de magnétophorèse, que les bactéries magnétiques qui produisaient les antigènes pouvaient reconnaitre les anticorps exprimés sur une autre population de *E. coli*, s'y fixer et les attirer contre un aimant (**Fig. 6**). Cette première preuve de concept ouvre la voie à des applications de diagnostic ou de dépollution amplifiées par tri magnétique. Une deuxième expérience consistait à faire produire par les bactéries magnétiques des invasines[17], des protéines impliquées dans le processus d'infection de cellules par contact bactérie/cellule. Grâce à un aimant localisé sous un tapis de cellules humaines, nous avons révélé que nos bactéries

magnétiques avec invasines, avaient tendance à rentrer en plus grande quantité au niveau de l'aimant. Les forces magnétiques ont permis d'attirer les bactéries plus facilement contre les cellules et ont favorisé (et localisé) leur entrée (**Fig. 6**). Ces deux expériences représentent des preuves de concept qui ouvrent la voie à des exemples d'utilisation du champ magnétique.

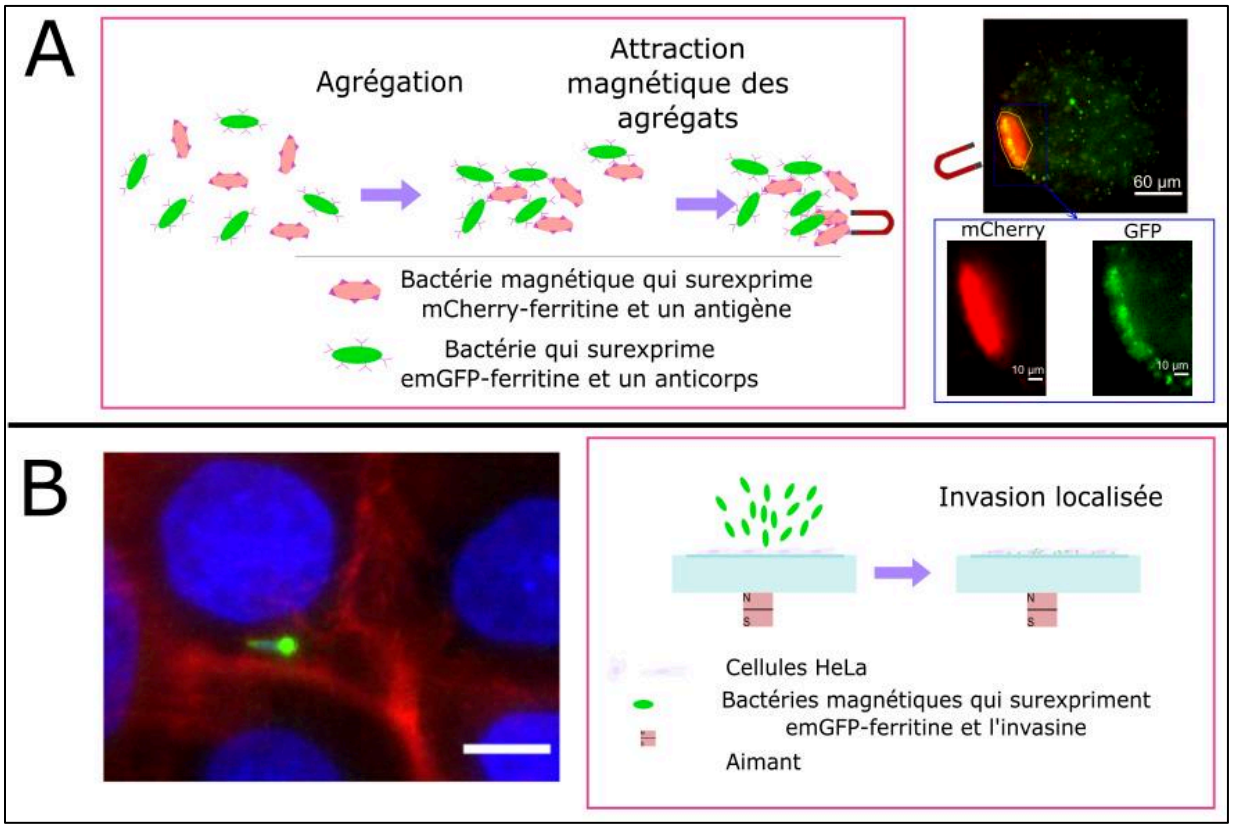

Figure 6 : Deux tests preuves-de-concept avec des bactéries magnétiques modifiées pour avoir de nouvelles propriétés de surface. (A) Test de capture de bactéries cibles contre un aimant par reconnaissant anticorps/antigène. **A gauche :** Schéma de principe. Des bactéries magnétiques fluorescentes rouges qui expriment à leur surface un antigène sont mises en contact avec et capturent des bactéries cibles fluorescentes vertes qui expriment l'anticorps correspondant. Le champ magnétique permet de récupérer des agrégats formés des deux types de bactéries. **A droite :** Résultats en goutte avec un aimant placé à gauche. Il y a accumulation de fluorescence rouge et verte contre l'aimant et donc localisation des deux populations bactériennes. **(B)** Test d'invasion bactérienne de cellules amplifiée par champ magnétique. **A gauche :** Image de fluorescence d'une bactérie magnétique qui surproduit l'invasine entrée dans une cellule LoVo. En bleu les noyaux, en rouge le cytosquelette, en vert la GFP-ferritine de la bactérie. Echelle, 10 µm. **A droite :** Schéma du principe de la localisation de l'invasion. Un aimant est placé sous les bactéries magnétiques qui produisent en surface l'invasine. La sédimentation permet un contact cellule/bactérie et favorise une entrée bactérienne. Les forces magnétiques s'ajoutent localement à la sédimentation et devraient augmenter et localiser l'invasion bactérienne.

2. Effet du magnétisme sur la communication par quorum sensing

Une fois que nous avons vu que des bactéries qui expriment des protéines spécifiques à leur surface peuvent devenir magnétiques, nous avons exploré d'autres preuves de concept. Nous avons essayé de voir si elles étaient capables de communiquer entre elles en temps réel par quorum sensing. Le quorum sensing est un mode de communication bactérien qui permet à une population de déclencher un phénotype lorsqu'elles sont assez nombreuses[18,19]. Il s'effectue grâce à des médiateurs, des auto-inducteurs comme les acyl homosérine lactones, AHL, chez les Gram-négatives. Ici, pour simplifier le problème, nous avons modifié génétiquement les *E. coli* avec soit un plasmide qui leur permet de sécréter un type d'AHL[20], les *senders*, soit de détecter la présence de cet AHL et de devenir fluorescentes (dans le rouge)[21], les *receivers.* Nous avons vérifié que les bactéries magnétiques sont toujours capables d'assurer leur fonction vis-à-vis d'AHL qu'elles soient *senders* ou *receivers.* Cela a prouvé que le magnétisme n'influençait pas leur capacité à produire des protéines ou des molécules post biominéralisation.

Ensuite, nous avons voulu tester l'effet du magnétisme sur la communication par quorum sensing dans notre système. Nous avons utilisé notre montage de magnétophorèse. Dans le cas où les bactéries magnétiques sont *senders*, il est possible de les localiser contre un aimant. Cependant, il n'est pas possible d'induire une réponse localisée vis-à-vis des *receivers*. Même si la source d'AHL est située à l'extrémité de la goutte, l'attraction n'est jamais totale et parfaite. Par ailleurs, AHL diffuse tellement vite, par rapport au temps de production/maturation de la protéine fluorescente détectrice des *receivers*, que tous les *receivers* s'allument de manière uniforme dans la goutte (**Fig. 7**). Pour essayer d'avoir une détection contrainte dans l'espace, à la périphérie des *senders*, l'une des solutions trouvée a été de se placer dans un milieu solide. En extrayant les *senders* magnétiques avec un aimant, et en déposant ce dernier sur une couche de gel recouvert de *receivers*, nous avons pu allumer (par fluorescence rouge) les bactéries détectrices seulement autour de l'aimant (**Fig. 7**). Cependant ce test gagnerait à être amélioré, notamment en revêtant l'aimant d'une matière qui empêcherait l'adsorption non spécifique des bactéries.

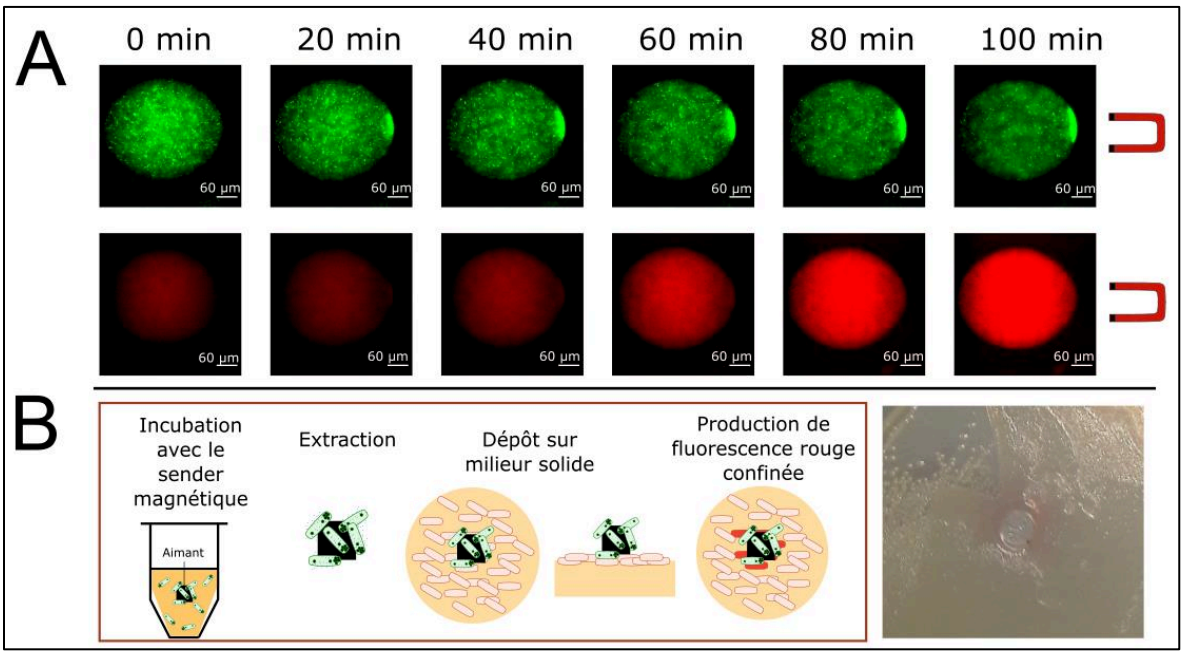

Figure 7 : Expérience de quorum sensing avec un *sender* magnétique et un *receiver*. (A) En milieu liquide. Images de fluorescence au cours du temps. En haut visualisation de *senders* magnétiques attirés par un aimant placé à droite. En bas, visualisation des *receivers* qui produisent de la fluorescence rouge quand AHL est dans le milieu. **(B)** En milieu solide. **A gauche** : schéma du principe de l'expérience. Des *senders* magnétiques sont extraits du milieu grâce à un aimant. L'aimant est ensuite déposé sur un gel recouvert de *receivers* qui peuvent produire de la fluorescence rouge en réponse à AHL et donc à proximité des *senders* magnétiques (autour de l'aimant). **A droite :** Photographie de l'empreinte laissée sur le gel. On note de la fluorescence rouge, visible à l'œil nu, confinée autour de l'aimant.

Dans un deuxième temps, nous avons testé l'autre configuration : des *senders* avec des *receivers* magnétiques. Cette deuxième expérience était d'autant plus importante qu'elle s'inscrit dans un contexte de biocapteur. Sachant que le quorum sensing est utilisé par des pathogènes, détecter *in situ* AHL, le médiateur de la communication, permettrait de détecter la présence de pathogènes vivants et actifs. Ici, notre idée était de tester la sensibilité de nos *receivers* magnétiques à différentes concentrations d'AHL, pour découvrir la limite basse de détection. Une idée supplémentaire était d'utiliser la localisation magnétique pour concentrer près d'un aimant tous les *receivers*, localement augmenter leur signal de fluorescence et améliorer possiblement la détection (**Fig. 8**). Nous avons montré qu'en présence de quantités variables d'AHL synthétique, ou de *senders*, avec notre montage de magnétophorèse, il était possible d'observer et de quantifier la détection d'AHL en moins de deux heures, et avec une concentration minimale de

10 nM. Cette valeur est assez comparable à la littérature[22,23]. La concentration magnétique n'a pas permis d'abaisser le temps de détection, hautement dépendant de la production/maturation de la protéine détectrice fluorescences, ni la limite de détection. En effet pour des concentrations de 1nM et moins, la fuite du promoteur du détecteur jouait trop pour pouvoir faire la distinction avec une condition sans AHL.

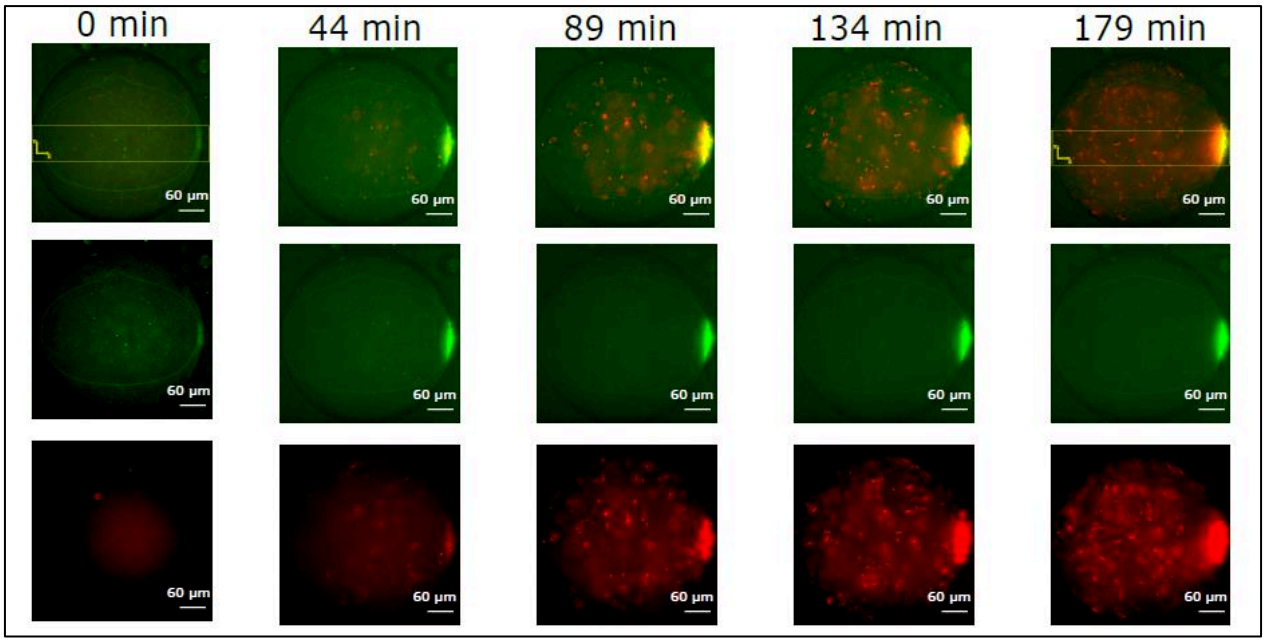

Figure 8 : Images de microscopie de fluorescence qui montrent la localisation spatiale et magnétique des *receivers* magnétiques en présence de 100 µM d'AHL, au cours du temps. L'aimant est à droite. **En haut** : superposition des deux canaux de fluorescence pour voir la ferritine (et donc les *receivers* magnétiques) en vert et la détection d'AHL par les *receivers* magnétiques apparaître en rouge. **Au milieu :** canal de fluorescence vert uniquement. **En bas :** canal de fluorescence rouge uniquement.

3. Résultats préliminaires sur l'utilisation *in vivo* des bactéries magnétiques

La dernière partie du travail de thèse s'est attardée à des études exploratoires sur d'autres utilisations des *E. coli* magnétiques. Nous avons mesuré la réponse IRM de nos bactéries minéralisées avec différentes concentrations de fer, et nous avons vu que les bactéries magnétiques ont une signature propre et se visualisent par IRM (**Fig. 9**). Elles pourraient donc être de bons agents de contraste IRM dans des applications *in vivo.* Ainsi, pour faire des premiers

tests *in vivo*, nous avons utilisé un modèle vivant très simple : *C. elegans*, un parasite qui se nourrit de bactéries *E. coli*. Nous avons voulu voir si nos bactéries survivaient dans *C. elegans*, et gardaient leurs propriétés magnétiques. En sélectionnant une souche de vers dont le grinder était anormal, nos bactéries se sont installées dans le lumen. Après lyse des vers, le lysat contenait encore des bactéries attirables par un aimant lors des tests de magnétophorèse (**Fig. 10**). Ces expériences sont à poursuivre pour les confirmer, mais elles nous laissent entrevoir la possibilité d'utiliser les bactéries magnétiques dans des échantillons plus complexes et même vivants.

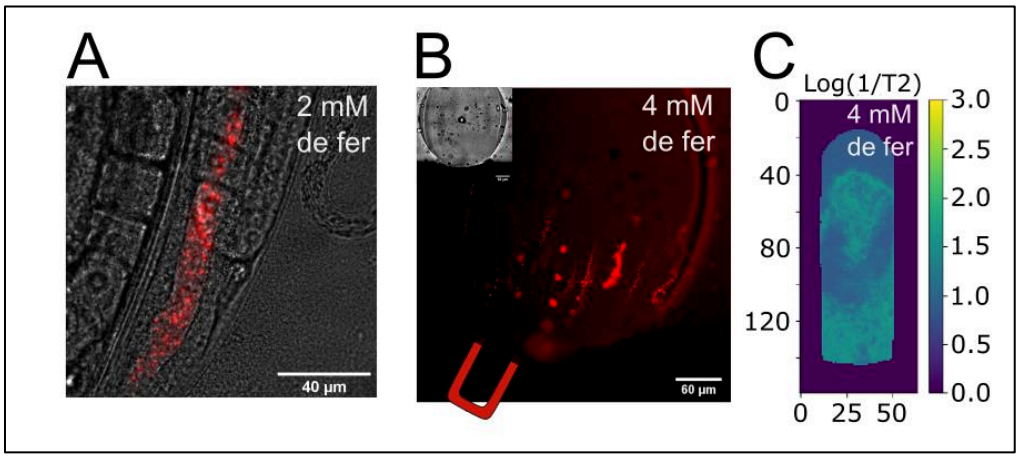

Figure 10 : Résultats préliminaires sur les bactéries magnétiques (qui surproduisent la mCherry-ferritine). (A) Image de microscopie de fluorescence de *E. coli* magnétiques intactes (minéralisées avec 2 mM de fer II) dans le lumen de la souche DA597 de *C. elegans*. Superposition du champ clair et du canal de fluorescence rouge. **(B)** Image de microscopie de fluorescence de magnétophorèse réalisée sur le lysat de *C. elegans* qui s'étaient préalablement nourrit de *E. coli* minéralisées avec 4 mM de fer II **(C)** Image par résonance magnétique d'un tube contenant des *E. coli* minéralisées avec 4 mM de fer II, réparties de manière inhomogène.

Enfin, des tests de lyse sur les *E. coli* magnétiques elles-mêmes, ont révélé que le lysat bactérien contenait des ferritines fluorescentes toujours attirées par des aimants. Ces derniers tests ouvrent de nouvelles perspectives : les bactéries pourraient être utilisées comme usines de nanoparticules magnétiques de taille contrôlée (celle de la ferritine) et génétiquement encodées avec des fonctions additionnelles : fluorescence, auto-agrégation, anticorps….

Conclusion :

En conclusion, cette thèse nous a permis d'explorer l'utilisation du magnétisme dans un système vivant : les bactéries *E. coli*. Nous avons montré, avec l'aide de techniques génétiques et chimiques, qu'il est possible de modifier une bactérie pour la programmer et la rendre manipulable avec des aimants. Nos bactéries magnétiques sont vivantes, localisables dans l'espace, visualisables par IRM et peuvent accomplir d'autres tâches. Le magnétisme permet de localiser leur action, augmentant dans certains cas leur efficacité.

Pour l'instant le champ magnétique n'a d'effet sur les bactéries qu'à faibles distances (de l'ordre de la centaine de micromètre). Il serait utile d'essayer d'optimiser les propriétés magnétiques. Cela pourrait se faire en changeant les conditions de biominéralisation, ou bien en changeant de protéines cages (en utilisant par exemple l'encapsuline qui est plus grande). Pour la suite, il serait aussi intéressant de se pencher sur les applications *in vivo* des *E. coli* magnétiques. Passer à une autre souche biocompatible, comme des probiotiques, permettrait d'envisager des tests plus poussés *in vivo.* Comme la reprogrammation des bactéries se fait aisément, l'une des directions possibles serait l'étude du microbiote du système digestif d'un organisme. Nos bactéries pourraient sonder les intestins, récupérer des informations quant à la présence de pathogènes ou de toxines, et à la fois être suivie par IRM ou bien être récupérées en sortie du tube digestif par tri magnétique comme l'ont fait certaines équipes[24].

Références :

1. Paddon, C. J. & Keasling, J. D. Semi-synthetic artemisinin: A model for the use of synthetic biology in pharmaceutical development. *Nat. Rev. Microbiol.* **12**, 355–367 (2014).
2. Paddon, C. J. *et al.* High-level semi-synthetic production of the potent antimalarial artemisinin. *Nature* **496**, 528–532 (2013).
3. Baeshen, N. A. *et al.* Cell factories for insulin production. *Microb. Cell Fact.* **13**, 1–9 (2014).
4. Inda, M. E. & Lu, T. Microbes as Biosensors. *Annu. Rev. Microbiol.* **74**, 337–359 (2020).
5. Hosseinidoust, Z. *et al.* Bioengineered and biohybrid bacteria-based systems for drug delivery. *Adv. Drug Deliv. Rev.* **106**, 27–44 (2016).
6. Danino, T. *et al.* Programmable probiotics for detection of cancer in urine. *Sci. Transl. Med.* **7**, (2015).
7. Riglar, D. T. & Silver, P. A. Engineering bacteria for diagnostic and therapeutic applications. *Nat. Rev. Microbiol.* **16**, 214–225 (2018).
8. Alphandéry, E., Faure, S., Seksek, O., Guyot, F. & Chebbi, I. Chains of magnetosomes extracted from AMB-1 magnetotactic bacteria for application in alternative magnetic field cancer therapy. *ACS Nano* **5**, 6279–6296 (2011).
9. Hill, P. J. *et al.* Magnetic resonance imaging of tumors colonized with bacterial ferritin-expressing Escherichia coli. *PLoS One* **6**, (2011).
10. Kengen, S. W. M. 'Pyrococcus furiosus, 30 years on'. *Microb. Biotechnol.* **10**, 1441–1444 (2017).
11. Tatur, J., Hagedoorn, P. L., Overeijnder, M. L. & Hagen, W. R. A highly thermostable ferritin from the hyperthermophilic archaeal anaerobe Pyrococcus furiosus. *Extremophiles* **10**, 139–148 (2006).
12. Dimov, I. & Maduro, M. F. The C. elegans intestine: organogenesis, digestion, and physiology. *Cell Tissue Res.* **377**, 383–396 (2019).
13. Blakemore, R. P., Maratea, D. & Wolfe, R. S. Isolation and pure culture of a freshwater magnetic spirillum in chemically defined medium. *J. Bacteriol.* **140**, 720–729 (1979).
14. Jacob, J. J. & Suthindhiran, K. Magnetotactic bacteria and magnetosomes – Scope and

challenges. *Mater. Sci. Eng. C* **68**, 919–928 (2016).

15. Liu, X. *et al.* Engineering Genetically-Encoded Mineralization and Magnetism via Directed Evolution. *Sci. Rep.* **6**, 1–10 (2016).
16. Glass, D. S. & Riedel-Kruse, I. H. A Synthetic Bacterial Cell-Cell Adhesion Toolbox for Programming Multicellular Morphologies and Patterns. *Cell* **174**, 649–658 (2018).
17. Isberg, R. R., Voorhis, D. L. & Falkow, S. Identification of invasin: A protein that allows enteric bacteria to penetrate cultured mammalian cells. *Cell* **50**, 769–778 (1987).
18. Bassler, B. L. How bacteria talk to each other: Regulation of gene expression by quorum sensing. *Curr. Opin. Microbiol.* **2**, 582–587 (1999).
19. Waters, C. M. & Bassler, B. L. Quorum Sensing: Cell-to-Cell Communication in Bacteria. *Annu. Rev. Cell Dev. Biol.* **21**, 319–346 (2005).
20. Prindle, A. *et al.* A sensing array of radically coupled genetic 'biopixels'. *Nature* **481**, 39–44 (2012).
21. Florea, M. *et al.* Engineering control of bacterial cellulose production using a genetic toolkit and a new celluloseproducing strain. *Proc. Natl. Acad. Sci. U. S. A.* **113**, E3431–E3440 (2016).
22. Kumari, A. *et al.* Biosensing systems for the detection of bacterial quorum signaling molecules. *Anal. Chem.* **78**, 7603–7609 (2006).
23. Struss, A., Pasini, P., Ensor, C. M., Raut, N. & Daunert, S. Paper strip whole cell biosensors: A portable test for the semiquantitative detection of bacterial quorum signaling molecules. *Anal. Chem.* **82**, 4457–4463 (2010).
24. Ramesh, P. *et al.* Ultraparamagnetic Cells Formed through Intracellular Oxidation and Chelation of Paramagnetic Iron. *Angew. Chemie - Int. Ed.* **57**, 12385–12389 (2018).

RÉSUMÉ

En programmant le comportement d'organismes vivants, la biologie synthétique a permis de réaliser diverses applications utiles jusqu'au secteur de la santé et de l'environnement. Des circuits synthétiques ont été développés pour du diagnostic *in vitro* ou *in vivo,* pour bio-produire de nouveaux matériaux, ou pour diriger l'assemblage de systèmes synthétiques multicellulaires. Par exemple, des bactéries programmées peuvent sentir des changements de l'environnement, détecter des molécules d'intérêt, surveiller ou diagnostiquer des maladies. Modifier des cellules pour qu'elles soient sensibles à des stimuli non-biologiques, comme des ondes acoustiques ou magnétiques, pourrait améliorer leur capacité à sonder ou à agir sur leur environnement. Ainsi, l'intégration de propriétés magnétiques dans des organismes vivants permettrait de manipuler leur position dans l'espace avec des forces magnétiques et de les utiliser comme agents de contraste pour l'imagerie par résonance magnétique. Durant ce travail de thèse, nous avons modifié des bactéries *Escherichia coli* pour qu'elles surproduisent une ferritine capable de stocker du fer, puis nous les avons minéralisées avec du fer. D'abord, nous avons caractérisé les propriétés des bactéries : nous avons trouvé qu'elles contenaient des compartiments enrichis en oxyde de fer leur conférant des propriétés magnétiques. Ensuite, nous avons montré que nous pouvions les manipuler dans l'espace grâce à des forces magnétiques : plus elles étaient chargées en fer, plus elles étaient attirées par un aimant. En outre, nous avons vu que les bactéries, en se divisant, transmettaient asymétriquement les ferritines riches en oxydes de fer, ce qui permettait d'éviter la dilution des propriétés magnétiques au cours de la croissance bactérienne. Enfin, nous avons démontré que ces bactéries peuvent être programmées pour réaliser des applications preuve-de-concept. Nous avons génétiquement encodé des fonctions d'adhésion sur les bactéries magnétiques pour réaliser la capture de cellules cibles suivi d'un tri magnétique, ou bien l'augmentation locale du taux d'invasion bactérienne de cellules humaines. Puis, nous avons utilisé les bactéries pour localiser ou détecter des molécules impliquées dans le quorum sensing, un mode de communication bactérien. Pour finir, nous avons étudié la réponse RMN des bactéries magnétiques et leur survie dans *Caenorhabditis elegans* ; cela représente une toute première étape vers leur utilisation comme agents de diagnostic ou de thérapie *in vivo.*

MOTS CLÉS

Biominéralisation – *E. coli* – Ferritine– Nanoparticules – Magnétisme – Biotechnologies

ABSTRACT

By programming the cellular behavior of living organisms, synthetic biology tools enable broad applications ranging from basic biology to health and environmental issues. Synthetic circuits have been developed for *in vitro* and *in vivo* diagnostics, to produce novel materials, or to direct the assembly of synthetic multicellular systems. For instance, programmed bacteria can report on environmental changes, detect specific molecules, or monitor and diagnose diseases. Programming cells to be sensitive to non-biochemical stimuli, such as acoustic or magnetic waves, could expand their capacity to probe or act on their environment. The integration of magnetic properties into living organisms could enable their spatial manipulation by magnetic forces and their use as contrast agents for magnetic resonance imaging. During this PhD work, we engineered iron-mineralized *Escherichia coli* expressing the iron-storage ferritin. First, we performed structural and magnetic characterization of the bacteria and found that they contained iron oxide-enriched bodies conferring magnetic properties. Next, we showed that they could be spatially manipulated when exposed to magnetic forces, with an efficiency that increased with iron loading. Moreover, the magnetic bacteria divided and transmitted asymmetrically iron oxide ferritin-enriched bodies during division, thus avoiding the dilution of the magnetic properties during population growth. Finally, we demonstrated that mineralized bacteria can be programmed to perform specific biochemical functions with spatiotemporal control using magnetic forces. We genetically encoded adhesion properties on magnetic bacteria to achieve the magnetic capture of specific target cells as well as the spatial modulation of human cell invasions. Next, we used magnetic bacteria for the localization or detection of molecules involved in quorum sensing communication. Lastly we studied the NMR response of magnetic *E. coli* and their survival in *Caenorhabditis elegans*, as a very first step toward their use as *in vivo* diagnostic or therapeutic agents.

KEYWORDS

Biomineralization – *E. coli* – Ferritin– Nanoparticles – Magnetism – Biotechnology